



**HAL**  
open science

# Prenatal dysfunctions of chloride-related inhibition in lumbar motoneurons of the SOD1G93A ALS

Hongmei Zhu

► **To cite this version:**

Hongmei Zhu. Prenatal dysfunctions of chloride-related inhibition in lumbar motoneurons of the SOD1G93A ALS. Neuroscience. Université de Bordeaux, 2023. English. NNT : 2023BORD0026 . tel-04116951

**HAL Id: tel-04116951**

**<https://theses.hal.science/tel-04116951>**

Submitted on 5 Jun 2023

**HAL** is a multi-disciplinary open access archive for the deposit and dissemination of scientific research documents, whether they are published or not. The documents may come from teaching and research institutions in France or abroad, or from public or private research centers.

L'archive ouverte pluridisciplinaire **HAL**, est destinée au dépôt et à la diffusion de documents scientifiques de niveau recherche, publiés ou non, émanant des établissements d'enseignement et de recherche français ou étrangers, des laboratoires publics ou privés.

THÈSE PRÉSENTÉE  
POUR OBTENIR LE GRADE DE  
**DOCTEUR DE L'UNIVERSITÉ DE BORDEAUX**

École Doctorale

Sciences de la Vie et de la Santé

Spécialité: Neurosciences

Par **Hongmei ZHU**

---

**DYSFONCTIONNEMENTS PRÉNATAUX DE L'INHIBITION  
LIÉE AU CHLORURE DANS LES MOTONEURONES  
LOMBAIRES DU MODÈLE DE SOURIS ALS SOD1<sup>G93A</sup>**

---

Présentée et soutenue publiquement le 10 février 2023

Composition du jury :

**Mme Muriel Darnaudéry**

*Pr, NutriNeurO, Université de Bordeaux*

**Présidente**

**M. Daniel Zytnicki**

*DR, SPPIN, Université Paris Cité*

**Rapporteur**

**M. Christophe Porcher**

*Pr, INMED, Université Aix-Marseille*

**Rapporteur**

**Mme Sabine Lévi**

*DR, INSERM UMRS-1270, Paris*

**Examineur**

**M. Pascal Legendre**

*DR, INSERM U1130-CNRS UMR 8246-Sorbonne Université, Paris*

**Examineur**

**M. Pascal Branchereau**

*Pr, INCIA, Université de Bordeaux*

**Directeur de thèse**

## **Research Unit :**

**INCIA - UMR 5287- CNRS Université de Bordeaux**

Team: MotoPsyn (Branchereau / Le Ray)

<https://www.bordeaux-neurocampus.fr/team/motopsyn/>

## **Address of the laboratory:**

INCIA - UMR 5287- CNRS

Université de Bordeaux

Zone nord Bat 2ab 2<sup>ème</sup> étage

146 rue Léo Saignat

33076 Bordeaux cedex

France

**“Nothing in life is to be feared, it is only to be understood. Now is the time to understand more, so that we may fear less.”**

*– Marie Curie*

**“No accumulation of single steps, can't reach a destination thousand miles away. No integration of small streams, can't merge into an ocean.”**

*– Xun Zi*

# Titre

## Dysfonctionnements prénataux de l'inhibition liée au chlorure dans les motoneurones lombaires du modèle de souris SOD1<sup>G93A</sup> ALS

### Résumé

La sclérose latérale amyotrophique (SLA) est une maladie neurodégénérative fatale de l'adulte caractérisée par la dégénérescence des motoneurones (MNs) et ayant une étiologie multifactorielle. La plupart des études sur la SLA se sont focalisées aux stades symptomatiques selon l'hypothèse que la pathogénicité apparaît lorsque la maladie devient symptomatique. Cependant, un nombre grandissant d'évidences indique que la pathogénicité se développerait bien avant les symptômes. Mon travail de thèse de Doctorat a été basé sur l'hypothèse selon laquelle la SLA – familiale et sporadique – découlerait de déficits présents dès le développement précoce. La première partie de ma thèse a consisté à analyser les courants post-synaptiques GABA/glycine (IPSCs) au niveau des MNs embryonnaire (E) E17,5, localisés dans la colonne motrice ventro-laterale, chez la souris SOD1<sup>G93A</sup> (SOD) modèle de la SLA, en parallèle à l'analyse de l'homéostasie chlorure. Nos résultats ont montré que les IPSCs sont moins fréquents chez les animaux SOD en accord avec une réduction des terminaisons synaptiques VIAAT autour des MNs. Les MNs SODs avaient un ECI 10 mV plus positif que les MNs sauvages (WT) de la même portée. Ce déficit était lié à une réduction du co-transporteur chlorure KCC2. Les IPSCs évoqués et spontanés présentaient une relaxation plus longue chez les MNs SOD, en corrélation à une [Cl<sup>-</sup>]<sub>i</sub> plus élevée. La modélisation a montré que cet excès de relaxation permettait de compenser la moindre efficacité de l'inhibition GABA/glycine liée au ECI dépolarisé. De manière intéressante, les simulations ont révélé la nature excitatrice des potentiels dépolarisants post-synaptiques GABA/glycine (dGPSPs) survenant à basse fréquence (<50Hz) sur les MNs SOD mais pas sur les MNs WT. A plus haute fréquence, les dGPSPs basculaient vers une inhibition du MN liée à une sommation de composantes « shuntantes ». La seconde partie de ma thèse a donc focalisé sur les effets de dGPSPs évoqués électriquement at différentes fréquences (7,5 - 100 Hz) sur de vrais MNs E17,5

au niveau desquels un ECl dépolarisant (sous le seuil du PA) était imposé. Le but était d'examiner si l'effet excitateur pouvait être lié aux changements morphologiques des MNs E17,5 décrits précédemment. Les résultats ont montré que certains MNs étaient bien excités par les dGPSPs basse fréquence et inhibés à plus forte fréquence (MNs bi-effet) alors que d'autres MNs étaient inhibés quelles que soient les fréquences (MNs inhibés). L'effet double était plus souvent détecté au niveau des MNs SOD. Les MNs WT ont été classés en deux groupes en fonction de leur résistance d'entrée ( $R_{in}$ ), les MNs bi-effet ayant une  $R_{in}$  élevée et les MNs inhibés une  $R_{in}$  basse. Les données morphométriques ont mis en avant un arbre dendritique réduit pour les MNs WT bi-effet ( $R_{in}$  élevée) et un arbre dendritique étendu pour les MNs inhibés ( $R_{in}$  basse). Ce n'était pas le cas des MNs SOD excités ou inhibés indépendamment de leur morphologie. En accord avec les simulations montrant qu'une baisse de la densité des courants inhibiteurs sur le soma du MN favorise l'excitation des dGPSPs, nous avons trouvé moins de terminaisons synaptiques VIAAT sur le soma et dendrites proximales des MNs SOD, et une fréquence réduite des dGPSPs spontanés. Dans leur ensemble, les données de ma thèse soulignent une altération précoce de l'homéostasie chlorure et de l'innervation GABA/glycine des MNs SOD1G93A. Avant la naissance, une population dominante de MNs avec  $R_{in}$  basse émerge chez les animaux WT. Ces MNs qui sont inhibés par les dGPSPs pourraient correspondre aux futures MNs vulnérables (rapides, FF). Ces MNs ne sont pas inhibés chez les animaux SOD. Le dysfonctionnement de l'inhibition pourrait être attribué à deux facteurs distincts : la morphologie et la densité des synapses inhibitrices péri-somatiques. Parmi ces facteurs, le deuxième joue un rôle majeur en contrôlant la capacité des neurones GABA/glycine à façonner la sortie motrice spinale.

**Mots clés** : homéostasie chlorure | intégration synaptique | KCC2 | inhibition | motoneurone spinal | sclérose latérale amyotrophique | modèle souris SOD1G93A | simulation | patch-clamp | stade prénatal | transmission synaptique GABAergique/glycinergique | GABA/glycine

# Title

## **Prenatal dysfunctions of chloride-related inhibition in lumbar motoneurons of the SOD1<sup>G93A</sup> ALS mouse model**

### **Abstract**

Amyotrophic lateral sclerosis (ALS) is a fatal and adult-onset neurodegenerative disease characterized by a progressive degeneration of motoneurons (MNs) with complex multifactorial aetiology. Most ALS studies have focused on symptomatic stages based on the hypothesis that ALS pathogenesis occurs when the disease becomes symptomatic. However, growing evidence indicates that ALS pathogenesis might start long before symptom onset. My PhD thesis work was based on the hypothesis that ALS - familial and sporadic - stems from deficits taking place during early development. With the aim of identifying early changes underpinning ALS neurodegeneration, the first part of my thesis analysed the GABAergic/glycinergic inhibitory postsynaptic currents (IPSCs) to embryonic (E) E17.5 MNs located in the ventro-lateral motor column from SOD1<sup>G93A</sup> (SOD) mice, in parallel with the analyse of chloride homeostasis. Our results showed that IPSCs are less frequent in SOD animals in accordance with a reduction of synaptic VIAAT-positive terminals in the close proximity of MN somata. SOD MNs exhibited an ECI 10 mV more depolarized than wild type (WT) MNs. This deficit in GABA/glycine inhibition was due to a reduction of the neuronal chloride transporter KCC2. SOD spontaneous IPSCs and evoked GABAAR-currents exhibited a slower decay correlated to elevated  $[Cl^-]_i$ . Using computer modelling approach, we revealed that the slower relaxation of synaptic inhibitory events acts as a compensatory mechanism to strengthen or increase the efficacy of GABA/glycine inhibition when ECI is more depolarized. Interestingly, simulations revealed an excitatory effect of low frequency (<50Hz) depolarizing GABA/glycine post-synaptic potentials (dGPSPs) in SOD-like MNs but not in WT-like littermates. At high frequency, dGPSPs switched to inhibitory effect resulting from the summation of the shunting components. The second part of my PhD thesis focussed on the effect of electrically evoked-dGPSPs, at different frequencies (7.5

to 100 Hz), on real lumbar E17.5 MNs in which a depolarized ECI (below spike threshold) was imposed. The aim was to examine whether the excitatory effect could be linked to morphological changes previously described in E17.5 SOD MNs. Results showed that some MNs were excited by low frequency dGPSPs and inhibited by high frequency dGPSPs (Dual MNs) and others were inhibited at all frequencies (Inhibited MNs). Dual effect was more often detected in SOD MNs. WT MNs were classified into two clusters according to their input resistance ( $R_{in}$ ), Dual MNs being specific to high  $R_{in}$  and Inhibited MNs to low  $R_{in}$ . Morphometric data pointed out a reduced dendritic tree in high  $R_{in}$  WT Dual MNs and a large dendritic tree in low  $R_{in}$  Inhibited MNs. This was not the case in SOD MNs that were excited or inhibited whatever their morphology and  $R_{in}$ . In agreement with simulation showing that a less density of inhibitory current on MNs soma favors excitatory dGPSPs, we found less synaptic VIAAT terminals on the soma and proximal dendrites of SOD MNs, compared to littermate WT MNs, as well as a lower frequency of spontaneous dGPSPs. Altogether, my thesis data emphasize a prenatal defect in the  $Cl^-$  homeostasis and GABA/glycine innervation in the SOD1<sup>G93A</sup> ALS MNs. Before birth, a dominant population of MNs with low  $R_{in}$  emerges in WT animals. These MNs that are inhibited by dGPSPs could represent future ALS vulnerable fast MNs (putative FF). Interestingly, those MNs are not inhibited in SOD animals. The inhibitory dysfunction could be attributed to two distinct factors: morphology and perisomatic inhibitory synapse density. Of these two factors, the latter plays a major role by controlling capability of GABAergic/glycinergic neurons for shaping spinal motor output.

**Keywords:** chloride homeostasis | synaptic integration | KCC2 | inhibition| spinal motoneurons| amyotrophic lateral sclerosis | SOD1G93A mouse model | simulation | patch-clamp | Prenatal stage | GABAergic/glycinergic synaptic transmission | GABA/glycine.

## **The impact of COVID-19 on my work**

The COVID-19 pandemic hit France during my PhD candidature, causing considerable uncertainty and disruptions to the daily activities in my lab, which affected my research and hence this thesis. The problems included government restrictions on access to workplaces, reduced interactions with other colleagues in the department. COVID-19 restrictions halted my laboratory-based work for several months, delaying the production of data and its analysis. They also caused delays in the delivery of KCC2 transgenic animal from USA and in the requisition of experimental animals. Moreover, I was caught by COVID during my PhD studies and it took me over 3 weeks to recover, but muscle or body aches lasted for more than one month, especially the pain and very heavy hands that made washing and brushing my hair difficult, as well as the inability to use the mouse for long hours per day for data analysis and making figures. Overall, COVID-19 significantly reduced my output during my PhD.

## **Funding acknowledgement**

Hongmei Zhu was granted by the China scholarship Council (CSC). We warmly thank the “Association pour la recherche sur la Sclérose Latérale Amyotrophique et autres maladies du Motoneurone” (ARSLA), as well as AFM-Téléthon for their financial support. This study received financial support from the French government in the framework of the University of Bordeaux's IdEx "Investments for the Future" program/GPR BRAIN\_2030 to Professor Pascal Branchereau.

# Acknowledgements

The completion of this thesis would not have been possible without the support of many people. Here, I wish to express my deep and sincere gratitude to all people who contributed to my research or PhD studies directly and indirectly, with experiments, supports, advices and encouragements.

## **To my supervisor – Professor Pascal Branchereau**

You are one of the best people I have ever met. Your invaluable guidance and immeasurable support throughout my doctoral studies. You have always been on my side and cared about what is best for me. You have been very generous in providing me with the available resources you have to broaden my research perspectives and achieve as many outcomes as possible during my four-year PhD studies. I really appreciate you offered me valuable opportunities to get involved into those exciting and interesting projects. Moreover, you have given me essential guidance and encouragement in dissection of spinal cords, electrophysiological experiments and data analysis, making posters, participating in international conferences, writing thesis, etc. You have always been patient in explaining to me when I had any questions. I sincerely thank you for your continuous help over the years and your patience with my dearth of knowledge. In most cases, you spent hours communicating and discussing projects, experimental results and project-related articles with me, and also extend some additional knowledge to me by sharing some good articles you reviewed and telling some stories about the authors. I really enjoy discussing scientific questions with you. In addition, you always went over the results very carefully, corrected any drafts I wrote, and led me to ask why and how. One scenario is still fresh in my mind: GraphPad Prism could directly provide the statistical results of the chi-square test, but you wanted to know how the Prism calculates. Finally, we re-learned together by searching online and using the statistics textbook in your office library, and then we manually calculated the p-values together by looking at the appendix tables of this book. You have set an example for me: know the what and endeavour to know the how and the why. Besides, during the years I worked with you, I observed a particularly good habit: you always write down a To-Do list on your desk or calendar, crossing one off as you completed it, and constantly review and use newly learned English words. You have taught me that every step must be very solid and conscientious in doing research and learning (new) knowledge. Another important lesson you taught me is that doing scientific research requires questioning, not trusting 100% of published articles or even recommended instructions for the use of antibodies without explaining why, but more importantly, trying. New results are often obtained through trying after questioning. I am indebted for the valuable knowledge I have learnt from you.

## **To three most important Collaborators**

A very big thank you to Prof. Daniel Cattaert of our institute for his guidance throughout the tenure of the main project. He gave me priority and excellent assistance in my thesis in spite of his packed schedule. His support has been incomputable in providing me with his simulation results and PCA analysis, the method of asymmetry analysis, correcting posters and manuscripts as well as offering me some instructive suggestions on complicated morphological results.

I am also very grateful to two key collaborators at University College London, Prof. Marco Beato and Dr. Filipe Nascimento, for their helpful discussions and keen insights in the side project. At the very beginning, for each low-power image I provided, Marco gave his opinion and that of an expert in the field to help me identify the dorsal and ventral nuclei at different lumbar levels. His serious academic attitude in annotating each image left a very deep impression on me. Unluckily, I did not obtain any positive outcomes or results in this tough side project because of the Confocal resolution limitation. However, through discussions and interaction with them, with specific questions or "questions - answer - discussion of results - problems - possible causes" process, I actively or passively absorbed a lot of topic-related knowledge and experienced the growing pleasure of answering questions and doing research. Furthermore, their very rigorous assessment to scientific results: results were analysed in multiple dimensions to determine the reliability of the results. The valid conclusion is based on the size of the group that is as large as possible and choose the correct statistical analysis method. Much more than that, I gradually got a lot of inspirations from them and drove myself to open my mind and try more scientific critical and comprehensive thinking. I really appreciated fruitful discussions and communications with them via email.

### **To Branchereau Lab**

To all the members of the Branchereau lab – a big shout out to you guys. To William Cazenave – thank you a lot for assistant in experiment of western blot and converting excel files from csv format to xltm. But also, thank you a lot for promptly accompanying me to hospital emergency room to check in and treat my wound when my finger was bitten by a pregnant FUS mouse. To two internship students of Master (Urvashi DALVI) and Bachelor (Alissa Dimitrova) – thank you for showing me instantaneous frequency analysis and helping me to re-check the labelled dendritic tree number, respectively. To Philippe Chauvet – laboratory engineer – special thank you for your assistance in the technical problems (i.e., fixing dissecting instruments) and also in enthusiastically teaching me French in the lab, although my French is still poor. To Antony Czarnecki – thank you for answering some of the project-related academic questions I asked and giving suggestions and proofreading my poster and PhD manuscript. To Alexandra Reichova – thank you for your care in the progress of my thesis and suggestions on the defense, and for your help in analysing the raw image data for the side project, even though we did not end up using it.

### **To all staff at INCIA and the University of Bordeaux**

Many others were part of my PhD journey. Gilles Courtand – Principal Engineer – I would like to give a big thank you for your excellent technical assistance in coding different macro files for image analysis of my IHC data and teaching me how to use the ZEISS Confocal microscopy for image acquisition and deconvolution processing. Dr.Thoby-Brisson Muriel – I really appreciate your kind assistance in lending me your team's powerful computer when my computer was running very slowly. Loïc GRATTIER and Christophe Halgand – our informatician – thank you for solving many problems related with my computer and servers. Cardoit Laura – Lab technician – thank you for teaching me use Leica cryostat and helping me cut few P20 spinal cords. Cabirol Marie-Jeanne – research engineer – thank you for teaching me CLARITY tissue clearing technique, although I eventually gave up using it because of the long processing time. Nathalie Argenta – thank you for breeding animals and offering the experimental animals I needed. Dr. Barriere Grégory – thank you for helping code macro in excel file

for efficient file format conversion from csv to xltm. Camille Lancelin – thank you for giving me helpful advices in the technical problems that I encountered during the side project. Anne Fayoux – thanks to your warm help in bringing the idle cooling fan from your home to the lab for me to use during the hot summer vacation of 2020 while I was analysing electrophysiological data in the lab.

### **To facility of Bordeaux Imaging Center**

To Fabrice Cordelieres – Engineer of BioImage Analyst in Photonic unit – thank you for your assistant in deconvolution processing for Airyscan images and suggestions for image analysis. To Lysiane Brocard and Matthieu Buridan – Technical manager and Engineer in Plant unit – Thank you for your professional technical assistance in teaching me to use the Zeiss confocal microscope equipped with the Airyscan module to capture super-resolution images in my side project and responding positively to any questions I asked. Special thanks to Matthieu Buridan for his handy help in delivering and upload the captured Airyscan images to me.

### **To the Doctorate Funding Program of the CSC and University of Bordeaux**

I am really grateful to the CSC (China Scholarship Council) for providing me with a 4-year scholarship, so that my PhD aspirations were fulfilled without financial worries.

I am especially grateful to Prof. Zhicheng Xiao who was my supervisor during my master study and early academic career. Thanks to his support and recommendations, I won the selection to study for a PhD overseas with a national scholarship.

I cannot thank the University of Bordeaux enough for providing me an opportunity to pursue a PhD at the prestigious Neuroscience Institute. I have been given access to a world of possibilities to develop my professional and research skills. In addition, I had the pleasure of taking a very high-quality online course - Computational Neuroscience Crash Course - with a professional teaching team and talented students from across the world to gain new knowledge and skill.

### **To my family, friends, flatmates and officemates**

I wish to express my heartfelt thanks to my officemates, Anne Bessaguet-Olechowski, Zoé Mazurie, Gabriel Barrios, Laura Puygrenier and Gabriel Pitollat, for their daily discussions and daily help with me. Among them, when I arrived in our lab, Zoé provided me with timely assistance in administrative procedures, share the experience of doing whole-cell patch clamp recording, and constantly cared about my life; Anne and Gabriel Barrios have shared with me unreservedly on the academic aspect (,sharing academic experiences and using Adobe illustrator).

I would like to extend my gratitude to the Chinese researchers and friends who I met in Bordeaux and have shared some journeys with me before COVID pandemic. They are Binbin Xu, Sze Ying Lam, Zhe Zhao, Wencan He, Xiaoyan Ma, Fang Tong, Li Lu, Wei Yuan, Linhan Shao, Zhenhui Chen, Jianqiao Jiang, Jiaojiao Wang, Oleg Solopchuck, et al. We exchanged various information (scientific news, some interesting knowledge in different fields, etc), and share the scientific methodology learned in France (e.g. reductionism) and learning resources. During the journey, I was so lucky to gain a Tai Chi instructor, Xiaoyan, who has been practicing martial arts since childhood. For me, she is also a good teacher and friend. Special thanks to Binbin for his great support and help in using R software for clustering analysis of my side project and teaching me how to use R. Sze Ying, a big thank you for your constant care and encouragement to me, and for some very helpful advices. You're just like my elder sister, caring about my life and studies,

bring me gifts and books after your travel, giving me red pocket for Chinese New Year (because you said in Hongkong, people who are not married are allowed to receive red packets no matter their ages), making food and bringing them to my residence or the lab, and letting me celebrate with you a very important event in your life. I also would like to give thanks to the students who got the same scholarship in the same year, they are Naixin Kang, Weiwei Cao, Yi Yu, Qilei Song, Junjin Che, Fenghuan Zhao, et al., for the happy time we have spent together.

I am grateful to have met some friendly flatmates in Bordeaux who are from different countries (i.e., France, Spain, Italy, Singapore, Syria, Germany, etc) and study different majors (i.e., mathematics, public health, computer science, chemistry, physics, political science, literature, etc). They are Antoine, Anne, Ahmad, David, Ali, Edgar, Lorenzo, Katie, Timothy, Alessa, Ahcene and Angela. We greet and communicate daily, share food or cuisines from our respective countries, run together, and go hiking together. We open our hearts to each other and get along like family: On weekends, we had family breakfast or dinner together, and Antoine and Anne often get up early to make crêpes and coffee for us, and then we enjoy a family breakfast and chat together. But when the kitchen and bathroom are untidy, we will have a harmonious family meeting to talk about the problems and improvement measures, and posted the family rules that each family member agrees to follow; When they learn some new knowledges (e.g. foreign language etc.) or obtain some important achievements (e.g. a finished product – a novel hands-on playable video game – designed by coding thousands of lines of code, Won award and certificate in oral presentations at the international conference, etc.), they share with me; When they buy new but very expensive chairs, they let me experience; When anyone finishes their study and will leave Bordeaux, they always say goodbye before leave, and also give gifts and good wishes for each other; Although Antoine had moved to another residence, he still came back to our residence to give us one COVID rapid test kit containing 5 tests after his institute had distributed two free kits to each staff member; Sometimes I discussed some English expressions or phrases with them, which is very interesting and funny. An example, I didn't know the meaning of "a can of worms" from an email reply from Marco, when I got home and asked Timothy from Singapore, "Do you know?", and then he blurted out "Don't want to open it". Honestly, this explanation is much better than the English-to-Chinese translation given by the translation software, because I had just such a picture in my mind that I can relate to a similar experience: we had cleaned a garbage bin with lots of worms together in the summer. There were many similar moments when I really appreciated the beauty and precision of the academic English used by people like Marco; When I was sick, Antoine and Edgar helped me contact the doctor and send me to the nearest emergency center; When I heard the news of my grandmother's death from my little niece, I felt very sad. It was Anne and Ahmed who first noticed my abnormality and offered me companionship and comfort; When I got Covid, Timothy took good care of me, buying food and cooking for me. Too many beautiful and vivid details of life cannot be written one by one.

I give my deepest thanks to my families, my Papa (Zhiwei Zhu) and Mummy (Huanying Zhu), grandma (Yuxian Xuan and Heshun Wang), grandpa (Guifu Zhu, and Jie Xuan, and Hexiang Xie), sister and brother (Hongguo Zhu, Yunqin Zhu, and Yunlou Zhu), aunt (Bin Xuan) and uncle (Ying Xuan), for giving me infinite love and supports. I will never be able to hug you again, my dear grandma and grandpa (Zhu Guifu and Jie Xuan), but I will remember you forever and wish you a second life and a happy life in another world.

The PhD journey in France is absolutely the most amazing and unforgettable experience in my whole life and great treasure to me. This is because not only the knowledge and expertise I've gained here, but also the unique and colourful oversea life I have had here. I really enjoy the time working here and all those after-work journeys.

I wish all my friends very best in their careers.  
Bonne santé à tous

## Abbreviations

ALS	Amyotrophic Lateral Sclerosis
AMPA	$\alpha$ -Amino-3-hydroxy-5-methyl-4-isoxazolepropionic acid
ANOVA	Analysis of variance
AP	Action potential
Ascl1	Achaete-scute complex homolog 1 ( <i>Drosophila</i> );
ATP	Adenosine triphosphate
BarH1	BarH-like homeobox
BSA	Bovine serum albumin
Bhlhb5	Basic-helix-loop-helix family, member e22
Bmp2	Bone morphogenetic protein 2
Bmp4	Bone morphogenetic protein 4
Bmp5	Bone morphogenetic protein 5
Bmp6	Bone morphogenetic protein 6
Bmp7	Bone morphogenetic protein 7
Bmpr1	Bone morphogenetic protein receptor, type 1a
Bmpr1b	Bone morphogenetic protein receptor, type 1b
Brn3a	POU domain, class 4, transcription factor 1
CCCs	Cation-chloride co-transporters
Chx10	Visual system homeobox
Cl <sup>-</sup>	Chloride
[Cl <sup>-</sup> ] <sub>i</sub>	Intracellular Cl <sup>-</sup> concentration
Cm	Membrane capacitance
Co-IP	Co-immunoprecipitation
CNS	Central nervous system
CPG	Central pattern generator
CSF	Cerebrospinal fluid
d	Day(s)
Dbx1	Developing brain homeobox 1
Dbx2	Developing brain homeobox 2
dGPSPs	Depolarizing GABA/glycine post synaptic potentials
DMSO	Dimethyl sulfoxide
E	Embryonic day
EAAT2	Excitatory amino acid transporter 2
E <sub>Cl</sub>	Chloride equilibrium
EDTA	Ethylenediaminetetraacetic acid
E <sub>GABAAR</sub>	Reversal potential for GABA <sub>A</sub> R
fALS	Familial ALS
FBL	Feedback loop
FDA	Food and Drug Administration
FFL	Feed-forward loop
FGF	Fibroblast growth factor
FSC	Forward scatter
FSC-A	Forward scatter area
FSC-H	Forward scatter height
FTD	Frontotemporal dementia
GABA	$\gamma$ -aminobutyric acid

GABA <sub>A</sub> R	GABA <sub>A</sub> receptor
GABA <sub>A</sub> Rs	GABA <sub>A</sub> receptors
GlyR	Glycine receptor
GlyRs	Glycine receptors
Glu	Glutamate
GluR	Glutamate receptors
IBC	Ice Bucket Challenge
IgG	Immunoglobulin
I-O	Input-output
i.p.	Intraperitoneally
IP	Immunoprecipitation
IPSCs	Inhibitory postsynaptic currents
iPSCs	Induced pluripotent stem cells
Isl1	ISL1 transcription factor, LIM homeodomain
Isl2	ISL2 transcription factor, LIM homeodomain
Lbx1	Ladybird homeobox homolog 1
Lhx1	LIM homeobox protein 1
Lhx2	LIM homeobox protein 2
Lhx4	LIM homeobox protein 4
Lhx5	LIM homeobox protein 5
Lhx9	LIM homeobox protein 9
Lmo4	LIM domain only 4
Lmx1b	LIM homeobox transcription factor 1 beta
KCC2	K <sup>+</sup> -Cl <sup>-</sup> transporter isoform 2
KCCs	K <sup>+</sup> -Cl <sup>-</sup> cotransporters
LMNs	Lower MNs
LTP	Long term potentiation
mAb	Monoclonal antibody
Math1	Atonal homolog 1 ( <i>Drosophila</i> )
Msx1	Homeobox, msh-like 1
mIPSCs	Miniature GABAergic/glycinergic inhibitory postsynaptic currents
MN	Motoneuron
MNs	Motoneurons
mSOD1	Mutant SOD1
NaCl	Sodium chloride
NDD	Neurodegenerative disorder
Ngn1	Neurogenin 1
Ngn2	Neurogenin 2
Ngn3	Neurogenin 3
NKCC1	Sodium (Na <sup>+</sup> )-potassium (K <sup>+</sup> )-Cl <sup>-</sup> transporter isoform 1
Nkx2.2	NK2 transcription factor related locus 2
Nkx2.9	NK2 transcription factor related, locus 9
Nkx6.1	NK6 homeobox 1
Nkx6.2	NK6 homeobox 2
NMDA	N-methyl-D-aspartate
NMJ	Neuromuscular junctions
Notch	Notch gene homolog 1 ( <i>Drosophila</i> )
Olig2	Oligodendrocyte transcription factor 2
Olig3	Oligodendrocyte transcription factor 3
OLs	Oligodendrocytes

OPCs	Oligodendrocyte precursor cells
OvExp	Over-expression
P	Postnatal day
p	p-value; probability value in statistical hypothesis testing
Pax2	Paired box gene 2
Pax3	Paired box gene 3
Pax6	Paired box gene 6
Pax7	Paired box gene 7
PBS	Phosphate-buffered saline
PFA	Paraformaldehyde
pH	Potential of hydrogen (measure of acidity or basicity)
PLCgamma	Phospholipase C, gamma 1
Ptf1a	Pancreas-specific transcription factor 1ax
Pitx2	Paired-like homeodomain transcription factor 2
RA	Retinoic acid
RC	Renshaw cells
Rin	Input resistance
Rm	Membrane resistance
RMP	Resting membrane potential
sALS	Sporadic ALS
Scl	T cell acute lymphocytic leukemia 1
SD	Standard deviation
SEM	Standard error of the mean
Shh	Sonic hedgehog; Sim1, single-minded homolog 1
SOD1	Cu-Zn superoxide dismutase-1
Sox1	SRY box-containing gene 1
Sox14	SRY box-containing gene 14
Sox21	SRY box-containing 21
TBI	Traumatic brain injury
TDP-43	TAR DNA Binding Protein 43 kDa (TARDBP)
Tg	Transgenic
Tlx1/3	T cell leukemia, homeobox 1/3
TM	Transmembrane
TMP	Transmembrane protein
TMS	Transcranial magnetic stimulation
TNF	Tumor necrosis factor
UMNs	Upper MNs
V/I	voltage-current
VLF	Ventro-Lateral Funiculus
WT	Wild type
Wt1	Wilms tumor homolog 1
YMCA	Young Men's Christian Association
$\alpha$ -MNs	Alpha motor neurons
$\alpha$ -S	Slow-twitch, fatigue-resistant $\alpha$ -MNs
$\alpha$ -FF	Fast-twitch, fatigable $\alpha$ -MNs
$\alpha$ -FR	Fast-twitch, fatigue-resistant $\alpha$ -MNs
$\gamma$ -MNs	Gamma motor neurons

## Glossary

<b>Transcription factor</b>	TF = a protein that binds to DNA and controls the transcription from DNA to RNA. TF is expressed in specific populations of neurons during development.
<b>Central pattern generator</b>	CPG = a specific group of neurons that autonomously generate rhythmic patterns of activity.
<b>Commissural Interneuron</b>	CIN = excitatory or inhibitory neuron that has an axon crossing the midline or between the left side and the right side of the nervous system.
<b>Rhythm-generating neuron</b>	Excitatory neuron that are primarily involved in rhythm generation.
<b>Ia interneuron</b>	Ia-IN = glycinergic/GABAergic ipsilaterally projecting inhibitory interneuron.
<b>Renshaw cell</b>	RC = inhibitory interneuron that is excited <i>via</i> recurrent collaterals from motor neurons (MNs). RC projects back to MNs and inhibit them. RC also inhibits reciprocal Ia interneurons.
<b>Recurrent inhibition</b>	Feedback inhibition linked to RCs activation.
<b>Fictive locomotion</b>	Locomotor activity that is initiated in the absence of sensory feedback and supra-spinal descending control.
<b>Drug-induced rhythmic activity</b>	Fictive locomotion induced by local application of molecules such as 5-HT, NMDA, noradrenaline, and dopamine (alone or in combination).
<b>Proprioception</b>	Sense of the body: the awareness of body and limb position. Mediated by proprioceptive movement-activated receptors in muscles, tendons and joints.
<b>Ventricular zone</b>	Innermost layer of the embryonic spinal cord that contains dividing progenitor cells.
<b>Chloride homeostasis</b>	A critical determinant of the strength and robustness of inhibition mediated by GABA <sub>A</sub> receptors (GABA <sub>A</sub> Rs).
<b>GABA<sub>A</sub>R</b>	ionotropic receptor of $\gamma$ -aminobutyric acid (GABA <sub>A</sub> R), a GABA-gated chloride (Cl <sup>-</sup> ) channel.
<b>GABA<sub>A</sub>R signalling</b>	Signalling delivered <i>via</i> the activation of GABA <sub>A</sub> R. The consequence of GABA <sub>A</sub> R signalling is dependent on intracellular Cl <sup>-</sup> concentration ([Cl <sup>-</sup> ] <sub>i</sub> ), which determines

the reversal potential for GABA<sub>A</sub>R currents ( $E_{GABAAR}$ ). GABA<sub>A</sub>R-mediated signalling consists of two main components: phasic and tonic inhibition.

**“Phasic” inhibition**

Synaptic inhibition (fast inhibition), one form of GABA<sub>A</sub>R-mediated inhibitory signalling. It is triggered by transient activation of synaptic GABA<sub>A</sub>Rs at GABAergic synapses and consists of individual inhibitory postsynaptic events.

**“Tonic” inhibition**

Non-synaptic constant (tonic) inhibition, one form of GABA<sub>A</sub>R-mediated inhibitory signalling. It is generated in large part through persistent activation of extrasynaptic GABA<sub>A</sub>Rs and may also involve spontaneously opening GABA<sub>A</sub>Rs whose activation does not require binding of GABA.

**IPSC**

Inhibitory postsynaptic current (IPSC) generated by phasic inhibition related to a synaptic release of GABA and/or glycine.

**Miniature IPSC**

mIPSC is triggered by the spontaneous release of GABA and/or glycine from a single synaptic vesicle, without any pre-synaptic action potential. mIPSCs are revealed in the presence of TTX.

**Spontaneous IPSC**

sIPSC is triggered by spontaneously occurring action potentials in presynaptic terminals and typically involve release of GABA and/or glycine from multiple synaptic vesicles.

**Evoked IPSC**

eIPSC is triggered following experimentally induced action potentials, and, like sIPSC, involves release of GABA and/or glycine from multiple synaptic vesicles.

# Table of contents

	Page
Abstract.....	4
The impact of COVID-19 on my work.....	8
Funding acknowledgement.....	9
Acknowledgements.....	10
Abbreviations.....	15
Glossary.....	18
List of figures.....	21
<b>CHAPTER 1 LITERATURE REVIEW.....</b>	<b>23</b>
<b>1.1 Physiology of spinal cord organization.....</b>	<b>23</b>
1.1.1 Locomotor system and spinal locomotor CPG.....	36
1.1.2 MNs subtypes.....	44
1.1.3 Recurrent inhibition.....	47
1.1.4 GABAergic/glycinergic inhibition and GABA/glycine transmission.....	51
1.1.5 Shunting inhibition.....	59
1.1.6 Chloride homeostasis.....	61
1.1.7 KCC2 and NKCC1.....	64
<b>1.2 ALS: an incurable disease.....</b>	<b>67</b>
1.2.1 SOD1 <sup>G93A</sup> and other ALS animal models.....	71
1.2.2 Pathophysiology of ALS.....	80
1.2.2.1 Neuronal loss.....	81
1.2.2.2 Motoneuronal alterations.....	83
1.2.2.3 Glutamate excitotoxicity.....	87
1.2.2.4 Synaptopathy.....	89
1.2.2.5 Electrophysiological changes.....	90
1.2.2.6 Glial defects.....	93
1.2.2.7 Hyperexcitability of MNs.....	99
1.2.2.8 Skeletal muscle alterations.....	101
<b>1.3 Hypothesis/aims of the thesis .....</b>	<b>102</b>
<b>CHAPTER 2 RESULTS – PAPER1.....</b>	<b>107</b>
<b>CHAPTER 2 RESULTS – PAPER2.....</b>	<b>133</b>
<b>CHAPTER 3 DISCUSSION.....</b>	<b>177</b>
<b>CHAPTER 4 PERSPECTIVES.....</b>	<b>194</b>
<b>CHAPTER 5 LIST OF PUBLICATIONS AND POSTERS.....</b>	<b>197</b>
<b>CHAPTER 6 REFERENCES.....</b>	<b>198</b>
<b>ANNEX.....</b>	<b>235</b>

# List of figures

## Chapter 1

- Figure 1. Organization of Motor cortex and spinal cord.
- Figure 2. A hierarchy of MNs identities.
- Figure 3. Columnar organization of spinal MNs by rostro-caudal axis patterning.
- Figure 4. Spinal MNs specification and connectivity.
- Figure 5. The development of the embryonic spinal cord
- Figure 6. Neuronal specification during spinal cord development along the dorso-ventral axis.
- Figure 7. Organization of the locomotor system in vertebrates
- Figure 8. Organization of Mouse Spinal Locomotor CPG Network.
- Figure 9. Positioning ipsilateral interneurons within the Spinal Locomotor CPG Network in ~P21 mice
- Figure 10. Schematic representation of the different types of motoneurons
- Figure 11. Local spinal motoneuronal network control excitation/inhibition balance in normal condition.
- Figure 12. The diagrams summarize the changes in the integration of Renshaw cells and Ia interneurons in the ventral spinal network during development.
- Figure 13. Schema of GABAergic (left) and glycinergic (right) axon terminal.
- Figure 14. Modes of GABAA receptor activation.
- Figure 15. Structure of Cys-loop receptor (GABAA receptor) ion channels.
- Figure 16. Structure of the glycine receptor.
- Figure 17. Development of the GABAAR-mediated inhibitory transmission in mouse lumbar spinal MNs.
- Figure 18. Developmental changes in the proportions of GABAergic and glycinergic synaptic activity in various areas of the CNS.
- Figure 19. Schema of shunting inhibition.
- Figure 20. Intracellular Cl<sup>-</sup> homeostasis.
- Figure 21. Schematic representation of GABAergic signaling in mouse.
- Figure 22. A developmental switch in cation-chloride cotransporter expression regulates excitatory GABAergic signaling in the developing CNS and inhibitory GABAergic signaling in the adult CNS
- Figure 23. Relationship between [Cl<sup>-</sup>]<sub>i</sub> and Cl<sup>-</sup> load (NKCC1 activity), KCC2 activity.
- Figure 24. Hypothetical structural model of the K<sup>+</sup>-Cl<sup>-</sup> cotransporter.
- Figure 25: Amyotrophic lateral sclerosis: muscle denervation and atrophy upon lower motor neurons loss.
- Figure 26. ALS Gene Discovery since 1990.
- Figure 27. Typical pathological hallmark features of ALS in human patients.
- Figure 28. ALS pathomechanisms and targets tested in recent preclinical trials in rodents.
- Figure 29. The “dying-forward” and “dying-back” hypotheses
- Figure 30. Schematic representation of the selective and progressive degeneration of MNs.
- Figure 31. Time course of neurodegeneration in the SOD1<sup>G93A</sup> mouse model of ALS.

- Figure 32. Embryonic morphological abnormalities in E17.5 SOD1<sup>G93A</sup> MNs.  
Figure 33. ALS-associated alterations in ventral spinal cord circuitry.  
Figure 34. Summary of the changes in motoneuron properties over time.  
Figure 35. Schematic of the evolution of MNs degeneration and glial activation during the course of SOD1 mutant-Initiated ALS disease.  
Figure 36. Graphic summary of natural killer cells modulates motor neuron-immune cell cross talk in models of ALS  
Figure 37. Hyperexcitability in SOD1G93A MNs at E17.5.  
Figure 38. Summary diagram of thesis aims.

### **Chapter 3**

- Figure 39. Summary diagram of the mechanisms involved in Cl<sup>-</sup> homeostasis regulating cellular hyperexcitability and affecting the synaptic inhibition efficacy of GABA/glycine in prenatal SOD<sup>G93A</sup> MNs.  
Figure 40. Recurrent inhibition is preferentially reduced in delayed firing motoneurons from SOD1G93A mice.  
Figure 41. Alterations in size of the postsynaptic GlyRs clusters onto Fast MNs.  
Figure 42. A summary of size measurements of GlyRs clusters on rodent spinal MNs.  
Figure 43. Schematic drawing of recorded MN receiving recurrent inhibition from the Renshaw cell but with variable glycinergic input efficacy under physiological conditions.

# CHAPTER 1 LITERATURE REVIEW

## 1.1 PHYSIOLOGY OF SPINAL CORD ORGANIZATION

A major task of the central nervous system (CNS) is to control behavioural actions, which necessitates a precise regulation of muscle activity. The final components of the circuitry controlling muscles are the motoneurons (MNs), which settle into pools in the ventral horn of the spinal cord in positions that mirror the musculature organization within the body (Figure 1). An animal's behavioural repertoire is evolved to suit its particular survival needs and originates from the nervous system circuitries that control movements. One major strategy for an animal to organize the neuronal networks for diverse behaviours is to possess ensembles of neurons that are distributed to form maps of external space or body space. These 'topographic' arrangements are a common theme in the vertebrate nervous system.

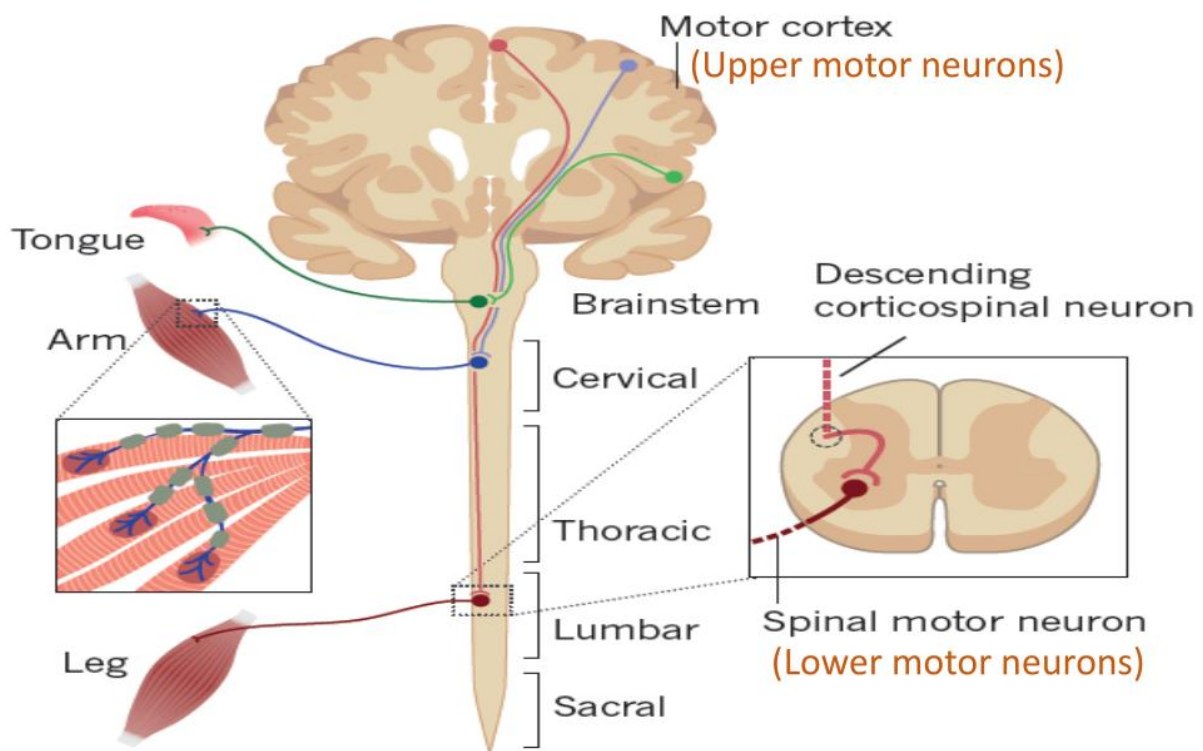


**Figure 1. Organization of motor cortex and spinal cord.** The descending corticospinal motor neurons (upper motor neurons) that project from the motor cortex make synapses in the brainstem and spinal cord, and the bulbar or spinal motor neurons (lower motor neurons) that project into skeletal muscles. Upper motor neurons from different areas of primary motor cortex control the functions of tongue (green), arm (blue), and leg (red). Adapted from Taylor et al., 2016.

Neurons have complex and extended morphologies compared to other cell types, and within the CNS, neurons can vary greatly in their properties. MNs are unique cells amongst neurons because they are large with very long axons, up to 1

m in length in an adult human. Motoneurons can be distinguished into two main categories according to their location in the CNS: upper motoneurons (UMNs) located in the cortex, and lower motoneuron (LMNs) located in the brainstem and spinal cord (Figure 1). The spinal MNs comprise both visceral “MNs” (pre-ganglionic neurons) of the thoracic and sacral regions, which control autonomic functions, and somatic MNs, which regulate the contraction of skeletal muscles and thus control movement. The diversity of MNs reflects the variety of targets they innervate, including a wide range of muscle fibre types. UMNs and LMNs differ in the location of their cell bodies, the neurotransmitters released, their targeting and symptoms resulting from their injury.

Terrestrial vertebrates possess hundreds of anatomically distinct muscle groups. Spinal MNs are located in the ventral horn of the spinal cord where they control effector muscles located in the periphery. MNs that innervate these discrete targets are organized into many diverse subtypes within the spinal cord. Diversity of spinal MNs is formed by hierarchical division and identified by the location of their cell bodies in the spinal cord, axon trajectory, and pattern of muscle innervation (Figure 2). Initially, all spinal MNs are generated from a single ventral progenitor domain. At a first level, columnar organization, MNs are spatially and molecularly allocated to columns according to the body region they innervate. These columns occupy a defined position along the rostral-caudal axis of the spinal cord. The first division among spinal MNs separates somatic MNs which innervate skeletal muscles, from the visceral “MNs”, which regulate the contraction of smooth muscle cells through a synaptic relay with the sympathetic neurons of the paravertebral ganglia. At a second level of organization, MNs within the main motor columns (e.g., LMC and MMC) are subdivided into medial and lateral divisions and project axons along different trajectories. The MMC contains MNs projecting axons towards proximal muscles whereas the LMC contains MNs projecting axons on distal (limbs) muscles. The LMC can be divided into two divisions: a medial-division projecting on ventral limb muscles and a lateral-division projecting on dorsally located limb muscles. Medial LMC axons typically innervate flexor muscles, whereas lateral LMC axons frequently innervate extensor muscles. The functional relevance of this anatomical segregation is still unclear (Dasen et al., 2009). At a third level, these two divisional subgroups have been linked to particular pools of MNs. Each pool innervate a dedicated target

muscle ([Jessell, 2000](#)). At limb levels, ~60 motor pools in the LMC control the alternation of flexor and extensor muscles about each joint, whereas at thoracic levels as few as 10 motor pools in the HMC supply muscle groups that support posture, inspiration and expiration. Such differences in MN identity and muscle fibre number associated with segmental distinctions in interneuron diversity have been proven by Jessell's lab ([Sweeney et al., 2018](#)).

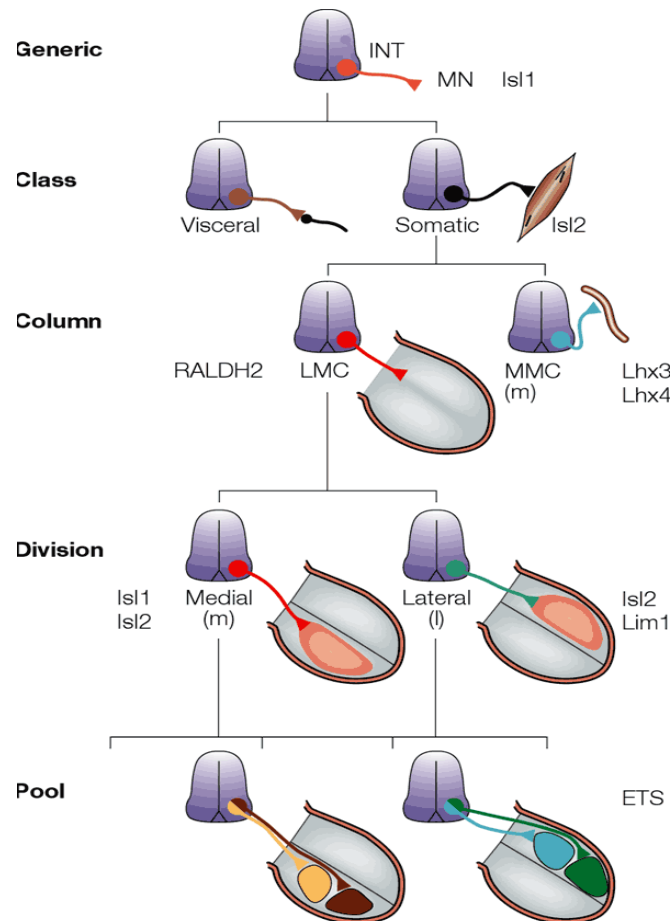


**Figure 2. A hierarchy of spinal MNs identities.** MNs subtype organization in the developing spinal cord depending on cell body position, axonal projections and gene expression. MNs are subdivided in two classes based on the innervation of skeletal muscle targets (somatic) and neuronal or glandular targets (visceral). Visceral and somatic MNs are derived from the same ventral progenitor domain at spinal levels. Somatic MNs reside in the motor column and are organized into distinct motor columns (e.g., LMC and MMC), where MNs sub-groups can be segregated into medial and lateral divisions. Medial/Lateral-division MNs are further subdivided into discrete MNs pools innervating separate muscle groups. *LMC*: lateral motor column, *MMC*: median motor column, *INT*: interneurons. Adapted from Jessell 2000.

Spinal MNs form the ultimate and irreplaceable component of the neuronal circuitry since there is no alternative route to convey the commands from the processing centers located in the CNS to the effector muscles in the periphery. Their axon extending through several meters in mammals constitute an exceptional and

unique anatomical feature. As explained before, spinal MNs are organized into distinct anatomical columns extending along the rostro-caudal axis and called motor columns (Figure 3 and 4). Previous studies have described four main columns: MMC, LMC, HMC and PGC (Prasad *et al.*, 1991; Tsuchida *et al.*, 1994; Jessell, 2000; Francius *et al.*, 2010; Alaynick *et al.*, 2011). MNs from the MMC are located in the medial region of the ventral grey matter of the spinal cord and target to the dermomyotome (Gutman *et al.*, 1993; Tsuchida *et al.*, 1994), which gives rise to the axial musculature later in development (Fetcho, 1987; Gutman *et al.*, 1993). Axial muscles are mainly involved in the maintenance of the body posture and are found all along the body axis. Consequently, MMC MNs are not segmentally restricted and are located all along the rostro-caudal axis of the spinal cord. MNs from the LMC are detected in the most lateral portion of the ventral spinal grey matter (Bueker, 1944). They connect to muscles of the appendages and therefore are present only at limb levels: LMC MNs are positioned at brachial level (C5 to T1), which innervates the forelimb, and at lumbar levels (L1–L5), which innervates the hindlimb (Hollyday *et al.*, 1977; Hollyday *et al.*, 1990).

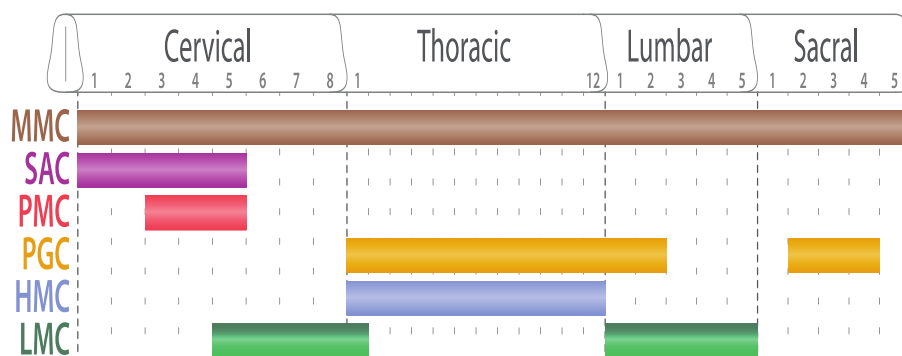


**Figure 3. Columnar organization of spinal MNs by rostro-caudal axis patterning.** Segmental distribution of spinal motor columns present along the rostro-caudal axis. *MMC*: median motor column, *SAC*: spinal accessory column, *PMC*: phrenic motor column, *PGC*: preganglionic column, *HMC*: hypaxial motor column, *LMC*: lateral motor column. Adapted from Stifani 2014.

MNs from the HMC are located in the ventro-lateral grey matter and innervate muscles derived from the ventral mesenchyme (Smith *et al.*, 1983). The ventral mesenchyme produces the body wall musculature composed of the intercostal and abdominal muscles present only at thoracic level (Prasad *et al.*, 1991). Thus, HMC MNs are only present at thoracic level (Tsuchida *et al.*, 1994; K. Sharma *et al.*, 2000). PGC “MNs” are located in the thoracic and upper lumbar spinal segments (T1–L2) where they occupy an intermedio-lateral location, and the sacral segments

(S2–S4). These cells known as spinal visceral “MNs” constitute the CNS component of the autonomic nervous system responsible for the control of smooth muscles (i.e., heart and arteries) and glands. Thoracic PGC MNs are connected to the sympathetic

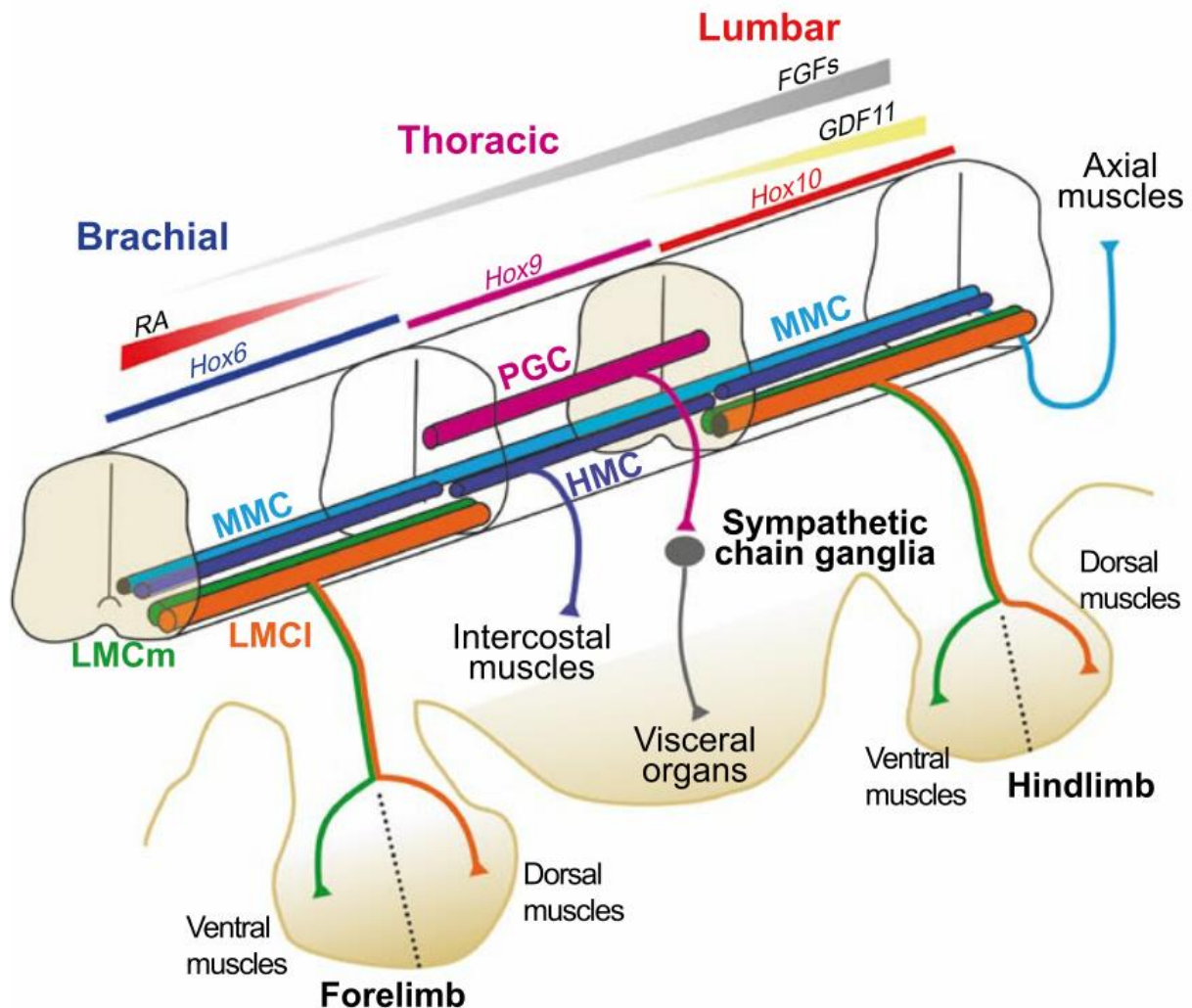


**Figure 4. Spinal MNs specification and connectivity.** Segmental identity of spinal MNs is established by specific Hox genes. Graded levels of the morphogens (FGFs, RA, and GDF11) determine spatial expression of Hox gene paralogues that shape the spinal cord into a brachial, a thoracic, and a lumbar segment. Spinal MNs congregate into four distinct motor columns organized in the rostro-caudal axis: LMC MNs innervate limb muscles, PGC MNs (Magenta) innervate sympathetic chain ganglia, MMC (formerly MMCm) MNs (light blue) innervate axial muscles and HMC (formerly MMCI) MNs (dark blue) innervate body wall muscles. LMC MNs are further subdivided into a medial (LMCm) and a lateral (LMCI) MNs pools innervating ventral and dorsal limb muscles. *FGFs*: fibroblast growth factors, *RA*: retinoic acid, *GDF11*: growth differentiation factor 11, *Hox*: homeobox. *Hox6*, *Hox9* and *Hox10* are MNs determinants at the brachial, thoracic and lumbar regions of spinal cord, respectively. Adapted from Francius et al., 2013.

chain ganglia in the proximity of the spine and belong to the sympathetic autonomic system (fight or flight), whereas sacral PGC MNs are connected to ganglia in the vicinity of the effector targets (kidney, bladder, gonads) and belong to the parasympathetic system (rest and digest). In addition, spinal MNs are also organized

into two less well-characterized motor columns: SAC and PMC. SAC MNs are located in the intermedio-lateral region of the spinal cord and expand from the end of the medulla until the 5th cervical segment (C1–C5) ([Ullah et al., 2007](#); [Jacobson et al., 2008](#)). Axons of the SAC MNs constitute the accessory nerve (XI), which supplies the sternocleidomastoid and trapezius muscles. PMC MNs are located in the cervical segments (C2–C6) at embryonic stages and become progressively confined between cervical levels (C3–C5) by birth ([Webber et al., 1976](#); [Allan et al., 1997a, 1997b](#); [A. Song et al., 2000](#)). Axonal projections from PMC MNs converge into phrenic nerves innervating the respiratory diaphragm. Each MMC, LMC, HMC and PGC column possesses a coherent gene expression profile as well as a uniform axonal projection pattern ([Stifani, 2014](#)).

Neural circuits are assembled with remarkable precision during embryonic development, and the selectivity inherent in their formation helps to define the behavioural repertoire of the mature organism. This developmental program begins with the differentiation of distinct classes of neurons from progenitor cells located at defined positions within the neural tube. The development of the embryonic spinal cord consists of four successive stages ([Figure 5](#)). At the neural plate stage: during gastrulation, the chordamesoderm induces neural “fate” in the overlying ectoderm that becomes the neural plate, a process known as neural induction. Newly formed neural cells are flanked laterally by epidermal ectoderm (ECT), while notochord cells (N) are positioned centrally in the neural plate and segmental plate mesoderm (S) is positioned laterally in the neural plate. At the neural fold stage: floor plate cells (F) are observed in the ventral midline regions and the somatic mesoderm begins to take shape. At the neural tube stage: the notochord (N) - forming from the chordamesoderm - induces ventral structure, while the dorsal lip of the neural plate fold inwards to generate the neural tube. Neural crest cells (R) differentiate at the dorsal midline, while neural crest cells (NC) cells delaminate from the dorsal neural tube. At the spinal cord stage: as development advances, the spinal cord develops a wide diversity of neuron classes arrayed across a dorso-ventral axis: MN and ventral interneurons (V) differentiate in the ventral region of the spinal cord, while dorsal root ganglion (DRG) neurons, commissural (C) neurons and association (A) neurons differentiate in the dorsal region of the spinal cord. DRG neurons differentiate from NC progenitors.

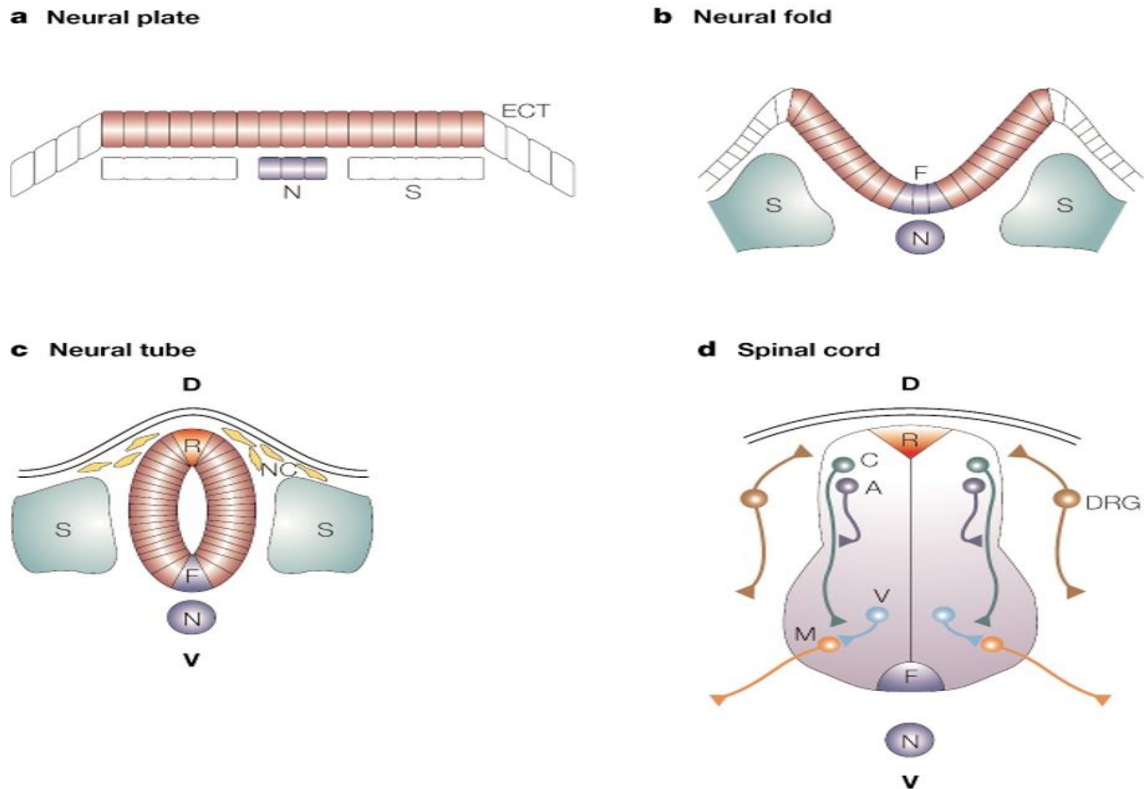


**Figure 5. The development of the embryonic spinal cord.** Abbreviations: **a**, epidermal ectoderm (ECT), notochord cells (N), segmental plate mesoderm (S). **b**, floor plate cells (F). **c**, roof plate cells (R), neural crest cells (NC). **d**, commissural (C) neurons, association (A) neurons, motor neurons (M), ventral interneurons (V), dorsal root ganglion (DRG) neurons, dorsal (D) and ventral (v) axes. Adapted from Jessell 2000.

Cellular identities are established by the inductive signalling of morphogen gradients within the ventricular zone of the ~E9.5 neural tube across two major spatial axes: 1) the dorso-ventral axis and 2) the rostro-caudal axis ([Jessell, 2000](#)). As development proceeds, neural progenitor cells within these axes differentiate into different neural categories with specific identities. Within mouse embryo, rostro-caudal patterning is established in early neural progenitors around the time of neural tube closure ([Ensini et al., 1998](#)) and in the developing spinal cord it is manifested by the differential expression of a phylogenetically conserved family of Hox transcription factors ([Figure 4](#)). Whilst the activity of rostro-caudal patterning signals is transient, it has a lasting effect on the pattern of Hox gene expression that is maintained for the rest of embryonic development ([Ensini et al., 1998](#)). Maintenance of Hox gene expression is essential for the generation of segment-specific types of spinal MNs including columnar and pool specific MN subtypes, which are necessary for proper wiring and functionality of spinal motor circuits ([Mazzoni et al., 2013](#)). Dorso-ventral patterning is regulated by two main secreted proteins or morphogens:

1) morphogen Sonic hedgehog (shh) secreted from the floor plate (FP) and the notochord (NC) modulates ventral patterning of the neural tube; 2) Bone morphogenetic proteins (Bmps) secreted from roof plate (R) and surface ectoderm modulate dorsal patterning of the neural tube. Within an idealized segment of spinal cord, these morphogen gradients establish 12 progenitor domains that grossly give rise to 7 dorsal interneuron progenitor divisions (pd1–6 and pdIL) to generate dorsal interneuron classes (dl1-dl6); 4 ventral interneuron progenitor divisions (p0–3) and 1 MN progenitor domain (pMN) to generate ventral interneuron classes (V0, V1, V2, V3) and MNs, respectively. All MNs are initially derived from ventral progenitor cells or domains (e.g., pMN) that are specified to become Olig2+ motor neuron progenitors *via* shh and retinoic acid (RA) signals. Thus, these ventral progenitor cells give rise to one cell type early (e.g., MNs) followed by another cell type later (e.g., oligodendrocytes) (Figure 6). Typically, the transcription factors in adjacent progenitor domains repress expression of factors in neighbouring domains, preventing cells from developing with hybrid identities. Transforming growth factor  $\beta$  (TGF- $\beta$ ) signalling is necessary for proper neural development, differentiation and function throughout life. The large number of elements of the nervous system are regulated by TGF- $\beta$  signals produced by sequential waves of activation, inhibition, and reactivation of TGF- $\beta$  family members (Meyers *et al.*, 2017). TGF $\beta$  family proteins from the overlying ectoderm (e.g., *Bmp4*) and roof plate (e.g., *Gdnf7*) produce dorsalizing signals. The dorsal-most progenitor domains, pd1–pd3, depend on TGF $\beta$ , whereas pd4–pd6 and pdIL are independent of TGF $\beta$ . The somite produces RA that controls subtype and dorsoventral identity through *Pax6*. RA signalling is required at several steps during the development of the spinal cord, from the specification of generic properties to the final acquisition of neuronal subtype identities.

As cells mature within their respective progenitor zones and begin to exit the cell cycle, an abrupt transition occurs in the transcriptional profile of cells. The postmitotic cells from some progenitor domains (e.g., p2) become further diversified through intercellular signalling interactions (e.g., Notch-Delta), resulting in the generation of excitatory V2a and inhibitory V2b neurons from common ancestral progenitor cells. The Delta/Notch pathway governs the specification, proliferation, and differentiation of neuronal precursors in embryonic and adult tissues. Notch

receptors and Delta ligands are transmembrane proteins that elicit signalling between adjacent cells. Delta/Notch interactions then trigger a metalloprotease-mediated cleavage in the Notch extracellular domain, followed by a  $\gamma$ -Secretase-dependent intramembrane proteolysis that releases the Notch IntraCellular Domain (NICD) into the cytoplasm. NICD enters the nucleus to interact with the DNA-binding CSL transcription factor and promote target gene transcription (Figure 6).

As neuron development progresses, the neurotransmitter properties of the cells emerge and express phenotypic markers, such as neurotransmitter biosynthetic enzymes (e.g., choline acetyltransferase (ChAT) or glutamic acid decarboxylase (GAD)) and vesicular transport proteins (e.g., vGluT2). During the formation of the CNS, cholinergic signalling, the binding of neurotransmitter acetylcholine (ACh) to its receptors, is essential for necessary physiological processes, including spontaneous neuronal activity, axon pathfinding and synaptogenesis (Rima et al., 2020). Glutamate decarboxylase (GAD) is the biosynthetic enzyme for the neurotransmitter  $\gamma$ -aminobutyric acid (GABA). GABA signalling plays several roles in neuronal development by modulating immature progenitor proliferation, neuron migration, survival and differentiation, proper morphological development of neurons, as well as potentially primes the earliest neuronal networks (Wu et al., 2015). Many progenitor domains tend to produce neurons with similar initial axonal growth trajectories, whereas other domains (e.g., pd1, p0, and p1) produce “V” interneuron subtypes with diverse axonal projection. Although each class of “V” cells is highly heterogeneous, the best example of the diversification of a single neuronal class is MNs (Figure 6).

Neuronal diversification produced in the embryonic nervous system during neurogenesis stems from cellular gene expression. The initial subdivision of MNs is driven by the action of the Hox factors according to the segmental level they occupy along the rostral-caudal axis. Afterwards, consolidation of their MN fate, newly-born MNs undergo a diversification process that results in the production of cell types displaying distinct molecular identities, migration pathways, axonal trajectories, and target connectivity located in the different motor columns and pools. However, defective consolidation of MN identity results in a partial or complete transformation of the MN population into dorsally adjacent V2a interneurons. This is likely due to the fact that MNs and V2a interneurons share some of their developmental determinants,

including *Nkx6* and *Lhx3* factors ([Francius & Clotman, 2013](#)). These molecular mechanisms are involved in the consolidation of MN identity: early MN markers include *Hb9*, *Isl1*, and *Hnf-6*; V2a interneuron markers include *Chx10*. Inactivation of *Hb9* results in defective consolidation of MN identity and partial conversion into V2a interneurons. MNs are subdivided by their cell body positions within motor columns. Each motor column consists of multiple MNs pools innervating individual muscles. Generic postmitotic MNs become subdivided into the medial and hypaxial motor columns (MMC and HMC), which innervate the back (epaxial) and trunk (hypaxial) musculature, respectively ([Figure 4](#)). MNs from both columns express *Isl1* and *Isl2*, although the ratio of expression varies, with greater *Isl1* expression in the HMC than MMC at E11.5 and greater *Isl2* in the MMC than HMC by E13.5 in mouse ([Tsuchida et al., 1994](#); [Thaler et al., 2004](#)). The MMC innervates dorsal or epaxial musculature, while HMC innervates ventral or hypaxial musculature ([Figure 4](#)). Initially, all MN progenitors express the LIM homeodomain transcription factor, *Lhx3*. *Lhx3* expression is maintained in the MMC, while its expression is downregulated in the HMC and LMC ([Tsuchida et al., 1994](#)). MN- (*Hb9* promoter) dependent expression of *Lhx3* results in conversion of LMC MNs to a MMC identity ([K. Sharma et al., 2000](#)). At limb levels, the medial and lateral portions of the lateral motor column (LMCm and LMCl) innervate the ventral and dorsal portions of the limb, respectively. MNs pools innervating the same muscle can be defined by unique combinations of transcription factors (e.g., *Nkx6* and *Ets* classes, which are a group of evolutionarily related, DNA-binding transcriptional factors) ([Figure 6](#)).

Currently, over 20 interneuron types have defined in the spinal cord. Historically, two broad groups have been defined: the “V” interneurons with progenitors that are found in the ventral cord and are grossly associated with motor function, and a dorsal interneuron, dl class, associated predominantly with sensory processing. Furthermore, each cardinal “V” class of ventral interneurons can be subdivided into several subsets according to further combinatorial expression of transcription factors ([Francius, Harris, et al., 2013](#)). As we can see on [Figure 6](#), V and dl interneurons are either excitatory (glutamatergic) or inhibitory (glycinergic and/or GABAergic).

## SnapShot: Spinal Cord Development

William A. Alaynick<sup>1</sup>, Thomas M. Jessell<sup>2</sup>, and Samuel L. Pfaff<sup>1</sup>

<sup>1</sup> HHMI, The Salk Institute for Biological Studies, La Jolla, CA 92037, USA; <sup>2</sup> HHMI, Columbia University, New York, NY 10032, USA

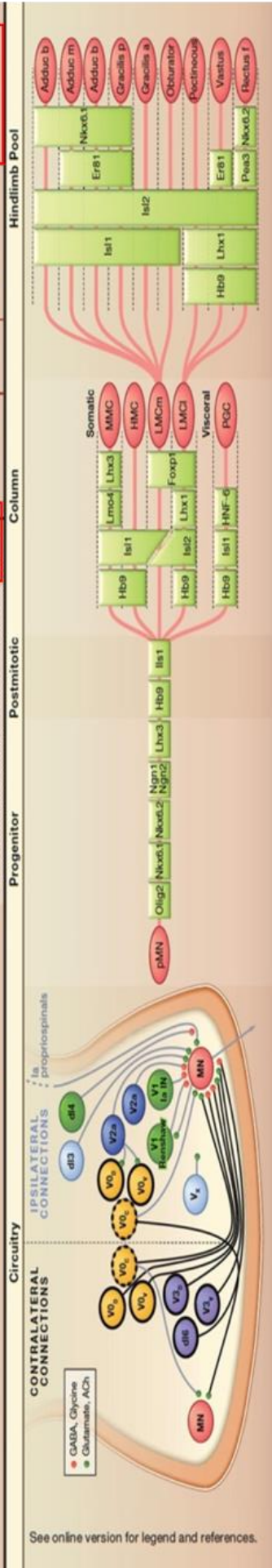
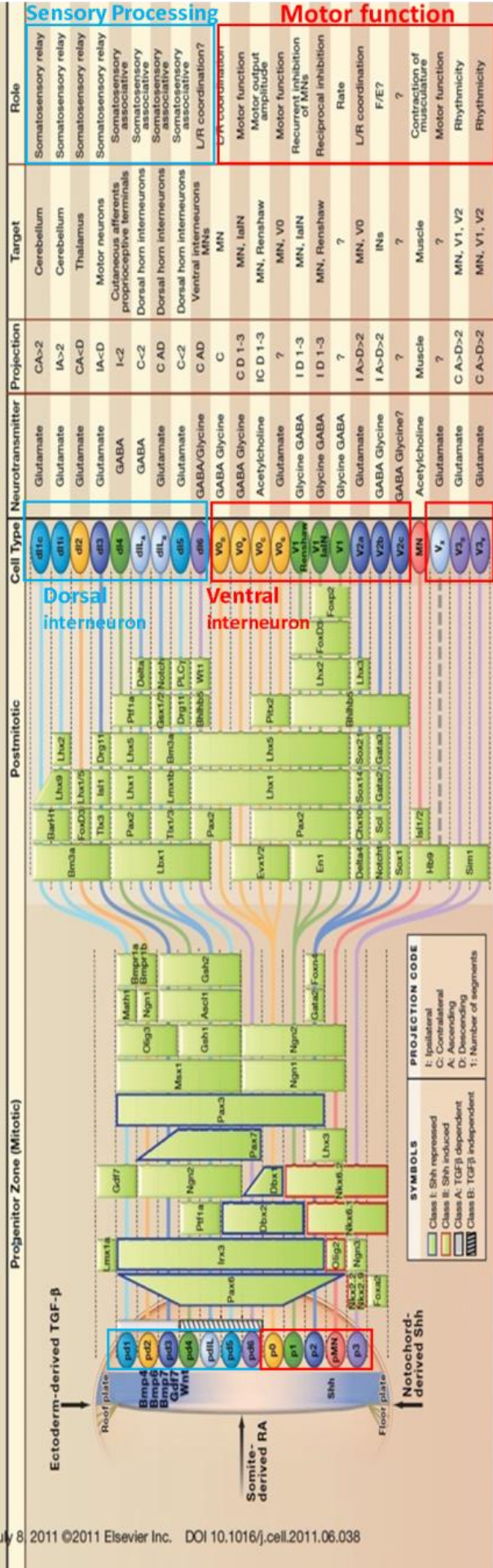


**Figure 6. Neuronal specification during spinal cord development along the dorso-ventral axis.** **Top panels** | In an idealized developing mouse spinal cord, the sequential genetic steps produce the patterning and specification of embryonic spinal cord progenitors and the diversity of their neuronal progeny including MNs, interneurons and oligodendrocytes. The progression from neural progenitor cells to postmitotic neurons spanning embryonic day 9.5 (E9.5) to E18.5 is shown from left to right, although some events are not strictly linear. At E9.5, morphogen gradients of Shh (ventrally), and Bmps and Gdf7 (dorsally) provide instructive positional signals to dividing progenitors in the ventricular zone. This leads to the restricted activation of patterning factors in distinct dorso-ventral domains, including Nkx6.1 (ventral), Pax6 (intermediate), and Pax3 and Pax7 (dorsal). At E11, eleven early classes of postmitotic neuron are present in the embryonic spinal cord: dl1-dl5 neurons that are derived from dorsal progenitors primarily contribute to sensory spinal pathways, whereas dl6, MN and V0–V3 neurons arising from intermediate/ventral progenitors are involved in the locomotor circuitry. A number of postmitotic transcription factors are indicated for the identification of each of generic neuronal population, e.g., Chx10 is a marker of V2a neurons and Isl1/2 is a marker of MNs. **Bottom panels** | Spinal premotor interneurons are organized in the contralateral medial ventral horn, and in the ipsilateral spinal cord in the deep dorsal horn, intermediate region, and ventral horn. The functions of the cardinal cell types in the spinal cord, particularly those that relate to locomotor behaviours, have been partially identified. *The differential expression patterns of transcription factor Hox (i.e., homedomain) paralogues along the rostro-caudal axis further subdivide MNs, but for clarity, these patterns are not reflected in this SnapShot.* Shh: Sonic hedgehog, Bmps: Bone morphogenetic proteins, Gdf7: Growth differentiation factor 7. Adapted from Alaynick, et al., 2011.

The spinal interneurons comprise a **central pattern-generating** circuitry (see below) that is capable of producing rhythmic left-right and flexor-extensor alternation in isolated spinal cord preparations, called fictive locomotion. Molecular genetic studies have defined roles for several classes of interneurons found in the ventral cord. Mutant mice lacking contralaterally projecting inhibitory *Dbx1*<sup>+</sup> V0 class interneurons display a disorganized left-right alternation. Talpalar and colleagues investigated the behavioural consequences of ablating either the entire V0 population (representing a major class of commissural neurons) or only the ventral (V0<sub>v</sub>) or the dorsal (V0<sub>D</sub>) subpopulation. Their results showed that mice lacking spinal V0 class interneurons lose the ability to alternate limbs and display rabbit-like hopping locomotor patterns, regardless of the speed of locomotion ([Talpalar et al., 2013](#)). Conversely, elimination of dorsal inhibitory V0<sub>D</sub> interneurons triggered hopping at slow locomotor frequencies, but the alternation remained conserved at fast locomotion while the phenotype was reversed during selective ablation of ventral glutamatergic V0<sub>v</sub> interneurons ([Talpalar et al., 2013](#); [Bellardita et al., 2015](#); [O. Kiehn, 2016](#)). These results demonstrate that the V0 population, through commissural projections, plays a critical role in setting the basic pattern of terrestrial locomotion, while also regulating the rhythm of left-right alternation. A genetic approach selectively eliminating Pax6<sup>+</sup> and En1<sup>+</sup> V1 class interneurons from the spinal cord ([Gosgnach et al., 2006](#)), showed that the overall pattern of left-right

alternation and rostro-caudal propagation of activity was normal when fictive locomotion was pharmacologically induced, whereas MN bursting episodes revealed longer cycle periods and durations (frequency). This resulted in a markedly slower locomotor activity rhythm in Pax6<sup>-/-</sup> and En1-DTA mice preparations compared to wild type preparations. These results demonstrate that the V1 population as a whole regulates the step-cycle period of fictive locomotion and is necessary for 'fast' locomotor outputs in mice. Given that, V1 class interneurons are more homogeneous compared to V0 in the sense that they are all inhibitory and characterized by the co-expression of glycine and GABA ([Wenner et al., 2000](#); [Alvarez et al., 2005](#)). These findings also suggest the important role for inhibition in regulating the frequency of the locomotor CPG rhythm. Ablation of ipsilateral projection of excitatory Chx10<sup>+</sup> V2a cells using diphtheria toxin also disturbs right-left alternation and, notably, at higher speeds, animals transition to a left-right synchronous gallop that is not seen in wild-type mice. Genetic ablation of Chx10<sup>+</sup> V2a in mice is also associated with defects in left-right coordination of locomotion activity and perturbs gait transitions ([Crone et al., 2008](#); [Zhong et al., 2011](#)). This effect is possibly mediated by a lack of excitatory drive onto contralateral glutamatergic interneurons as suggested by the pattern of V2a synaptic connectivity in mice, in turn weakening left-right alteration ([Crone et al., 2008](#)). These results demonstrate that a group of ipsilaterally projecting excitatory interneurons, Chx10<sup>+</sup> V2a interneurons, has an important role in driving the excitatory commissural interneurons (a subset of CIN) responsible for left-right alternation. Moreover, in neonatal (P0-P4) mice, spinal V2a interneurons are dispensable for left-right coordination at low locomotor frequencies, but their function is essential for maintaining left-right coordination at high frequencies, i.e., frequency-dependent recruitment of V2a interneurons during fictive locomotion ([Zhong et al., 2011](#)). Half of the V2a interneurons receive rhythmic locomotor synaptic drive, which increases with cycle frequency, recruiting more of the neurons to fire at higher frequencies, while the other V2a interneurons do not receive locomotion-related synaptic drive and are not recruited into the locomotor network at any frequency. This gradual recruitment of V2a interneurons underlies the maintenance of left-right alternation in normal mice during acceleration from low speeds, in which V2a interneurons do not have a major role, to higher speeds, in which maintenance of left-right alternation depends on the increasing recruitment of rhythmic V2a interneurons. The increased role of V2a interneurons at higher locomotor frequencies arises from increased synaptic drive to

recruit subthreshold oscillating V2a neurons, and not from recruitment of a second set of silent V2a interneurons ([Zhong et al., 2011](#)). Inactivation of contralaterally projecting excitatory *Sim1*<sup>+</sup> V3 interneuron class disrupts the regularity of the rhythm. The ipsilaterally projecting glutamatergic Hb9<sup>+</sup> Vx class is rhythmically active during locomotion ([Hinckley et al., 2005](#)). Inactivation of the *Pitx2*<sup>+</sup> V0<sub>C</sub> class disrupts aquatic locomotion due to altered integration of sensory feedback. The Ptf1a<sup>+</sup> dl4 class forms inhibitory presynaptic contacts on glutamatergic proprioceptive sensory neurons in the ventral spinal cord. The dl6 and dl3 interneuron classes make direct connections onto MNs, however, their roles have not been determined ([Figure 6](#)). As a whole, we can see that many subtypes of spinal interneurons are involved in the genesis of an appropriate locomotor activity.

### 1.1.1 LOCOMOTOR SYSTEM AND SPINAL LOCOMOTOR CPG

MNs acquire molecular properties during their differentiation throughout embryonic development as a result of dynamic interplay between spatial and temporal expression of families of transcription factors and diffusible morphogens. In the terminal step of differentiation, the combinatorial activity of terminal effector genes defines the features of individual postmitotic MNs. This battery of terminal identity genes governs the synthesis of neurotransmitters and expression of neurotransmitter receptors, ion channels, and axon guidance and synaptic adhesion molecules ([Deneris et al., 2014](#); [Li et al., 2020](#)). At these early stages of development, the first wirings of neuronal circuits proceed with axon outgrowth toward appropriate targets and by the complex interaction of both intrinsic genetic instructions and environmental cues. Spinal MNs are organized into motor columns along the rostro-caudal and ventro-dorsal axes that project to a single muscle target in the periphery. Long descending premotor projection neurons from the spinal cord and supraspinal centres, as well as proprioceptive afferents, begin to establish the spinal motor circuitry during embryonic development ([Glover, 2000](#); [Arber, 2017](#)). The extensive dendritic arborization of MNs that integrates synaptic inputs critical for circuit formation and plasticity ([Dong et al., 2015](#)). Also, the diversity of local interneuron subtypes that direct early motor output enable further adaptive motor behaviour ([Berg et al., 2018](#)).

Animals rely on locomotion or movements to explore their environment, to feed, to escape from predators, to dominate habitats and to find partners for

reproduction. These locomotor behaviours are fundamental motor acts that give animals the ability to exploit their surroundings to seek the essential resources, to rapidly change their gait to adapt their locomotion to various terrains and avoid hazards, and also give humans the ability to move. To perform these locomotor movements, the central nervous system generates elaborate goal-directed locomotor sequences translating intent into action through the transformation of the activity of neuronal circuits into the orderly contraction of muscles (*McNeill Alexander, 2002; Bellardita et al., 2015; O. Kiehn, 2016*). Work over many years has demonstrated that the motor control system exhibits a multitude of interleaved layers of organization in a modular manner (*Goulding, 2009*). Topography of neural circuits is clearly a major organizational strategy of the CNS. Thereby, the motor network is presented as topographic spatial organization within the spinal MNs, motor cortex, spinal sensory system, and spinal interneurons function together with the thalamus, basal ganglia, brainstem, cerebellum, and other brain regions to initiate and coordinate movements (*Figure 7*).

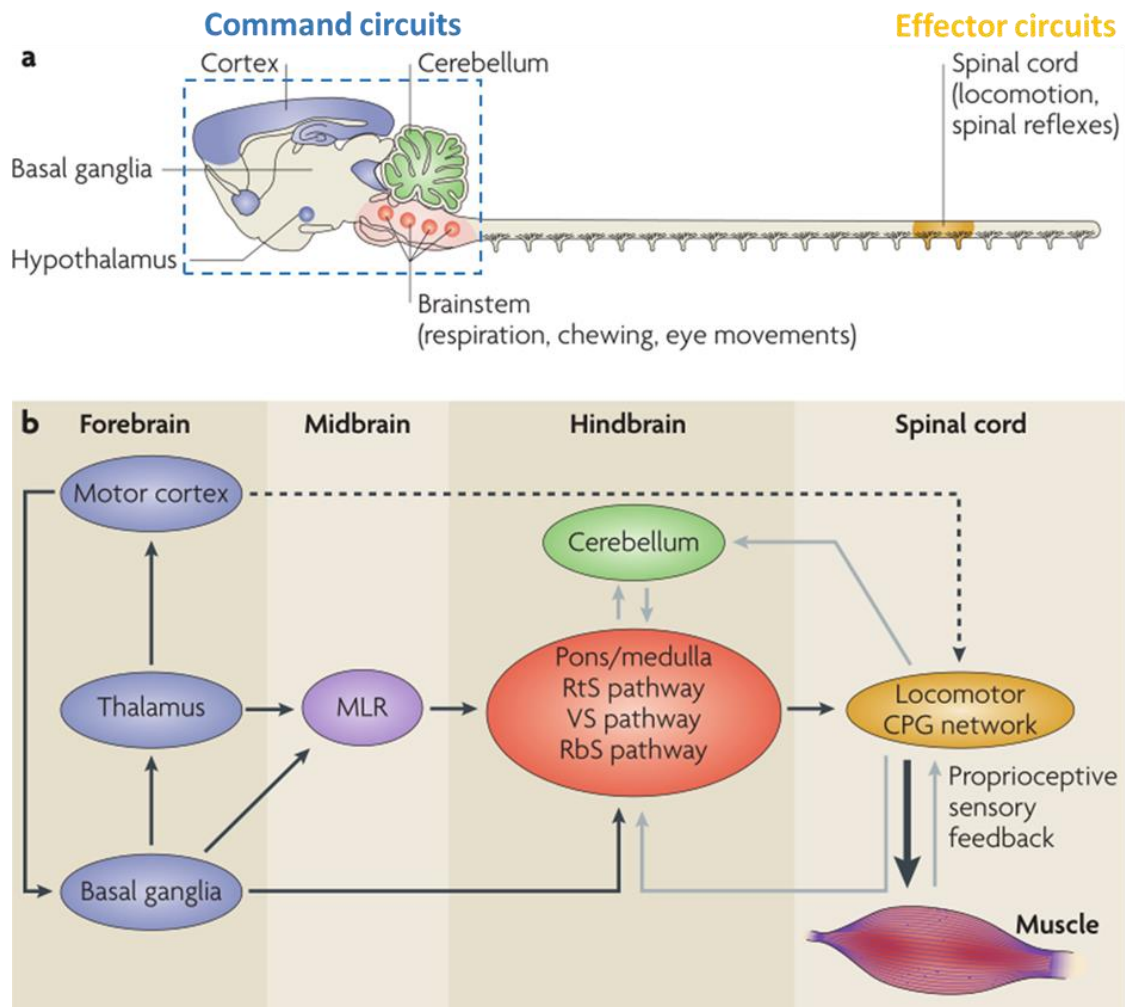


**Figure 7. Organization of the locomotor system in vertebrates.** (a) Schematic of the rodent central nervous system, showing the neural structures that configure the motor pathways that control simple behaviours such as respiration, chewing, and locomotion. (b) Motor pathways in aquatic and terrestrial vertebrates share a similar neuroanatomical structure. Local control of muscle movements is regulated by pools of MNs in the spinal cord that are part of a decentralized locomotor CPG network. Spinal motor centers are modulated by proprioceptive sensory feedback via sensory afferents. Descending reticulospinal (RtS), vestibulospinal (VS) and rubrospinal (RbS) pathways control the locomotor network in the spinal cord, although the RtS pathway is the primary pathway for initiating locomotion. The RtS pathway can be activated by the mesencephalic locomotor region (MLR), which has inputs from the basal ganglia and thalamus. The cerebellum coordinates motor behaviors by mediating sensory and internal feedback and optimizing the motor pattern to the task at hand. It also coordinates spinal motor actions by the supraspinal motor pathways. Connections from the motor cortex refine and initiate motor actions. The black lines indicate direct command pathways, the grey lines indicate feedback pathways. Adapted from Goulding 2009.

In vertebrates, the best example of modular organization of motor circuits is the central pattern generators (CPGs) in the spinal cord, which generate neural oscillations and control rhythmic movements, providing an experimentally tractable model system for investigating how moderately complex ensembles of neurons generate specific motor behaviours. These CPGs are involved in many important

functions, including different forms of locomotion, such as swimming, walking, running, and flying. The planning and initiation of locomotion take place in supraspinal areas, including the cortex, the basal ganglia, the midbrain and the hindbrain, but the precise timings and patterns of locomotor movements in vertebrates are generated by activity of locomotor CPG network in neuron assemblies that are located in the spinal cord itself (for review, see(O. [Kiehn, 2016](#))).

The first schematic of the locomotor CPG, called the “half-center” model, is proposed by Graham Brown (1914) and elaborated on by Lundberg (1981) ([McCrea et al., 2008](#); [Stuart et al., 2008](#)). This model includes two (flexor and extensor) half-centers reciprocally inhibiting each other. The mutual inhibitory interactions between the half-centers are mediated by inhibitory interneurons, which ensure that only one half-center can be active at a time. Due to some fatigue or adaptation mechanism, the activity of the active half-center gradually decreases, leading to the activation of the antagonistic half-center. The antagonistic half-center then inhibits the active half-center, thus switching the locomotor phase. It is suggested that the flexor and extensor half-centers directly project to and activate the flexor and extensor MNs, respectively. At a very general level of organization, locomotor CPG networks in all vertebrates need to secure two basic functions: rhythm-generation and pattern-generation. The rhythm is the clock. For example, rhythmic spinal circuits control locomotor gait, thalamic oscillations detect attentional state, cerebellar rhythms are important for motor coordination, and circadian rhythms entrain our biological clocks to a 24-hour cycle. In the spinal cord, the pattern-generation involves the rhythmic activation of MNs and left–right alternation. The pattern generators are neuronal ensembles capable of generating the basic spatiotemporal patterns underlying "automatic" movements (e.g., locomotion, respiration, swallowing and defence reactions), in the absence of peripheral feedback.

### **Dual inhibitory CIN pathways controlling left–right alteration**

We have seen above the role of different commissural interneurons in the pattern-generation. A series of lesion experiments have demonstrated that walking mammalian locomotor CPG network or core CPG components are located in the ventral half of the caudal spinal cord ([Kjaerulff et al., 1996](#)) (for review, see ([Goulding, 2009](#))). The spinal locomotor CPG comprises a distributed network of

premotor interneurons and MNs that may generate basic movement patterns by mediating the synergistic drive to multiple muscles, such as limb and body muscles (O. Kiehn, 2016; Takei et al., 2017). The core of the network consists of groups of excitatory and inhibitory premotor interneurons that serve designated roles in the network operation. The central organizing feature of the motor circuitry is the grouping of MNs into discrete operational units, motor pools, each of which innervates a single muscle. These premotor interneurons receive activating inputs from the brain and are able to produce the rhythms and patterns of locomotion that are conveyed to MNs and then to the axial and limb muscles (Figure 8). Anatomical tracing and electrophysiological studies in mice reveal that the neural substrate for driving left-right coordination consists of at least two components: commissural interneurons (CINs) and a class of ipsilateral interneurons (Crone et al., 2008). These neurons have converged towards a common network structure controlling left-right coordination at the segmental level. CINs must coordinate activity on the two sides of the body through a complex segmental CIN system in newborn rodents with: a dual inhibitory CIN pathway and a single excitatory CIN pathway (Crone et al., 2008; Kiehn, 2011). The dual inhibitory pathway is composed of two distinct projections: a direct inhibitory CIN input to contralateral MNs, and an indirect excitatory CIN projection that provides input to contralateral inhibitory interneurons, including Renshaw cells (RC) and other inhibitory interneurons (e.g., Ia interneurons) (“alteration” in solid-line path, Figure 8). These pathways appear well-suited to the control of left-right alternation during locomotion since they are likely to connect to rhythm-generating neurons on the contralateral side of the cord (“alteration” in dash-line path, Figure 8). The single excitatory pathway is composed of a set of glutamatergic CINs that directly excite contralateral MNs (“Synchrony” in solid-line path, Figure 8), with possible additional connections to contralateral rhythm-generating neurons (“Synchrony” in dash-line path, Figure 8). This pathway is therefore positioned to promote synchrony in left-right motor bursting. Accordingly, these two types of CIN pathways produced the different locomotion patterns: the dual inhibitory pathway might be active during a pattern of alternation activity (walking), whereas the direct excitatory pathway might be active during a pattern of synchronized movements (hopping). The general organization of these pathways seems to be similar in the adult cat spinal cord (Jankowska, 2008).

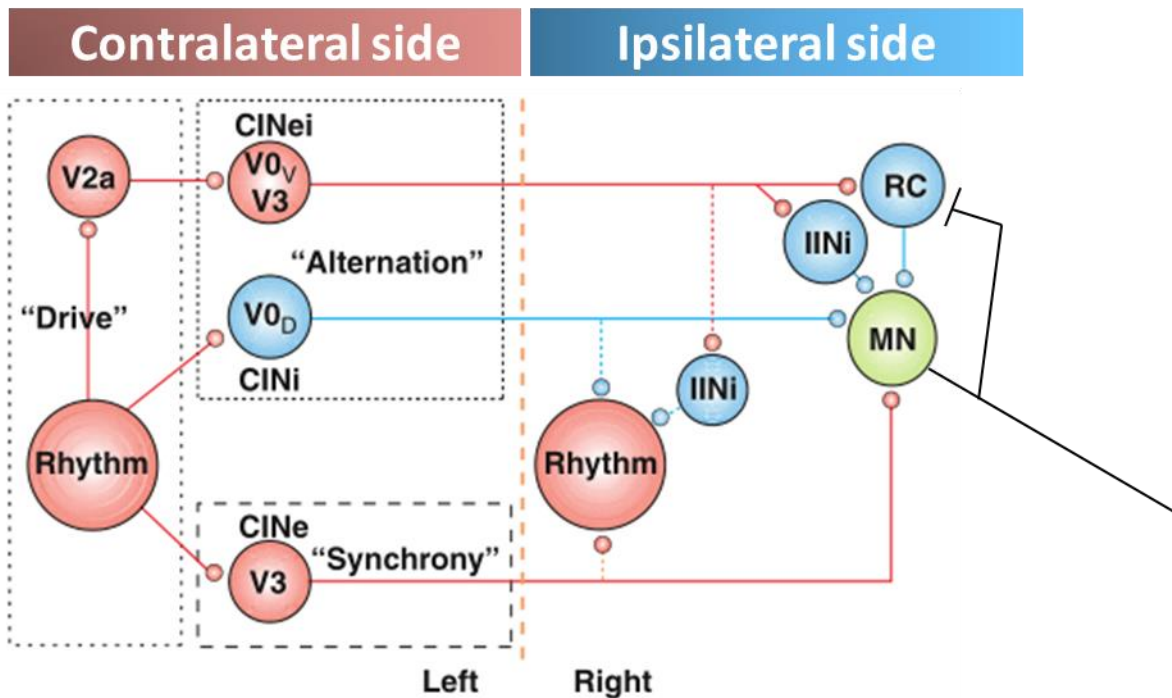


**Figure 8. Organization of Mouse Spinal Locomotor CPG Network.** Commissural interneurons (CINs) are the core of the assembly of the locomotor CPG network in rodents that ensures left-right alternation in motor activity. Two CIN populations are involved in left-right “alteration”: a set of inhibitory CINs (CINi) inhibit directly on contralateral MN, whereas a set of excitatory CINs (CINE) inhibit contralateral MN indirectly by acting on GABAergic/glycinergic inhibitory INs including ipsilaterally projecting inhibitory interneuron (IINi) and Renshaw cells (RC). Left-right “synchrony” is obtained via a single CINE acting directly on MN, or driven directly from the rhythm-generating core on the ipsilateral side. To obtain left-right coordination during locomotion, these crossed connections should also connect to the rhythm-generating core (dotted lines) on the other side of the cord and/or corresponding commissural interneurons. The “Drive” of left–right coordinating pathways is mediated through multiple ipsilaterally projecting glutamatergic neurons including the V2a population, and a group of rhythm-generating neurons. *In this diagram, a single neuron represents a group of neurons.* Adapted from Kiehn 2011 and Crone et al., 2008.

Based on neuronal elimination experiments and genetic tracing studies, at least four classes of interneurons (INs), including V0, V2, V3 and V1, can be defined in the locomotor CPG region in the embryonic and early postnatal spinal cord (Figure 8). Almost all the V0-INs and most of the V3-INs are commissural. V0 interneurons were the first of the parent genetically defined classes to be characterized, and have their functional role in stepping determined (Lanuza et al., 2004; Gosgnach, 2022). V0-CINs are composed of two subclasses: one-third of V0-CINs are glutamatergic and Evx1-positive (V0<sub>V</sub>), while the remaining two-thirds are inhibitory and Evx1-negative (V0<sub>D</sub>). V3-CINs are Sim1-positive and all excitatory. Upon genetic loss of function experiments, in normal mice where: 1) V0-CINs are ablated, left–right alternation is upset result in a hopping rabbit-like gait, which indicate that the V0-

CINs may be important for left–right alternation through the action of  $V0_V$  via the excitatory indirect pathway and  $V0_D$  via the inhibitory direct pathway. Therefore, lacking these  $V0$ -CINs pathways, the default option for rhythmic outputs is hopping gait. 2) The  $V3$  population is excitatory and was initially shown to extend contralaterally projecting axons at early embryonic time points ([Y. Zhang et al., 2008](#); [Gosgnach, 2022](#)).  $V3$ -CINs are removed, spinal locomotor activity showed increased variability in the locomotor burst amplitude and period, and imbalance between the left–right activity, which suggest that the  $V3$ -CINs play a minor role in left–right alternation, although the known projections to inhibitory INs via indirect inhibitory pathway mediated by subset of  $V3$ -CINs ( $V3$ -CINei).  $V3$ -CINs also project directly to contralateral MNs indicating that  $V3$ -CINs ( $V3$ -CINe) may be active under conditions of left–right synchrony via direct excitatory pathway ([Kiehn, 2011](#)). These findings suggested that  $V3$ -CINs population expressing the same gene can be functionally divided into two distinct sub-populations:  $V3$ -CINei (involved in “left–right alternation” circuits) and  $V3$ -CINe (involved in “left–right synchrony” circuits). This also implies that the direct pathway may play a more important role than the indirect pathway in terms of functional effects. Moreover,  $V3$ -CINs class enable to receive rhythmic excitation during fictive locomotion. The  $V2$  interneuronal population can be divided up into two distinct subpopulations, excitatory  $V2a$  neurons which express the transcription factor *Chx10* ([Al-Mosawie et al., 2007](#); [Lundfald et al., 2007](#)), and inhibitory  $V2b$  cells which express *Gata3* ([Lundfald et al., 2007](#); [J. Zhang et al., 2014](#); [Britz et al., 2015](#)).  $V2a$  is a subclass of  $V2$ -INs, which are ipsilateral, *Chx10*-positive and glutamatergic. In ablation of  $V2a$ -INs using *Chx10*-DTA mice, the locomotor frequency and motor burst amplitude of drug-induced locomotor-like activity becomes more variable than it is with the  $V2a$ -INs present. The left–right alternation is disrupted especially at medium to high locomotor frequencies with no disruption of the left–right synchronous activity.  $V2a$ -INs therefore provide significant drive to one pathway of the dual inhibitory system without being the main source of the rhythm-generation, indicating that  $V2a$ -INs are critical for the initiation of left–right alternation circuits and are recruited in a frequency-dependent manner (i.e., at medium to high locomotor frequencies).  $V1$ -INs express the transcription factor *En1* and, as a whole, more than 90% of this population has been shown to be inhibitory ([Sapir et al., 2004](#); [Gosgnach, 2022](#)).  $V1$ -INs are ipsilateral, *Pax6* and *En1*-positive, and GABAergic and glycinergic. This set constitutes over one third of all inhibitory

interneurons in the ventral spinal cord, and includes all Renshaw and many ipsilaterally projecting inhibitory interneurons ([Sapir et al., 2004](#); [J. Zhang et al., 2014](#)). Genetic ablation of V1-INs slows the speed of rhythmic locomotor output and perturbs flexor-extensor alternation ([Gosgnach et al., 2006](#); [J. Zhang et al., 2014](#)).

### **Ipsilateral inhibitory circuits underlying flexor–extensor alternation**

The spinal locomotor CPG network generating flexor–extensor alternation is organized in flexor and extensor modules which are reciprocally connected through ipsilateral inhibitory interneurons ([Kiehn, 2011](#)). During locomotion, both flexor and extensor MNs receive alternating inhibitory and excitatory drives to secure alternation around individual joints of limbs, inhibitory interneurons are therefore important network elements. The ipsilaterally projecting inhibitory interneuron (IINi) includes V1 population and possibly the V2b population, which are connected in a reciprocal pattern between flexor and extensor rhythm-generating modules. Among these two populations of INs, V1 interneurons (V1-INs) are a major inhibitory population that control motor output. V1 population are highly homogeneous in neurotransmitter that they are all inhibitory and characterized by the expression of GABA and glycine. They consist of three main subclasses: Renshaw Cells (RCs), reciprocal Ia inhibitory interneurons (rIa-IN), and non-reciprocal group I interneurons, all of which project monosynaptically to MNs. Through the formation of inhibitory microcircuits with highly selective synaptic input and output connectivity, inhibitory interneurons mediate feedback (recurrent), reciprocal, and feedforward inhibition. The connectivity patterns of these inhibitory premotor neurons were identified first in cats and then shown to be similar in the neonatal rodent spinal cord (for review, see ([Kiehn, 2011](#))). However, recent experiments in ~P21 mice spinal cord have shown that V1-INs are highly diverse subgroups based on the expression of 19 transcription factors, exhibit distinct physiological signatures, and settle in highly localized positions along both the mediolateral and dorsoventral axes of the spinal cord, a feature that constrains patterns of sensory and motor input ([Bikoff et al., 2016](#)). The study by Bikoff et al. have provided insight into: 1) the position of interneurons is a determinant of microcircuit organization; 2) the diversity of V1-INs based on the position (e.g., dorsally-positioned V1Sp8 and ventrally-positioned V1R subsets) exhibited that different inhibitory microcircuits exist for motor pools controlling hip, ankle, and foot muscles ([Figure 9](#)). From an evolutionary perspective, the diversity displayed by

mammalian V1 neuronal circuits may be an adaptation to the complex control features of multi-jointed limbs.

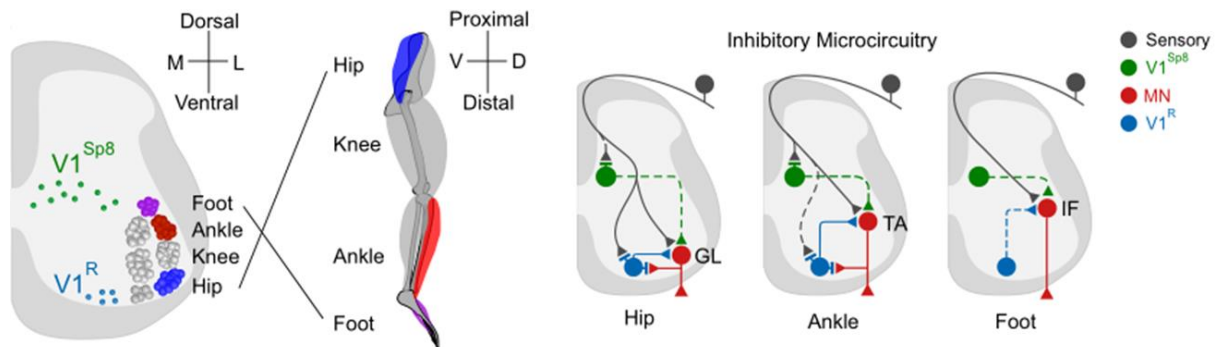


**Figure 9. Wiring diagram of inhibitory interneuron microcircuits within the Spinal Locomotor CPG Network in ~P21 mice.** Ipsilateral interneurons are mainly from two groups: sensory afferent neurons and V1 groups including  $Sp8^+$  expressing V1 spinal neurons ( $V1^{Sp8}$ ) and V1 Renshaw cells ( $V1^R$ ), which send direct monosynaptic inputs to three hindlimb pools of MNs on hip, ankle and foot. Gluteus (GL) MNs innervate hip extensor muscles and occupy an extreme ventral position in the LMC. Tibialis anterior (TA) and intrinsic foot (IF) MNs innervate ankle flexor and foot plantar-flexor muscles, respectively, and occupy a similar dorsal position within the LMC.  $V1^R$  interneurons do not receive collateral input from IF MNs, but can receive collateral input from Hip and Ankle MNs. However,  $V1^{Sp8}$  interneurons receive no motor axon collateral contacts, suggesting that the collateral branches of MNs are restricted to  $V1^R$  interneurons, which mediate a feedback or recurrent inhibition. The solid and dotted lines represent prevalent and sparse synaptic connectivity. From Bikoff et al., 2016.

### 1.1.2 MNs SUBTYPES

The spinal cord is a highly organized final executive center for body movement and MNs are the final stage of neural processing for the execution of locomotor behaviours. As all motor-related circuitries with their particular organizational schemes must signal or converge to the MNs that control muscles, it is helpful to examine the arrangement of MNs first. Romanes and colleagues have used retrograde neuronal fills from the muscles or nerves in the periphery and identified discrete clusters of MNs, called pools, devoted to each muscle ([George J. Romanes, 1951](#); [G.J. Romanes, 1964](#); [S et al., 1981](#); [Nicolopoulos-Stournaras et al., 1983](#); [Vanderhorst et al., 1997](#)). These studies also identified the organizational principles of inter-pool relationships. Behaviourally relevant movements naturally involve muscles within the same part of the body leading to a significant local clustering of neurons that control neighbouring body regions.

The MN population can be divided in many sub-populations in adults ([Figure 10](#)).  $\gamma$ -MNs innervate intrafusal fibres whereas  $\alpha$ -MNs innervate extrafusal fibres and  $\beta$ -MNs innervate both.  $\gamma$ - and  $\beta$ -MNs further divide between static and dynamic MNs

according to the way they modulate the spindle activity. When investigating the properties of the motor units, Burke et al. ([Burke et al., 1971](#); [Burke et al., 1973](#)) defined three physiological types: fast and slow motor units according to the contraction time of the muscle fibres and within the fast motor units fatigue-resistant and fatigable motor units according to the way the contractile material of their muscle fibers is able or not to sustain repeated stimulations. Each motor unit comprises slow MNs (S MNs), fast fatigue-resistant MNs (FR MNs) and fast fatigue-fatigable MNs (FF MNs). The investigation of the motor unit properties was initially carried out in the cat but similar results were obtained in many other mammals (rat, rabbit, human, guinea-pig) ([Kernell, 2006](#)). However, some authors argued that, in the mouse, FR and FF motor units form a continuum rather than discrete populations, especially in rodents in which motor neuron size differences are less marked ([R Bakels et al., 1993](#); [R. Bakels et al., 1993](#); [Gardiner, 1993](#)). In mammals every muscle embodies the three types of muscle units although in highly variable proportions. Burke et al. ([Burke et al., 1971](#); [Burke et al., 1973](#)) further demonstrated that all the muscle fibers of a given motor unit exhibited the same histochemical profile. Furthermore, they found a correlation between the physiological types and the histochemical profiles: type S motor units have type I muscle fibers, type FR motor units have type IIa muscle fibers, and type FF motor units have type IIb muscle fibers ([Figure 10](#)). Therefore, Burke et al. ([Burke et al., 1971](#); [Burke et al., 1973](#)) showed an exquisite correlation between the muscle unit contractile properties (contraction velocity and fatigue resistance) and the molecular identity of the fibers (difference in the amount of oxidative enzymes such as SDH or in the amount of myofibrillar ATPases) ([Edstrom et al., 1968](#); [Schiaffino et al., 2011](#)). Later on, staining of the different isotypes of the myosin heavy chain proteins was established ([Schiaffino et al., 1988](#)) allowing to tighten the link between the contractile proteins and the muscle unit properties.

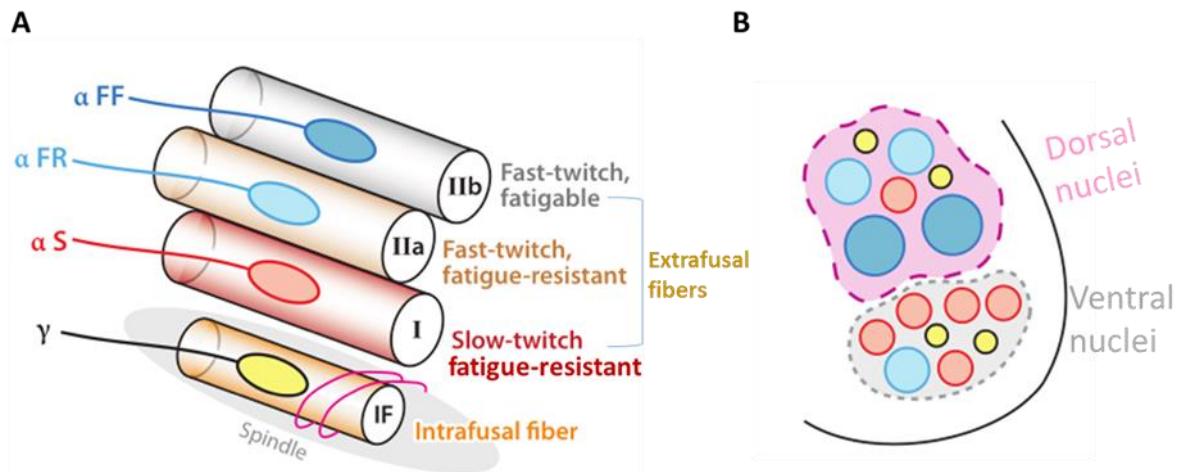


**Figure 10. Schematic representation of the different types of motoneurons.**

MNs in the adult can be classified into functionally diverse classes and subtypes. (A). One division - into alpha ( $\alpha$ ), beta ( $\beta$ ), and gamma ( $\gamma$ ) MNs - is made according to the type of muscle fiber that each class innervates:  $\alpha$ -MNs innervate extrafusal fibers,  $\gamma$ -MNs innervate intrafusal fibers,  $\beta$ -MNs innervate both intrafusal and extrafusal fibers but this class is not shown in this schema.  $\alpha$ -MNs target distinct muscle fibers, thus this class continue to be subdivided into three subtypes: FF (fast-twitch fatigable), FR (fast-twitch, fatigue-resistant) and S (slow-twitch, fatigue-resistant). (B). A typical motor pool contains all types of MNs—fast and slow,  $\alpha$  and  $\gamma$ :  $\alpha$ -FF,  $\alpha$ -FR,  $\alpha$ -S and  $\gamma$ . The upper pool innervates a fast muscle but also contains  $\alpha$ -S and  $\gamma$  MNs. Similarly, the lower pool would be classified as slow. Adapted from Kanning et al., 2010.

The fact that different MNs impinge on different muscle units and that a given MN connects exclusively to a homogenous muscle fiber population calls for a matching between a MN and its efferent fibers characteristics (i.e, the MNs electrophysiological properties need to be tuned to their output). Indeed, MNs properties are widely different. Among all characteristics, MNs of a given kind segregate according to their electrotonic size (evaluated by the measure of the input conductance) (Zengel et al., 1985). In addition, Friese et al. (Friese et al., 2009) showed that the average size of the soma already allowed to discriminate between  $\gamma$ - and  $\alpha$ -MNs as early as P14 in the mice. MN size therefore increases from  $\gamma$ -MN to  $\alpha$ -FF MN ( $\gamma < \alpha$ -S <  $\alpha$ -FR <  $\alpha$ -FF). Given the evidence indicating that  $\alpha$ -MNs receive a common input (Elwood Henneman, 1957; Mendell et al., 1968; E. Henneman, 1985) posited an orderly recruitment of the motor units based on the size principle. That is to say that considering a fixed input, the most electronically compact MNs will see their voltage rise more and will reach their firing threshold prior the less compact ones.

In the neonatal rodent, heterogeneity between motor units is already established (Close, 1967) and motor units present a biased composition in fiber types as early as E16 (Condon et al., 1990). But what about the putative differences

between the electrical intrinsic properties of neonatal MNs? So far, we do not know how the functional properties of the different subtypes of spinal MNs mature. It is well known that, in adult mammals, spinal MNs start to fire without any delay at the onset of a liminal current pulse (*Elwood Henneman, 1957; Manuel et al., 2009*). In sharp contrast, at least two different firing behaviours were reported during the second postnatal week for the rat abduces MNs (*Russier et al., 2003*) or the mouse spinal MNs (*Pambo-Pambo et al., 2009*). Upon injection of liminal current pulses, the discharge starts at the current onset in some MNs but it is delayed in others. Neonatal and adult bistable motoneurons display delayed spike-frequency acceleration. Delayed spike-frequency acceleration reflects slow inactivation of Kv1.2 channels (*Bos et al., 2018*).

### 1.1.3 RECURRENT INHIBITION

An important and relatively simple circuit that controls MN firing is the recurrent inhibitory circuit established between Renshaw cells (RCs) and MNs (*Figure 11*), which form a recurrent inhibitory circuit in order to adjust the motor output. RCs receive synaptic inputs from intraspinal collaterals of motoneuronal axons and, once activated, inhibit the same MNs and close synergists (*Birdsey Renshaw, 1946; Eccles et al., 1954; Fyffe, 1991; Francisco J. Alvarez et al., 2007*). In this manner, RCs slow down and stabilize MN firing and shape input–output relations to excitatory drive (*Windhorst, 1996*).

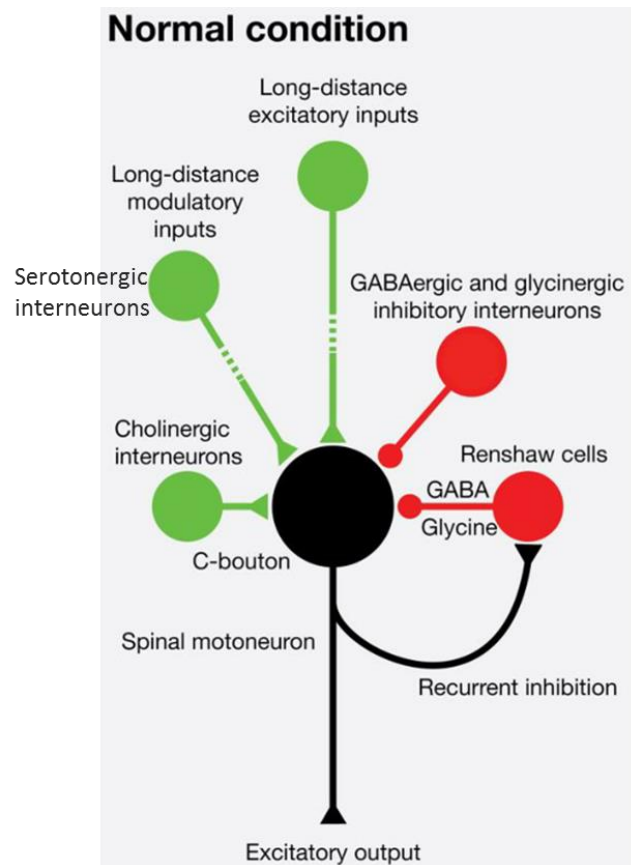


**Figure 11. Local spinal motoneuronal network control excitation/inhibition balance in normal condition.** Lower motoneurons execute voluntary movements by integrating central descending and peripheral commands, and local inhibitory (GABAergic and/or glycinergic interneurons and Renshaw cells) and modulatory (cholinergic and serotonergic interneurons) inputs. Adapted from Crabé et al., 2020.

Renshaw cells were first identified in cats by their high-frequency discharge in response to antidromic motor axon action potentials ([Willis, 1971](#)) and are located in the most ventral regions of laminae VII and IX of the spinal cord ([R. C. Thomas et al., 1965](#)). They belong to the V1 interneuron subclass ([Gonzalez-Forero et al., 2005](#)) and can be identified by their medium to large size, expression of biochemical markers such as GlyT2, calbindin, and parvalbumin, location, and electrophysiological properties such as a high postsynaptic sensitivity to acetylcholine and large glycine- and GABA-evoked currents ([Francisco J. Alvarez et al., 2007](#)). Their inhibitory action is mediated by both GABA and glycinergic synapses, although synaptic boutons immunoreactive to glycine alone are MNs than boutons that are immunoreactive to both GABA and glycine ([Shigenaga et al., 2005](#)). Since Renshaw cells release both GABA and glycine, the recurrent inhibition they induce exerts a longer inhibitory synaptic action than the inhibition induced by Ia interneurons, in which neurotransmission is more phasic and solely glycinergic

([Bhumbra, 2012](#); [Ole Kiehn, 2016](#)). Renshaw cells are the only interneurons that receive direct excitatory synaptic inputs from MNs and, in turn, exert inhibitory feedback on them, known as recurrent inhibition ([Francisco J. Alvarez et al., 2013](#)). However, inhibitory synapses of Renshaw cells are located on dendrites rather than on the cell body ([Fyffe, 1991](#)) and the effectiveness of recurrent inhibition at reducing the MN firing rate is limited ([Mattei et al., 2003](#)). This is in keeping with the small amplitude of the postsynaptic inhibitory potential or current generated by Renshaw cells ([Windhorst, 1996](#)). In contrast, the synapses of Ia inhibitory interneurons are close to the MN soma and have a more significant impact in counteracting the excitatory input arriving in the dendrites. Thus, Renshaw cells and Ia interneurons present distinct synaptic connectivity that serves different functions. Individual Renshaw cells receive inputs from particular motor pools and spread their inhibitory output to the same MNs, either directly or through inhibition of Ia inhibitory neurons mediating reciprocal inhibition of antagonistic muscles (flexor and extensor alternation activity), to  $\gamma$ -MNs controlling muscle spindle length, and to other Renshaw cells ([Francisco J. Alvarez et al., 2007](#)) ([Figure 12](#)). Thus, recurrent inhibition is primarily generated by input from motor axon collaterals.

In summary, Renshaw cells are activated by axon collaterals of  $\alpha$ -MNs, in particular those in proximal motor pools that are vulnerable in ALS, and in turn inhibit  $\alpha$ - and  $\gamma$ -MNs in homonymous and synergist MN pools. The functional role of Renshaw inhibition is not clear. Several hypotheses have been proposed: Renshaw inhibition may serve to limit MN firing ([Noga et al., 1987](#)), curtail plateau potentials and persistent firing ([Hultborn et al., 2003](#); [Bui et al., 2008](#)), or even support high firing rates of MNs ([Obeidat et al., 2014](#)), to restructure recruitment at the motor pool level ([Hultborn et al., 1979](#)), or to guide the tuning of MN properties at the microcircuit level ([Brownstone et al., 2015](#)).

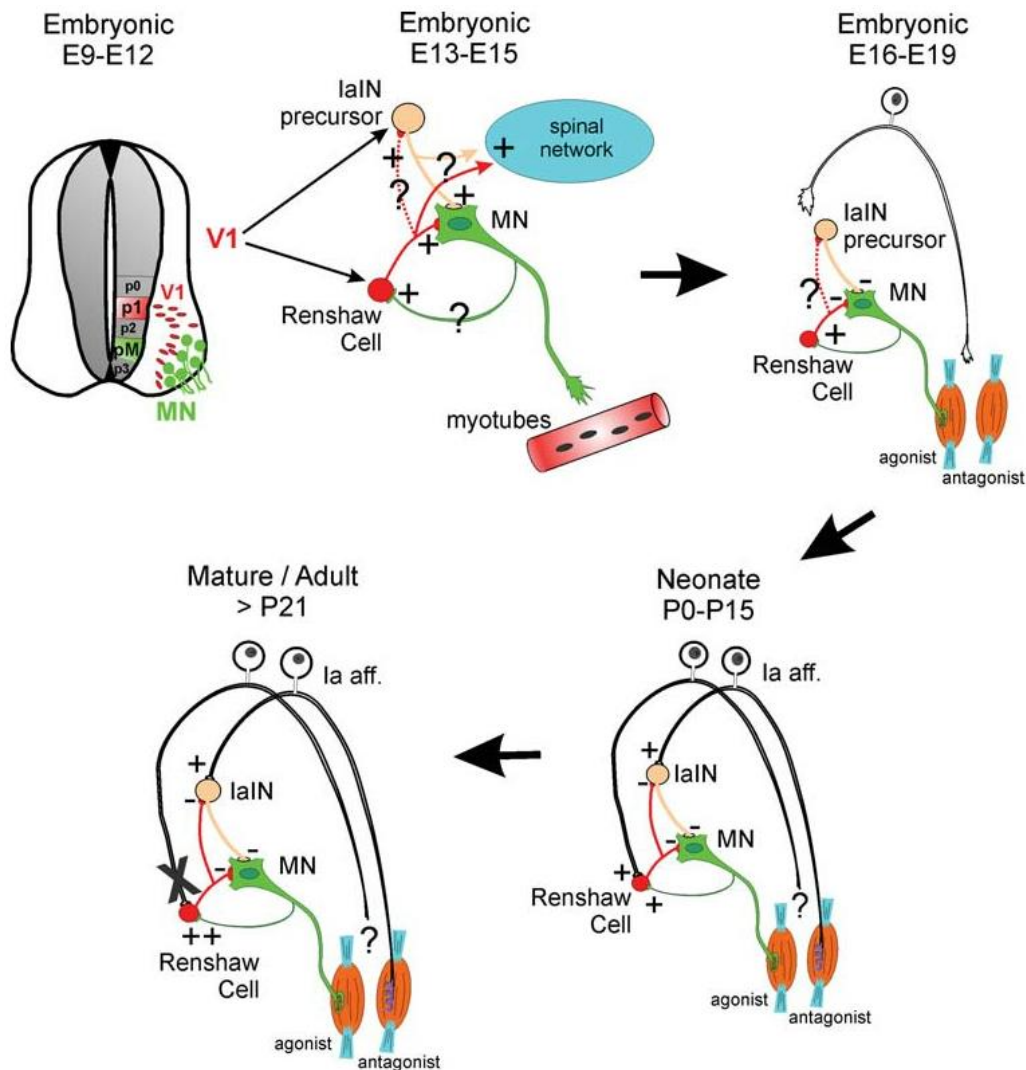


**Figure 12. The diagrams summarize the changes in the integration of Renshaw cells and Ia interneurons in the ventral spinal network during development.** Renshaw cells and Ia interneurons are derived from V1 interneurons that are generated from p1 progenitors in the early neural tube (**top, left**). | V1 interneurons take a ventral-lateral migratory path and position themselves in close relationship to MNs with whom they start to interact synaptically. V1 interneurons produce several classes of ipsilaterally projecting GABAergic/glycinergic premotor interneurons: RCs and IaIN precursors (**top, middle**). At mid-embryonic stages, all early connectivity (primarily cholinergic and GABAergic and less glycinergic and glutamatergic) is excitatory, however, morphological details of these early connections are largely unknown (question marks). It is believed that this early connectivity has important roles in transmitting motoneuron spontaneous activity to the whole spinal network and that this spontaneous activity is important during early axonal guidance and target recognition. An amplifier role for early MN-initiated spontaneous activity could be accomplished by RCs directly or indirectly through connections with other interneurons like IaINs. The anatomical nature and organization of these connections remains speculative at present. Current studies are actively pursuing clarification of this early synaptology. | At late embryonic stages (**top, right**), inhibitory synapses become hyperpolarizing and the role of RCs in transmitting excitation down-regulates in favor of exerting inhibitory influences over the MNs. Primary afferent axons commence to invade the ventral horn of the spinal cord in late embryos at the same time that they induce the differentiation of the sensory apparatus in the periphery (muscle spindles and Golgi tendon organs). By the time of birth (**bottom, right**), RCs are contacted by both sensory afferents and motor axons and, in this sense, they are a class of proprioceptive inhibitory interneuron that also has direct excitation from MNs. The source of the sensory input is as yet unknown. If it originates from antagonist muscles, then Renshaw cells could behave at this stage as a special class of IaIN. After maturation and onset of weight-bearing locomotion (**bottom, left**) this sensory input is functionally lost (indicated by an X), although the sensory inputs are still present structurally, and the role of RCs then becomes more focused to recurrent inhibition, as it is in the adult. From Alvarez and Fyffe 2007.

### 1.1.4 GABAergic/Glycinergic INHIBITION AND GABA/Glycine TRANSMISSION

There are two major inhibitory neurotransmitters that modulate excitatory signals in the CNS:  $\gamma$ -aminobutyric acid (GABA) and glycine. Inhibitory circuits across different brain regions rely preferentially on GABAergic (brain) or glycinergic transmission (brainstem and spinal cord), but some neural circuits utilize both GABA and glycine at an individual synapse (*Andréa Dumoulin et al., 2001*). GABA and glycine can also be co-released from the axon terminal of an individual interneuron allowing a wider dynamic range of inhibitory modulation than could be conferred by the action of a single neurotransmitter type (*Nerlich et al., 2014*) (*Figure 13*). In the spinal cord sensory-motor circuit, distinct populations of proprioceptive sensory afferents target specific MNs and different populations of inhibitory interneurons form synapses onto the sensory afferent terminals and MNs, respectively. Inhibitory synapses onto the sensory afferents are usually GABAergic, whereas those on MNs are glycinergic and/or GABAergic (*Hughes et al., 2005; Betley et al., 2009*).

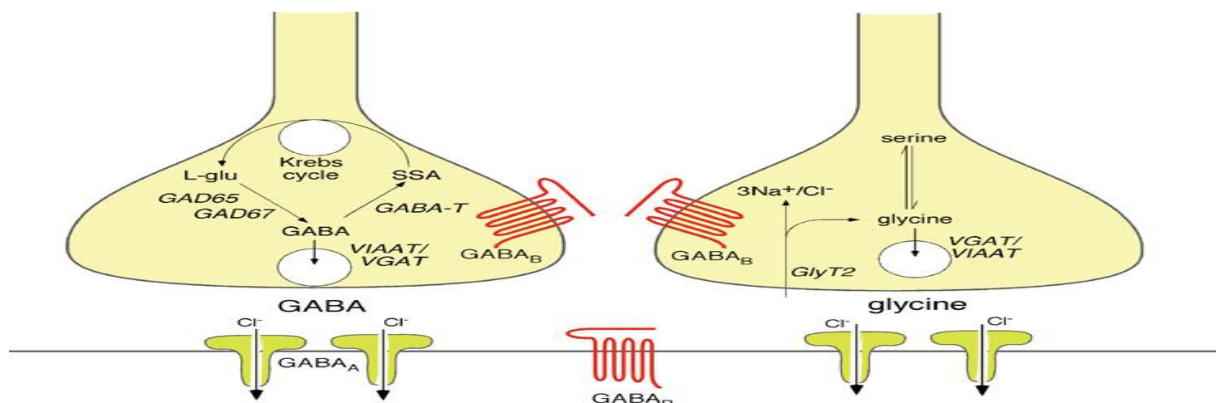


**Figure 13. Schema of GABAergic (left) and glycinergic (right) axon terminal.** GABA is synthesized from L-glutamate by GAD-65 and GAD-67 and transported into presynaptic storage vesicles by VGAT/VIAAT. Degradation of GABA occurs through GABA transaminase (GABA-T) to form succinic semialdehyde (SSA) which is further metabolized in the Krebs cycle. Glycine is formed from serine-by-serine methyl transferase and taken up from extracellular space by GlyT2. Transport into presynaptic vesicles occurs again through VGAT/VIAAT. GABA acts at postsynaptic GABA<sub>A</sub> receptors and presynaptic and postsynaptic GABA<sub>B</sub> receptors. Some neurons, in particular primary sensory afferent neurons, carry GABA<sub>A</sub> receptors also on their presynaptic terminals. Glycine acts at postsynaptic glycine receptors (modified from Zeilhofer et al., 2012a).

Inhibitory neural transmission in the adult nervous system is mediated by GABA and glycine (*Figure 13*), which are inhibitory neurotransmitters with fast synaptic inhibition occurring largely through the ionotropic GABA<sub>A</sub> receptor (GABA<sub>A</sub>R) (*Hevers et al., 1998; Martin Heubl et al., 2017; Siucinska, 2019*). As a GABA-gated chloride (Cl<sup>-</sup>) channel, the consequence of GABA<sub>A</sub>R signalling is dependent on intracellular Cl<sup>-</sup> concentration, which determines the reversal potential for GABA<sub>A</sub>R

currents ( $E_{\text{GABA}}$ ). In the mature CNS, which includes the spinal cord, GABA and glycine negatively regulate neuronal activity ([Richard W. Olsen et al., 1990](#); [R L Macdonald et al., 1994](#); [Legendre, 2001a](#); [Kirsch, 2006](#)). In the spinal cord, there are three types of inhibitory neurons and terminals: GABAergic, GABA/glycine co-releasing, and glycinergic ([Jonas et al., 1998](#); [Vaaga et al., 2014](#); [Tritsch et al., 2016](#)). These neurons and terminals are arranged in the spinal cord neural circuit and are involved in many vital roles, such as regulating locomotive movement and respiratory rhythms ([Andrew J. Todd et al., 1990](#); [Hanns Ulrich Zeilhofer et al., 2005](#); [Mehdi Hossaini et al., 2007](#)).

At the spinal cord level, in adults, the activation of  $\text{GABA}_A$  and glycine receptor-gated  $\text{Cl}^-$  channels inhibits neurons as a result of low intracellular chloride concentration ( $[\text{Cl}^-]_i$ ) and hyperpolarized  $\text{Cl}^-$  equilibrium potential ( $E_{\text{Cl}}$ ). Low  $[\text{Cl}^-]_i$  is maintained by the potassium-chloride cotransporter KCC2 ([Delpire et al., 2002](#); [J. A. Payne et al., 2003](#)), which extrudes  $\text{Cl}^-$ . However, at early developmental stages, GABA and glycine are often excitatory because  $E_{\text{Cl}}$  is very depolarizing ([Ziskind-Conhaim, 1998](#)). The decrease of inhibition would be caused mainly by downregulation of KCC2, which induce depolarized  $E_{\text{Cl}}$  ([Figure 13](#)) ([Coull et al., 2003](#); [Boulenguez et al., 2010](#)). The GABAergic system plays an important role in motor control and sensory transmission in the spinal cord ([Cramer et al., 2008](#); [Sibilla et al., 2009](#)). GABA receptors are present in the pre- and post-synaptic sites of primary afferent terminals, at laminae I-III ([Bowerly et al., 1987](#)) and at MNs ([Delgado-Lezama et al., 2013](#)). This system modulates the motor performance and sensory processing ([Rudomin, 2009](#)).

The fast actions of GABA and glycine are mediated by their ionotropic receptors, which are ligand-gated ion channels. Fast inhibition is mostly mediated by glycine receptors and  $\text{GABA}_A$  receptors.  $\text{GABA}_C$  receptors are also ionotropic, but their expression is more reduced than for  $\text{GABA}_A$  receptors, mainly in the retina ([S. M. Jones et al., 2009](#)). Since their contribution to fast inhibition is minor in this sense, it is sometimes omitted.  $\text{GABA}_B$  receptors are also inhibitory, but they are metabotropic receptors, which means they are G-protein coupled receptors. They do not contribute to fast inhibitory transmission, because the consequences of their activation are slower ([Purves et al., 2001](#)).

GABA<sub>A</sub> receptors mediate two modes of inhibitory neurotransmission ([Robert L. Macdonald et al., 2009](#)) ([Figure 14](#)). The first, termed “phasic” inhibition, involves the transient activation of postsynaptic GABA<sub>A</sub> receptors by nearly saturating concentrations of GABA released from presynaptic vesicles. GABA<sub>A</sub> receptors are also involved in slower forms of non-synaptic inhibition, a phenomenon termed “tonic” inhibition, both forms were illustrated in [Figure 14](#). Phasic inhibition gives rise to inhibitory postsynaptic currents (IPSCs) that activate rapidly (rise times of 1ms or less) but decay slowly ([Maconochie et al., 1994](#); [M. V. Jones et al., 1995](#)). Several types of IPSCs can be recorded, each having slightly different kinetic properties ([Otis et al., 1994](#); [Mody et al., 2004](#)). 1). Miniature IPSCs (mIPSCs) are triggered by the spontaneous release of GABA from a single synaptic vesicle (i.e., action potential independent) ([Figure 14A](#)). 2). In contrast, spontaneous IPSCs (sIPSCs) are triggered by spontaneously occurring action potentials in presynaptic terminals and typically involve release of GABA from multiple synaptic vesicles ([Figure 14B](#)). 3). Evoked IPSCs (eIPSCs) are triggered following experimentally induced action potentials, and, like sIPSCs, involve release of GABA from multiple synaptic vesicles. Tonic inhibition is mediated by peri- and extra-synaptic GABA<sub>A</sub> receptors that are persistently activated by sub-saturating concentrations of ambient GABA ([Figure 14C](#)). While the sources and precise concentration of ambient GABA are still uncertain, it is generally believed to arise from a combination of synaptic overflow and non-vesicular release, and to reach concentrations of 1M ([Attwell et al., 1993](#); [Zoli, 1999](#); [Mark Farrant et al., 2005](#)). Interestingly, the contribution of the tonic current to overall inhibitory tone may actually be greater than the summed charge transfer of phasic currents ([Brickley et al., 1996](#); [Hamann et al., 2002](#)).

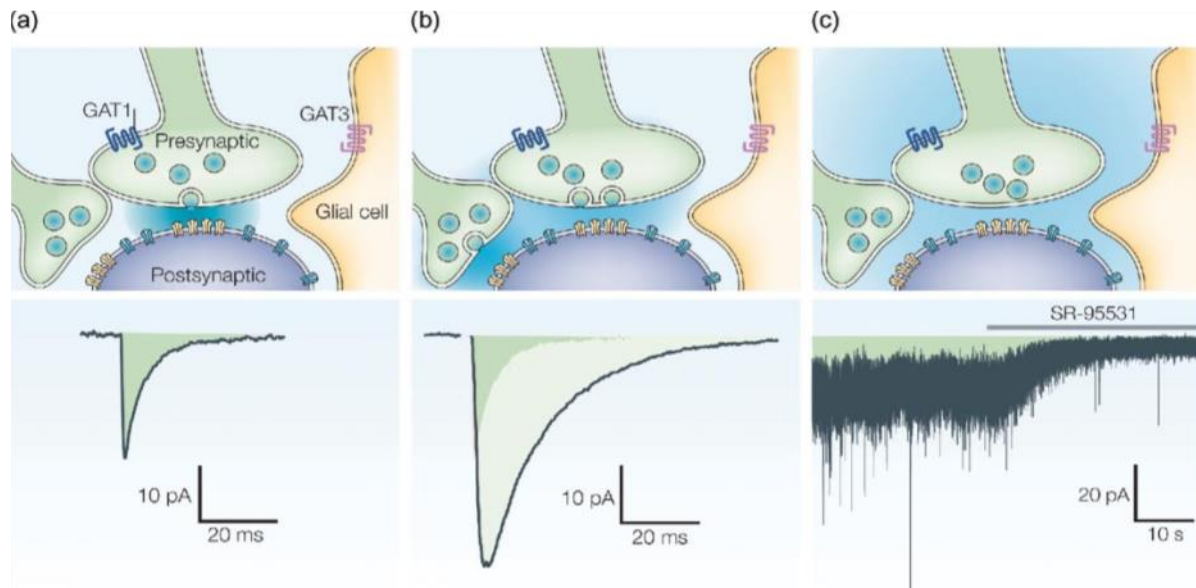


**Figure 14. Modes of GABA<sub>A</sub> receptor activation.** (a) The release of GABA (blue shading) from a single presynaptic vesicle activates only those postsynaptic GABA<sub>A</sub> receptors clustered immediately beneath the release site (yellow). The current record shows an averaged waveform of the resulting miniature inhibitory postsynaptic currents (mIPSCs). (b) Action potential-dependent release of multiple vesicles or evoked release from several terminals promotes GABA “spillover”, which activates both synaptic and extrasynaptic receptors (blue). The current record shows the larger and much slower averaged waveform of the resulting eIPSCs. The area of the mIPSC shown in panel (a) is superimposed for comparison. (c) A low concentration of ambient GABA, which persists despite the activity of the neuronal and glial GABA transporters (GAT1 and GAT3, respectively), tonically activates extrasynaptic GABA<sub>A</sub> receptors. The trace shows the tonic current that results from stochastic opening of these high-affinity receptors, with superimposed phasic currents. The GABA<sub>A</sub> receptor antagonist gabazine (SR-95531) blocks phasic IPSCs and tonic channel activity, causing a change in the “holding” current and a reduction in current variance. The shaded area beneath the current record before SR-95531 application represents the charge carried by tonically active GABA<sub>A</sub> receptors. The current records are from whole-cell patch-clamp recordings of granule cells in acute cerebellar slices from adult mice. Adapted from Macdonald and Botzolakis 2009.

GABA<sub>A</sub> receptors, like other Cys-loop receptors, are ligand-gated channels mediating inhibition in the CNS and assembled from homologous subunits (Figure 15A) as pseudo-symmetrical heteropentamers (Figure 15B) (Robert L. Macdonald et al., 2009), which facilitate folding and oligomerization of GABA<sub>A</sub> receptor subunits and provide a stringent quality control system (Bollan et al., 2003; Ellgaard et al., 2003). There are also specific subunit requirements for GABA<sub>A</sub> receptor assembly that serve to limit receptor heterogeneity (Angelotti et al., 1993). While the functional and pharmacological signature of receptors has been identified in a subset of hippocampal neurons (Mortensen et al., 2006), the overwhelming majority of native receptors are composed of ternary subunit combinations (McKernan et al., 1996; R. W. Olsen et al., 2009). Recently, Garifulina and colleagues (Garifulina et al., 2022) demonstrated that β- subunit homomers are proton-gated anion channels. Mutation of a single H267A in β3 subunits completely abolishes channel activation by protons.

In molecular dynamic simulations of the  $\beta 3$  crystal structure protonation of H267 increased the formation of hydrogen bonds between H267 and E270 of the adjacent subunit leading to a pore stabilising ring formation and accumulation of  $\text{Cl}^-$  within the transmembrane pore.

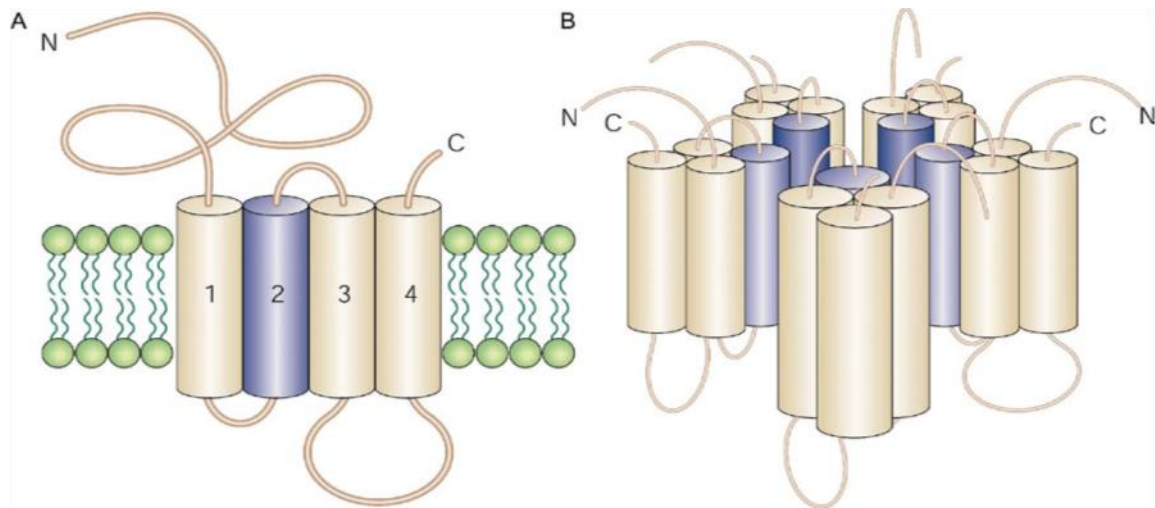


**Figure 15. Structure of Cys-loop receptor (GABA<sub>A</sub> receptor) ion channels.** **A.** Individual subunits contain four hydrophobic Transmembrane (TM) domains. The large N-terminal domain is located extracellularly and is believed to contain neurotransmitter and modulator binding sites. The C-terminal domain is also located extracellularly; however, it is typically only a few amino acids long. The intracellular domain between TM3 and TM4 is the most divergent region and contains Numerous consensus sites for the action of both serine/threonine and tyrosine protein kinases. **B.** Receptors are assembled as pseudo-symmetrical pentamers. The ion channel is formed by a ring of TM2 domains (blue). This is surrounded by a second ring composed of TM1 and TM3 domains, which is in turn surrounded by a third ring composed of TM4 domains. Adapted from Macdonald and Botzoulakis 2009.

Different subunits are also involved in the formation of GlyRs with different functional properties ([Legendre, 2001a](#)). The quaternary structure of GlyR has been examined by chemical cross-linking of its subunits ([Langosch et al., 1988](#)) ([Figure 16](#)), demonstrating a pentameric quaternary structure with an invariant stoichiometry of three  $\alpha$  and two  $\beta$  subunits ([Langosch et al., 1988](#)). Neurons express both homomeric and heteromeric GlyRs. Homomeric GlyRs are the dominant form in foetal rat spinal cord neurons ([Virginio et al., 1997](#)) and are also expressed by foetal neurons of the rat neocortex ([Flint et al., 1998](#)) and cerebellar granule cells ([Kaneda et al., 1995](#); [Virginio et al., 1997](#)), where glycine synapses have not been detected. Homomeric GlyRs seem to be located extrasynaptically and responsible of a “tonic” inhibition ([E. Muller et al., 2008](#)), whereas heteromeric  $\alpha/\beta$  GlyRs are predominantly expressed at postsynaptic sites ([Takahashi et al., 1992](#); [Rampon et al., 1996](#); [Kneussel et al., 2000](#)). The existence of numerous subtypes of GlyR represents a

functional diversity of inhibitory glycinergic synapses as GlyRs have functions distinct from their role in inhibitory synaptic transmission during brain development.

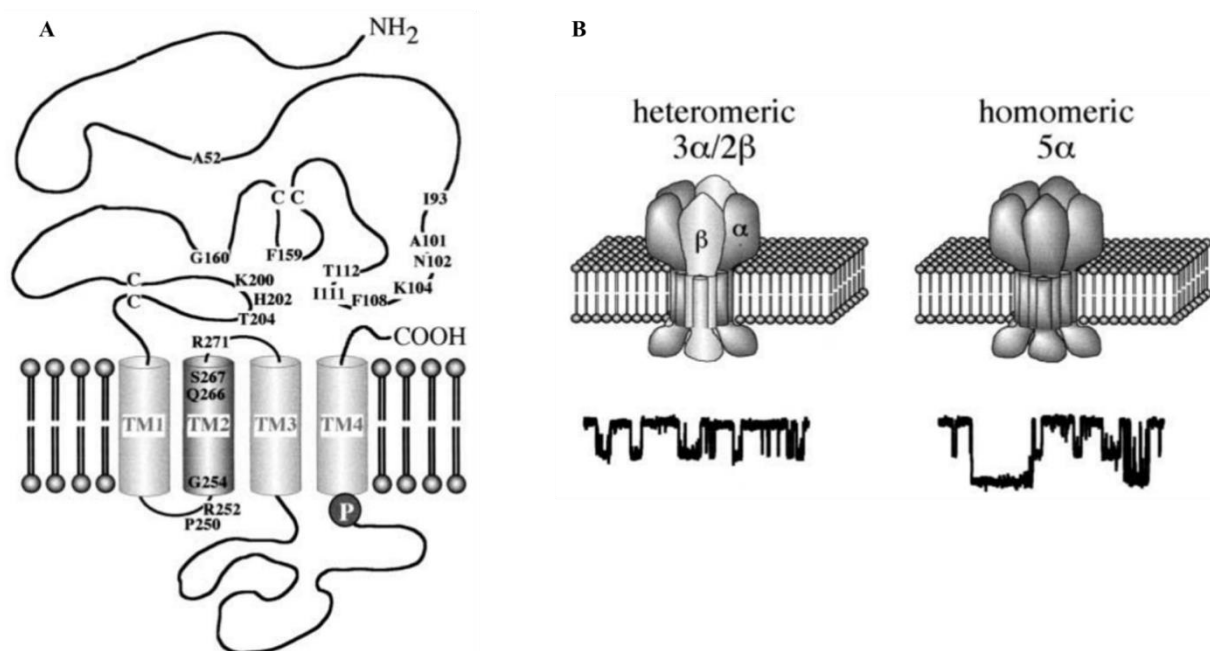


**Figure 16. Structure of the glycine receptor.** **A.** Membrane topology of a subunit with the four transmembrane domains, showing the position of functionally important amino acid residues (see text). The filled circle (black) in the TM3–TM4 intracellular cytoplasmic loop (serine 391) is the phosphorylation site for PKC. The transmembrane domain M2 forming the pore of the chloride channel is in black. **B.** arrangement of  $\alpha$  and  $\beta$  GlyR subunits in the heteromeric (left) and homomeric receptors (right). The single-channel recordings (bottom) show the subconductance levels, depending on GlyRs subunit combinations. Adapted from Legendre 2001.

The intracellular  $\text{Cl}^-$  concentration ( $[\text{Cl}^-]_i$ ) in neurons is developmentally regulated, with a relatively high postnatal concentration that drops to a lower value going into adulthood, which has been confirmed in a wide range of animal species from worms to higher mammals, tissue structures (i.e., retina, olfactory bulb, hippocampus, neocortex, spinal cord, etc.) and preparations from neuronal cultures to slices, intact organs in vitro and in vivo [see the large table in Ben-Ari et al Physiological reviews ([Y. Ben-Ari et al., 2007](#))] ([Ben-Ari et al., 2012](#)). During early neuronal development, GABA<sub>A</sub>R responses are often depolarizing and excitatory, and this property is important for the facilitation of neuronal proliferation, migration, and synaptic integration ([Ge et al., 2006](#)). The developmental switch of GABA<sub>A</sub>R transmission towards a hyperpolarizing, inhibitory response is due primarily to changes mediated by neuronal sodium-potassium-chloride cotransporter 1 (NKCC1, mediating  $\text{Cl}^-$  influx) ([Yamada et al., 2004](#)) and the potassium-chloride cotransporter 2 (KCC2, mediating  $\text{Cl}^-$  efflux), in particular, an enhanced KCC2 surface expression

and function shortly after birth ([Rivera et al., 1999](#)). There is heterogeneity in the timing of this developmental switch in polarity of GABA. In rodent hippocampus the change of polarity of GABA appears during the first 2 postnatal weeks ([M. Farrant et al., 2007](#); [Tyzio et al., 2008](#); [Valeeva et al., 2016](#)). In embryonic mouse spinal cord, this switch occurs after E15.5 ([Jean-Xavier et al., 2006](#); [Alain Delpy et al., 2008](#); [Stil et al., 2009](#); [Allain et al., 2011](#)).

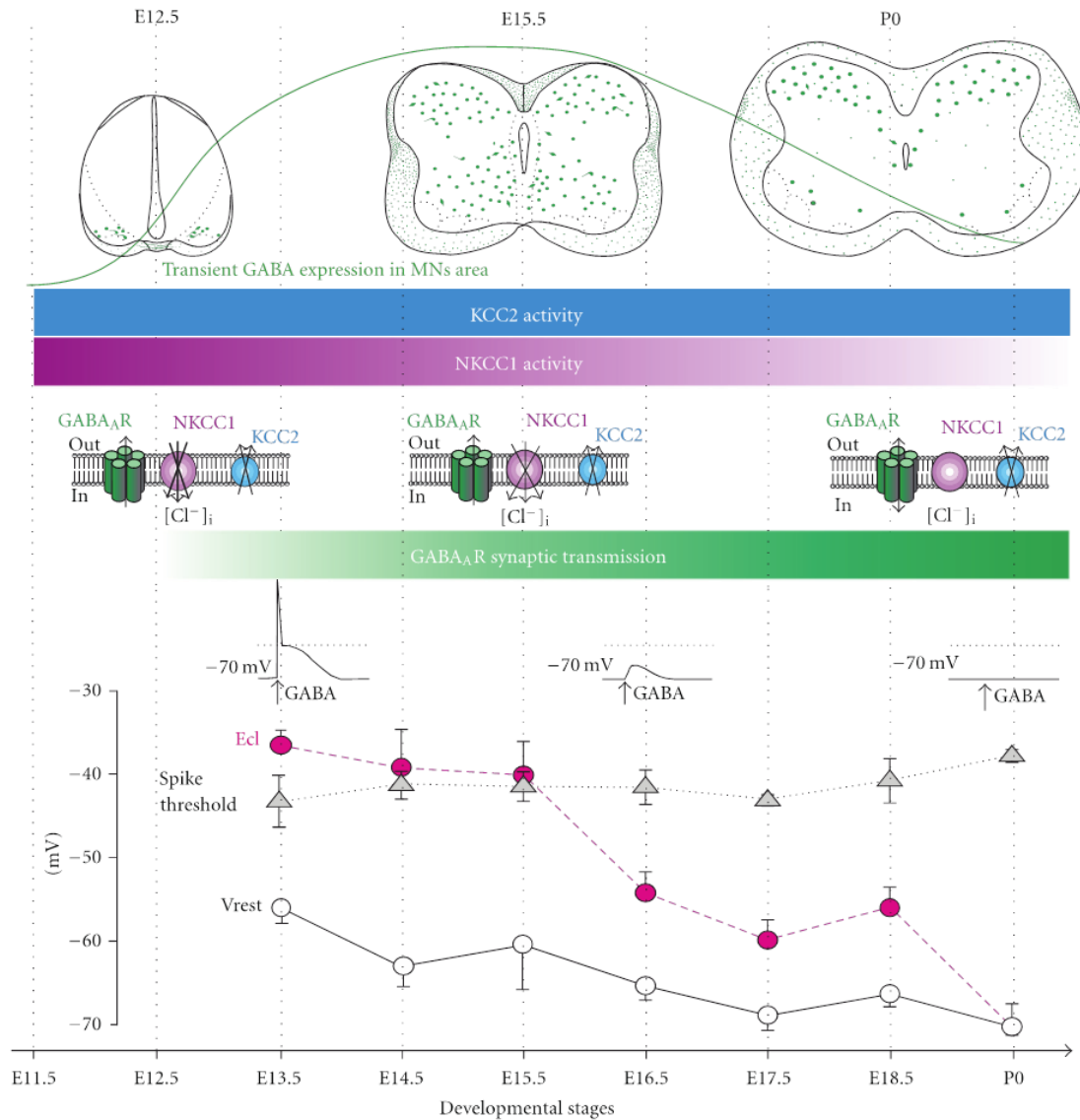


**Figure 17. Development of the GABA<sub>A</sub>R-mediated inhibitory transmission in mouse lumbar spinal MNs.** From top to bottom: schematic drawings (frontal views) depict the transient expression of GABA in spinal ventral interneurons (in green), while horizontal bars indicate the permanent KCC2 (in blue) and transient NKCC1 activity (in violet). The color intensity encodes the level of activity. NKCC1 inactivation combined to KCC2 activity leads to a significant decrease in  $[Cl^-]_i$  and a disappearance of GABA<sub>A</sub>R-mediated excitatory effects. In parallel to the maturation of the chloride cotransporters KCC2 and NKCC1, the spinal cord starts to convey first synaptic activity at E12.5 that is GABAergic (green horizontal bar). Bottom: maturation of the chloride equilibrium potential ( $E_{Cl}$ ), spike threshold and resting membrane potential ( $V_{rest}$ ) across the embryonic stages of developmental. *Note: the drop of  $E_{Cl}$  at E16.5 accounts for the GABA<sub>A</sub>R-mediated “shunting” effect.* Adapted from Allain et al., 2011.

Our laboratory has showed that there is a shift of  $E_{GABA_{AR}}$  toward negative values during the embryonic development of mouse lumbar spinal MNs (*Alain Delpy et al., 2008*). Until E15.5, the reversal potential of  $Cl^-$  ions (chloride equilibrium,  $E_{Cl}$ ) is above the spike threshold, whereas after E16.5, it drops significantly below spike threshold. During the course of the embryonic development, the resting membrane potential ( $V_{rest}$ ) of mouse spinal MNs remains below the  $E_{Cl}$ . However, if  $GABA_{AR}$  activation may trigger the firing of MNs until E15.5, after this embryonic developmental stage, such activation, although producing a depolarization, fails to trigger action potentials (*Alain Delpy et al., 2008*) (Figure 17). This shunting depolarizing GABA effect likely persists during postnatal stages even though our experimental measurements indicate that  $E_{Cl}$  reaches MNs  $V_{rest}$  at P0 (*Alain Delpy et al., 2008*). During the first 3 weeks of rodent postnatal development, inhibitory synaptic transmission changes in multiple ways that differ depending on brain areas. The respective contribution of the glycinergic and GABAergic transmission to the overall inhibitory message received by postsynaptic neurons may vary during the developmental period. For example, a developmental switch from a predominant GABAergic to main glycinergic neurotransmission occurs in the lumbar spinal cord (*B.-X. Gao et al., 2001*) and in the lateral superior olive of young rodents (*Kotak et al., 1998; Nabekura et al., 2004*), while GABAergic neurotransmission dominates in developing collicular neurons (*Meier et al., 2002*) (Figure 18).

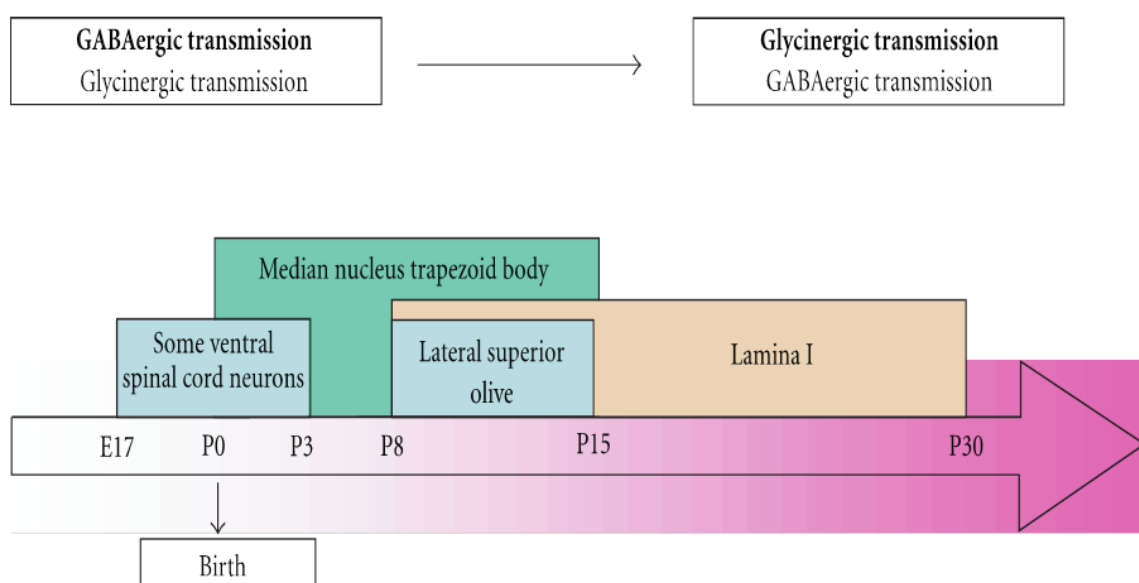


**Figure 18. Developmental changes in the proportions of GABAergic and glycinergic synaptic activity in various areas of the CNS.** A developmental switch from a predominant GABAergic to main glycinergic neurotransmission occurs in the lumbar spinal cord and in the lateral superior olive of

young rodent, while GABAergic neurotransmission dominates in developing collicular neurons. Adapted from Allain et al., 2011.

### 1.1.5 SHUNTING INHIBITION

Shunting inhibition, also known as divisive inhibition, is a form of postsynaptic potential inhibition that can be represented mathematically as reducing the excitatory potential by division, rather than linear subtraction. The term "shunting" is used because of the synaptic conductance short-circuit currents that are generated at adjacent excitatory synapses. If a shunting inhibitory synapse is activated, the input resistance is reduced locally. According to Ohm's law, the amplitude of subsequent excitatory postsynaptic potential (EPSP) is thus reduced (Figure 19). Consider a model neuron with an excitatory channel and inhibitory channel. The reversal potential for the excitatory channel is typically much more depolarized than the resting potential. This provides the depolarizing current flow of an excitatory input. The reversal potential of the inhibitory channel, however, is assumed to be slightly above the resting potential. Both excitatory and inhibitory channels are organized such that preferred motion leads to temporally non-overlapping activation of the channels. For a two-flash preferred direction stimulus this arrangement will lead to a depolarizing current from the excitatory channel as well as a depolarizing current from the inhibitory channel. When motion in the antipreferred direction is presented to the model shunting neuron, the excitatory and inhibitory conductances are activated at the same time. Under these circumstances the inhibitory channel essentially creates a large hole in the membrane. Any current flow caused by the simultaneous activation of excitatory channels will simply seep out through this hole (Figure 19). In other words, this so-called shunting inhibitory channel can veto nearby excitatory currents.

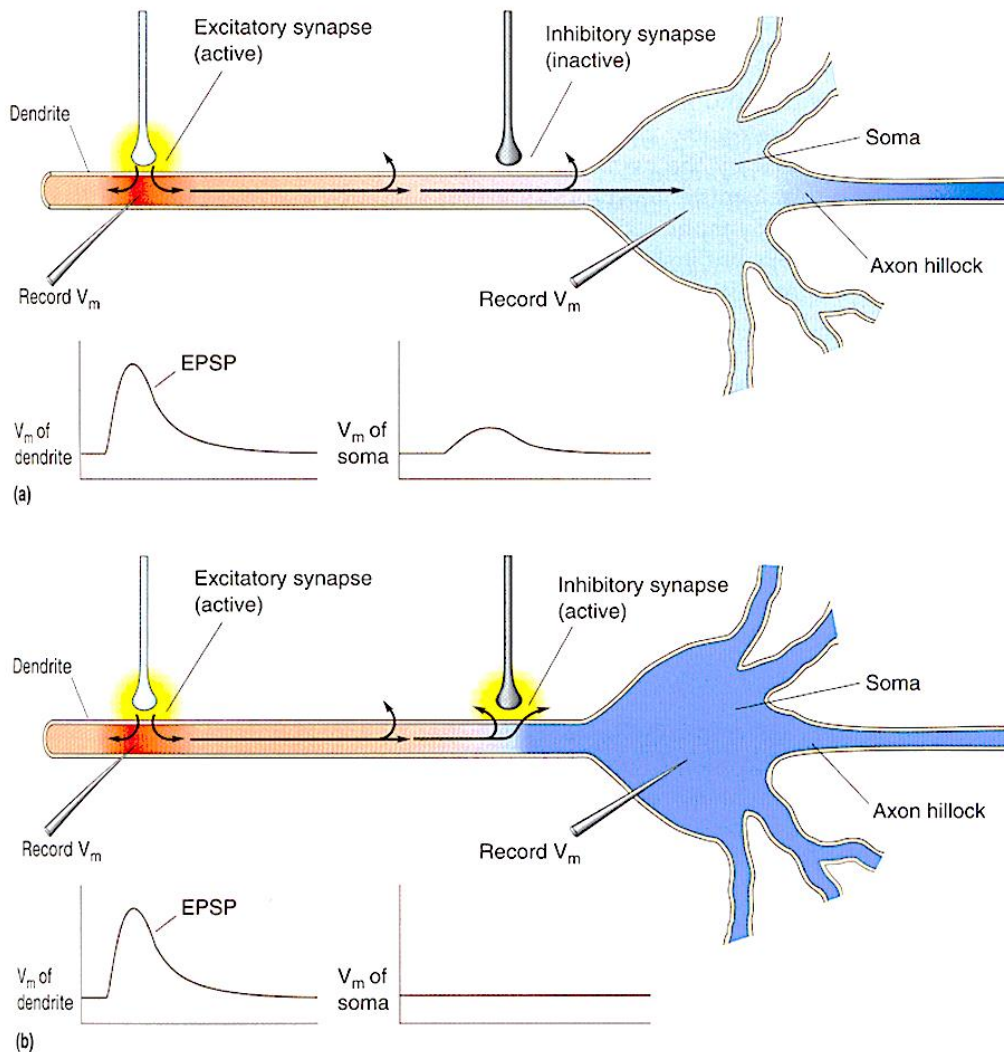


**Figure 19. Schema of shunting inhibition.** A neuron receives one excitatory and one inhibitory input. **(a)** Stimulation of the excitatory input causes inward post-synaptic current that spreads to the soma, where it can be recorded as an EPSP. **(b)** When the inhibitory and excitatory inputs are stimulated together, the depolarizing current leaks out before it reaches the soma. Adapted from Paulus and Rothwell 2016.

The shunting inhibition model provides a possible mechanism to implement a multiplicative nonlinearity, but what is the evidence that shunting inhibition is actually used in neural systems? Many direction-selective neurons contain gamma-aminobutyric acid (GABA) activated chloride channels whose reversal potential is close to the resting potential. Thus, the GABAergic synapse could function as a shunt. When GABAergic synapses are inactivated pharmacologically, *Direction selectivity* (DS) in many systems is greatly reduced ([Sillito, 1977](#); [Ariel et al., 1982](#); [Schmid et al., 1988](#)).

GABA<sub>A</sub> receptor activation causes Cl<sup>-</sup> channels to open in the membrane and the usual consequence is a change in the membrane potential. Since the Cl<sup>-</sup> equilibrium potential is usually more negative than the resting membrane potential,

this gives rise to an influx of  $\text{Cl}^-$  and hyperpolarization of the postsynaptic neuron observed as an IPSP ([Glickfeld et al., 2009](#)). However, the synaptic equilibrium potential for chloride is not always more negative than the resting potential, particularly in early development, or after a period of sustained  $\text{Cl}^-$  influx sufficient to increase the chloride concentration inside the cell ([Staley et al., 1995](#)). If the synaptic reversal potential is more positive, lying between the resting potential and the threshold for the generation of action potentials, activation of the GABAergic synapse can depolarize the membrane and produce an EPSP. Finally, if the  $\text{Cl}^-$  equilibrium potential is equal to resting potential, then there will be no obvious PSP after activation of a GABA receptor ([Alain Delpy et al., 2008](#); [Branchereau et al., 2016](#)).

Shunting inhibition can be quantified by the sum of the EPSP, the IPSP and a nonlinear term proportional to their product ( $k \times \text{EPSP} \times \text{IPSP}$ ), where the coefficient  $k$  reflects the strength of shunting effect ([J. Hao et al., 2009](#)). The  $k$  value strongly depends on the locations (dendritic trunk, oblique branches, soma) of excitatory and inhibitory inputs and the distance between them. The duration of shunting inhibition is relatively short in comparison with the membrane polarization that is produced at the GABAergic synapse. This is because transmembrane resistance is reduced while the  $\text{Cl}^-$  channel is open, it returns to normal when the channel closes.

### 1.1.6 CHLORIDE HOMEOSTASIS

The intraneuronal ionic composition is an important determinant of brain functioning. There is growing evidence that aberrant homeostasis of  $[\text{Cl}^-]_i$  evokes, in addition to that of  $\text{Na}^+$  and  $\text{Ca}^{2+}$ , robust impairments of neuronal excitability and neurotransmission and thereby neurological conditions. Thus, understanding the mechanisms underlying regulation of  $[\text{Cl}^-]_i$  is crucial for deciphering the variability in GABAergic and glycinergic signalling of neurons, in both health and disease. The homeostatic level of  $[\text{Cl}^-]_i$  is determined by various regulatory mechanisms, including those mediated by plasma membrane  $\text{Cl}^-$  channels and transporters ([Rahmati et al., 2018](#)).

$\text{Cl}^-$  is the most abundant transportable anion in all cells of the body where it triggers fundamental biological functions in all tissues. The  $[\text{Cl}^-]_i$  is regulated and maintained by a delicate functional balance between the operations of plasma

membrane  $\text{Cl}^-$  channels and those of transporters, as well as those of local impermeant anions (Rivera et al., 1999; J. Glykys et al., 2014). In the CNS,  $\text{Cl}^-$  channels and transporters play key roles in neuronal growth and development, neurotransmitter uptake, intracellular pH modulation, cell volume regulation and, perhaps most importantly, setting  $[\text{Cl}^-]_i$  either above or below its equilibrium potential (Figure 20) (Sangan et al., 2002; Deidda et al., 2014; Ruffin et al., 2014; Jentsch, 2016; Joseph Glykys et al., 2017).

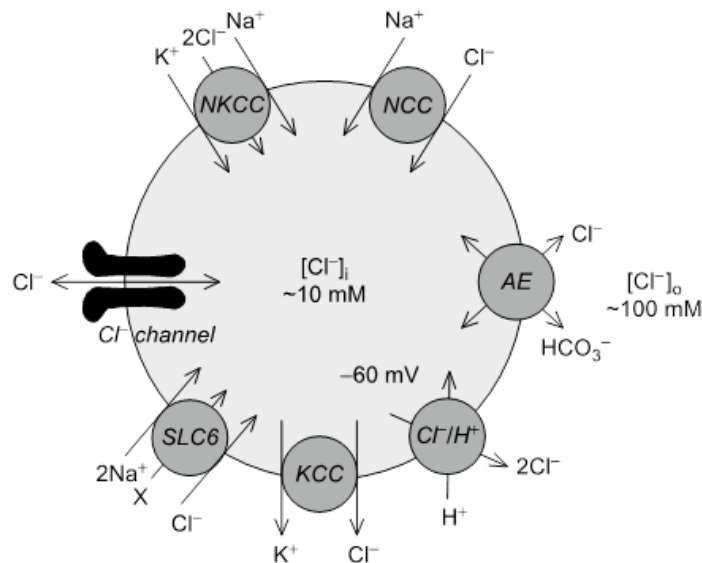


**Figure 20. Intracellular  $\text{Cl}^-$  homeostasis.** Intracellular  $\text{Cl}^-$  homeostasis is determined by the functional activities of various  $\text{Cl}^-$  transporters expressed in the plasma membrane of a given cell. These  $\text{Cl}^-$  transporter molecules include the cation-chloride cotransporters NKCC, NCC, KCC, members of the SLC6 family,  $\text{Cl}^-/\text{HCO}_3^-$  antiporters (AEs), and  $\text{Cl}^-/\text{H}^+$  antiporters (ClC-3, -4, -5 or -7). X represents a neurotransmitter such as GABA, dopamine, glycine, etc. (Chen et al., 2004). Direction of  $\text{Cl}^-$  transport depends on the chemical or the electro-chemical potential gradients across the plasma membrane. Adapted from Yasunobu et al., 2009.

In addition,  $[\text{Cl}^-]_i$  plays a crucial role in moderating neuronal excitability by determining the postsynaptic responses to the neurotransmitters GABA and glycine (Figure 21) (Yehezkel Ben-Ari et al., 2007; Branchereau et al., 2016; Nicolas Doyon et al., 2016). One of the most studied roles of  $[\text{Cl}^-]_i$  in neurons is its modulatory function in postsynaptic responses evoked by activation of ligand-gated  $\text{Cl}^-$  channels, such as GABA<sub>A</sub> receptors (GABA<sub>A</sub>Rs) (J Bormann et al., 1987). The direction of the  $\text{Cl}^-$  flow depends on the difference between  $E_{\text{Cl}}$  and the resting membrane potential (RMP) (Figure 21). If  $E_{\text{Cl}}$  is more negative than the RMP of the neuron,  $\text{Cl}^-$  flows inside the neuron. GABA<sub>A</sub>Rs in these types of cells mediate inward (hyperpolarizing)  $\text{Cl}^-$  currents, which in turn lead to inhibition of the postsynaptic neuronal activity (Figure 21a). In contrast, if  $E_{\text{Cl}}$  becomes more positive than the RMP,

outward (depolarizing)  $\text{Cl}^-$  flow through  $\text{GABA}_A\text{Rs}$  leads to excitation of the postsynaptic neuron (Figure 21c). Therefore, the activities of  $\text{Cl}^-$  channels and transporters that regulate  $[\text{Cl}^-]_i$  are critical for determining the polarity of the impact of  $\text{GABA}_A\text{Rs}$  on the neuronal membrane potential.

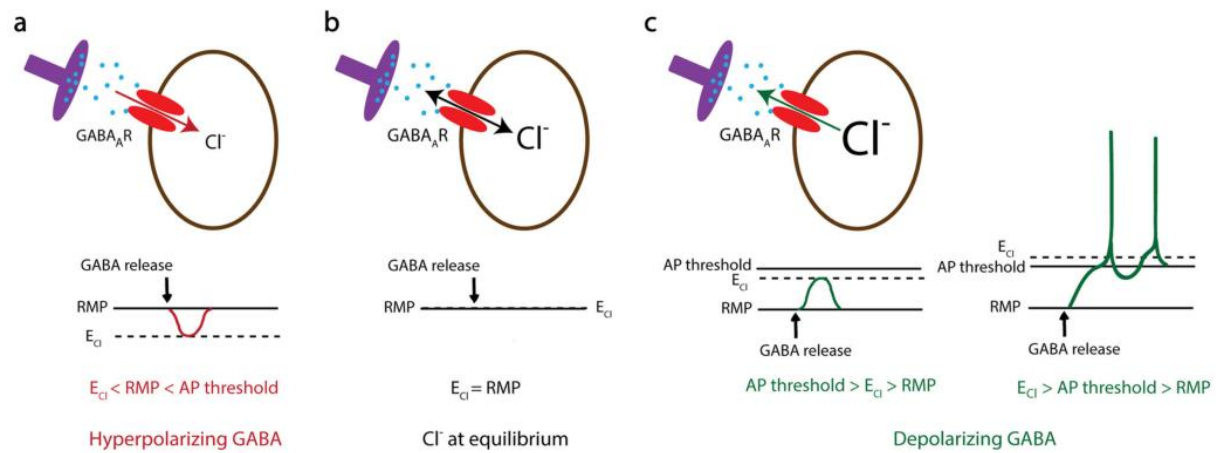


**Figure 21. Schematic representation of GABAergic signaling in mouse.** The level of intracellular chloride concentration ( $[\text{Cl}^-]_i$ ) dictates the polarity of the current through  $\text{GABA}_A$  receptors ( $\text{GABA}_A\text{Rs}$ ). If  $[\text{Cl}^-]_i$  is low, the reversal potential of  $\text{Cl}^-$  ( $E_{\text{Cl}}$ ) becomes negative compared to the resting membrane potential (RMP). In this condition  $\text{GABA}_A\text{Rs}$  mediate an inward  $\text{Cl}^-$  current that results in hyperpolarization of the cell membrane (a). In contrast, high  $[\text{Cl}^-]_i$  results in a positive shift of  $E_{\text{Cl}}$  and leads to an outward  $\text{Cl}^-$  current through  $\text{GABA}_A\text{R}$  and depolarization of the cell membrane that potentially induces action potential firing (c). In conditions where  $E_{\text{Cl}}$  shifts to values similar to RMP, there will be no net  $\text{Cl}^-$  current through  $\text{GABA}_A\text{Rs}$  (b). Adapted from Rahmati et al., 2018.

Mutations or deletions of  $\text{Cl}^-$  channels and transporters in the brain have been linked to genetic disorders, such as particular forms of neonatal seizures and epilepsy, ataxia, hyperekplexia (startle disease), and autism spectrum disorders (Cohen et al., 2002; Vermeer et al., 2010; Pizzarelli et al., 2011; Deidda et al., 2014). In addition, impaired  $\text{Cl}^-$  homeostasis has been associated with pathology of the brain following acute injuries, such as hypoxic-ischemic encephalopathy, brain edema, and post-traumatic seizures (Galeffi, 2004; Jin et al., 2005; Pond et al., 2006; Papp et al., 2008). Therefore, targeting  $\text{Cl}^-$  channels/transporters has been investigated as a therapeutic tool for re-balancing neuronal  $[\text{Cl}^-]_i$  and rescuing the consequential neurological symptoms. One example of such a  $\text{Cl}^-$  based intervention is dampening the elevation of  $[\text{Cl}^-]_i$  following traumatic brain injury (TBI), so as to prevent further neuronal swelling, excitatory GABA signalling, and seizure susceptibility (Annegers et al., 1998; Hung et al., 2012; Goubert et al., 2019). Developing drugs that specifically target  $\text{Cl}^-$  channels or transporters may thereby not only ameliorate the short-term pathological processes induced by TBI, but also

have long-term behavioural consequences ([Rungta et al., 2015](#); [Ben-Ari, 2017](#); [Goubert et al., 2019](#)).

Chloride channels and transporters may become activated in response to membrane potential changes (such as Cl<sup>-</sup>-channels), intracellular Ca<sup>2+</sup> signalling (such as anoctamin-channels), and changes in intracellular pH (SLC4 and SLC26). Although regulated by different actors ([Figure 20](#)), [Cl<sup>-</sup>]<sub>i</sub> mostly relies on cation-chloride co-transporters (CCCs). In fact, Cl<sup>-</sup> is transported across the membrane by CCCs, mainly represented by the Na<sup>+</sup>-K<sup>+</sup>-Cl<sup>-</sup> cotransporter (NKCC1), and K<sup>+</sup>-Cl<sup>-</sup> cotransporters (KCCs). Investigating the impact of such a rich set of widely expressed ion channels/transporters on neuronal functioning is a complex matter because of the heterogeneity of the neuronal populations and the diverse functional interactions of Cl<sup>-</sup> channels/transporters with each other and other ion carriers.

### 1.1.7 KCC2 AND NKCC1

[Cl<sup>-</sup>]<sub>i</sub> is regulated by CCCs in neural cells and it changes during development. The chloride importer NKCC1 and the chloride exporter KCC2 are key regulators of neuronal chloride concentration ([Williamson et al., 1999](#); [John A Payne et al., 2003](#); [Medina et al., 2014](#); [Pisella et al., 2019](#)), which work by accumulating and extruding Cl<sup>-</sup>, respectively. KCC2 is encoded by *Slc12a5* and is exclusively expressed in the plasma membrane of somata and dendrites on pyramidal neurons and interneurons from the hippocampus, neocortex to the spinal cord. It pumps Cl<sup>-</sup> across the plasma membrane out of the cell. In contrast, NKCC1, which is widely expressed in central and peripheral neurons as well as glial cells, is encoded by *SLC12a2* and facilitates uptake of Cl<sup>-</sup> into cells ([Benarroch, 2013](#); [Rahmati et al., 2018](#)). KCC2 is composed of two splice variants: KCC2a and KCC2b. KCC2b is responsible for establishing hyperpolarizing GABA<sub>A</sub> receptor-mediated transmission ([Zhu et al., 2005](#)). NKCC1a and NKCC1b are two highly homologous NKCC1 isoforms. The NKCC1a isoform exhibits mRNA expression primarily in the brain ([Cutler et al., 2002](#)). NKCC1 and KCC2 are comprised of 12 membrane-spanning segments, 6 extracellular loops, and intracellular N- and C-terminals. They differ in the position of regulatory sequences, phosphorylation sites, and long extracellular loops ([Gamba, 2005](#); [Acton et al., 2012](#); [Hartmann et al., 2014](#)). In immature neurons, an age-specific upregulation of NKCC1 and a relative deficiency in KCC2 loads more Cl<sup>-</sup> into the cell, resulting in a

net  $\text{Cl}^-$  outflow and subsequent depolarization when GABA activates  $\text{GABA}_A$ Rs (Figure 22). Conversely, higher KCC2 and less NKCC1 expression results in a net  $\text{Cl}^-$  influx in adult neurons (Plotkin et al., 1997; Dzhala et al., 2005; Löscher et al., 2013). The developmental shift in expression and/or function of NKCC1 and KCC2 has sparked a large number of studies to understand the physiological and pathological mechanisms of this reverse function in GABA. Additionally, cation-chloride cotransporters also regulate cell volume (Kahle et al., 2008). Dysfunction of these cotransporters has been associated with the damaging secondary effects of cerebral edema after ischemic and traumatic brain injury, and in neurodegeneration in the CNS and PNS (Kahle et al., 2008).

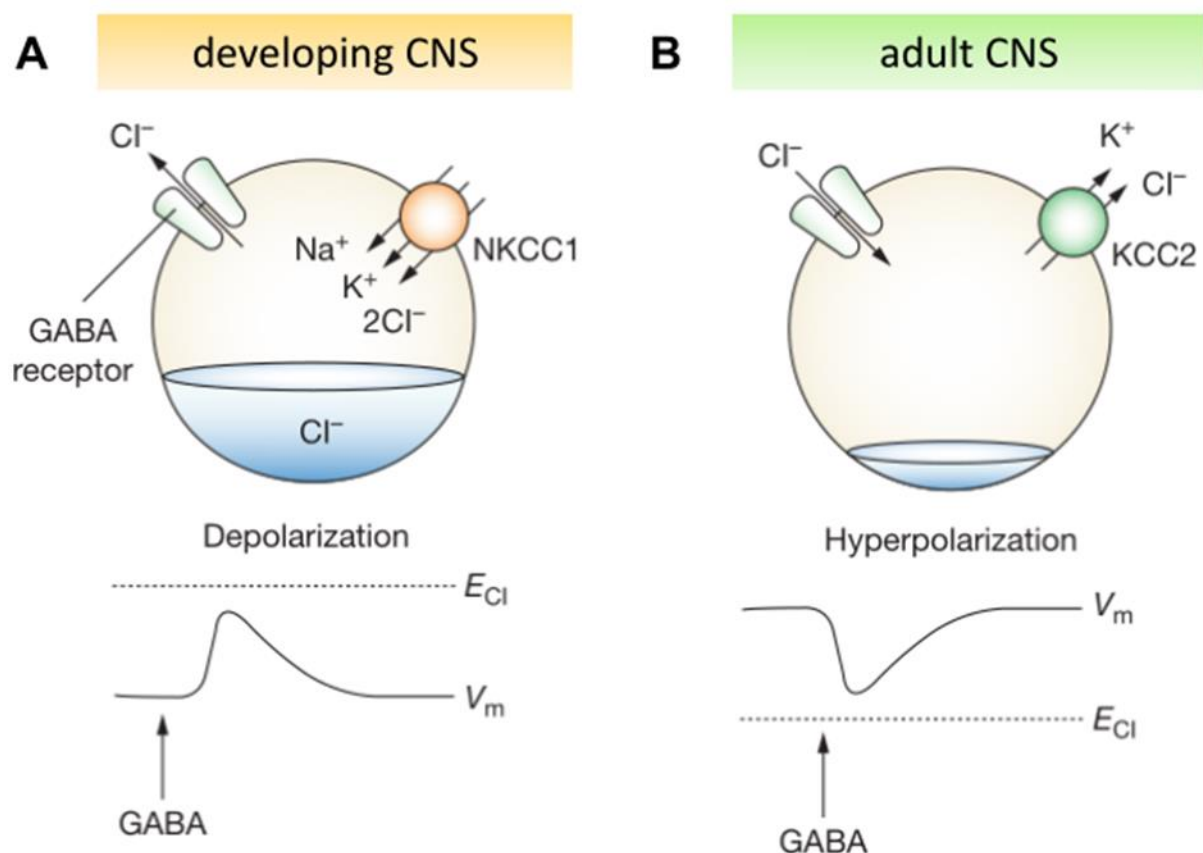


**Figure 22. A developmental switch in cation–chloride cotransporter expression regulates excitatory GABAergic signaling in the developing CNS and inhibitory GABAergic signaling in the adult CNS. A.** During embryonic and early postnatal life, immature hippocampal and spinal neurons express chloride-intruding Na–K–2Cl cotransporter NKCC1 higher than chloride-extruding K–Cl cotransporter KCC2. Owing to high activity of NKCC1 and minimal activity of KCC2,  $[\text{Cl}^-]_i$  is high, and  $E_{\text{Cl}}$  is positive relative to the  $V_m$  of the neuron. When  $[\text{Cl}^-]_i$  is high, opening of chloride channels by  $\text{GABA}_A$ -receptor activation results in chloride efflux, thereby depolarizing and exciting the neuron. **B.** During neuronal maturation, NKCC1 activity decreases and KCC2 activity increases. KCC2 maintains a low  $[\text{Cl}^-]_i$ , and the  $E_{\text{Cl}}$  is negative relative to the  $V_m$ . Therefore, activation of the  $\text{GABA}_A$  receptors results in chloride influx, hyperpolarization and inhibition of the neuron.  $[\text{Cl}^-]_i$ , intracellular chloride concentration;  $E_{\text{Cl}}$ , equilibrium potential for chloride;  $V_m$ , membrane potential; GABA,  $\gamma$ -aminobutyric acid. Adapted from Kahle et al., 2008.

In neurons, NKCC1 and KCC2 (*Miho Watanabe et al., 2015*) are key regulators of  $[Cl^-]_i$  (**Figure 23**). The fine regulation of  $[Cl^-]_i$  by NKCC1 and KCC2 is essential for brain development, including cell proliferation and apoptosis, and neuronal migration and maturation (*Peerboom et al., 2021*). Moreover, NKCC1 and KCC2 are key for neuronal synaptic plasticity and for maintaining a proper excitatory/inhibitory balance, which is fundamental for brain functions (*Peerboom et al., 2021*).

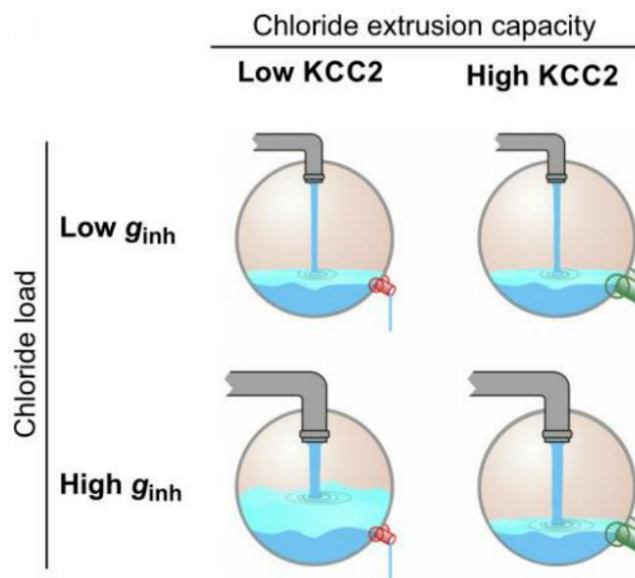


**Figure 23. Relationship between  $[Cl^-]_i$  and  $Cl^-$  load (NKCC1 activity), KCC2 activity.** Relationship between  $Cl^-$  load, KCC2 activity, and  $[Cl^-]_i$ . High  $[Cl^-]_i$  results from a combination of low  $Cl^-$  extrusion capacity (left) and high  $Cl^-$  load (bottom). Low  $Cl^-$  load coupled with low  $Cl^-$  extrusion capacity (top left) or high  $Cl^-$  load coupled with high  $Cl^-$  extrusion capacity (bottom right) will both yield low  $[Cl^-]_i$ . Adapted from Doyon et al., 2016.

Among the cation-chloride cotransporter gene family, the  $K^+-Cl^-$  cotransporters exhibit the greatest genetic diversity. Four distinct isoforms of the  $K^+-Cl^-$  cotransporter have been identified, KCC1 (Slc12a4), KCC2 (Slc12a5), KCC3 (Slc12a6) and KCC4 (Slc12a7). In brains of new-born mice, transcript expression of KCC2a and KCC2b are similar. Upon postnatal development, however, KCC2b is steeply up-regulated whereas KCC2a is not (*Uvarov et al., 2007*). KCC2b appears to be the predominant variant in the mature rodent cortex. KCC2a exhibits significant levels of mRNA expression in the brainstem and spinal cord during prenatal and early postnatal development, indicating it may play an important developmental role in these CNS regions. Structure–function studies have examined some unique operational and

structural features of KCC2, which had a large extended region in the carboxy-terminus, exhibiting little identity with the other KCCs (Figure 24).

Three phosphoacceptor sites were identified in the N-terminal domain of the protein NKCC1: Thr189 is necessary for activation of the protein, whereas phosphorylation at Thr184 and Thr202 are modulatory (Darman *et al.*, 2002). Phosphorylation of S940 (Silayeva *et al.*, 2015) and dephosphorylation of T906/T1007 (Moore *et al.*, 2018; M. Watanabe *et al.*, 2019) are essential for the potentiation of KCC2 activity. In contrast, phosphorylation of T906/T1007 residues reduces KCC2 membrane expression which can lead to spine swelling (M. Heubl *et al.*, 2017), thereby affecting both GABA signaling and dendritic spine morphology.

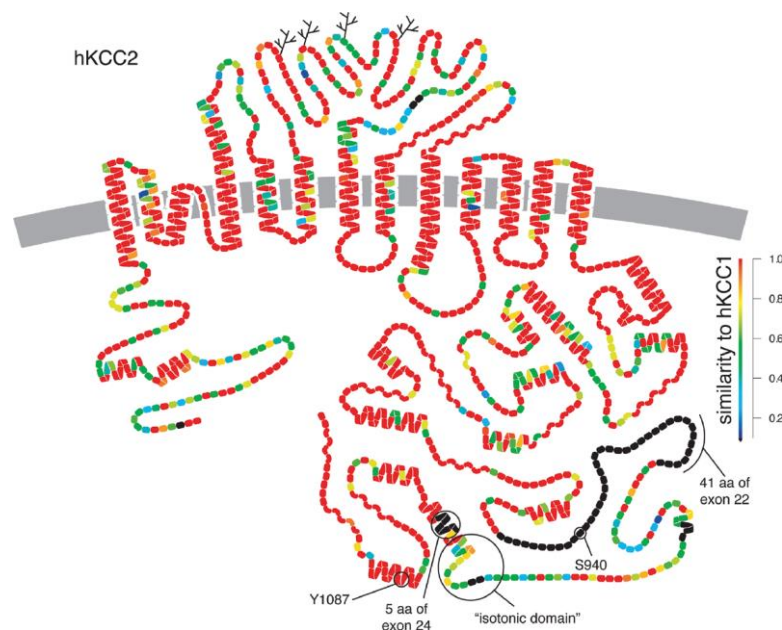


**Figure 24. Hypothetical structural model of the  $K^+$ - $Cl^-$  cotransporter.** Human KCC2 (hKCC2) and human KCC1 (hKCC1) are compared to one another by colors that indicate the degree of similarity on a per residue basis: red residues are identical and black residues are absent from hKCC1. The branched lines are potential N-linked glycosylation sites between putative transmembrane segments 5 and 6. Predicted secondary structural elements are shown as helices for predicted alpha-helix and wavy lines for predicted beta-sheet. A reentrant loop between putative transmembrane segments 2 and 3 has been predicted for NKCC2 and is shown for KCC2. Adapted from Payne 2009.

## 1.2. ALS: AN UNCURABLE DISEASE

Amyotrophic lateral sclerosis (ALS) is a fatal adult-onset neurodegenerative disease characterized by progressive muscular weakness and atrophy due to degeneration of corticospinal motor neurons in the brain and spinal motoneurons (MNs). Upper motor neurons are glutamatergic descending neurons that synapse directly or indirectly *via* interneurons onto lower MNs typically through the

corticobulbar and corticospinal tracts. Lower MNs are multipolar cholinergic neurons whose axons exit the CNS to innervate skeletal muscles to produce movement. Consequently, ALS leads to progressive muscle atrophy and weakness and eventual paralysis (Figure 25). In fact, the name “Amyotrophic Lateral Sclerosis” reflects the strikingly selective degeneration of MNs in ALS. It is derived from a combination of three words: “Lateral” refers to the lateral spinal cord, given that corticospinal MNs are particularly vulnerable to degeneration; “Amyotrophic” is from the Greek “amyotrophia,” meaning lacking muscle nourishment; and “Sclerosis” (fibrosis) refers to gliosis of the crossed corticospinal tract in the dorsolateral quadrant of the spinal cord (J.-M. Charcot, 1874; Frey et al., 2000; Pun et al., 2006).

Sir Charles Bell, an Edinburgh surgeon (Martin R Turner et al., 2015), first discovered the clinical features of ALS in the mid-19th century. In 1862, Charles Radcliffe and Lockhart Clarke further classified the disease as a nerve-based disease consisting of paralysis and muscular atrophy (Martin R Turner et al., 2015). In 1874, Jean-Martin Charcot, a French neurologist, bridged the knowledge gap between patient symptoms and neurological presentations and officially named the disease amyotrophic lateral sclerosis (Martin R Turner et al., 2015). However, in the decades since that time, neurologists and clinical researchers have been mystified and challenged to solve the puzzle to the disease’s pathogenesis, aetiology, and epidemiology. Over time, neurologists gradually improved the diagnostic procedures and attempted to understand ALS pathology, but, because ALS has not been well understood and was virtually unknown to the public (Martin R Turner et al., 2015), it was not until 1990 that researchers developed a uniform diagnostic procedure (Geevasinga et al., 2019).

In 1939, the famous New York Yankee baseball player, Lou Gehrig, was diagnosed with ALS and delivered his famous farewell speech at Yankee Stadium (Smith, 2015), bringing the disease out of obscurity. Later, the disease would become informally known in the United States as Lou Gehrig’s disease. In 1963, Stephen Hawking, a 21-year-old doctoral student, was diagnosed and became a public face for ALS as he completed his doctorate, made groundbreaking scientific discoveries, and taught cosmology and physics (Smith, 2015). As the longest recorded ALS survivor, Hawking contributed a lifetime of scientific publications,

inspirational documentaries, and television show appearances, which sparked an awareness movement for the ALS community.

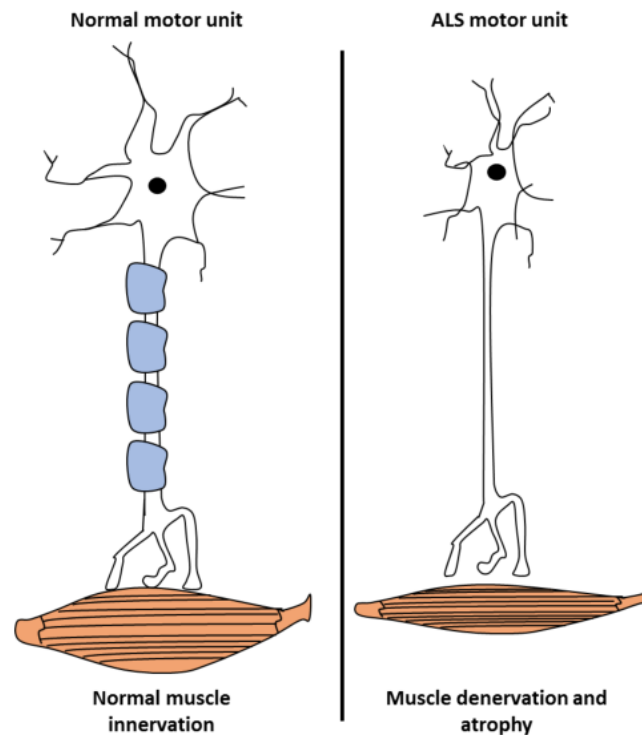


**Figure 25: Amyotrophic lateral sclerosis: muscle denervation and atrophy upon lower MNs loss.** Note the loss of the myeline sheath in ALS MNs. From Hajer EL OUSSINI-BEN CHAABANE's PhD manuscript, 2016.

Within the last decade, other well-known people with ALS have established non-profit organizations to raise funds for ALS medical research and patient services. Steve Gleason, a retired New Orleans Saints football player who was diagnosed with ALS in 2011, started a non-profit organization, the Team Gleason Foundation ([Moustafa, 2018](#)). The Gleason Foundation has granted people with ALS with end of life adventure trips, speech and eye gaze equipment, and has advocated for law reform to leverage biotechnology and assistive technology in people with ALS' favor ([Moustafa, 2018](#)). Hope Loves Company is a non-profit organization that teams with Young Men's Christian Association (YMCA) camps throughout the country to provide healing experiences and emotional support to children who have parents or grandparents with ALS ([O'Donnell-Ames, 2008](#)). In 2014, the ALS Ice Bucket Challenge (IBC), a ground-breaking social media fundraising phenomenon, significantly increased ALS public awareness and raised over \$115 million within eight weeks for the ALS Association and over \$220 million globally for ALS medical

research ([Sohn, 2017](#)). Since the IBC, hundreds of people have established fundraising efforts and non-profit organizations geared toward funding research for an ALS cure.

While medical research efforts have increased dramatically since the IBC, social researchers have not followed the same trajectory to inform social welfare and clinical interventions for people with ALS. Many organizations, including the ALS Association, a nationwide ALS helping organization, was established in the United States in 1985 ([Stephens et al., 2015](#); [Ward et al., 2015](#)), have attempted to expand their resources and diversify their clinical research and investment portfolios. Nevertheless, given the history of ALS being an untreatable and incurable disease that kills tens of thousands of people throughout the world every year, many people with ALS, ALS advocates, and allies are growing impatient for clinical progress ([K. Traynor, 2018](#)). Given that it is unknown when researchers will find a cure, increased financial emphasis in social research is needed to guide social programs that help people with ALS and their families adaptively cope with the emotional and mental health challenges associated with this disease.

ALS, also known as Lou Gehrig's or Charcot disease, was first described by Jean-Martin Charcot in 1874 ([Rowland, 2001](#)). ALS is a progressive motor neuron disease in which motor neurons die in the motor cortex, brain stem, and spinal cord ([Boillée et al., 2006](#)). Two forms of ALS have been identified; sporadic ALS (sALS) and familial ALS (fALS) ([Harikrishnareddy et al., 2015](#)). Almost 90% of ALS patients suffer from the sporadic form and only 10% patients suffer from the familial form ([Harikrishnareddy et al., 2015](#)). In general, recent studies have shown that the incidence of ALS is lower in Asian countries than in Europe and North America ([Longinetti et al., 2019](#)). Two to three people suffer from ALS per 100,000 of the general European populations using the person-year calculation ([Al-Chalabi et al., 2013](#); [Longinetti et al., 2019](#)). The incidence rate of ALS is higher in males than in females, possessing a risk ratio of 1:350 and 1:400 for males and females respectively ([Al-Chalabi et al., 2013](#)). ALS is a fatal disorder in which most patients do not survive more than 3 to 5 years following diagnosis ([Wijesekera et al., 2009](#)). Despite decades of research, riluzole ([Bensimon et al., 1994](#)) and edaravone ([Abe et al., 2014](#)) remain the only drugs approved by Food and Drug Administration,

however both have limited efficacy on ALS patients. Riluzole is a drug that blocks the persistent sodium current, likely reducing the chronic glutamate excitotoxicity. Edaravone is a scavenger of peroxy radicals and peroxynitrites that promotes cell survival against oxidative stress and potentially inhibits apoptosis. There is an urgent need of more effective drugs for the treatment of this incurable disorder. The hallmark of ALS is the presence of lower and upper motor neuron signs and symptoms. ALS can present with four different types of onset: limbic onset, bulbar onset, primary lateral sclerosis and progressive muscular atrophy ([Matthew C. Kiernan et al., 2011](#); [Al-Chalabi et al., 2013](#)). In limbic onset, voluntary muscles of both upper and lower limbs are affected causing muscles weakness, fasciculation, spasticity, wasting and tendon reflexes. Bulbar onset is mainly characterised by difficulty in speaking, breathing and swallowing. Primary lateral sclerosis and progressive muscular atrophy involve dysfunction in the upper and lower motor neurons, respectively.

The disease mechanism in ALS is a complex process involving multiple factors. Despite numerous studies, disease pathogenesis in ALS is still not clear. Gene mutation, epigenetic regulation and environmental exposure have been associated with ALS causes ([Paez-Colasante et al., 2015](#)). Gene mutation is considered one of the major reasons for the occurrence of fALS. Mutation in genes such as C9orf72, SOD1, TARDBP (TDP-43) and FUS occur frequently, however mutation in 40 other genes have also been associated with ALS ([Al-Chalabi et al., 2017](#)). Among all genetic mutations, mutation in C9orf72 is the most common, accounting for 40-50% of total familial cases. Mutation in SOD1 accounts for 20% of fALS, TARDBP and FUS account for 1-5% of fALS, and ANG accounts for <1% of fALS ([Robberecht et al., 2013](#)). Although genetic mutation is closely associated with fALS, studies conducted in monozygotic twins discovered an association of epigenetic regulation such as deoxyribonucleic acid (DNA) methylation, histone remodeling, ribonucleic acid (RNA) editing and non-coding RNAs in ALS patients with no family history of ALS ([Paez-Colasante et al., 2015](#)). Along with genetic contribution, different environmental factors are also known to contribute in the onset of ALS ([Al-Chalabi et al., 2013](#)).

### 1.2.1 SOD1<sup>G93A</sup> AND OTHER ALS ANIMAL MODELS

At least 25 genes have now been reproducibly implicated in familial ALS, sporadic ALS, or both (Figure 26). The SOD1 gene was the first gene identified as the genetic cause of ALS (Rosen et al., 1993). The SOD1 gene is located on chromosome 21 in humans. Five exons in this chromosome encode the Cu-Zn superoxide dismutase-1 (SOD1) subunit, a protein consisting of 153 amino acids, which when bound with copper and zinc forms a SOD1 homodimer (B. Turner et al., 2008). The dimeric form of SOD1 acts as an antioxidant, metabolising the toxic radical superoxide to molecular oxygen and hydrogen peroxide (Rosen et al., 1993; Kaur et al., 2016). Mutations in the SOD1 gene result in conformational instability of the protein, which leads to the formation of large intracellular protein aggregates that contribute to motor neuron death (Lucie I. Bruijn et al., 1998).

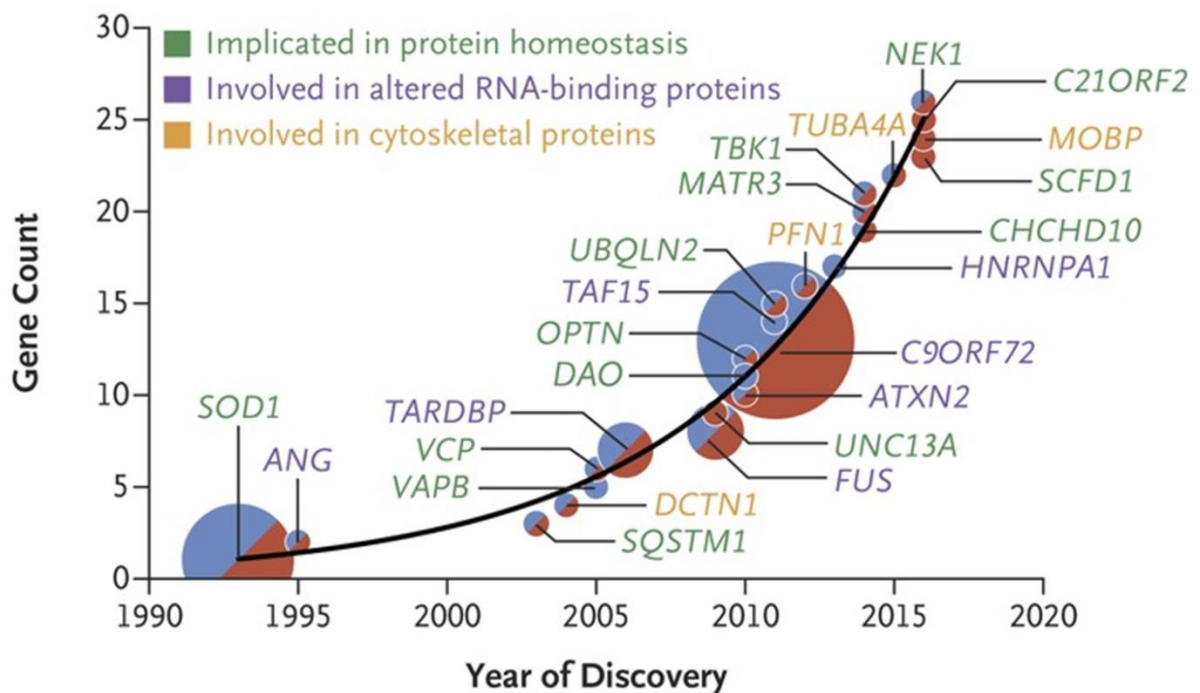


**Figure 26. ALS Gene Discovery since 1990.** The size of each circle reflects the proportion of all familial ALS cases associated with that gene (e.g., 20% for SOD1 and 45% for C9ORF72). Blue circles indicate genes associated only with familial ALS, red circles indicate genes associated only with sporadic ALS, and circles that are half blue and half red indicate genes associated with both familial and sporadic ALS. Each of these genes has been found to be mutated in more than one ALS-affected family or in multiple, unrelated cases of sporadic ALS. From Brown et al., 2017.

Some 130 mutations, such as G93A, G37R, and G85R, occur in the SOD1 gene (Al-Chalabi et al., 2017), among which the G93A missense mutation is the most studied. The G93A mutation results in the substitution of the glycine residue at position 93 by an alanine residue in the SOD1 subunit (Kaur et al., 2016). Following the discovery of this mutation in ALS, a number of rodent models of ALS

overexpressing human mutant SOD1 (mSOD1) have been developed that resembles human ALS (*B. Turner et al., 2008*). However, the deletion of SOD1 gene failed to develop ALS-like phenotype in mice (*Reaume et al., 1996*), which suggest that mutant SOD1 cause toxicity by gain of other pathogenic mechanisms rather than loss of enzymatic function of SOD1. The transgenic mice and rat models have been important tools to further understand early and late pathophysiological mechanisms associated with mSOD1 and to evaluate potential therapeutic strategies in ALS (*McGoldrick et al., 2013*).

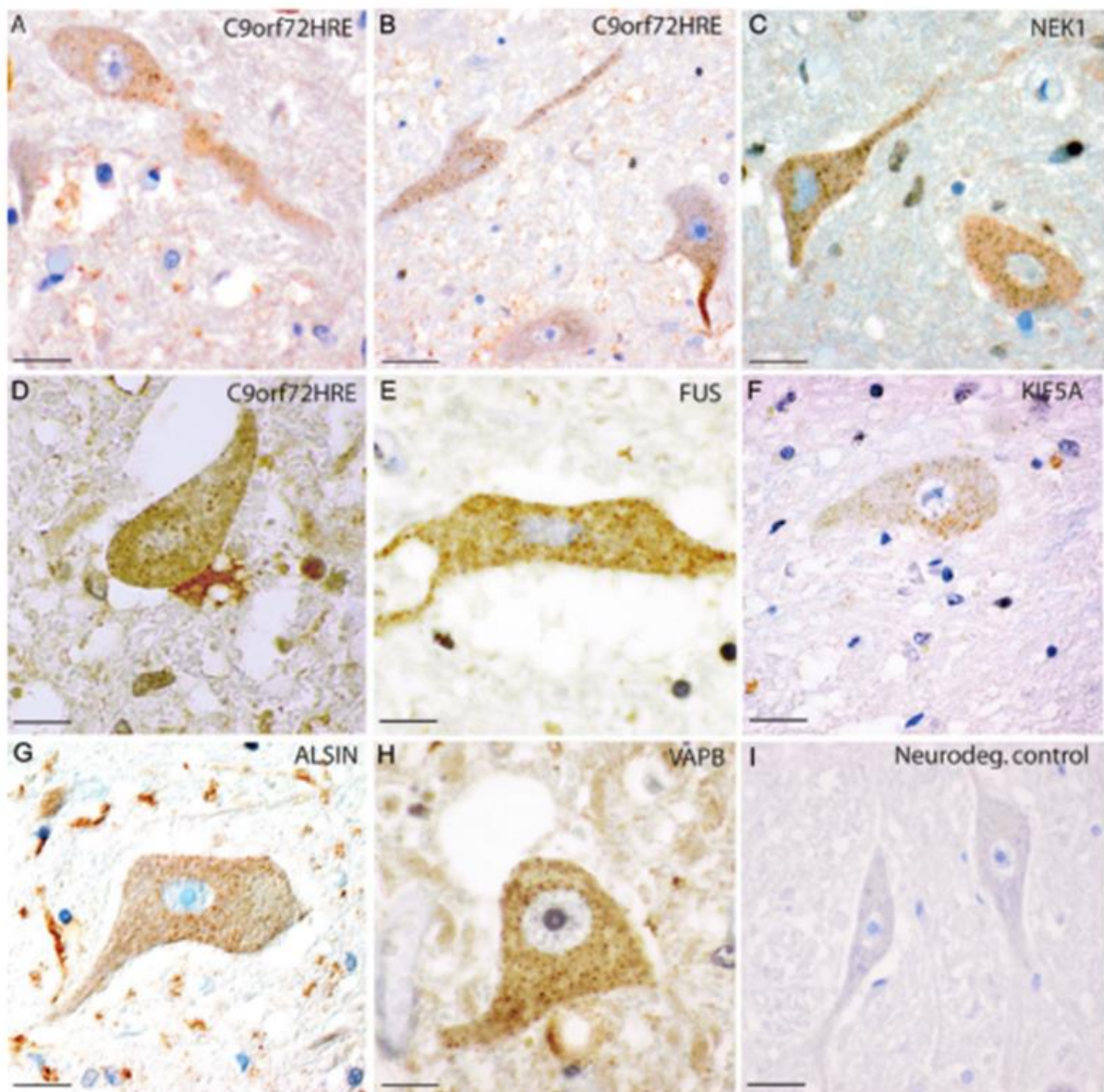


**Figure 27. Typical pathological hallmark features of ALS in human patients.** Affected spinal MNs accumulate small dot-like granular aggregated proteins (**inclusions**) in spinal cord sections of misSOD1<sup>WT</sup> patients with mutations in six ALS-associated genes: C9orf72HRE (**A–B**, cases #2 and #8), NEK1 (**C**), C9orf72HRE (**D**, cases #16), FUS (**E**), KIF5A (**F**), ALSIN (**G**), VAPB (**H**). In patients with different SOD1 gene mutations, affected spinal MNs accumulate larger or skein-like inclusions (images not shown here). Adapted from Forsberg et al., 2019.

A hallmark pathology of ALS is protein deposition and inclusion formation within motor neurons and/or motoneurons (MNs) (Figure 27). Study of the mSOD1 mouse model reveals a number of cell and non-cell autonomous mechanisms that are involved in the pathophysiology of ALS (Figure 28). Cell autonomous mechanisms include changes within motor neurons such as axonal transport defects, mitochondrial dysfunction, increased endoplasmic reticulum (ER) stress, glutamate toxicity and caspase activation, abnormal RNA metabolism and impaired proteostasis (Soo et al., 2015; Mathis et al., 2017). Non-cell autonomous mechanisms include neuroinflammation centrally mediated by astrocytes and microglia (Hooten et al., 2015) and oligodendrocytes that develop spontaneous neuroinflammation, or/and involve peripherally (Schwann cells, skeletal myocytes, and T - cells) acting contributors to the survival of MNs (Taylor et al., 2016). Overall, both cell and non-cell autonomous mechanisms contribute to motor neuron death in ALS.

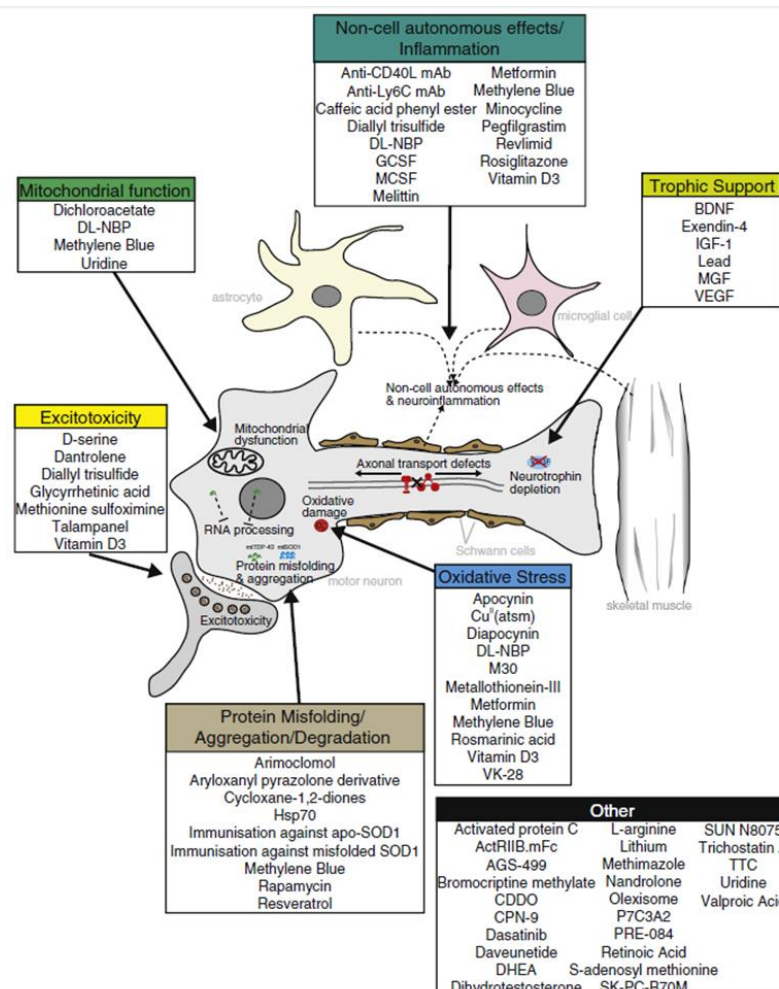


**Figure 28. ALS pathomechanisms and targets tested in recent preclinical trials in rodents.** ALS pathophysiology encompasses both cell and non-cell autonomous mechanisms. From McGoldrick et al., 2013.

Despite the above and other knowledge in disease mechanisms leading to ALS, the primary factors that trigger ALS remain unknown. Findings from studies in mSOD1 mice suggest that mSOD1 in motor neurons initiate toxic actions, which in combination with non-neuronal cells also possessing mSOD1, accelerates motor neuron death and disease progression. Initially, two studies failed to demonstrate ALS in transgenic mice such as SOD1<sup>G37R</sup>, SOD1<sup>G93A</sup>, SOD1<sup>G85R</sup> specifically expressing mSOD1 in neurons ([Pramatarova et al., 2001](#); [Lino et al., 2002](#)). In contrast, in a third study, SOD1<sup>G93A</sup> transgenic mice overexpressing mSOD1 selectively in neurons developed ALS ([Jaarsma et al., 2008](#)). In another study, disease onset in chimeric SOD1<sup>G37R</sup> mice was accelerated when mSOD1 was present in cells other than motor neuron cells ([Yamanaka et al., 2008](#)). Conversely, the presence of wild-type non-neuronal cells substantially delayed disease onset in chimeric SOD1<sup>G37R</sup> and SOD1<sup>G85R</sup> mice ([Clement et al., 2003](#); [Yamanaka et al., 2008](#)). Similarly, in transgenic SOD1<sup>G93A</sup> mice, wild-type microglia slowed motor neuron loss and prolonged disease duration and survival compared to mice possessing mSOD1 expressed microglia ([Beers et al., 2006](#)). Together, these findings clarify that the presence of mSOD1 promotes motor neuron loss by both cell and non-cell autonomous processes in transgenic mSOD1 mice.

Following motor neuron death, mSOD1 aggregates are released into the extracellular environment to provide a positive feedback loop to further induce motor neuron death ([Brundin et al., 2010](#)). These extracellular mSOD1 aggregates are not directly toxic to motor neurons, but rather activate microglia, which then mediate neurotoxicity. SOD1 aggregates in the extracellular space are taken up by neighbouring cells via micropinocytosis or in association with vesicles ([Zeineddine et al., 2015](#); [Silverman et al., 2016](#)). In vitro studies have demonstrated that the extracellular mSOD1 cause detectable injury to motor neurons when co-cultured with microglia, but had no effect on motor neurons in the absence of microglia ([W. Zhao et al., 2010](#)).

Over the last 20 years, several transgenic mouse strains expressing human mutant SOD1 have been generated. These mice have been used to either examine disease mechanisms or trial potential therapeutic strategies for ALS, although the latter has led to questionable success ([Perrin, 2014](#)). The transgenic line harboring

the Gly93 → Ala substitution (SOD1<sup>G93A</sup>) has been used most extensively (*M. E. Gurney, Pu, Chiu, Dalcanto, et al., 1994*), followed by the SOD1<sup>G37R</sup> (*Wong et al., 1995*), SOD1<sup>G85R</sup> (*L.I. Bruijn et al., 1997*), SOD1<sup>G86R</sup> (*Ripps et al., 1995*) and SOD1<sup>G90A</sup> (*Jonsson et al., 2006*) models.

The B6SJL-TgN(SOD1-G93A)1Gur mouse (*M. E. Gurney, Pu, Chiu, Dalcanto, et al., 1994*) carries  $25 \pm 1.5$  copies of the transgene within chromosome 12 and as a result, it expresses very high levels of human mutant SOD1<sup>G93A</sup> (*Alexander et al., 2004*). Whilst these significant levels of overexpression are criticized as a major limitation (*Alexander et al., 2004*), these animals remain the most widely used mouse model for therapeutic studies in ALS (*M. E. Gurney, Pu, Chiu, Dalcanto, et al., 1994*). These SOD1<sup>G93A</sup> mice become paralyzed in the hindlimbs as a result of MN loss from the spinal cord, resulting in death by 5 months of age. Another variant of this model, B6SJL-TgN(SOD1-G93A)dl1Gur, possesses fewer copies of the transgene;  $8 \pm 1.5$  (*Mark E Gurney, 1997; Alexander et al., 2004*). This “low-copy” mouse, hereafter referred to as “G93A-slow” (s-SOD1<sup>G93A</sup>), develops a slower disease course in comparison, where paralysis begins at 6–8.5 months of age (*Alexander et al., 2004; F. L. Muller et al., 2008; Acevedo-Arozena et al., 2011*). In addition, several other “low-copy” mouse lines have subsequently been generated, with even fewer copies of the human SOD1G93A transgene. These models also exhibit greater life spans compared to the higher copy lines (*Alexander et al., 2004*). Similarly, four lines of mice expressing another SOD1 mutant, SOD1G37R, at different levels (5–14 times) have been produced, with variable phenotypes (*Wong et al., 1995*). Multiple mouse models based on transgenic expression of wild type or mutant TDP-43 have also been generated (*Philips et al., 2015*). Overexpressing human TDP-43 with a defective nuclear localization signal (NLS) in mice in the absence of an ALS mutation results in cytoplasmic expression of hTDP-43 and nuclear TDP-43 clearance. This results in a severe motor phenotype and reduced survival in the resulting ‘rNLS8’ mice compared to littermate controls (*Walker et al., 2015*). Several mouse models also exist based on transgenic expression of mutant FUS. These mice display progressive, age- and mutation-dependent degeneration that also model aspects of ALS (*A. Sharma et al., 2016*). Furthermore, several newer models based on the C9orf72 repeat expansion have

also been produced, although the phenotypes are more reminiscent of FTD rather than ALS ([Batra et al., 2017](#)).

The pathomechanisms caused by *C9orf72* repeat expansions are increasingly understood. A GGGGCC hexanucleotide repeat expansion in intron 1 of chromosome 9 open reading frame 72 (*C9ORF72*) gene is the most common genetic cause of and frontotemporal dementia. Repeat-associated non-ATG translation of dipeptide repeat proteins (DPRs) contributes to the neuropathological features of c9FTD/ALS. Among the five DPRs, arginine-rich poly-PR are reported to be the most toxic. A study by Maor-Nof and colleagues elucidated how the dipeptide protein poly-proline-arginine (poly-PR), which is generated from the repeat expansion, induces apoptotic pathways and, ultimately, neurodegeneration by epigenetic modulation of gene transcription via the transcription factor p53, thereby indicating nucleoporin p54 ablation as a novel therapeutic strategy ([Maor-Nof et al., 2021](#)). Hao and colleagues generated a mouse model that the transgenic animals specifically expressed poly-PR (GFP-PR<sub>28</sub>), but without repeat RNA in neurons driven by Thy1 promoter. The GFP-PR<sub>28</sub> homozygous mice showed reduced body size, decreased body weight, and reduced premature survival. GFP-PR<sub>28</sub> heterozygous mice showed motor deficits, especially in progressive gait and balance impairment. Consistent with abnormal behaviours that are associated with the cerebellum, loss of Purkinje cells, but not hippocampal neurons, were presented in GFP-PR<sub>28</sub> heterozygous mice. Moreover, microglia and astrocytes in the cerebellum and lumbar spinal cord of GFP-PR<sub>28</sub> heterozygous mice were significantly activated. Finally, the poly-PR expressing neurons developed synaptic transmission-related genes dysregulation. These data demonstrated that GFP-PR<sub>28</sub> transgenic mice partly model neuropathological features of c9FTD/ALS ([Z. Hao et al., 2019](#)). However, BIIB078, an investigational antisense oligonucleotide for *C9orf72*-associated ALS, did not show clinical benefit in Phase 1 study. This clinical program was discontinued in March 2022 (<https://investors.biogen.com/news-releases/news-release-details/biogen-and-ionis-announce-topline-phase-1-study-results>).

Since its discovery as a primary component in cytoplasmic aggregates in post-mortem tissue of patients with ALS, the identification of mutations in TAR DNA Binding Protein 43 kDa (TARDBP, encoding TDP-43) have provided crucial insight

into common pathogenic themes in ALS ([Kabashi et al., 2008](#); [J. Sreedharan et al., 2008](#); [Van Deerlin et al., 2008](#); [Pesiridis et al., 2011](#)). TDP-43 links both familial and sporadic forms of ALS as mutations are causative for disease and cytoplasmic aggregates are a hallmark of nearly all cases, regardless of TDP-43 mutational status. Research has focused on the formation and consequences of cytosolic protein aggregates as drivers of ALS pathology through both gain- and loss-of-function mechanisms. Not only does aggregation sequester the normal function of TDP-43, but these aggregates also actively block normal cellular processes inevitably leading to cellular demise in a short time span. TDP-43 pathology appears to be tightly linked with its mislocalization from the nucleus to the cytoplasm, making it difficult to decouple the consequences of nuclear-to-cytoplasmic mislocalization from protein aggregation. Studies focusing on the effects of TDP-43 mislocalization have demonstrated both gain- and loss-of-function consequences including altered splicing regulation, over responsiveness to cellular stressors, increases in DNA damage, and transcriptome-wide changes. Additionally, mutations in TARDBP confer a baseline increase in cytoplasmic TDP-43 thus suggesting that small changes in the subcellular localization of TDP-43 could in fact drive early pathology ([Suk et al., 2020](#)). Certainly, early events in TDP-43 pathogenesis (i.e., to the protein mislocalization stage) will provide insight into disease mechanisms, therapeutic targets, and novel biomarkers for ALS.

Fused in sarcoma (FUS) is a DNA/RNA binding protein containing 526 amino acids. The *FUS* gene was initially identified as a fusion oncogene on chromosome 16 in human liposarcoma ([Croizat et al., 1993](#)), the translocation and fusion of which to transcription factors results in strong transcriptional activation of the proteins. FUS is one of the components of the heterogeneous nuclear ribonucleoprotein (hnRNP) complex. Increasing evidence suggests that FUS is involved in various cellular processes, including gene transcription and regulation, DNA repair, RNA shearing, RNA transport, translation, processing of microRNAs, and maintenance of genomic stability ([Lagier-Tourenne et al., 2010](#)). FUS is genetically and pathologically involved in frontotemporal lobar degeneration (FTLD)/ALS. Multiple lines of evidence across diverse models suggest that functional loss of FUS can lead to neuronal dysfunction and/or neuronal cell death. Loss of FUS in the nucleus can impair alternative splicing and/or transcription, whereas dysfunction of FUS in the cytoplasm,

especially in the dendritic spines of neurons, can cause mRNA destabilization. Alternative splicing of the MAPT gene at exon 10, which generates 4-repeat Tau (4R-Tau) and 3-repeat Tau (3R-Tau), is one of the most impactful targets regulated by FUS. Additionally, loss of FUS function can affect dendritic spine maturation by destabilizing mRNAs such as Glutamate receptor 1 (GluA1), a major AMPA receptor, and Synaptic Ras GTPase-activating protein 1 (SynGAP1). Moreover, FUS is involved in axonal transport and morphological maintenance of neurons. These findings indicate that a biological link between loss of FUS function, Tau isoform alteration, aberrant post-synaptic function, and phenotypic expression might lead to the sequential cascade culminating in FTL (Ishigaki et al., 2018).

The first generation of transgenic pigs expressing mutant G93A hSOD1 was reported (Yang et al., 2014). This model shows hind limb motor defects, which are germline transmissible, and motor neuron degeneration in dose- and age-dependent manners. Importantly, in the early disease stage, mutant hSOD1 did not form cytoplasmic inclusions, but showed nuclear accumulation and ubiquitinated nuclear aggregates, as seen in some ALS patient brains, but not in transgenic ALS mouse models. SOD1 binds PCBP1, a nuclear poly(rC) binding protein, in pig brain, but not in mouse brain, suggesting that the SOD1-PCBP1 interaction accounts for nuclear SOD1 accumulation and that species-specific targets are key to ALS pathology in large mammals and in humans. Another transgenic (Tg) cloned swine model expressing the human pathological hSOD1G93A allele was reported (Crociara et al., 2019). As in patients, these Tg pigs transmitted the disease to the progeny with an autosomal dominant trait and showed ALS onset from about 27 months of age. Post mortem analysis revealed MN degeneration, gliosis and hSOD1 protein aggregates in brainstem and spinal cord. Severe skeletal muscle pathology including necrosis and inflammation was observed at the end stage, as well. Remarkably, as in human patients, these Tg pigs showed a quite long presymptomatic phase in which gradually increasing amounts of TDP-43 were detected in peripheral blood mononuclear cells. Thus, these transgenic swine models open the unique opportunity to investigate ALS biomarkers even before disease onset other than testing novel drugs and possible medical devices (Figure 28).

## 1.2.2 PATHOPHYSIOLOGY OF ALS

ALS is a rapidly progressive neurodegenerative disorder of the human motor system, clinically characterized by dysfunction of the upper and lower motor neurons, which forms the basis of diagnosis (*J. Charcot et al., 1869; Brooks et al., 2000; Geevasinga et al., 2016*). While disease onset is typically focal involving upper or lower limbs, bulbar or respiratory regions, the ensuing progressive course affects contiguous body regions resulting in global muscle weakness, with respiratory dysfunction representing a terminal phase of the disease (*Steve Vucic et al., 2014; Dharmadasa et al., 2017*). Understanding the relationship between upper and lower motor neuron dysfunction is critical for unravelling ALS pathogenesis and three opposing theories have been proposed (*Eisen et al., 2017*). A first school of thought suggested that ALS originates at a cortical level, with corticomotoneuronal hyperexcitability mediating neuronal degeneration via a transsynaptic anterograde mechanism, the dying forward hypothesis (*Eisen et al., 1992*). A second school of thought proposed a contrasting theory, whereby lower motor neuron dysfunction was postulated to occur as a primary event, the dying back hypothesis (**Figure 29**) (*Williamson et al., 1999; Fischer et al., 2004*). A third school of thought, the independent hypothesis, proposed an independent and random degeneration of upper and lower motor neuron degeneration with patterns of disease spread being contiguous and random, conforming to underlying neuroanatomical boundaries (*J. Ravits et al., 2007; J. M. Ravits et al., 2009*).

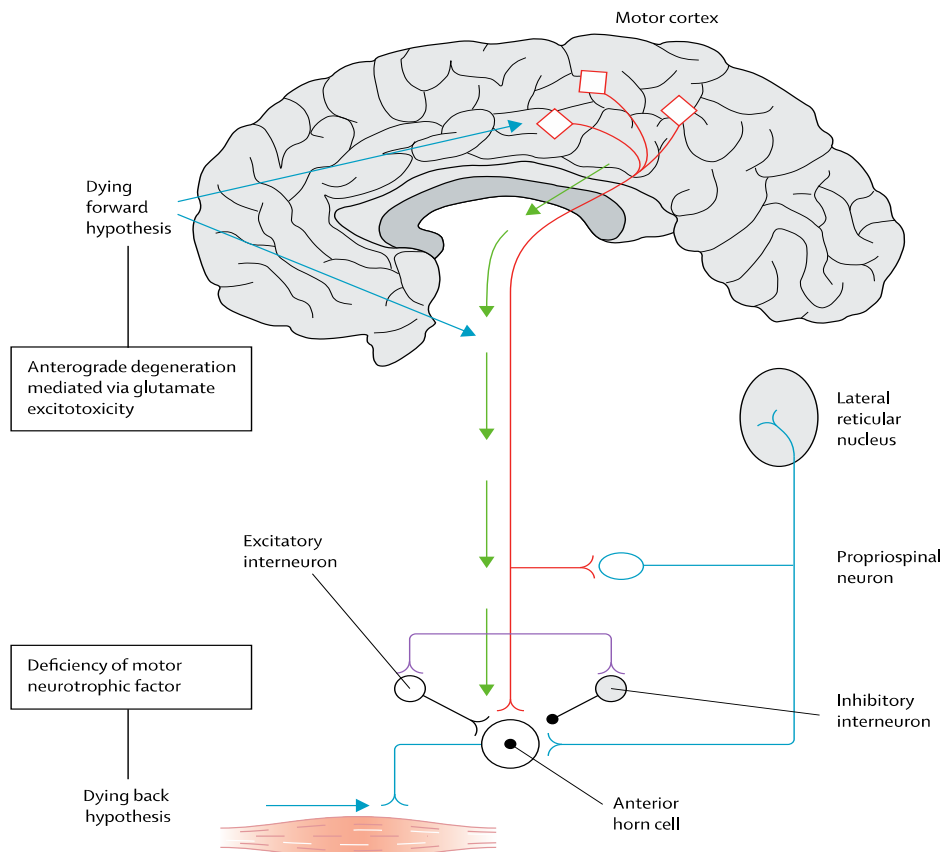


**Figure 29. The “dying-forward” and “dying-back” hypotheses.** The “dying-forward” hypothesis postulates that ALS commences in the motor and pre-motor cortices’ pyramidal neurons and, through anterograde mechanisms, causes dysfunction and death of the bulbar and spinal MNs. Excitotoxicity is important but not the only factor. The hallmark TAR DNA-binding protein 43 (TDP-43) pathology, seen in >95% of patients with ALS, is largely restricted to corticofugal projecting neurons (“dying forward”). In broader terms, this site of origin may be considered as the nidus of a spreading network disorder associated with frontotemporal dementia in ALS. In any event, ALS is best regarded as a degenerative brain disease. The figure indicates that there are alternative hypotheses of origin site which include dying-back and independent degeneration of the upper and lower MNs. The “dying-back” hypothesis proposes that ALS begins within the muscle cells or at the neuromuscular junction. Specifically, there is deficiency of a motor neurotrophic hormone, which is normally released by postsynaptic cells and retrogradely transported up the presynaptic axon to the cell body where it exerts its effects. Adapted from Kiernan et al., 2011.

### 1.2.2.1 NEURONAL LOSS

ALS is a late-onset, progressive and fatal neurodegenerative disease which primarily affects motor neurons (MNs) located in the motor cortex of the brain, brainstem motor nuclei and anterior horn of the spinal cord ([Matthew C. Kiernan et al., 2011](#); [Renton et al., 2014](#); [Alsultan et al., 2016](#); [Taylor et al., 2016](#)). In ALS, as MNs degenerate, the ability to control movement of the muscles is progressively lost ([Figure 30](#)). Specific MNs in the brain, brainstem and spinal cord are selectively targeted, and pathology appears first in these restricted MN populations.

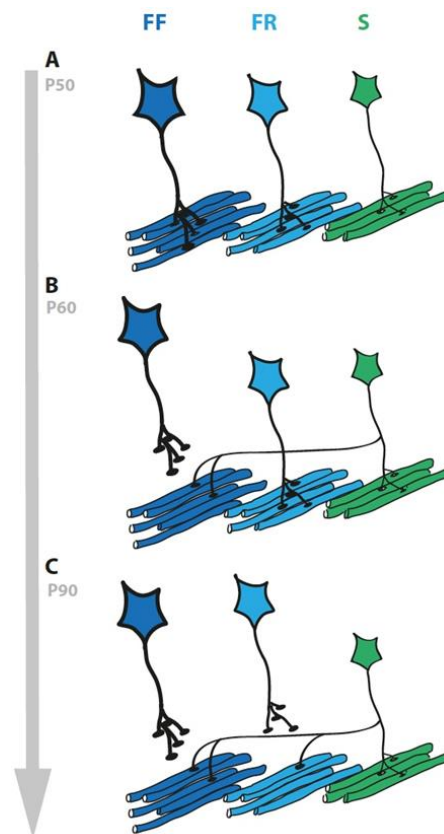


**Figure 30. Schematic representation of the selective and progressive degeneration of MNs.**

In ALS, as MNs axonal dieback at the NMJ, the ability to control movement of the muscles is progressively lost. The general sequence of degeneration is from FF to FR to S. **(A)** at P50 day, FF, FR, and S are normal in terms of controlling the movement of the muscles. **(B)** at P60 day, there is selective dieback of FF motor axons, resulting in failure to control the movement of the muscles. However, denervated endplates can, for a period, be reinnervated by axonal regrowth or sprouting from either FR or S MNs (only S shown for simplicity). **(C)** at P90 day, both FF and FR MNs fail to control the movement of the muscles. Similarly, due to the high sprouting capacity of S motor axon, their denervated endplates can be reinnervated over a period by sprouting from S MNs. However, at late stages, even S axons die back (not shown in the drawing). Motor units: FF (Fast-twitch fatigable): high force, fast contraction speed but fatigue in a few seconds; FR (Fast-twitch fatigue-resistant): intermediate force, fast contraction speed and resistant to fatigue; S (Slow-twitch fatigue-resistant): low force, slower contraction speed, highly fatigue resistant. Adapted from Kanning et al., 2010 and Clemence Martinot's PhD manuscript, 2011.

It is unknown why MNs are specifically targeted in ALS and remarkably, MNs are not equally affected ([Rochat et al., 2016](#); [Nijssen et al., 2017](#)). Whilst both UMNs and LMNs are involved, some LMN subtypes are relatively resistant to neurodegeneration. Spinal cord and hypoglossal MNs are amongst the first to degenerate, hence the ability to speak, breath and move is lost early in disease course. As ALS progresses, specific MN subtypes then preferentially deteriorate. However, some MNs are spared until disease end stage, such as oculomotor neurons and Onuf's nuclei MNs, and as a result, patients retain normal visual, sexual and bladder function throughout the disease course. The resistant MNs differ significantly from the vulnerable MNs anatomically and functionally, and they possess

distinct transcriptomes, metabolic and developmental profiles. Surprisingly, there are also differences in vulnerability amongst spinal MNs, because those that are part of the faster motor units degenerate before those in the slower motor units ([Frey et al., 2000](#); [Pun et al., 2006](#); [Hegedus et al., 2007](#); [Hadzipasic et al., 2014](#); [A. Sharma et al., 2016](#); [Spiller et al., 2016](#)), thus adding further complexity to the question of MN vulnerability.

To investigate the progression of motor neuron loss, through morphological techniques, reactive astrocytosis, and expression of ubiquitin and neurofilament proteins, by immunohistochemistry, loss of MNs in SOD1<sup>G93A</sup> mice followed a biphasic progression, with an initial loss at 126 days of age, followed by a gradual loss from onset of symptoms through to end-stage disease. Reactive astrocytosis was first observed at 70 days of age and showed a gradual increase through to end-stage disease ([Feeney et al., 2001](#)). The progression of clinical and pathological disease was studied in a line of mice designated human SOD1. Clinical disease started at 91 ± 14 days of age with fine shaking of the limbs, followed by paralysis and death by 136 ± 7 days of age. Pathological changes begin by 37 days of age with vacuoles derived from swollen mitochondria accumulating in motor neurons. At the onset of clinical disease (90 days), significant death of somatic MNs innervating limb muscles has occurred; mice at end-stage disease (136 days) show up to 50% loss of cervical and lumbar MNs. However, neither thoracic nor cranial MNs show appreciable loss despite vacuolar changes. Autonomic MNs also are not affected. Mice that express wild-type human SOD1 remain free of disease, indicating that mutations cause neuron loss by a gain-of-function ([Chiu et al., 1995](#)). Thus, the age-dependent penetrance of MN disease in this transgenic model is due to the gradual accumulation of pathological damage in select populations of cholinergic neurons.

### 1.2.2.2 MOTONEURONAL ALTERATIONS

One of the main pathological characteristics of ALS is the presence of insoluble protein inclusions in the soma of MNs. TAR DNA binding protein-43 (TDP-43) is the major component of these cytoplasmic inclusions ([Arai et al., 2006](#); [Neumann et al., 2006](#)) in almost all (97%) ALS patients and ~50% of frontotemporal dementia (FTD) patients ([Arai et al., 2006](#); [Neumann et al., 2006](#); [I. R. A. Mackenzie et al., 2007](#); [I. R. Mackenzie et al., 2010](#); [Scotter et al., 2015](#); [Le et al.,](#)

2016; Tan et al., 2017). Loss of TDP-43 from the nucleus is evident in MNs from ALS/FTD patient tissues, concomitant with the formation of TDP-43 inclusions in the cytoplasm of both MNs and glia. Neuropathological studies have also revealed that the clinical course of ALS reflects the presence of TDP-43 pathology, from its deposition at an initial site of onset, to its spread to contiguous regions of the CNS (Brettschneider et al., 2013). Mutations in TDP-43 are also present in 5% of familial forms of ALS (Jemeen Sreedharan et al., 2008). In the genetic types of ALS, it remains unclear why MNs are specifically affected when the mutant proteins are ubiquitously expressed. Males are affected more by ALS than females, and ethnic populations show differences in the incidence rates of ALS, further highlighting the contribution of genetics to ALS.

The expression of specific proteins can vary between MN subpopulations and this may be linked to their vulnerability to degenerate. Evidence for this hypothesis comes from the existing mouse models of ALS. Whilst mutant SOD1<sup>G93A</sup> is expressed in all MNs in these mice (Jaarsma et al., 2008), its propensity to induce neurodegeneration and disease is proportional to its expression level (M. E. Gurney, Pu, Chiu, Dal Canto, et al., 1994; L.I. Bruijn et al., 1997; Alexander et al., 2004). At lower levels of expression, pathology is restricted to MNs in the spinal cord and brainstem only, whereas higher expression levels also induce severe abnormalities in the brain. Fewer copies of the SOD1<sup>G37R</sup> transgene correlate with delayed disease progression and a significant increase in lifespan compared to animals with higher copy numbers (Zwiegers et al., 2014). Similarly, in TDP-43 models, higher levels of overexpression are associated with a worse phenotype (Philips et al., 2015). Moreover, disease is evident in both wildtype and mutant TDP-43 models, indicating that the expression levels of TDP-43, rather than the presence of a mutation per se, induces neurodegeneration. Hence, the effect of the TDP-43 mutation can be difficult to segregate from the effects of overexpression in these models (Philips et al., 2015). Both retaining the physiological expression levels and normal nuclear localization of TDP-43 have been linked to maintaining cellular homeostasis (Swarup et al., 2011; Philips et al., 2015). These studies together highlight the role of differing protein expression levels in the development and progression of ALS.

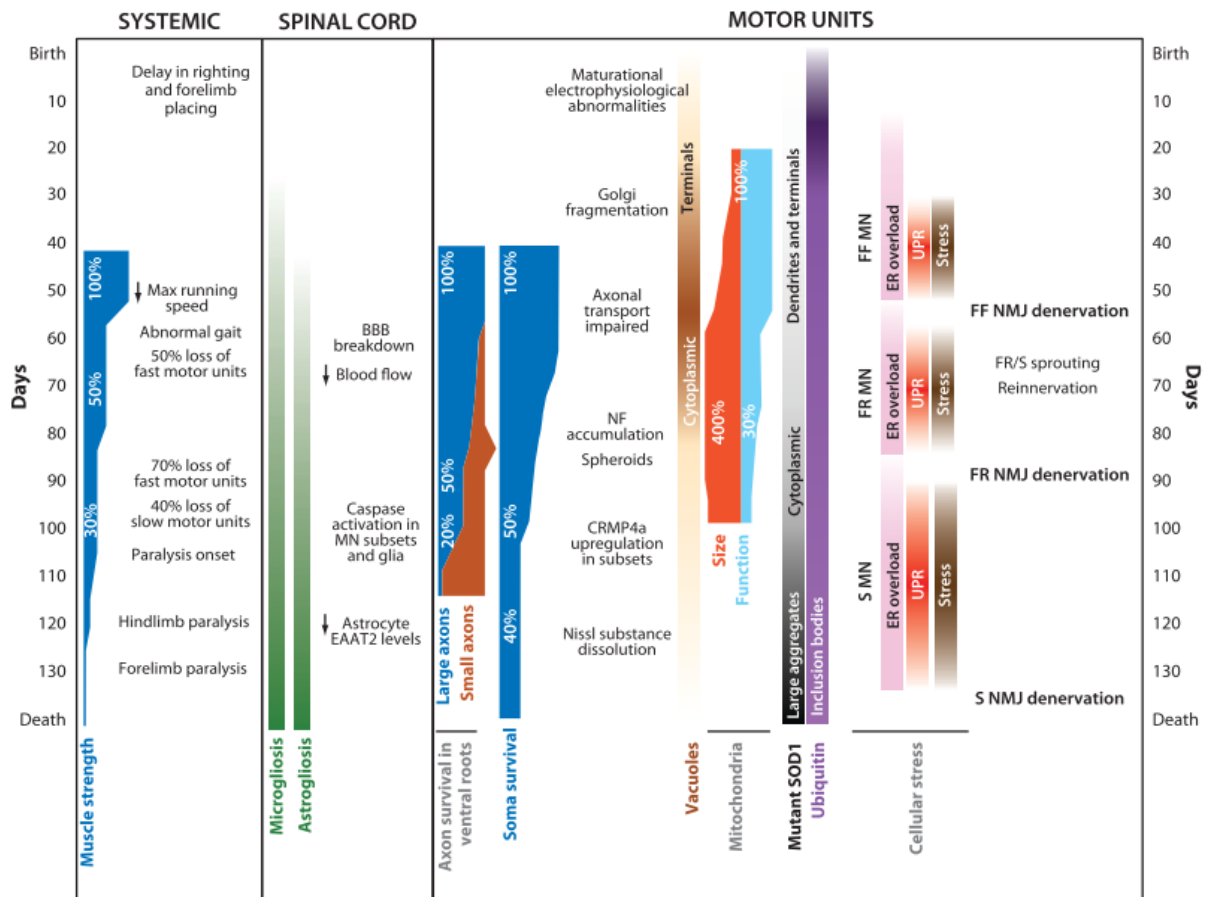


**Figure 31. Time course of neurodegeneration in the SOD1<sup>G93A</sup> mouse model of ALS.** The diagram provides an overview of the complex ballet of cellular and molecular mechanisms that lead over six months to the death of this severe model of ALS. Many changes occur before muscle strength is reduced by half, including initial alterations in electrophysiology and behaviour followed by ubiquitination and ER stress in susceptible FF motor neurons leading to axonal dieback and microgliosis and astrogliosis in the spinal cord. These are accompanied by subcellular changes such as Golgi fragmentation and mitochondrial swelling. During the following months, these changes become exacerbated and generalized to other motor units, leading to extensive MNs loss and muscle paralysis. Indicated stages (scale in days) represent those in the G93A high-expressor line. Some parameters have not been studied at earlier stages, so the indicated dates represent the latest possible onset. The overall layout progresses from systemic and behavioural changes on the left toward molecular and cellular changes in motor units on the right. Adapted from Kanning et al., 2010.

Time course of neurodegeneration in the SOD1<sup>G93A</sup> mouse model of ALS was compiled from multiple publications over the ten years (Figure 31) (Kanning et al., 2010). In the spinal cord, the earliest detectable pathological alterations occur before muscle denervation. The earliest reported phenotypes concern cultured embryonic motor neurons, which show remarkably increased sensitivity to external stressors such as Fas ligand, which triggers their death by activating caspase-8 and p38 (Raoul et al., 2002). They are also hyperexcitable owing to abnormally strong persistent inward currents (Jason J. Kuo et al., 2004; Kuo et al., 2005). Axonal

transport defects (both anterograde and retrograde) are also found in cultured motor neurons ([Kieran et al., 2005](#); [De Vos et al., 2007](#)). In vivo, the earliest change detected to date is an increase in the electrical excitability of hypoglossal motor neurons at P4, reflecting an abnormally strong persistent inward sodium current. In parallel, early pruning of dendrites may reflect premature functional maturation ([van Zundert et al., 2008](#)). Not all motor neuron subtypes are equally affected by the disease. This is first apparent at the morphological level. FF motor units undergo atrophy earliest in mutant SOD mice, with near total loss of FF terminals from type IIb muscle fibres in the triceps surae of SOD1<sup>G93A</sup> mice by P50 ([Frey et al., 2000](#)). Notably, dendritic morphometric parameters in foetal E17.5 WT and SOD1<sup>G93A</sup> MNs presented striking differences in [Figure 32](#), a ~ 60% reduction of the terminal dendritic length was found in SOD1<sup>G93A</sup> MNs after topologic and morphologic analysis ([Martin et al., 2013](#)). As the role of dendritic trees is to collect and transmit synaptic inputs to the soma, its structural properties are crucial for local integration of distal inputs or all inhibitory and excitatory inputs to shape the state of excitability of a circuit throughout life. Neurite outgrowth is an important process in the formation of neuronal networks ([Aoki et al., 2005](#)). The morphology of neurons and network plays an important role in processing electrical and biochemical signals, and can be interpreted as a strong indicator that the anatomy of the cellular and network level is deeply involved on various functional levels ([Breit et al., 2016](#)).

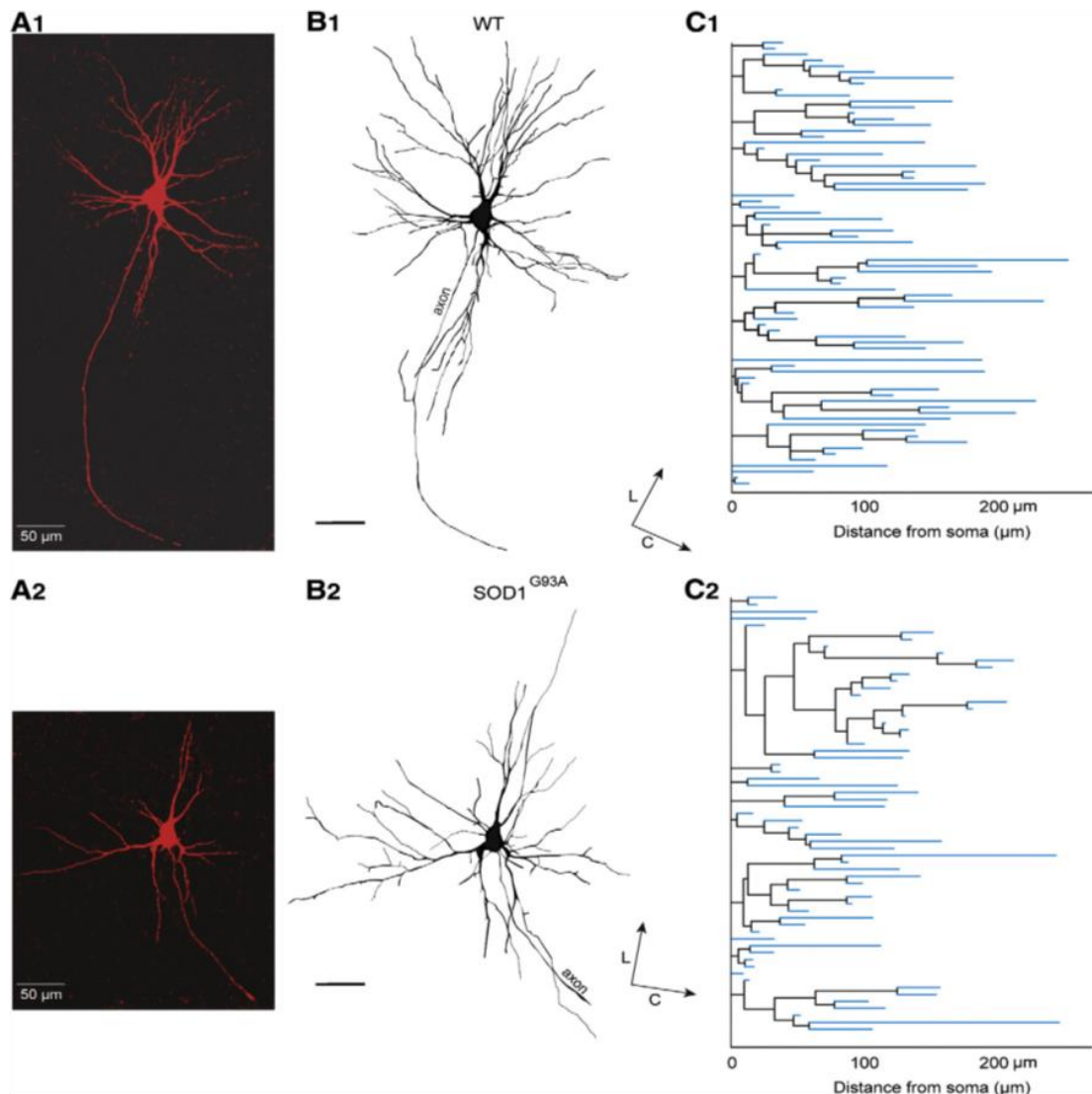


**Figure 32. Embryonic morphological abnormalities in E17.5 SOD1<sup>G93A</sup> MNs. (A1–A2)** Representative WT and SOD1<sup>G93A</sup> MNs filled with neurobiotin. Illustrations correspond to projected images of 54 and 61 optical sections stack (0.6 μm in Z) for WT and SOD1<sup>G93A</sup> MN, respectively (×20 magnification). **(B1–B2)** 3D reconstructions of complete dendritic trees of the WT and SOD1<sup>G93A</sup> MNs illustrated in A. Reconstructions were made from ×60 high magnification confocal acquisitions (0.2 μm in Z). **(C1–C2)** Two-dimensional representations of whole dendritic arborization (dendrograms) obtained from the 3D reconstructions illustrated in B1–B2. Intermediate segments are shown in black and terminal segments in blue. L = lateral, C = caudal. Adapted from Martin et al., 2013.

### 1.2.2.3 GLUTAMATE EXCITOTOXICITY

Glutamic acid is an excitatory neurotransmitter involved in long term potentiation (LTP). Neuronal cell death decreases neuronal glutamate (Glu) uptake, which is required for the rapid removal of Glu from the extracellular space, thus terminating the excitatory signal and reducing the excitotoxic neuronal damages ([Heath et al., 2002](#); [Geevasinga et al., 2016](#)). A large number of studies with

SOD1G93A ALS-model mice provide strong evidence for the role of oxidative stress in the disease pathogenesis ([Geevasinga et al., 2016](#); [Spalloni et al., 2016](#)). Additionally, ROS-mediated mitochondrial dysfunction, in connection with glutamate excitotoxicity, has been implicated in ALS pathogenesis ([Z. Xu et al., 2004](#)). Glutamate is abundant in the diet, and is the most abundant excitatory neurotransmitter in the nervous system, binding to receptors such as the NMDA (N-methyl-D-aspartate) receptor ([Meldrum, 2000](#)). The NMDA ionotropic glutamate receptor can mediate Ca<sup>2+</sup> influx in response to agonist binding. Excitotoxicity refers to a situation where neurons are killed due to excessive stimulation, leading to uncontrolled Ca<sup>2+</sup> influx, activating cellular signalling processes which can then lead to cell death. Glutamate excitotoxicity is thought to be involved in the generation of ROS and involved in mitochondrial permeability transition, which causes an increase in membrane permeability to smaller molecules, leading to mitochondrial dysfunction ([Schinder et al., 1996](#)). The mitochondria remain sensitive to oxidative damages, resulting in further mitochondrial dysfunction ([Spalloni et al., 2016](#)). The mitochondrial dysfunction, in turn, enhances glutamate-mediated excitotoxicity by disrupting the normal voltage-dependent Mg<sup>2+</sup>-mediated blockade of glutamate receptors ([Bowling et al., 1995](#); [Z. Xu et al., 2004](#)). Glutamate excitotoxicity is currently being studied as a key pathological mechanism in several neurodegenerative diseases including dementia, Parkinson's disease, and ALS. Excitotoxicity is currently being targeted pharmacologically in dementia patients, with the FDA approved therapeutic memantine ([Molinuevo et al., 2005](#)).

Changes in excitability of neurons may also play an important role in ALS progression. Over-stimulation of neuronal glutamate receptors (GluR) leads to excitotoxicity, thus leading to neuronal dysfunction and ultimately to cellular death through activation of Ca<sup>2+</sup>-dependent enzymatic pathways ([Arundine et al., 2003](#); [Kuo et al., 2005](#)). Defects in glutamate transport that may contribute to excessive extracellular glutamate have been noted in patients with sporadic ALS and in the transgenic mutant SOD1 mouse model of ALS ([Rothstein et al., 1995](#); [Lin et al., 1998](#); [Dunlop et al., 2003](#)). Numerous reports of alterations to glutamate receptors have also been central to the development of the excitotoxicity hypothesis in ALS or ALS-parkinsonism dementia complex ([Wilson et al., 2007](#); [P. Zhao et al., 2008](#); [Blasco et al., 2014](#)). In humans, low GluR2 expression was found in both upper and

lower motor neurons compared to other neuronal types (*P. Shaw et al., 2000*). Specific downregulation of GluR1 was also reported in a FUS depletion model of ALS (*Udagawa et al., 2015*).

Currently, the only approved pharmacological therapeutic for the treatment of ALS (Riluzole or Rilutek™) is thought to act as a mitigator of glutamate excitotoxicity. The drugs Riluzole and Edaravone, have been reported to work by an anti-glutamate mechanism (*Cheah et al., 2010; Rothstein, 2017*). Given that this therapeutic extends life by approximately 3 months in ALS patients, it is likely that ALS has some degree of glutamate excitotoxicity involved in pathogenesis, although it may not be the predominant mechanism of neurodegeneration in ALS (*Bensimon et al., 1994; Doble, 1996*).

#### **1.2.2.4 SYNAPTOPATHY**

Synaptopathy is a broad definition of diseases with synaptic dysfunction, regardless of the disease mechanisms (*Lepeta et al., 2016*). In the broadest definition, synaptopathy encompasses a wide range of features, which in due course, will lead to synaptic dysfunction. These features include changes in Ca<sup>2+</sup> levels at synapses, glutamate excitotoxicity, structural changes in pre- and postsynaptic anchoring proteins, altered synaptic structure and function, which is often associated with dendritic spine loss, dysfunctional neurotransmitter release (quantal content and frequency), impaired maintenance, and regeneration of axons by Schwann cells, and cognitive deficit (*Lepeta et al., 2016; M. Fogarty, 2019*). Furthermore, synaptopathies lead to neuronal loss, mitochondrial dysfunction, accumulation of misfolded proteins associated with defective proteostasis, and defective neuromuscular junctions (NMJ) (*Wishart et al., 2006; Lepeta et al., 2016; M. Fogarty, 2019*).

In the motor system the synapse is critically important for the integration of signals between motor neurons and target muscles, as well as between neurons in the cortex (*Azpurua et al., 2015*). Neuronal morphology as well as synaptic form, number and structure are tightly regulated, and are essential for appropriate and functional connections. This developing nervous system, stimulated by changes in spontaneous activity, regulates the formation of the synapse. Effectively, cortical

circuits require the elimination of redundant synapses during synaptogenesis and rely on intimate communication between pre- and post-synaptic compartments ([Cohen-Cory, 2002](#)).

The majority of excitatory glutamatergic neurotransmission in the CNS is mediated by  $\alpha$ -Amino-3-hydroxy-5-methyl-4-isoxazolepropionic acid (AMPA) receptors, as glutamate plays its effects through postsynaptic receptors. Increased extracellular glutamate concentration or sensitivity of the postsynaptic neuron to glutamate result in increased activation of glutamate receptors ([Van Damme et al., 2005](#)). In the CNS, NMDA receptors are abundantly expressed, the affect synaptic plasticity and alterations are implicated in many neurodegenerative diseases, such as in learning and memory disorders ([Castellano et al., 2001](#)) and depression-related disorders ([Dang et al., 2014](#)). The regulation of neuronal signalling occurs in parallel with the trafficking of neurotransmitter transporters, shuttling rapidly to and from the plasma membrane in response to the excitatory release of the neurotransmitter itself ([Deken et al., 2003](#)).

Abnormal synaptogenesis and synaptic signalling has been implicated in the initiation and progression of a range of neurodegenerative diseases including ALS ([Gillingwater et al., 2013](#); [J. R. Bae et al., 2017](#)). investigations have shown that synaptic loss was not due to cortical atrophy, but instead was strongly related to the severity of cognitive impairment of the individual patients, suggesting that synapse loss occurs before neurodegeneration ([Henstridge et al., 2018](#)).

#### **1.2.2.5 ELECTROPHYSIOLOGICAL CHANGES IN ALS disease**

ALS is a fatal neurological disorder affecting both upper MNs in the cerebral cortex and lower MNs in the brainstem and spinal cord. The primary feature of ALS is the selective loss of MNs in the brain and spinal cord. However, changes in synaptic transmission and MN excitability are among the first events that take place during development and accompany the relentless deterioration of motor circuitry. The earliest signs, which are detected during embryonic and postnatal development and that will pave the way for the rest of the disease course in ALS mice, are linked to the electrophysiological properties and circuitry of MNs. In SOD1<sup>G93A</sup> mice, the first motor symptoms appear at around 90 days of age, but activation of cellular stress pathways

can be observed in vulnerable MNs as early as postnatal day (P)12, and dysfunction of the neuromuscular junction is already noticeable at P50 ([Pun et al., 2006](#); [Smita Saxena et al., 2009](#)). The earliest alterations that evidence a functional defect are those observed during the developmental stages of the motor system and are associated with MNs' acquisition of electrophysiological properties and the integration of MNs into the motor circuitry. Both isolated embryonic SOD1<sup>G93A</sup> expressing MNs ([Pieri et al., 2003](#)) and those in slice preparation ([Quinlan et al., 2011](#)) consistently exhibit an increased rate of repolarization compared to controls. Action potential (AP) frequency is increased in ALS embryonic MNs in culture ([Pieri et al., 2003](#); [Jason J. Kuo et al., 2004](#); [Qing Chang et al., 2016](#)), embryonic spinal cord preparation ([Martin et al., 2013](#)), postnatal spinal cord, and brainstem slices ([Jason J. Kuo et al., 2004](#); [van Zundert et al., 2008](#)), as well as in human MNs derived from induced pluripotent stem cells (iPSCs) obtained from patients with ALS ([Brian J. Wainger et al., 2014](#); [A.-C. Devlin et al., 2015](#)), relative to controls. Spinal MNs from P6–P10 spinal cord slices or preparations show decreased firing frequency compared with wildtype, although by age, the gain is lower in motoneurons from P6–P7 transgenic mice and unchanged in MNs from older P8–10 transgenic mice versus those from wildtype mice ([Bories et al., 2007](#)). Altogether this evidence highlights altered MN excitability, inhibitory imbalance, and changes in spinal locomotor networks as salient traits of the earliest origins of the pathology described to date.

LMN activity/excitability in humans was indirectly measured through nerve conduction studies (NCS) and electromyography (EMG) ([Joyce et al., 2013](#)). These studies revealed an increase in motor unit excitability, evidenced by the increased presence of fasciculation potentials, double discharges of the motor unit ([Kostera-Pruszczyk et al., 2002](#); [Piotrkiewicz et al., 2008](#)) and aberrant single motor unit firing ([Piotrkiewicz et al., 2008](#)) and increased axonal excitability ([Bostock et al., 1995](#); [Kanai et al., 2006](#); [Nakata et al., 2006](#)) ([Figure 33](#)). Increased axonal excitability in ALS is likely due to enhanced persistent axonal Na<sup>+</sup> conductance and impairments in axonal K<sup>+</sup> conductance ([Bostock et al., 1995](#); [Horn et al., 1996](#); [Mogyoros, 1998](#); [Kanai et al., 2006](#); [Nakata et al., 2006](#); [Tamura et al., 2006](#); [Steve Vucic et al., 2006](#); [S. Vucic et al., 2010](#)) and was suggested to contribute to fasciculation potentials typical of ALS ([de Carvalho et al., 2013](#); [Howells et al., 2018](#); [Gunes et al., 2020](#)) ([Figure 33](#)).

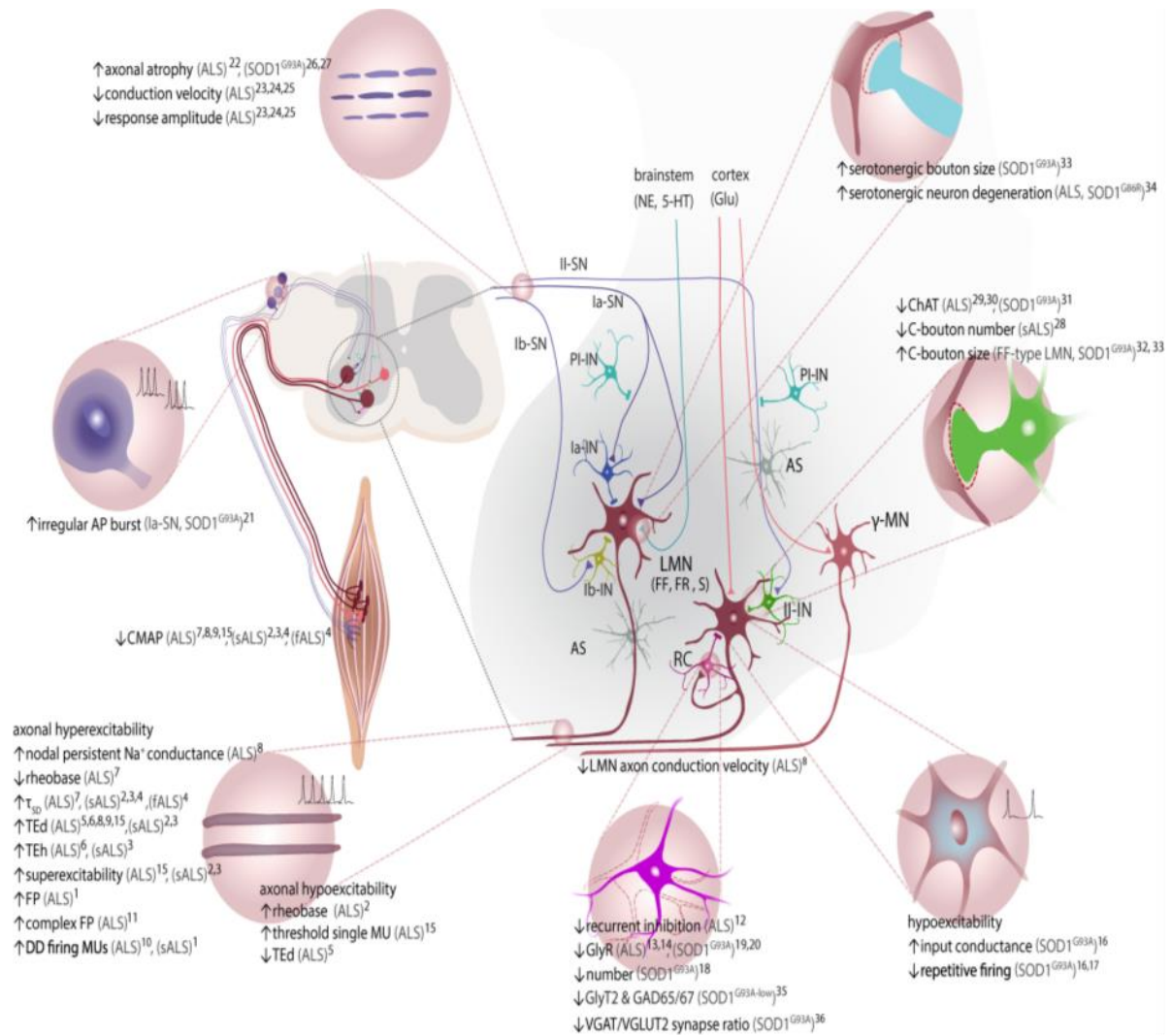


**Figure 33. ALS-associated alterations in ventral spinal cord circuitry.** LMN receive inhibitory input via Ia-IN, Ib-IN, and RC, and excitatory inputs from corticospinal tract (UMN), II-IN and SN.  $\gamma$ -motor neurons, which are spared in ALS, do not receive direct inputs from Ia-SN. Excitatory inputs to LMNs via Ia afferent terminals are controlled by PI-IN. Both excitatory and inhibitory inputs are tightly regulated by the proprioceptive feedback provided by sensory afferents (Ia, Ib and II-SN) and astrocytes. Axonal hyperexcitability and hypoexcitability are reported in ALS patients. Decreased RC synapses on LMN and lower number of RC is reported. LMN hypoexcitability is present *in vivo* in SOD1G93A tg mouse model. Ia-SN neurons exhibit irregular firing patterns as an indication of their altered excitability/activity. Cholinergic C-bouton number is decreased in sALS patients, but C-boutons are enlarged especially onto vulnerable FF LMN in SOD1G93A tg mice. Protein and mRNA levels of ChAT are decreased in spinal cord of ALS patients. Reduced ChAT expression is reported in II-IN and C-boutons on MN of SOD1G93A tg mice. Serotonergic boutons on LMN are increased in low-copy SOD1G93A tg mice, whereas serotonergic neurons in brainstem degenerate in both ALS patients and SOD1G86R tg (not shown). Please note that monosynaptic connections between UMN and LMN are only present in humans. Neuromodulatory synapses are depicted as one (somata located in brainstem). Studies with unspecified type of ALS are referred to as (ALS). AP, action potential; AS, astrocytes; CMAP, compound muscle action potential; ChAT, choline acetyltransferase; CPG, central pattern generator; DD, double-discharge; fALS, familial ALS; FF, fast-fatigable; FP, fasciculation potential; FR, fast-resistant; gamma ( $\gamma$ )-motor neuron,  $\gamma$ -MN; GAD65/67, glutamic acid decarboxylase 65/67; Glu, glutamate; GlyT2 & GAD65/67 (SOD1<sup>G93A-bony</sup>)<sup>35</sup>; VGAT/GLUT2 synapse ratio (SOD1<sup>G93A</sup>)<sup>36</sup>.

Although ALS is an adult-onset neurodegenerative disease, MN electrical properties are already altered during embryonic development. Summary of the changes in MN properties over time in the SOD1<sup>G93A</sup> mouse was illustrated in **Figure 34** (Huh et al., 2021). Schematic representation of the changes in four key electrophysiological properties over time.

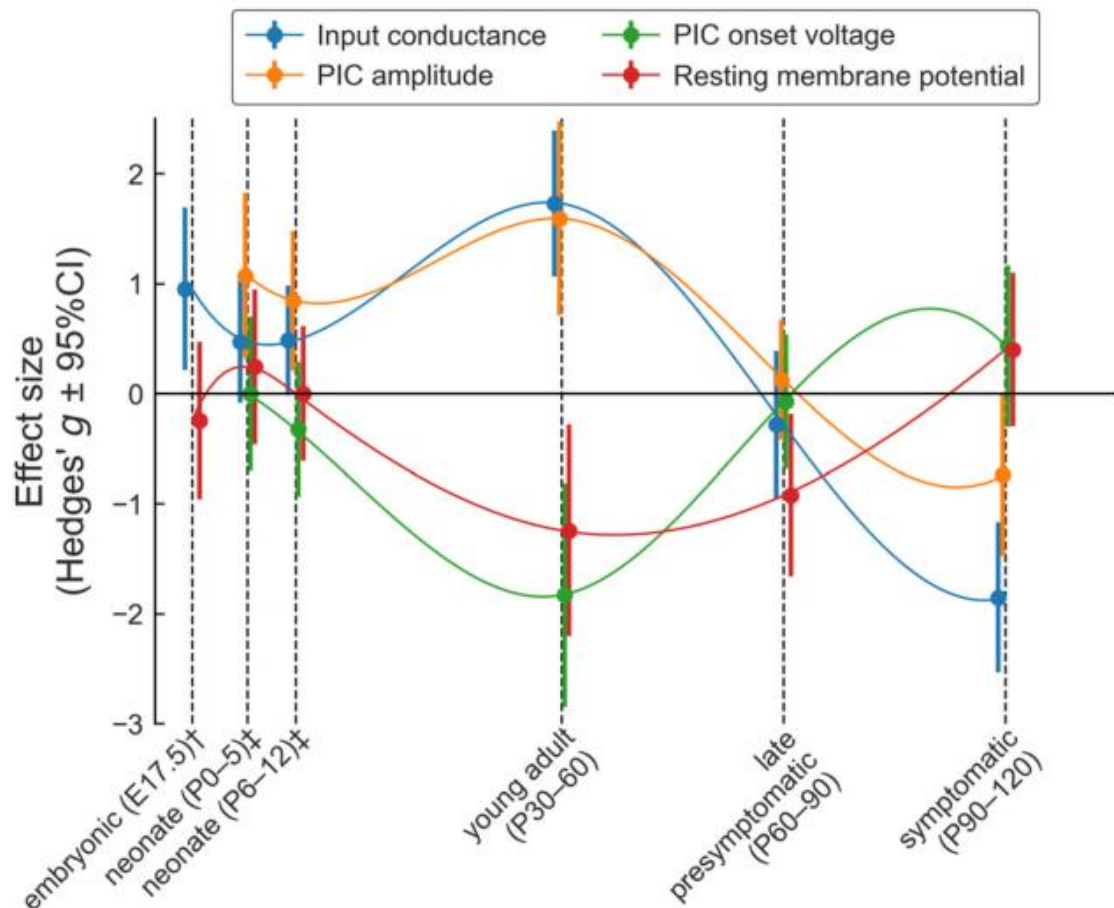


**Figure 34. Summary of the changes in motoneuron properties over time.** Schematic representation of the changes in four key electrophysiological properties over time. The dots represent the effect size (Hedges' *g*) and the vertical bars show the 95%CI around *g*. The thin lines are cubic splines interpolation of the data over time. The points have been slightly staggered so that the vertical bars do not occlude each other. †Data from embryonic motoneurons are from Martin et al. (2013). These authors did not measure PICs in embryonic motoneurons. Kuo et al. (2004) did measure PICs, but their embryonic motoneurons were cultured for 10–30 d *in vitro*, and their development stage is therefore uncertain. ‡Data from neonates (P0–P5 and P6–P12) are from Quinlan et al. (2011). Adapted from Huh et al., 2021.

### 1.2.2.6 GLIAL DEFECTS

The neuroglia includes the neuroectoderm-derived macroglia that comprise astrocytes, oligodendrocytes, and NG2-positive progenitors and the microglia, the resident macrophages of the CNS that have a mesodermal origin. Astrocytes and microglia are major players in neuroinflammatory response (**Figure 35**). Both cell types can be polarized to a neurotoxic/proinflammatory or neurotrophic/resolutive

phenotype in response to different signals, and close molecular conversations and reciprocal modulation are established between them during the course of activation (Jha et al., 2019).

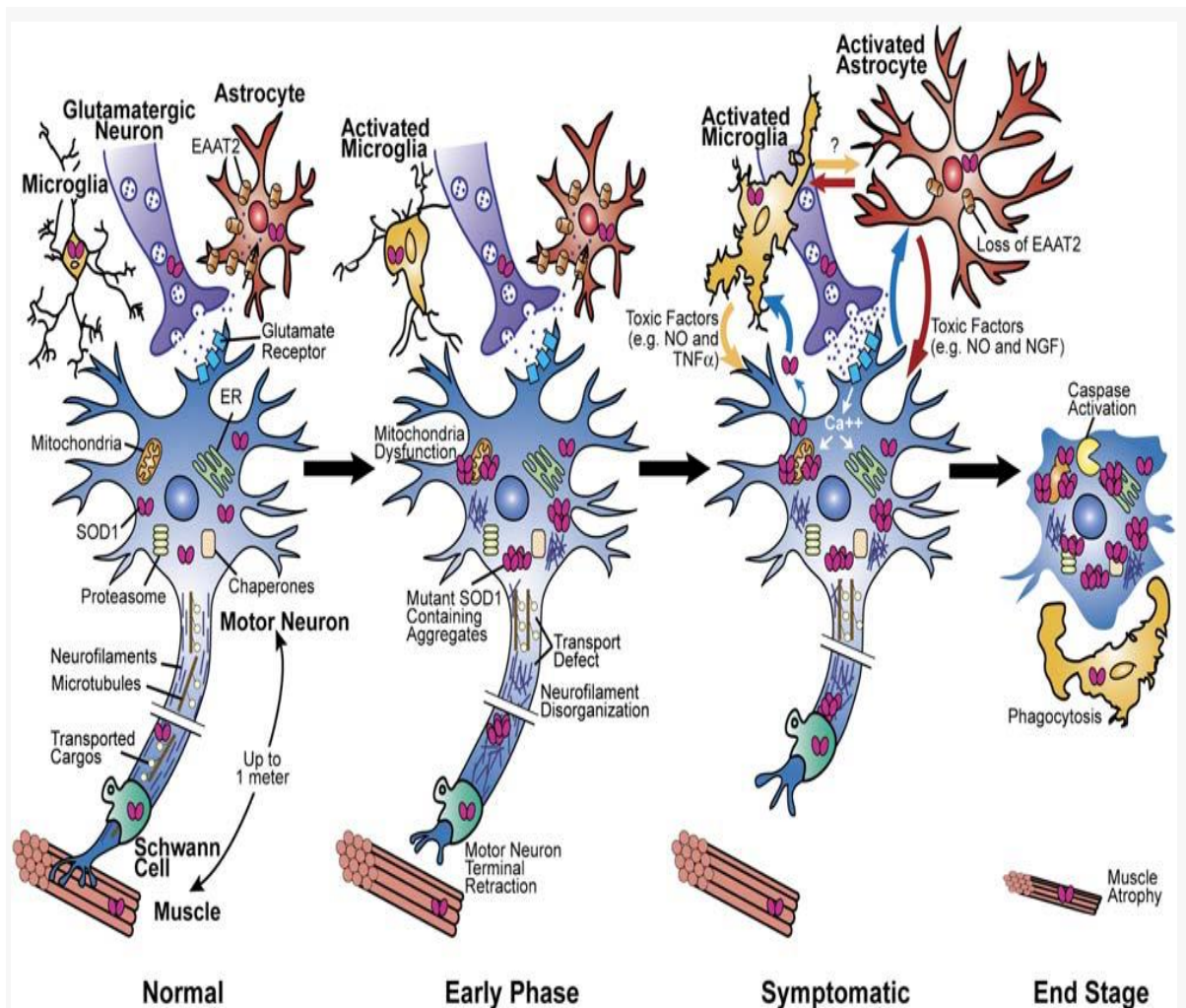


**Figure 35. Schematic of the evolution of MNs degeneration and glial activation during the course of SOD1 mutant-initiated ALS disease.** Four stages are defined (normal, early phase, symptomatic, and end stage). Toxicity is non-cell-autonomous, produced by a combination of damage incurred directly within motor neurons that is central to disease initiation and damage within nonneuronal neighbors, including astrocytes and microglia, whose actions amplify the initial damage and drive disease progression and spread. Selective vulnerability of motor neurons to ubiquitously expressed mutant SOD1 is determined by the unique functional properties of motor neurons (e.g., they are very large cells with large biosynthetic loads, high rates of firing, and respond to glutamate inputs) and damage to their supporting cells in the neighborhood. Adapted from Boillee et al., 2006.

Astrocytes are a large portion of the glial cell population in the CNS and accomplish a plethora of essential functions that have been extensively summarized (Verkhratsky et al., 2019). In the human cortex, a single astrocyte enwraps >1 million synapses and most, if not all, have at least 1 process with endfeet contacting a blood vessel (von Bartheld et al., 2016). Therefore, astrocytes are polarized cells that are in a key position to provide structural, metabolic, and trophic support to

neurons. Astrocytes react to CNS damage with a phenotypic shift characterized by morphological, molecular, and functional changes including increased proliferation rate, higher levels of astrocytic glial fibrillary acidic protein expression, and extension of thicker processes ([Sofroniew et al., 2010](#)). Since many terms have been used to describe these astroglial responses leading to confusing terminologies, it was recently proposed to reserve “reactive astrocytes” as an umbrella term encompassing multiple potential states of astrocytes undergoing disease-associated remodelling ([Escartin et al., 2021](#)). During ALS progression, increased number of reactive astrocytes are identified in the spinal cord, even before motor symptoms are detected ([Yamanaka et al., 2018](#)). Astrocytes overexpressing the fALS-linked SOD1 mutation [G93A] reduce motor neuron survival in coculture conditions, whether they are isolated from neonatal rats ([Vargas et al., 2006](#)), mice ([Nagai et al., 2007](#)), or derived from human cells ([Di Giorgio et al., 2007](#)).

Microglia, the resident macrophages of the CNS, play a crucial role in neuroinflammation to promote motor neuron loss in ALS ([Hooten et al., 2015](#)). Microglia invade the brain early in development, convert into a highly ramified cell type, and constantly screen their environment. Microglia are activated by any type of pathologic event or change in brain homeostasis and can strongly influence the outcome or response to a stressor due to the release of a variety of substances, including cytokines, chemokines, and growth factors. They are the professional phagocytes of the brain and help orchestrate the immunological response by interacting with infiltrating immune cells ([Wolf et al., 2017](#)). Increased microgliosis has been observed in spinal cords of ALS patients ([Yiangou et al., 2006](#)). In ALS, the dual role of microglia is well established. In response to damage or injury, microglia become activated, inducing their migration to the site of injury, proliferation and causing the release of damage-associated molecular patterns, cytokines, chemokines and reactive nitrogen and oxygen species to promote neuroinflammation ([Becher et al., 2017](#)). It is generally considered that activated microglia exhibit two different phenotypes in ALS, M1 and M2 phenotypes ([Parisi et al., 2016](#); [Geloso et al., 2017](#)), although this concept remains controversial and is considered an oversimplification ([Ransohoff, 2016](#)). In ALS, microglia possess early protective M2 phenotype characterised by small cell bodies with shorter and simple processes, and late neurotoxic M1 phenotype exhibiting large cell bodies with short and extensively

branched processes ([Ohgomori et al., 2016](#)). In ALS mice, mutant SOD1 (mSOD1) expressing M2 microglia isolated at disease onset protected co-cultured motor neurons, whilst mSOD1 expressing M1 microglia isolated at disease end-stage damaged co-cultured motor neurons ([Liao et al., 2012](#)). The activation of microglia (microgliosis) and subsequent neuroinflammation is a major cause of fALS ([Hooten et al., 2015](#)), although it remains unknown if a similar mechanism is a major cause of sALS. In humans, increased microgliosis has been demonstrated in the spinal cords of specimens from ALS patients ([Yiangou et al., 2006](#)). Microgliosis occurs specifically with motor neuron injury in the motor cortex, along the corticospinal tract, and in the ventral horn of the spinal cord ([Philips et al., 2011](#)).

During early phases of disease, M2 phenotype possess a protective response against signals triggered by motor neuron damage. M2 phenotype release anti-inflammatory cytokines and neurotrophic factors including interleukin IL-4, IL-10, IL-13, and insulin-like growth factor-1 to promote motor neuron survival ([Tang et al., 2016](#); [Du et al., 2017](#)). Consistently, in SOD1G93A and SOD1G37R mice, overexpression of anti-inflammatory IL-10 have been demonstrated at the pre-onset phase of disease progression ([Gravel et al., 2016](#)). An anti-inflammatory cytokine, IL-4, has also been shown to suppress the release of reactive oxygen species and nitric oxide, and protected co-cultured primary motor neurons against microglia-mediated motor neuron damage ([W. Zhao et al., 2006](#)). Despite, the actual processes that transform protective microglia into a toxic form is still unknown, it is believed that the prolonged period of microglial activation will transform protective M2 phenotype into deleterious M1 phenotype. M1 phenotypes promote the release of pro-inflammatory factors such as IL-1 $\alpha$ , IL-1 $\beta$ , IL-6, IL-12, IL-23 and tumor necrosis factor (TNF)- $\alpha$ , chemokines, prostaglandin E2, chemokine (C-C motif) ligand 2, ROS and inducible nitric oxide synthase to proliferate motor neuron death ([Hooten et al., 2015](#); [Du et al., 2017](#); [Geloso et al., 2017](#)). Furthermore, the death of motor neurons results in the release of mSOD1 to provide a positive feedback loop to further induce microglia-mediated motor neuron death. Thus, the dual role of microglia in ALS is well established. The modulation of microglial function serves as a promising therapeutic strategy.

Myelin is the lipid-rich structure formed by oligodendrocytes (OLs) that wraps the axons in multilayered sheaths, assuring protection, efficient saltatory signal conduction and metabolic support to neurons. The impact of OL dysfunction and myelin damage is now considered to be a major contributing factor to neurodegeneration in several neurological diseases, including ALS. Upon OL injury, oligodendrocyte precursor cells (OPCs) of adult nervous tissue sustain the generation of new OLs for myelin reconstitution, but this spontaneous regeneration process fails to successfully counteract myelin damage. The functions of OPCs exceed the formation and repair of myelin, and also involve the trophic support to axons and the capability to exert an immunomodulatory role ([Raffaele et al., 2021](#)), which are particularly relevant in the context of neurodegeneration. Intriguingly, degeneration of mature OLs and myelin defects were found to start at pre-symptomatic phase in SOD1 G93A mice spinal cord ([Niebroj-Dobosz et al., 2007](#); [Kang et al., 2013](#); [Rodolfo G. Gatto et al., 2018](#); [R. G. Gatto et al., 2018](#); [Bonfanti et al., 2020](#)), suggesting that myelin disruption anticipates MN degeneration and directly contributes to disease exacerbation. In line with this, the presence of OL abnormalities in the lumbar spinal cord of SOD1 G93A mice is at very early developmental stages (P7-10), including increased levels of immature markers like NG2 and GPR17 and reduced density of CC1+ mature cells ([Bonfanti et al., 2020](#)). However, despite the growing understanding of oligodendrocyte maturation in the developmental myelination, the underlying molecular mechanisms or factors involved in the context of ALS disease remain poorly investigated. The possible mechanisms underlying OL degeneration, defective OPC maturation, and impairment in energy supply to MNs have also been examined to provide insights on future therapeutic interventions.

In ALS, immune cells also contribute to MN degeneration. There is clear evidence of immune activation in some patients with ALS and in animal models of disease, which is evidence of abnormalities of the peripheral immune system, with alterations of T lymphocytes, monocytes, complement and cytokines in the peripheral blood of patients with ALS. For instance, the total leukocyte count is elevated in patients with ALS, and correlates with progression of disease ([Murdock et al., 2017](#)). The ratio of neutrophils to monocytes was also shown to be increased ([Murdock et al., 2016](#)), as was the total number of granulocytes ([Gustafson et al., 2017](#)). In the

SOD1<sup>G93A</sup> transgenic mouse, circulating neutrophils are increased ([Lee et al., 2017](#)), and neutrophils and mast cells are present along peripheral motor axons. As with inflammation in the CNS, peripheral immune activation could be a reaction to tissue damage, but once established, could exacerbate disease. We report the presence of NK cells in post-mortem ALS motor cortex and spinal cord tissues, and the expression of NKG2D ligands on MNs. Using a mouse model of hSOD1<sup>G93A</sup>, Garofalo and colleagues ([Garofalo et al., 2022](#)) demonstrated NK cell accumulation in the motor cortex and spinal cord, with an early CCL2-dependent peak. NK cell depletion reduces the pace of MN degeneration, delays motor impairment and increases survival. This is confirmed in another ALS mouse model, TDP43<sup>A315T</sup>. NK cells are neurotoxic to hSOD1<sup>G93A</sup> MNs which express NKG2D ligands, while IFN $\gamma$  produced by NK cells instructs microglia toward an inflammatory phenotype, and impairs FOXP3<sup>+</sup>/Treg cell infiltration in the spinal cord of hSOD1<sup>G93A</sup> mice. Together, these data suggest a role of NK cells in determining the onset and progression of MN degeneration in ALS, and in modulating Treg recruitment and microglia phenotype ([Figure 36](#)).

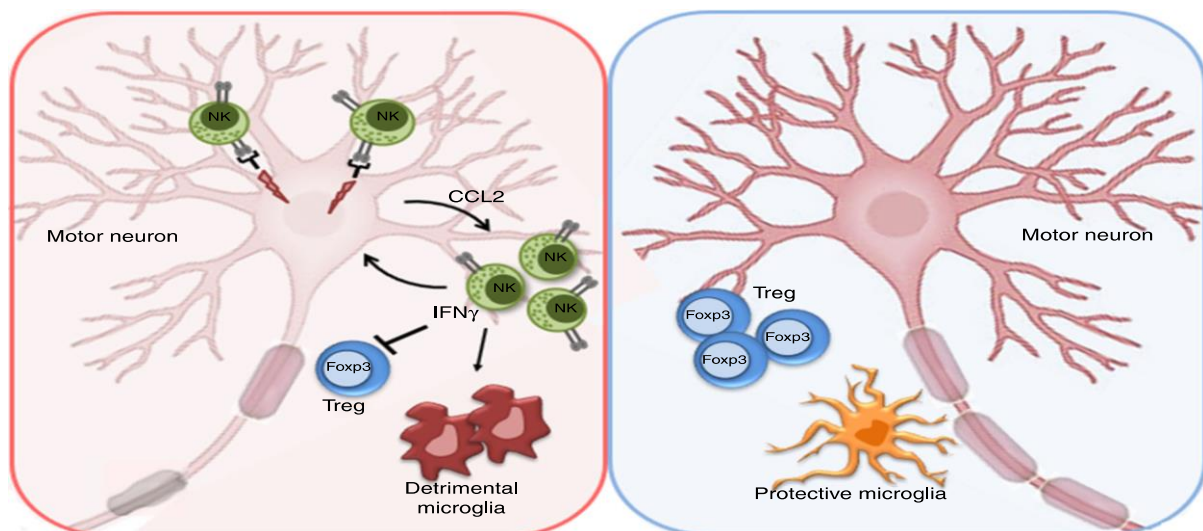


**Figure 36. Graphic summary of natural killer cells modulates motor neuron-immune cell cross talk in mouse model of ALS hSOD1<sup>G93A</sup>.** (Left) NK cells' effects in the spinal cord of hSOD1<sup>G93A</sup> mice at the early symptomatic stage. NK cells directly exert cytotoxic activity against MNs through the NKG2D-Mult-1 axis. Furthermore, IFN $\gamma$  released by NK cells: (i) increases the release of CCL2 by damaged neurons; (ii) reduces the number of Treg Foxp3<sup>+</sup> cells; (iii) shapes microglia toward a pro-inflammatory phenotype. (Right) NK cell depletion, in hSOD1<sup>G93A</sup> mice, induces neuroprotective microglia phenotype and increases the number of Treg Foxp3<sup>+</sup> cells that protect the MNs. Adapted from Garofalo et al., 2020.

### 1.2.2.7 Hyperexcitability of MNs

Electroneurography studies revealed marked variability in the hyperexcitability index scores of patients with ALS studies focused on spinal motor neurons revealed that affected neurons within the anterior horn present with both synapse loss and narrowed synaptic contact, with this occurring at an early stage in ALS patients ([Sasaki et al., 1994](#)). Moreover, transcranial magnetic stimulation (TMS) studies indicated that both the UMNs and LMNs of the motor cortex and of the spinal cord exhibit hyperexcitability in sporadic and SOD1 familial ALS cases, months prior to the onset of motor symptoms ([Steve Vucic et al., 2006](#); [van Zundert et al., 2008](#); [Martin R. Turner et al., 2012](#); [J. S. Bae et al., 2013](#); [Menon et al., 2015](#)).

Hyperexcitability enables neurons to have a lower threshold to fire action potentials upon stimulation, which is often described as a condition in which the neuron is excessively excitable. The mechanism leading to hyperexcitability has also been documented in the most characterised SOD1<sup>G93A</sup> mouse model of ALS ([Figure 37](#)), with changes in excitability occurring prior to cell loss ([Pieri et al., 2003](#); [M. J. Fogarty et al., 2015](#); [Murdock et al., 2015](#)). Furthermore, in vitro and in vivo studies using experimentally induced excitotoxicity have demonstrated the vulnerability of both UMNs and LMNs ([King et al., 2007](#); [Southam et al., 2013](#); [Blizzard et al., 2015](#)).

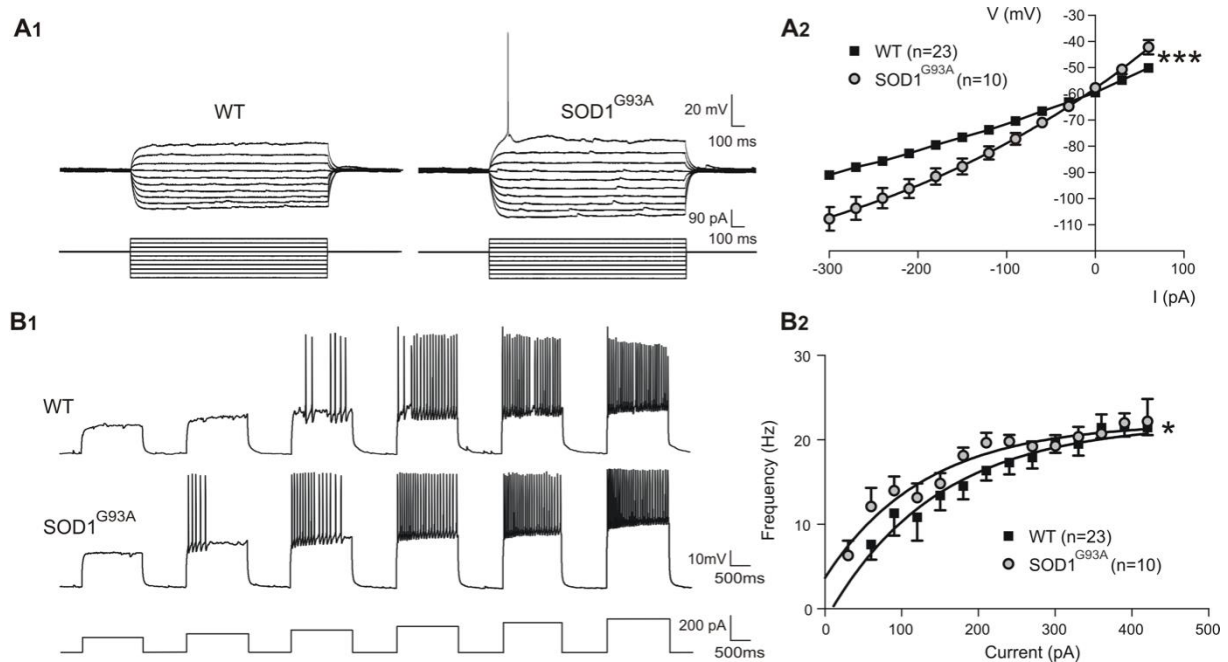


**Figure 37. Hyperexcitability in SOD1<sup>G93A</sup> MNs at E17.5.** **A1.** Membrane potential responses to similar current steps in WT and SOD1<sup>G93A</sup> MN. Note that, in response to the largest positive current

pulse, the SOD1<sup>G93A</sup> MN fires an action potential (AP) whereas the WT MN remains silent. **A2.** Mean voltage–current (V/I) relationship in WT (black squares) and SOD1<sup>G93A</sup> MNs (gray circles) revealing the increased input resistance in SOD1<sup>G93A</sup> MNs (steeper slope). **B1.** Characteristic membrane response of a WT MN (top trace) and a SOD1<sup>G93A</sup> MN (middle trace) to current injection of increasing steps (bottom trace). Note the SOD1<sup>G93A</sup> MN fires APs in response to the second current step, unlike the WT MN. **B2.** Average AP frequency, plotted against current intensity, revealing the hyperexcitability of SOD1<sup>G93A</sup> MNs (same symbols as in A2). \*p < 0.05, \*\*\*p < 0.001, two-way ANOVA. Adapted from Martin et al., 2013.

Hyperexcitability was also found in human iPSC-MNs derived from SOD1, FUS and C9orf72 associated familial patients ([Brian J. Wainger et al., 2014](#)). This hyperexcitability might damage nerve cells and lead to excitotoxicity. The critical role of excitotoxicity in ALS is an enduring concept and poses an attractive target for potential therapeutic strategies. Accordingly, until the recent approval of the drug Edaravone ([Rothstein, 2017](#)), the drug on the market for the treatment of ALS was Riluzole, which is thought to positively alter ALS progression by preventing excitotoxic pre-synaptic glutamate uptake ([Miller et al., 2012](#)). Supporting the role excitotoxic mechanisms play in disease genesis and progression, ALS patients display elevated levels of cerebrospinal fluid (CSF) glutamate ([P. J. Shaw et al., 1995](#)), and reduced expression and activity of the excitatory amino acid transporter 2 (EAAT2) in pathologically affected areas of the CNS ([Rothstein et al., 1992](#); [Rothstein et al., 1995](#); [Fray et al., 1998](#)). Moreover, findings in transgenic mice expressing a rare ALS-causing G127X mutant SOD1 protein indicate the protein is linked to excitotoxicity in ALS pathology by increasing sensitivity of motor neurons to excitotoxicity ([Meehan et al., 2010](#)), reducing the expression and activity of EAAT2 ([Boston-Howes et al., 2006](#)) and altering the inhibitory-excitatory synaptic ratio ([Sunico et al., 2011](#)).

Renshaw cell alterations may lead to hyperexcitability and eventually to MN degeneration. Loss of Renshaw cell function could be the result of degeneration of the corticospinal fibers directed to these cells and that the loss of cortical inhibitory influence, in association with ion channel alterations, may participate in increased motor network excitability ([Brunet et al., 2020](#)). Two hypotheses have been proposed to explain how Renshaw cell alterations may lead to a hyperexcitable state and eventual degeneration of MNs ([Scamps et al., 2021](#)). The first hypothesis postulates that the hyperexcitability is caused by loss of recurrent Renshaw cell-mediated inhibition and is based on electrophysiological findings suggesting an impairment of Renshaw cells in patients with ALS ([Raynor et al., 1994](#); [Shefner et al., 1998](#)). The second hypothesis proposes that the recurrent inhibitory circuit is

altered prior to MN hyperexcitability and neurodegeneration, but this was not a consequence of Renshaw cell loss due to the finding that loss of inhibitory spinal interneurons occurred after loss of motoneurons ([M. Hossaini et al., 2011](#)).

#### 1.2.2.8 SKELETAL MUSCLE ALTERATIONS

ALS had long been considered a pure motor neuron disease; however, recent studies have shown that motor neuron protection is not sufficient to prevent the course of the disease since the dismantlement of NMJs occurs before motor neuron degeneration. Skeletal muscle alterations have been described in the early stages of the disease. Studies in ALS mouse models have corroborated this hypothesis and described ALS as a distal axonopathy also caused by alterations in skeletal muscle ([Fischer et al., 2004](#)). Motor neuron activity regulates muscle physiology and function; in turn, muscles affect the neuronal activity by sending retrograde signals that preserve NMJ functionality and structure ([Heckman et al., 2012](#)). The so-called “dying back” hypothesis suggests that retrograde signals contribute to the centripetal motor neuron degeneration in ALS ([Dadon-Nachum et al., 2011](#)).

The NMJ connects muscle fibers and motor neurons, allowing their communication. The trophic factors (i.e. retrograde messenger) play an important role in the selection process of NMJ connections at nerve terminals ([Je et al., 2012](#); [Hurtado et al., 2017](#)). One of the most studied neurotrophic factors is brain-derived neurotrophic factor (BDNF), showing a neuroprotective effect under adverse conditions, such as glutamatergic stimulation, cerebral ischemia, hypoglycemia, and neurotoxicity ([Maisonpierre et al., 1991](#); [Bathina et al., 2015](#)). proBDNF-p75(NTR) signaling promotes retraction of the less active terminals, whereas mature BDNF-tyrosine-related kinase B (TrkB) p75NTR (p75 neurotrophin receptor) facilitates stabilization of the active ends ([Je et al., 2012](#)). Significantly higher levels of BDNF in CSF were found in ALS patients with faster disease progression and lower serum levels of proBDNF were associated with a shorter survival, indicating that BDNF and proBDNF might be used as ALS prognostic biomarkers ([Riolo et al., 2022](#)). ALS is the classic example of severely compromised communication between muscles and nerves ([Lepore et al., 2019](#)). NMJ degradation is the first event of denervation, and it occurs before motor neuron loss ([Fischer et al., 2004](#); [Loeffler et al., 2016](#)). NRG1-ErbBs signalling and, hence, NMJ development and maintenance depend on the

activation of muscle-specific receptor tyrosine kinase (MuSK) ([Burden, 2002](#)). MuSK orchestrates the muscle-derived retrograde signal through the interaction with LRP4 and agrin, ensuring NMJ stability and maintenance while preventing disassembly ([Kong et al., 2004](#); [Hesser et al., 2006](#); [Herbst, 2020](#); [Rodríguez Cruz et al., 2020](#)). MuSK overexpression in SOD1<sup>G93A</sup> double transgenic mice delayed the onset of ALS, improved motor ability, and preserved the integrity of NMJs ([Pérez-García et al., 2012](#)).

Preclinical genetic interventions on skeletal muscle highlighted the importance of this tissue in ALS progression as modifying the expression of genes involved in skeletal muscle physiology, metabolism, and functions had a strong impact (either positive or negative) on the disease. For example, IGF-1 regulates skeletal muscle physiology and promotes satellite cell proliferation and neuronal survival ([Musaro et al., 2002](#); [Y.-H. Song et al., 2013](#); [Ahmad et al., 2020](#); [Yoshida et al., 2020](#)). The expression of IGF-1 in skeletal muscle of ALS models gave the most remarkable results on disease progression and survival, delaying the death of SOD1<sup>G93A</sup> mice by about one month ([Dobrowolny et al., 2005](#)). In these mice, the regeneration pathways through calcineurin and CDK5 were induced, while apoptotic and ubiquitin pathways were inhibited, protecting muscles against atrophy and denervation and preserving NMJs and motor neurons ([Dobrowolny et al., 2005](#); [Dobrowolny et al., 2008](#)). Interestingly, high concentrations of IGF-1 in patients' serum correlate with a better prognosis but not with a lower risk of ALS, suggesting that IGF-1 plays a role in the survival of ALS patients ([Nagel et al., 2020](#)).

### **1.3. HYPOTHESIS / AIMS OF THE THESIS**

As we have seen, ALS is an adult-onset neurodegenerative disease characterized by a progressive and selective degeneration of MNs. Most ALS studies have focused on symptomatic adult stages based on the hypothesis that ALS pathogenesis occurs when the disease becomes symptomatic. However, growing evidence indicates that ALS pathogenesis might start long before symptom onset ([Jason J. Kuo et al., 2004](#); [Kuo et al., 2005](#); [Avossa et al., 2006](#); [Bories et al., 2007](#); [Amendola et al., 2008](#); [van Zundert et al., 2008](#); [Pambo-Pambo et al., 2009](#); [Q. Chang et al., 2011](#); [Quinlan et al., 2011](#); [Filipchuk et al., 2012](#); [Leroy et al.,](#)

[2014](#); [Milan et al., 2014](#); [Qing Chang et al., 2016](#); [Medelin et al., 2016](#)). A large number of abnormal cellular and molecular mechanisms underlying MNs degeneration have been identified, but to date such efforts have led to few improvements in therapy and no cure for ALS ([X. Xu et al., 2021](#)). “Hit hard, hit early” applies to any disease, including ALS ([Keon et al., 2021](#)). Earlier initiation of therapy is favorable for ALS patients to slow the fundamental neurodegenerative process, resulting in cost savings and prolonged survival. Hence, how can we facilitate an earlier diagnosis and mechanism-based therapies of ALS? Investigating a very early initiation of ALS pathogenesis is crucial. Interestingly, a recent study published in the journal *Science* demonstrated that Huntington's disease is one of the neurodegenerative diseases whose pathogenesis originates in the neurodevelopmental stage ([Braz et al., 2022](#)). Thereby, my PhD thesis hypothesized that **the pathogenesis of ALS disease originates in the prenatal development period**.

Changes in excitability of diseased MNs in ALS mouse models occur remarkably early, which are detected during prenatal development ([Pieri et al., 2003](#); [Jason J. Kuo et al., 2004](#); [Kuo et al., 2005](#); [Martin et al., 2013](#); [Qing Chang et al., 2016](#)) and postnatal first 2-week development ([van Zundert et al., 2008](#); [Pambo-Pambo et al., 2009](#)). Hyperexcitability is consistently exhibited in embryonic spinal SOD1<sup>G93A</sup> MNs in culture (embryonic day (E) 15.5 (E15.5), ([Pieri et al., 2003](#)); E12-14, ([Jason J. Kuo et al., 2004](#)); E13, ([Qing Chang et al., 2016](#))), E17.5 brainstem-spinal cord preparation ([Martin et al., 2013](#)), postnatal P0-12 spinal cord slices ([Quinlan et al., 2011](#)), and brainstem slices ([van Zundert et al., 2008](#)), as well as in human MNs derived from iPSCs obtained from patients with ALS ([Brian J. Wainger et al., 2014](#); [A.-C. Devlin et al., 2015](#)), relative to controls. Based on these findings, hyperexcitability in ALS is triggered much earlier, prior to the manifestation of symptoms. This early sign - cellular hyperexcitability - could be considered a hallmark during early pathogenesis of ALS and maybe a first or primary pathological event.

Cellular excitability is tightly regulated by, for example, intrinsic mechanisms such as ion channel density and function, and synaptic mechanisms that regulate the balance of excitation to inhibition. The intrinsic mechanisms for hyperexcitability in ALS at prenatal stage are well delineated and are mainly mediated by voltage-gated ion channels, including Na<sup>+</sup> ([Kuo et al., 2005](#)) and Ca<sup>2+</sup> ([Qing Chang et al., 2016](#))

channels. Moreover, our lab previously found that E17.5 SOD<sup>G93A</sup> MNs are hyperexcitable because of a shorter dendritic tree and increased input resistance ([Martin et al., 2013](#)). In our study, we cannot exclude a participation of the persistent Na<sup>+</sup> current in hyperexcitability of E17.5 SOD<sup>G93A</sup> MNs, but our study demonstrates that its contribution would be minor *versus* the alteration of the dendrite morphology (this is summarized in [Figure 38](#)). However, little is known about the synaptic mechanisms underlying the hyperexcitability of prenatal SOD<sup>G93A</sup> MNs. Does a reduction in the inhibitory inputs or an increase of the excitatory inputs lead to higher firing rates? How are altered synaptic inputs and dendritic morphology integrated (i.e., dendritic integration), leading to hyperexcitability?

From a theoretical viewpoint, increasing the excitability of a network or cellular hyperexcitability can be achieved equally well by increasing excitatory input or removing inhibitory input. In fact, silent interconnections can be achieved better by disinhibiting than by enhancing excitability. Furthermore, among the numerous potential causative links in ALS associated dysfunction and degeneration, more and more evidences point to the key role of inhibitory alteration ([Ramirez-Jarquin et al., 2014](#); [Clark et al., 2015a](#); [Ramírez-Jarquín et al., 2018](#); [Van den Bos et al., 2018](#)), with vulnerability being induced in the perinatal period ([Eisen et al., 2014b](#)). Therefore, this thesis focused on investigating changes of prenatal (E17.5) inhibition in spinal locomotor CPG networks. At E17.5 GABA/glycine is still depolarizing but a powerful shunting effect allows adult-like alternated activities between ipsi- and contra-lateral lumbar spinal CPGs. It is therefore worthy examining the inhibitory system in the E17.5 SOD1<sup>G93A</sup> mouse.

As summarized in the [Figure 38](#), the aims of my PhD thesis were to:

- 1- analyze the Cl<sup>-</sup> homeostasis in SOD<sup>G93A</sup> and littermate spinal lumbar MNs from the lateral motor column in order to identify whether the deficit of GABA/glycine inhibition leads to hyperexcitability in prenatal SOD<sup>G93A</sup> MNs. Also, understand cellular mechanisms underlying putative Cl<sup>-</sup> homeostasis changes. (Examination of the alteration in pre-synaptic compartments by analyzing the density of GABAergic/glycinergic inputs).
- 2- investigate functional outcome of putative altered Cl<sup>-</sup> homeostasis on fictive locomotor-like activity.

- 3- unravel early compensatory or pathological mechanisms.
- 4- study the involvement of the morphology in the physiological integration of inhibitory GABA/glycine synaptic inputs in parallel to other parameters such as ECI.

First part of this thesis (i.e., the first article) addresses the first three aims, focusing on two factors - pre-synaptic GABAergic/glycinergic inputs density and post-synaptic GABA<sub>A</sub>R/GlyR responses (i.e., E<sub>Cl</sub>) - that regulate GABA/glycine inhibition, while the second part of this thesis (i.e., the second article) addresses the last objective by considering the MN morphology, ECI, inhibitory synaptic input density to integrate together to regulate GABA/glycine inhibition.

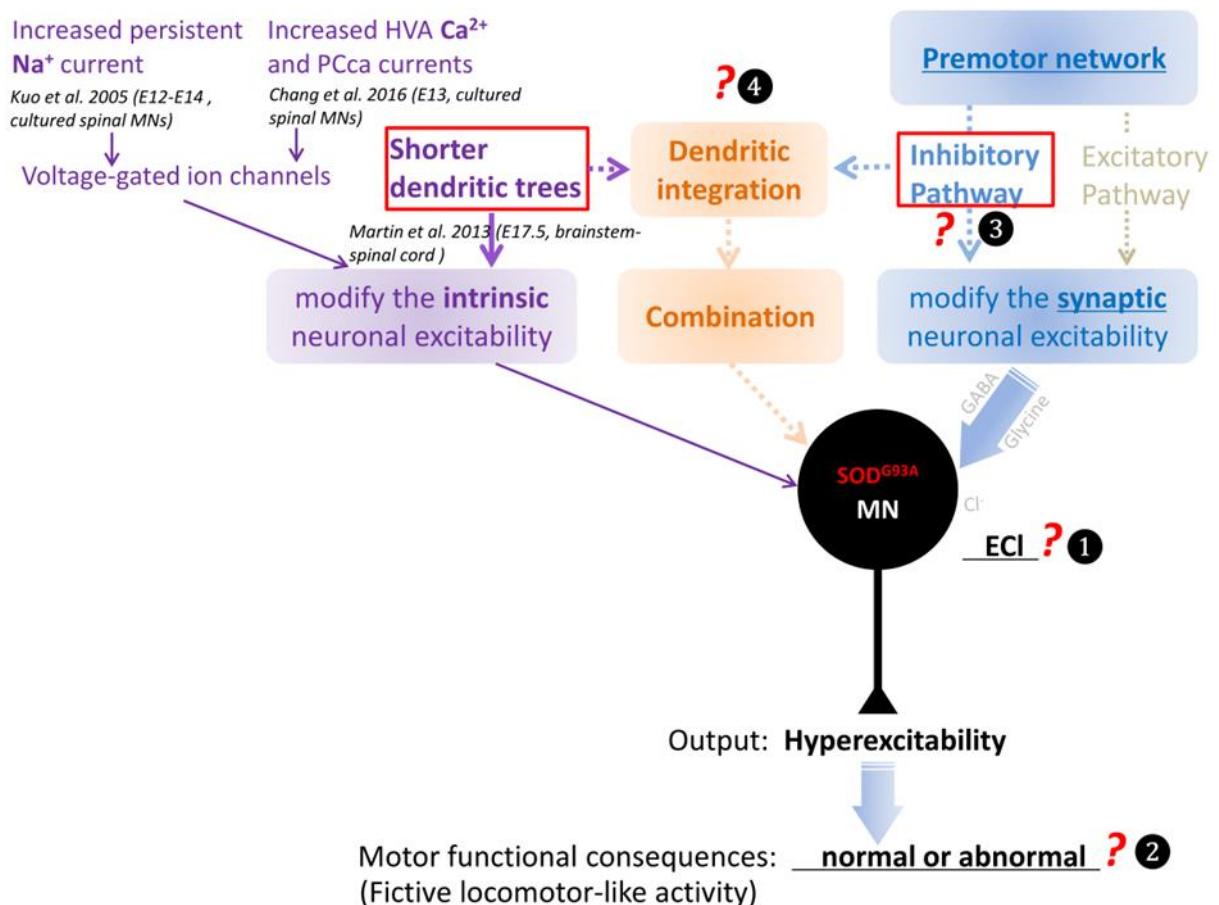


**Figure 38. Summary diagram of thesis aims.** The thin solid arrows represent proven whereas the washed dashed arrows have not been proven. In mouse spinal cord organotypic cultures and *ex vivo* brainstem-spinal cord preparation, output of spinal SOD<sup>G93A</sup> MNs that exhibited hyperexcitability was demonstrated at middle and late embryonic stages (see **text in purple**). Such alterations in neuronal excitability may be regulated by intrinsic mechanisms and/or synaptic mechanisms (i.e., extrinsic or network). The intrinsic mechanisms for hyperexcitability of immature SOD<sup>G93A</sup> MNs have been well studied, but synaptic mechanisms have not been demonstrated (see **text in blue**). Therefore, my PhD

thesis investigated whether the hyperexcitability of SOD<sup>G93A</sup> MNs could be induced by mechanisms besides these intrinsic mechanisms, such as an alteration in the synaptic inputs received by a motoneuron. We focused on the GABA/glycine inhibitory pathway from the premotor network to investigate whether this pathway is involved in hyperexcitability of E17.5 SOD<sup>G93A</sup> MNs. Accordingly, four scientific questions needed to be addressed: 1) How is the GABAAR/GlyR-mediated inhibition in SOD<sup>G93A</sup> MNs? (To evaluate changes in Cl<sup>-</sup> homeostasis) | What are the mechanisms of GABA/glycine inhibition deficiency, leading to hyperexcitability of prenatal SODG93A MNs? = Does a reduction in the inhibitory inputs lead to higher firing rates? (To analyse the density of GABAergic/glycinergic inputs); 2) What's the consequence of putative alterations in inhibitory pathways on motor function? (To assess outcome on fictive locomotor-like activity). Answering this question will help to determine whether the properties of hyperexcitability caused by inhibitory dysfunction are maintained in a compensatory state or have been transformed into a fully pathological state; 3) What early compensatory or pathological mechanisms are involved in the putative alteration of Cl<sup>-</sup> homeostasis? 4) Is it the integration of multiple factors such as morphology, inhibitory synaptic inputs and ECl that synergistically regulates neuronal hyperexcitability? *HVA: high voltage activated, PCca: Persistent Ca<sup>2+</sup> current. Cl<sup>-</sup> homeostasis - evaluating [Cl<sup>-</sup>]<sub>i</sub> - calculated from individual ECl (ECl = E<sub>GABAAR</sub>, because Cl<sup>-</sup> ions are mainly involved in GABA<sub>A</sub>R currents in foetal MNs (J Bormann et al., 1987; B. X. Gao et al., 1995))*

## **CHAPTER 2 RESULTS – PAPER 1**



# Relaxation of synaptic inhibitory events as a compensatory mechanism in fetal SOD spinal motor networks

Pascal Branchereau\*, Elodie Martin, Anne-Emilie Allain, William Cazenave, Laura Supiot, Fara Hodeib, Amandine Laupénie, Urvashi Dalvi, Hongmei Zhu, Daniel Cattaert

University of Bordeaux, CNRS, INCIA, UMR 5287, Bordeaux, France

**Abstract** Amyotrophic lateral sclerosis (ALS) is a devastating neurodegenerative disease affecting motor neurons (MNs) during late adulthood. Here, with the aim of identifying early changes underpinning ALS neurodegeneration, we analyzed the GABAergic/glycinergic inputs to E17.5 fetal MNs from SOD1<sup>G93A</sup> (SOD) mice in parallel with chloride homeostasis. Our results show that IPSCs are less frequent in SOD animals in accordance with a reduction of synaptic VIAAT-positive terminals. SOD MNs exhibited an  $E_{GABAAR}$  10 mV more depolarized than in WT MNs associated with a KCC2 reduction. Interestingly, SOD GABAergic/glycinergic IPSCs and evoked GABA<sub>A</sub>R-currents exhibited a slower decay correlated to elevated [Cl<sup>-</sup>]. Computer simulations revealed that a slower relaxation of synaptic inhibitory events acts as compensatory mechanism to strengthen GABA/glycine inhibition when  $E_{GABAAR}$  is more depolarized. How such mechanisms evolve during pathophysiological processes remain to be determined, but our data indicate that at least SOD1 familial ALS may be considered as a neurodevelopmental disease.

## Introduction

Amyotrophic Lateral Sclerosis (ALS), also known as Lou Gehrig's disease, is a rapidly progressive neurodegenerative disease that targets motor neurons (MNs). It is one of the most common and most devastating neurodegenerative diseases. The incidence rate of ALS in the general European population has been estimated as ~2 per 100 000 person per year (*Logroscino et al., 2010*). What makes ALS particularly devastating is that there is no known curative treatment. Death often occurs due ultimately to respiratory paralysis that concludes the progressive pattern of the disease, with the mean survival time of patients post-diagnosis being 3 to 5 years.

In 90% of cases, ALS is idiopathic and sporadic (sALS). Only 10% of ALS cases are familial (fALS) in origin, inherited through an autosomal dominant pattern. Around 20 genes are associated with ALS, with the most common causes of typical ALS being associated with mutations in SOD1, TARDBP, FUS and C9orf72 (*Van Damme et al., 2017*). Mutations in C9orf72 are the most common cause of fALS (10% of total ALS) followed by mutations in SOD1 (superoxide dismutase 1) (2% of total ALS). Interestingly, misfolded SOD1 was found in MNs in a subset of patients with sALS that did not have SOD1 mutations, suggesting that there is a SOD1-dependent pathway common to both sALS and fALS (*Bosco et al., 2010; Pare´ et al., 2018*).

Because ALS is a lethal adult-onset neurodegenerative disease, most studies have focused on symptomatic adult stages. However, a growing body of evidence indicates that ALS pathogenesis might develop earlier than previously expected (*Kuo et al., 2004; Kuo et al., 2005; Avossa et al., 2006; Bories et al., 2007; Amendola and Durand, 2008; van Zundert et al., 2008; Pambo-Pambo et al., 2009; Chang and Martin, 2011; Quinlan et al., 2011; Filipchuk and Durand, 2012; Leroy et al., 2014; Milan et al., 2015; Chang and Martin, 2016; Medelin et al., 2016*). Using the

\*For correspondence:  
pascal.branchereau@u-bordeaux.fr

Competing interests: The authors declare that no competing interests exist.

Funding: See page 21

Received: 27 August 2019

Accepted: 20 December 2019

Published: 23 December 2019

Reviewing editor: Inna Slutsky, Tel Aviv University, Israel

© Copyright Branchereau et al. This article is distributed under the terms of the [Creative Commons Attribution License](#), which permits unrestricted use and redistribution provided that the original author and source are credited.

transgenic mouse model SOD1<sup>G93A</sup> (SOD, Gly93fiAla substitution), which expresses a large degree of human mutant SOD1 and faithfully recapitulates a vast majority of the pathology's abnormalities seen in ALS patients (Fogarty, 2018), we previously found that SOD MNs are hyperexcitable at the prenatal (embryonic day (E) 17.5) stage because of a shorter dendritic tree and increased input resistance (Martin et al., 2013).

Among the numerous potential causative link in ALS associated dysfunction and degeneration, more and more evidence point to the key role of inhibitory alteration (Ramírez-Jarquín et al., 2014; Clark et al., 2015; Ramírez-Jarquín and Tapia, 2018; Van den Bos et al., 2018), with vulnerability being induced in the perinatal period (Eisen et al., 2014).

Here, using gramicidin intracellular recordings of SOD and wild type (WT) lumbar spinal prenatal E17.5 MNs from the lateral motor column (LMC, ventral pool), we first analyzed chloride homeostasis and found that  $E_{GABAAR}$  was 10 mV more depolarized in the SOD fetus compared to WT associated with a KCC2 down-regulation. Interestingly, locomotor-like activity remained normal. We then examined the premotor network at the same fetal developmental stage in order to determine underlying mechanisms that could compensate for MN hyperexcitability and chloride homeostasis deficiency. This was performed by combining whole-cell patch-clamp recordings and immunohistochemistry. Miniature (m), spontaneous (s) inhibitory postsynaptic currents (IPSCs) as well as evoked (e) IPSCs and puff-evoked GABA<sub>A</sub>R currents were quantified in parallel with the staining of synaptic VIAAT boutons. Our results show a significant reduction in IPSC frequency in SOD MNs compared to WT MNs, in agreement with a reduction in synaptic VIAAT-positive terminals. Our result also show a significantly slower decay time in SOD IPSCs and GABA<sub>A</sub>R-currents compared to WT. Interestingly, this slower decay is associated with a higher intracellular chloride concentration  $[Cl]_i$  in SOD MNs compared to WT. In prenatal E17.5 MNs, GABAergic/glycinergic postsynaptic potentials are depolarizing (dGPSPs) and exert mixed excitatory (depolarizing) and inhibitory (shunting) effects on the input-output (I-O) relationship (Gulledge and Stuart, 2003; Alger and Nicoll, 1982; Michelson and Wong, 1991; Misgeld et al., 1982; Staley and Mody, 1992). Higher  $[Cl]_i$  would then result in shifting the balance dGPSPs toward more excitation (Branchereau et al., 2016). However, Using computer simulations, we demonstrate that longer decay time reinforce the inhibitory component of dGPSPs. Therefore longer relaxation of dGPSPs constitutes a partial compensatory mechanism sustaining a well-coordinated, although slightly slower, locomotor activity in prenatal SOD mice. Together, our findings show that although the presynaptic network of SOD MNs is altered at fetal stages, cellular mechanisms leading to long-lasting IPSCs operate to compensate for the depolarized  $E_{GABAAR}$  and hyperexcitability of E17.5 SOD MNS in order to maintain a coordinated locomotor activity.

## Results

### Fetal MNs exhibit a perturbed chloride homeostasis but normal locomotor-like activity

Initially, gramicidin perforated patch-clamp recordings from L4-L5 MNs were used to obtain Rin and Cm values for individual MNs. SOD MN values for Rin and Cm were  $148.2 \pm 13.5$  MW,  $n = 21$  and  $105.6 \pm 5.9$  pF,  $n = 21$ ,  $N = 16$ , respectively, and were significantly different ( $p < 0.05$ , Mann Whitney test) from WT MNs values ( $104.9 \pm 10.8$  MW,  $n = 16$  and  $143.7 \pm 14.2$  pF,  $n = 16$ ,  $N = 10$ ) (Table 1). These values corresponded to the previously reported differences between WT and SOD MNs (Martin et al., 2013).

Table 1. Passive membrane properties of E17.5 MNs and GABA<sub>A</sub>R conductances.

Data are from perforated patch-clamp recordings and are shown as mean  $\pm$  SEM. Statistical significance was calculated by a non-parametric Mann Whitney test. ns,  $p > 0.05$ ; \* $p < 0.05$ .

	Rin (MW)	Cm (pF)	$g_{GABAAR}$ (pS)	$g_{GABAAR}/Cm$ (MW/pS)	N	N
WT	$104.9 \pm 10.8$	$143.7 \pm 14.2$	$3.90 \pm 0.97$	$0.029 \pm 0.007$	16	10
SOD	$148.2 \pm 13.5^*$	$105.6 \pm 5.9^*$	$1.91 \pm 0.24^{ns}$	$0.019 \pm 0.003^{ns}$	21	16

Puff application of the GABA<sub>A</sub>R agonist isoguvacine allowed us to measure the reversal potential of GABA<sub>A</sub>R ( $E_{\text{GABAAR}}$ ) in individual SOD and WT MNs (Figure 1A), while our pooled data indicated that mean  $E_{\text{GABAAR}}$  was significantly different in SOD MNs ( $-50.5 \pm 2.4$  mV,  $n = 25$ ,  $N = 18$ ) and WT MNs ( $-62.0 \pm 2.0$  mV,  $n = 24$ ,  $N = 17$ ) ( $p < 0.001$ , Mann Whitney test) (Figure 1B1). From these  $E_{\text{GABAAR}}$  values, and because  $\text{Cl}^-$  ions are mainly involved in GABA<sub>A</sub>R currents in fetal MNs (Bormann *et al.*, 1987; Gao and Ziskind-Conhaim, 1995), we calculated the intracellular chloride concentration  $[\text{Cl}^-]_i$  as being  $19.5 \pm 1.5$  mM and  $12.2 \pm 0.9$  mM in SOD and WT MNs, respectively ( $p < 0.001$ , Mann Whitney test) (Figure 1B2). Interestingly,  $[\text{Cl}^-]_i$  values reported in E17.5 WT MNs are in agreement with those previously reported, i.e., 12 mM (Delpy *et al.*, 2008). The resting membrane potential ( $E_m$ ) was not significantly different between SOD and WT MNs ( $-73.1 \pm 0.5$  mV in SOD and  $-74.1 \pm 1.0$  mV in WT MNs ( $p > 0.05$ , Mann Whitney test MNs) (Figure 1B3), in contrast to the mean driving force ( $\text{DF} = E_m - E_{\text{GABAAR}}$ ), which was  $22.6 \pm 2.3$  mV and  $12.1 \pm 2.2$  mV in SOD and WT MNs, respectively ( $p < 0.001$ , Mann Whitney test) (Figure 1B4).

The dissipation of an elevated intracellular  $\text{Cl}^-$  concentration is mediated by the activation of the neuronal  $\text{K}^+/\text{Cl}^-$  co-transporter type 2 (KCC2) (Payne *et al.*, 1996; Rivera *et al.*, 1999). This protein, which extrudes  $\text{Cl}^-$ , is expressed at early stages in the embryonic SC (Delpy *et al.*, 2008). The  $[\text{Cl}^-]_i$  is also related to the  $\text{Na}^+ - \text{K}^+ - 2\text{Cl}^-$  co-transporter NKCC1, which intrudes chloride ions (Russell, 2000; Delpy *et al.*, 2008). Therefore, in order to identify the cellular mechanisms underlying the higher  $[\text{Cl}^-]_i$  in SOD MNs, we firstly assessed the amount of KCC2 and NKCC1 in lumbar SCs using WB. Our data showed that KCC2 was reduced by ~19% in SOD lumbar SCs compared to WT ( $p < 0.05$ , Mann Whitney test) (Figure 2A1) whereas NKCC1 was unchanged (Figure 2A2). When analyzed in the MN area (Hb9-eGFP), the KCC2 staining appeared as significantly reduced in SOD SCs ( $181.5 \pm 16.2$  arbitrary unit (AU),  $n = 43$ ,  $N = 4$ ) compared to WT ( $395.0 \pm 20.3$  AU,  $n = 42$ ,  $N = 4$ ) ( $p < 0.001$ , Mann Whitney test) (Figure 2B1–B2 and B5). At the level of the MN membrane, the KCC2 density was also significantly reduced in SOD SCs ( $5.8 \pm 0.6$  AU,  $n = 81$ ,  $N = 4$ ) compared to WT SCs ( $8.5 \pm 0.6$  AU,  $n = 116$ ,  $N = 4$ ) ( $p < 0.01$ , Mann Whitney test) (Figure 2B3–B4 and B6). Functionally, we found that the KCC2 efficacy, assessed using indirect measurements, was reduced in SOD MNs:  $E_{\text{GABAAR}}$  reached a maximum of  $-43.8 \pm 0.8$  mV ( $n = 19$ ,  $N = 16$ ) in SOD MNs and  $-46.5 \pm 0.7$  mV ( $n = 24$ ,  $N = 17$ ) in WT ( $p < 0.05$ , Mann Whitney test) after 30 s isoguvacine pressure ejection (Figure 2C) and returned to control values:  $-49.3 \pm 1.2$  mV ( $n = 19$ ) in SOD MNs and  $-54.8 \pm 1.0$  mV ( $n = 24$ ) in WT ( $p < 0.001$ , Mann Whitney test) after a 4 min isoguvacine washout (Figure 2C). This difference was absent when the specific KCC2 blocker VU0240551 was applied (Figure 2C).

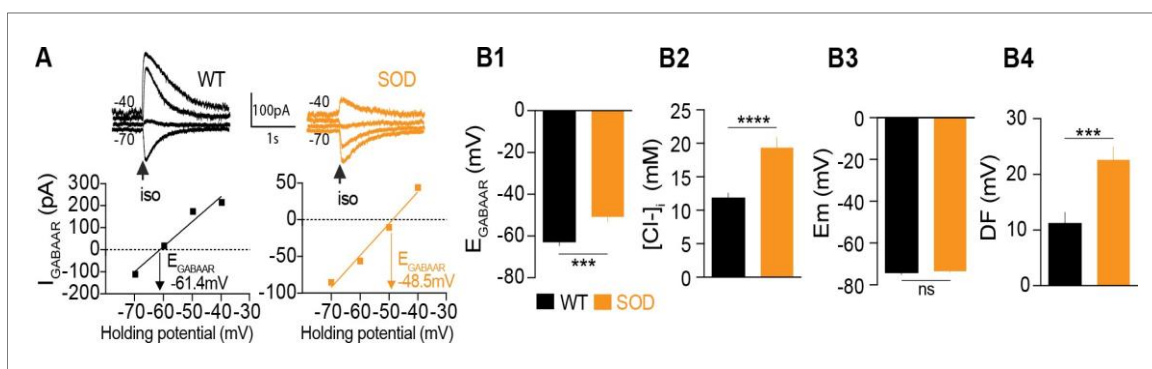


Figure 1. Alterations in chloride homeostasis. (A) Representative traces of isoguvacine (Iso) responses illustrating the reversal of the evoked GABA<sub>A</sub>R-related current ( $E_{\text{GABAAR}}$ ) in WT and SOD MNs. Holding voltage  $-70$  mV,  $-60$  mV,  $-50$  mV and  $-40$  mV. I/V relationships, plotted below the traces, revealed that  $E_{\text{GABAAR}}$  was  $-61.4$  mV and  $-48.5$  mV in the representative WT and SOD MNs, respectively. (B1) Mean  $E_{\text{GABAAR}}$  was significantly lower in E17.5 WT ( $n = 25$ ) compared to SOD ( $n = 24$ ) MNs from the same litter. (B2) Accordingly, the mean  $[\text{Cl}^-]_i$ , calculated from individual  $E_{\text{GABAAR}}$  values, indicated that SOD MNs had a higher  $[\text{Cl}^-]_i$  than WT. (B3) Mean resting membrane potential ( $E_m$ ) did not differ in WT and SOD MNs. (B4) Mean driving force (DF) for chloride ions was doubled in SOD MNs compared to WT MNs. Values illustrated were from the same set of MNs. \*\*\*\* $p < 0.0001$ , \*\*\* $p < 0.001$ , ns non-significant, Mann Whitney test.

The online version of this article includes the following figure supplement(s) for figure 1:

Figure supplement 1. Recorded MNs belong to the lateral motor column (LMC).

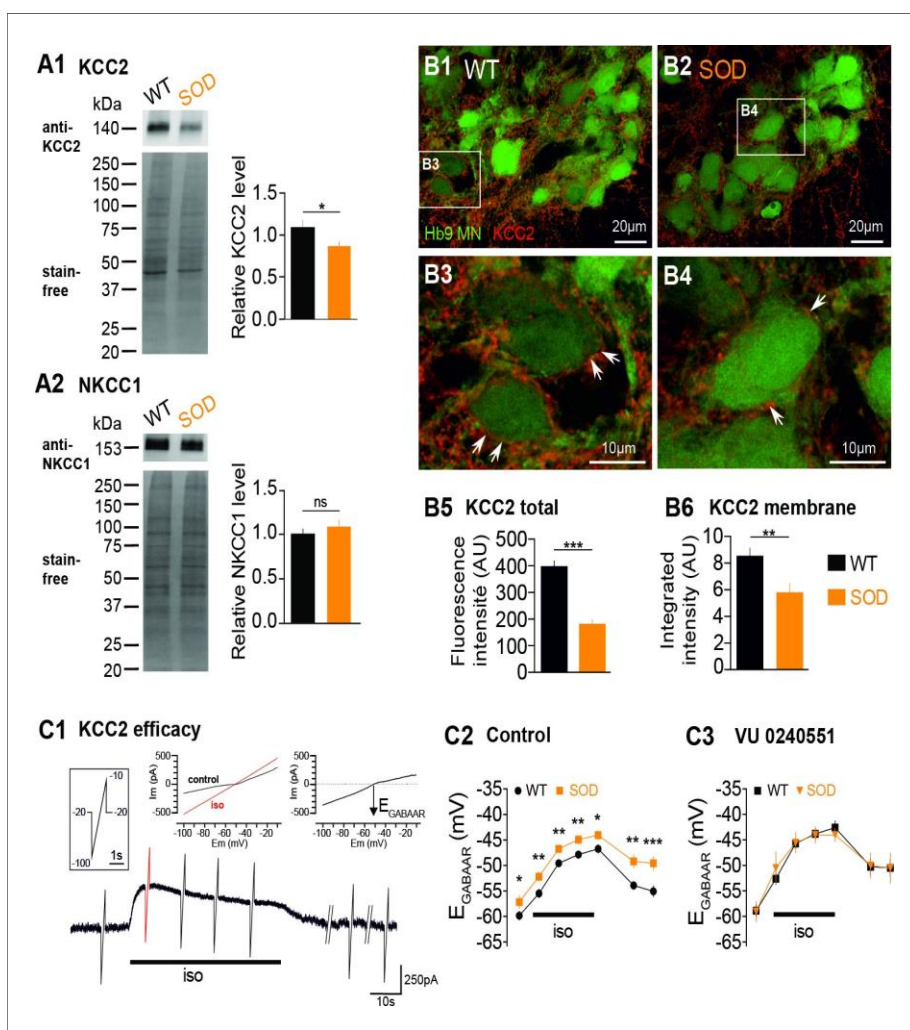


Figure 2. Expression of KCC2 and NKCC1 in the E17.5 SOD spinal cord. (A1) Analysis of the KCC2 protein in SOD and WT SCs. The stain-free staining of total proteins loaded (lower left panel) was used as the normalization control to quantify the ~140 kDa KCC2 band (upper left panel). Right panel: quantification of KCC2 WB. (A2) Analysis of the NKCC1 protein in SOD and WT SCs. The ~150 kDa NKCC1 band (upper left panel) was analyzed. Quantification of NKCC1 WB. Three loads (20 mg of protein) from SOD and WT lumbar spinal cord extracts were used, each load including five individual SCs from four different litters. (B1-B4) Representative immunohistochemical KCC2 (red) staining in WT (B1-B3) and SOD (B2-B4) lumbar 0.2 mm thickness optical sections (L3-L5 level) containing Hb9-eGFP MNs (green). Images correspond to x60 confocal acquisitions. White arrows point the KCC2 labeling surrounding spinal MNs. (B5-B6) Quantification of the global KCC2 staining (B5) in the MN area and membrane KCC2 staining (B6) in E17.5 SOD and WT SCs. (C1) Illustration of the protocol applied to assess the KCC2 efficacy as explained in the Materials and method section. (C2-C3) Evolution of  $E_{Cl}$  values with time during the isoguvacine (iso) application in control aCSF (C2) and in the presence of the highly specific KCC2 blocker VU0240551 (10 mM) (C3). \*\*\* $p < 0.001$ , \*\* $p < 0.01$ , \* $p < 0.05$ , ns non-significant, Mann Whitney test.

In order to assess whether the alteration of chloride homeostasis in SOD MNs could affect the left-right alternation in locomotor-like activity expressed by E17.5 mouse spinal lumbar networks due to half-centers organization and commissural inhibition (Branchereau *et al.*, 2000), we recorded this activity in L3-L5 ventral roots after exogenous application of 5-HT/NMDA/DA. As illustrated in Figure 3A1, this cocktail evoked stable bilateral segmental alternation between left and right ventral roots in WT SC preparations. Chemically-activated locomotor-like activity was also expressed in the ventral roots of SOD SCs (Figure 3A2), although analysis (Rayleigh's test) revealed a slower rhythm period in SOD SCs ( $2.01 \pm 0.03$  s,  $n = 8$ ,  $N = 5$ ) compared to WT controls where bursts recurred with

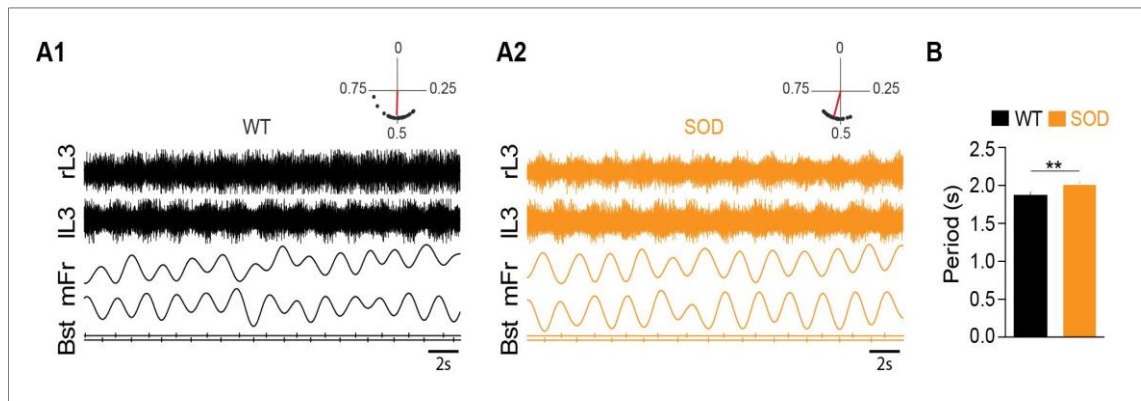


Figure 3. Motor activity in the E17.5 SOD spinal cord. (A) Fictive locomotor-like activity evoked by 5-HT/NMDA/DA (see Materials and methods) recorded from contralateral lumbar ventral roots (IL3, rL3; two first traces) displayed regular alternating activities (see circular plots above each raw data panel) in both WT (A1) and SOD (A2) SCs. Below the raw data are traces of the floating mean spike frequencies (mFr) and the corresponding troughs of activity (burst start, Bst) from which the phase relationships between the left and right SC sides were calculated (circular plots). (B) The cycle period was significantly longer in SOD SCs ( $n = 9$ ) compared to WT ( $n = 8$ ) SCs.  $**p < 0.01$ , ns non-significant, Mann Whitney test.

a period of  $1.88 \pm 0.03$  s ( $n = 9$ ,  $N = 7$ ) ( $p < 0.01$ , Mann Whitney test) (Figure 3B). However, the rhythm phase relationship between left and right sides was close to anti-phase in both genotypes ( $0.49 \pm 0.003$  and  $0.52 \pm 0.004$  in SOD and WT SCs, respectively) (see polar plots in Figure 3A1–A2). Therefore, surprisingly, alteration of chloride homeostasis in SOD MNs has limited consequences on the locomotor-like activity and therefore little physiological consequences. Could compensatory mechanisms in the SOD spinal synaptic network explain this result?

In order to gain information about the synaptic inputs from the premotor inhibitory neuronal networks that underlies this MN activity, we then compared the occurrence and properties of GABA/glycinergic synaptic events in SOD and WT E17.5 MNs in the absence of rhythmic fictive locomotion. We found that miniature GABAergic/glycinergic inhibitory synaptic currents (mIPSCs), which persisted in the presence of TTX, were significantly ( $p < 0.001$ ; K-S test) less frequent in SOD: the mean inter-event interval (IEI) was  $887 \pm 30$  ms ( $n = 19$ ,  $N = 9$ , 1589 events) for SOD MNs and  $838 \pm 33$  ms ( $n = 15$ ,  $N = 7$ , 1366 events) for WT MNs from the same littermate ( $p < 0.001$ , Mann Whitney test) (Figure 4A1,A2). The mIPSCs of SOD MNs were also slightly smaller ( $52.8 \pm 0.9$  pA) compared to WT MNs ( $57.9 \pm 1.2$  pA) ( $p < 0.05$ , Mann Whitney test) (Figure 4A3).  $\tau_{\text{rise}}$  was not significantly different between SOD MNs ( $1.25 \pm 0.03$  ms) and WT MNs ( $1.11 \pm 0.02$  ms) ( $p > 0.05$ , Mann Whitney test), whereas  $\tau_{\text{decay}}$  was strongly significantly larger in SOD MNs ( $20.53 \pm 0.08$  ms) compared to WT MNs ( $16.11 \pm 0.40$  ms) ( $p < 0.0001$ , Mann Whitney test) (Figure 4A4, see inset traces). The total charge of mIPSCs, calculated for best-fitted ( $R > 0.98$ ) mIPSCs, was similar in SOD MNs ( $-1.14 \pm 0.04$  pA.s,  $n = 841$ ,  $N = 9$ ) and WT MNs ( $-1.18 \pm 0.04$  pA.s,  $n = 901$ ,  $N = 7$ ) ( $p > 0.05$ , Mann Whitney test), indicating that the longer relaxation for SOD mIPSCs likely compensated their reduced amplitude. The development of synaptic inhibition in spinal MNs involves a functional switch between GABA to glycine events (Gao et al., 2001). We therefore focused on pharmacologically dissected GABA and glycine mIPSCs, isolated using strychnine and GABAzine, respectively. Interestingly, strychnine application revealed a tonic glycine current in 5/7 SOD MNs and 4/6 WT MNs (Figure 4A5) without any significant difference in amplitude between SOD MNs ( $11.72 \pm 3.34$  pA,  $n = 5$ ,  $N = 5$ ) and WT MNs ( $11.15 \pm 2.36$  pA,  $n = 4$ ,  $N = 4$ ) ( $p > 0.05$ , Mann Whitney test). We found a tonic GABA current in only 3/8 SOD MNs and 2/7 WT MNs, this tonic current being comparable in both genotypes:  $15.03 \pm 1.09$  pA ( $n = 3$ ,  $N = 3$ ) for SOD MNs and  $10.40 \pm 0.60$  pA ( $n = 2$ ,  $N = 2$ ) for WT MNs ( $p > 0.05$ , Mann Whitney test). This tonic glycine and GABA current likely favors tonic shunting effect as previously demonstrated (Branchereau et al., 2016; Song et al., 2011).

The pharmacological dissection revealed that mIPSCs were ~50% pure glycine, ~40% pure GABA, the remaining events ~10% being mixed (see Figure 4A6–A8). No difference was found between SOD MNs ( $48.43 \pm 8.26\%$  glycine,  $n = 5$ ,  $N = 5$ ;  $39.65 \pm 16.77\%$  GABA,  $n = 3$ ,  $N = 3$ ) and WT MNs ( $51.46 \pm 9.41\%$  glycine,  $n = 3$ ,  $N = 3$ ;  $41.79 \pm 7.97\%$  GABA,  $n = 5$ ,  $N = 5$ ) ( $p > 0.05$ , Mann Whitney

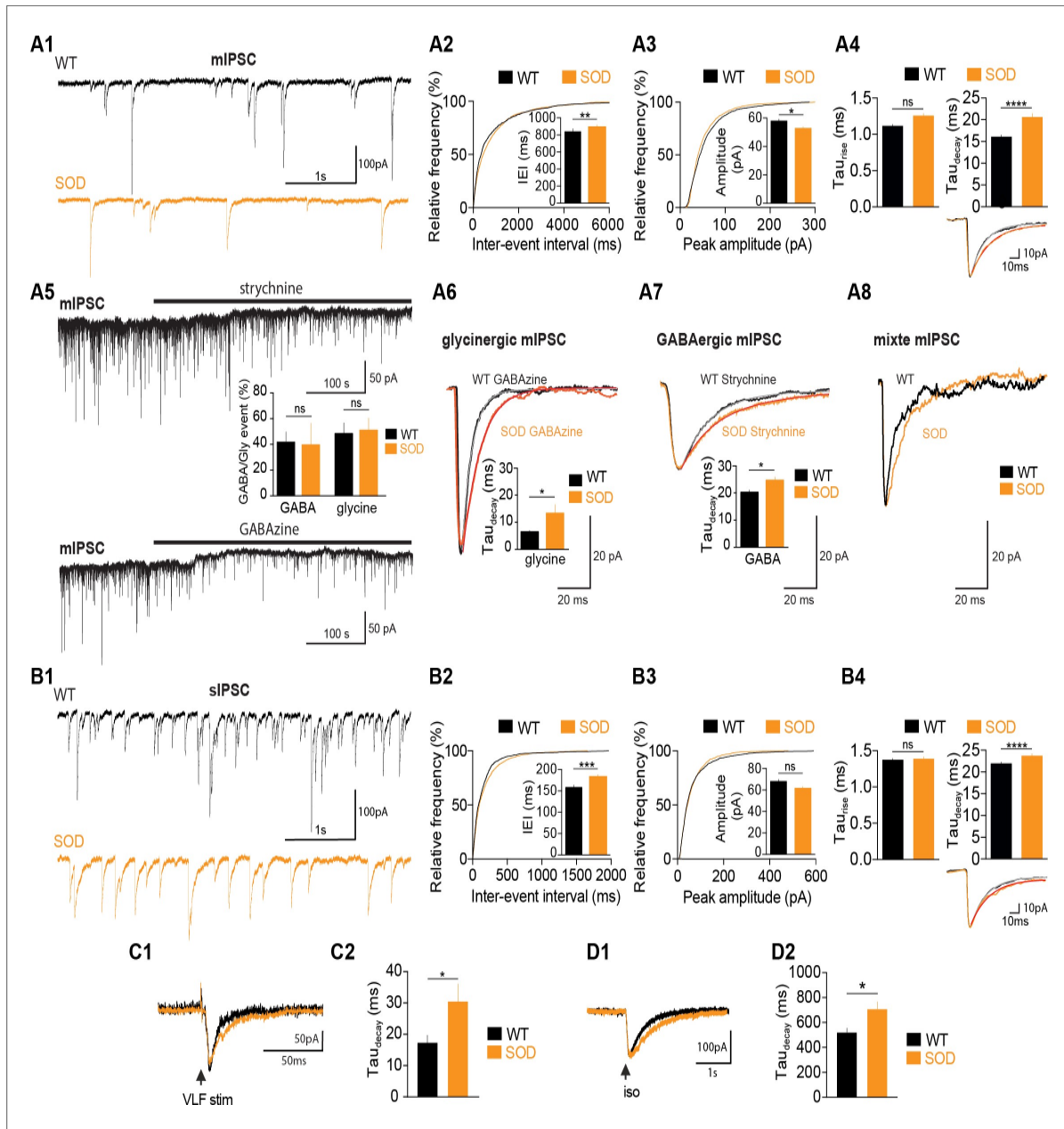


Figure 4. SOD E17.5 MNs exhibit a reduced IPSC frequency compared with WT MNs along with a persistent increase in their  $\tau_{decay}$ . (A1) Sample miniature IPSC (mIPSC) recordings obtained from representative SOD and WT MNs (holding membrane potential  $-70$  mV). (A2) Cumulative frequency of inter-event interval (IEI) and mean values of mIPSCs revealed a small but significant reduction in frequency in SOD MNs ( $n = 19$ ) compared with WT ( $n = 15$ ) MNs. (A3) mIPSC peak amplitude was slightly smaller in SOD than in WT MNs (same layout as in A2). (A4) Mean  $\tau_{rise}$  was unchanged but mean  $\tau_{decay}$  was significantly increased in SOD mIPSCs compared with WT mIPSCs. Inset traces (mean of 30 events) from representative experiments. (A5) Blocking the GlyR or GABA<sub>A</sub>R (black horizontal bars) reveals a tonic current. The distribution of pure GABA<sub>A</sub>R-mediated mIPSCs in WT ( $n = 5$ ) and SOD ( $n = 3$ ) MNs and pure GlyR-mediated mIPSCs in WT ( $n = 3$ ) and SOD ( $n = 5$ ) MNs is shown between the two traces. (A6)  $\tau_{decay}$  of pure GlyR-mediated mIPSCs is significantly increased in SOD MNs ( $n = 3$ ) compared to WT MNs ( $n = 5$ ). Traces are mean of 53 events (WT) and 57 events (SOD) from representative experiments. (A7) Relaxation of pure GABA<sub>A</sub>R-mediated mIPSCs is significantly longer in SOD MNs ( $n = 3$ ) compared to WT MNs ( $n = 5$ ). Traces are mean of 35 events (WT) and 35 events (SOD) from representative experiments. (A8) Mixed GlyR-GABA<sub>A</sub>R-mediated events from representative experiments. (B1) Samples of spontaneous IPSC (sIPSC) recordings from representative SOD and WT MNs. (B2) Cumulative frequency of IEI and mean values of sIPSCs revealed a slight frequency reduction in SOD MNs ( $n = 17$ ) compared to WT MNs ( $n = 14$ ). (B3) sIPSC peak amplitudes were similar in SOD and WT MNs. (B4) Mean  $\tau_{rise}$  was not significantly different in WT sIPSCs, but SOD sIPSCs exhibited a higher  $\tau_{decay}$ . Inset traces (mean of 30 events) from representative experiments. (C1-C2) SOD eIPSCs ( $n = 6$ ) displayed a higher  $\tau_{decay}$  than WT eIPSCs ( $n = 10$ ). (D1-D2) Puff-

Figure 4 continued on next page

## Figure 4 continued

evoked SOD GABA<sub>A</sub>R currents (n = 21) exhibited a higher  $\tau_{decay}$  than WT GABA<sub>A</sub>R currents (n = 16). Left traces in C1) and D1) are from representative SOD and WT eIPSCs and puff-evoked GABA<sub>A</sub>R currents. \*\*\*\*p<0.0001, \*\*\*p<0.001, \*\*p<0.01, \*p<0.05, ns non-significant, Mann Whitney test.

test). Interestingly, E17.5 SOD MNs, recorded at a holding potential of  $-70$  mV with  $E_{Cl}$  set at  $\sim 0$  mV displayed pure glycine and GABA mIPSCs with a longer relaxation than E17.5 WT animals from the same littermate.  $\tau_{decay}$  of pure glycine mIPSCs was  $13.35 \pm 3.14$  ms (n = 3, N = 3) in SOD MNs and  $6.53 \pm 0.44$  ms in WT MNs (n = 5, N = 5) (p<0.05, Mann Whitney test) (Figure 4A6) whereas  $\tau_{rise}$  were similar in both genotypes ( $1.24 \pm 0.12$  ms for SOD and  $1.18 \pm 0.07$  ms for WT, p>0.05, Mann Whitney test).  $\tau_{decay}$  of pure GABA mIPSCs was also larger in SOD MNs ( $24.69 \pm 1.18$  ms, n = 5, N = 5) compared to WT MNs ( $19.51 \pm 0.56$  ms, n = 3, N = 3) (p<0.05, Mann Whitney test) (Figure 4A7) whereas  $\tau_{rise}$  were similar in both genotypes ( $3.02 \pm 0.24$  ms for SOD and  $2.12 \pm 0.52$  ms for WT, p>0.05, Mann Whitney test).

Most of the differences found between SOD and WT mIPSCs were also observed in spontaneous GABAergic/glycinergic inhibitory synaptic currents (sIPSCs). An increase in IEI was found for sIPSCs (p<0.001; K-S test): mean IEI was  $182.3 \pm 5.9$  ms (n = 14, N = 10, 1499 events) and  $157.9 \pm 5.6$  ms (n = 17, N = 11, 1685 events) in SOD and WT MNs, respectively (p<0.001, Mann Whitney test) (Figure 4B1–B2). No difference was found in the amplitude of sIPSCs (p>0.05; K-S test):  $68.0 \pm 1.8$  pA in SOD MNs and  $61.7 \pm 1.4$  pA in WT MNs (p>0.05, Mann Whitney test) (Figure 4B3). Again the  $\tau_{rise}$  was not significantly different between SOD MNs ( $1.38 \pm 0.02$  ms) and WT MNs ( $1.37 \pm 0.02$  ms) (p>0.05, Mann Whitney test), whereas  $\tau_{decay}$  was again strikingly larger in SOD MNs compared to WT MNs:  $21.89 \pm 0.42$  ms in WT MNs and  $23.58 \pm 0.53$  ms in SOD MNs (p<0.0001, Mann Whitney test) (Figure 4B4, see inset traces). VLF (ventro-lateral funiculus)-evoked IPSCs (eIPSCs) recorded in MNs at a holding potential  $-70$  mV with an imposed  $E_{Cl}$  of  $-45$  mV also revealed a longer  $\tau_{decay}$  ( $30.3 \pm 5.7$  ms, n = 6, N = 3) in SOD MNs compared to WT MNs ( $18.3 \pm 2.7$ , n = 10, N = 4) (p<0.05, Mann Whitney test) (Figure 4C1–C2), the amplitude and  $\tau_{rise}$  of eIPSCs being not significantly different ( $62.4 \pm 16.6$  pA,  $2.8 \pm 0.5$  ms in SOD, n = 6 and  $72.1 \pm 13.2$  pA,  $2.3 \pm 0.3$  ms in WT, n = 10). This was in agreement with our data showing a reduced efficacy of KCC2 (Figure 2C) leading to a higher  $[Cl^-]_i$  in SOD MNs compared to WT and therefore a slower relaxation of IPSCs (Pitt et al., 2008; Houston et al., 2009). Finally,  $\tau_{decay}$  of puff-evoked GABA<sub>A</sub>R current was also affected in the same way:  $707.8 \pm 57.8$  ms (n = 21, N = 16) in SOD MNs versus  $521.3 \pm 33.3$  ms (n = 16, N = 10) in WT (p<0.05, Mann Whitney test) (Figure 4D1–D2), the amplitude and  $\tau_{rise}$  of evoked IPSCs (eIPSCs) being not significantly different ( $49.3 \pm 5.9$  pA,  $34.9 \pm 3.6$  ms in SOD, n = 21 and  $58.1 \pm 8.6$  pA,  $43.3 \pm 5.8$  ms, n = 16).

The transport of GABA/glycine (GABA/Gly) into synaptic vesicles is mediated by VIAAT transporters. Therefore, in order to seek for anatomical correlates of our electrophysiological findings, we performed an immunohistochemical analysis of GABAergic/glycinergic (VIAAT positive) synaptic puncta (Figure 5A, red) in the lumbar MN area identified by the presence of Hb9-eGFP neurons (Figure 5A, green). Synaptic terminals were identified using double staining for the synaptic vesicle protein synaptophysin (Figure 5A, white) that is ubiquitously expressed in the marginal zone of the SC in close proximity of Hb9 somata. We did not detect any significant difference in the percentage of VIAAT puncta between SOD and WT SCs:  $0.47 \pm 0.10\%$  of analyzed area in SOD (n = 5, N = 4) and  $0.54 \pm 0.14\%$  in WT (n = 6, N = 5) (p>0.05, Mann Whitney test) (Figure 5B1–B2). Synaptophysin staining in SOD SCs was decreased by 44% compared to WT:  $2.17 \pm 0.47\%$  of area in SOD and  $3.93 \pm 0.72\%$  of area in WT (p<0.01, Mann Whitney test) (Figure 5B3). We then calculated the percentage of the synaptophysin surface colocalized with VIAAT and found a  $\sim 23\%$  decrease in this percentage of colocalization in SOD SCs compared to WT:  $24.50 \pm 2.55\%$  and  $32.05 \pm 2.73\%$  for SOD and WT, respectively (p<0.001, Mann Whitney test) (Figure 5B4).

Our electrophysiological data indicated a clear alteration in the frequency and shape of miniature and spontaneous synaptic currents in SOD MNs, with IPSCs being less frequent in SOD animals. This reduced basal network activity was therefore consistent with the anatomical labeling of GABAergic/glycinergic synaptic terminals. Prenatal SOD MNs also exhibited a more depolarized  $E_{GABAAR}$  than WT MNs, which would in turn impinge on the efficacy of GABA/Gly inhibition (Branchereau et al., 2016). In SOD MNs  $E_{GABAAR}$  was 10 mV more depolarized, which could preclude efficient inhibition.

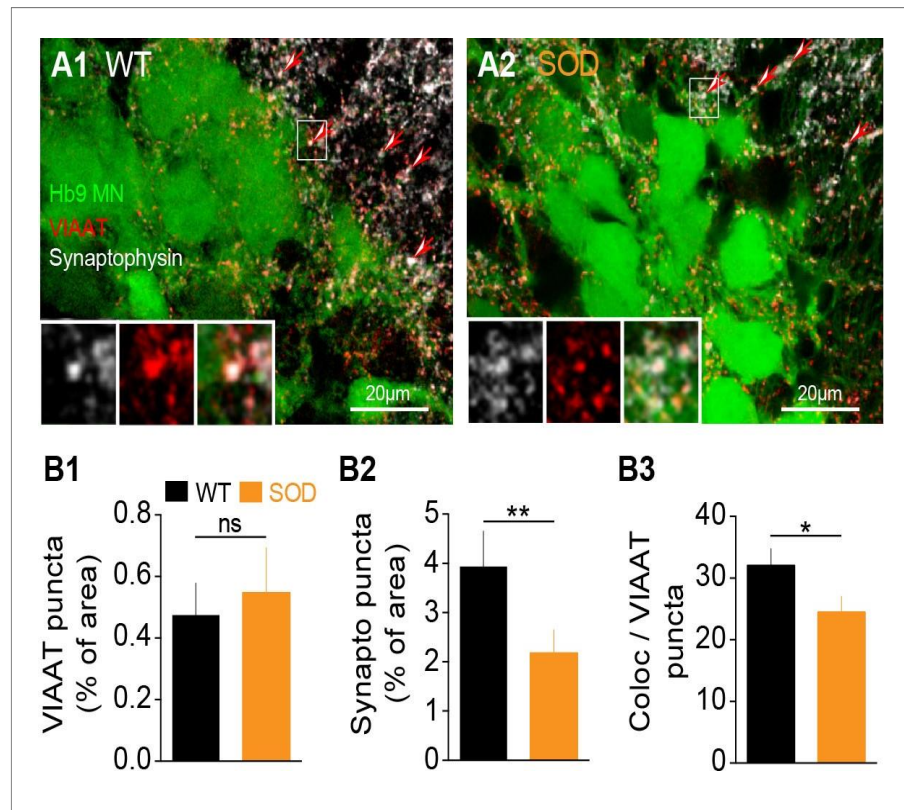


Figure 5. Inhibitory terminal staining in E17.5 SOD and WT SCs. (A1-A2) Confocal visualization of Hb9-eGFP MNs (green) along with VIAAT (red) and synaptophysin (white) staining in lumbar E17.5 WT (A1) and SOD1 (A2) (frontal sections). Arrows point the synaptophysin-VIAAT co-localized staining highlighted in the left corner insets (0.2 mm thickness optical section). (B1) The density of VIAAT puncta was similar in WT ( $n = 6$ ) and SOD1 ( $n = 5$ ) SCs. (B2) SOD SCs again exhibited a significant reduction in their density of synaptophysin terminals. (B3) VIAAT puncta co-localizing with synaptophysin puncta were slightly reduced in SOD SCs compared with WT SCs. \*\*\* $p < 0.001$ , \*\* $p < 0.01$ , \* $p < 0.05$ , *ns* non-significant, Mann Whitney test.

Surprisingly on the other hand, well-coordinated locomotor-like activity was still elicited in SOD SCs (Figure 3A), indicating the presence of putative compensatory mechanisms. In this respect, the slower decay times of both IPSCs and puff-evoked GABA<sub>A</sub>R currents recorded in SOD MNs could be one of such mechanisms. Therefore, in order to test this idea further, we conducted a series of computer simulations of SOD-like and WT-like E17.5 spinal MNs in which the effect of  $\tau_{U_{decay}}$  on the strength of GABA/Gly inhibition was assessed.

### A slower decay time of GABA/Gly synaptic currents to strengthen inhibition in SOD MNs

The impact of synaptic current shape on MN activity was assessed using numerical simulations of WT-like and SOD-like MNs with a NEURON simulation environment (Carnevale and Hines, 2006). The topology and morphometry of canonical WT and SOD E17 MNs were issued from Martin et al. (2013). The two MN types differed only in the length of their terminal dendrites, being shorter in SOD-like MNs (i.e. 60% of WT-like MNs) (Figure 6—figure supplement 1A-B). As a result, the SOD-like MNs are more excitable (Martin et al., 2013). A continuous depolarizing current was injected into the somata of both the WT-like (250 pA) and SOD-like MNs (200 pA) (Figure 6—figure supplement 1C) to produce a spiking discharge of ~12.5 Hz (Figure 6A1, B1). This spike frequency in E17.5 MNs was reached during bursts of activity occurring during fictive locomotion (Figure 6—figure supplement 2A, B). During this MN discharge, a train of GABA/Gly synaptic events was delivered to the MN soma. Various frequencies of GABA/Gly synaptic events were tested to assess the frequency (cut-off frequency) needed to totally block the ongoing MN discharge. When  $E_{GABAAR}$  was

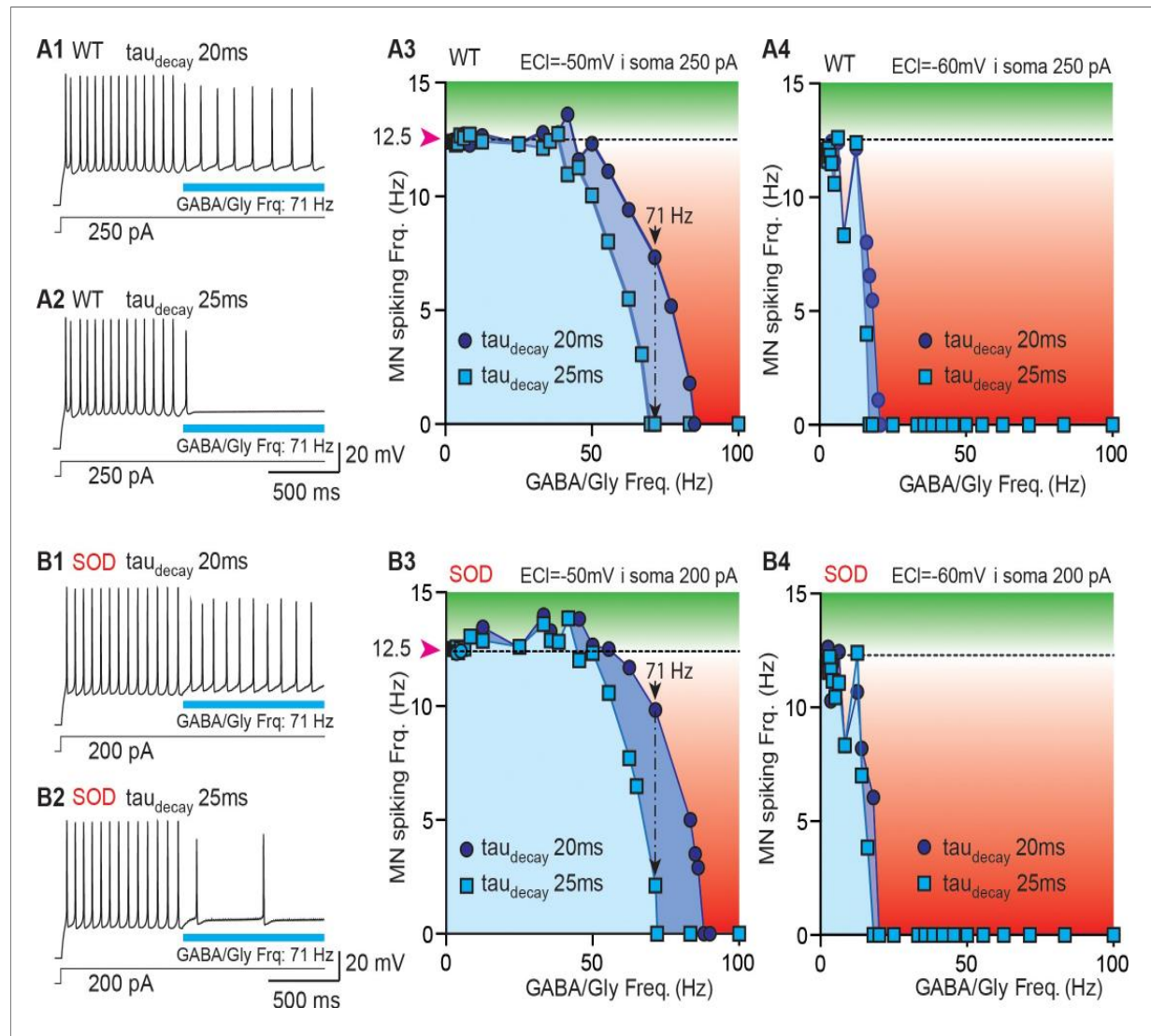


Figure 6. Simulation of a putative compensatory role of  $\tau_{decay}$  for the inhibitory strength of GABA/gly synaptic events in SOD-like MNs. (A) Simulations made with a WT-like MN whose soma was continuously injected with depolarizing current (250 pA) to induce spiking discharge at a rate of ~12.5 Hz. After the spiking discharge was stabilized ( $t = 2$  s), a train of GABA/Gly synaptic events was delivered to the soma at a frequency of 71 Hz, with either a  $\tau_{decay}$  of 20 ms (A1) or 25 ms (A2) and  $E_{GABAAR}$  set at  $-50$  mV. Using these two values of GABA/Gly  $\tau_{decay}$  (20 ms: dark blue circles; 25 ms: light blue squares), various frequencies of GABA/Gly synaptic train (from 0 to 100 Hz) were tested with either  $E_{GABAAR} = -50$  mV (A3) or  $E_{GABAAR} = -60$  mV (A4). The horizontal dashed line represents the stabilized spiking frequency before application of the GABA/Gly synaptic train. Inhibitory effects (below dashed line) are in red, excitatory effects (above this line) are in green. (B1-B5) Simulations made with a SOD-like MN, in which the soma was continuously depolarized (200 pA injection) to induce spiking discharge at ~12.5 Hz (same layout as in A). Note that in the SOD-like MN with  $E_{GABAAR} = -50$  mV, excitatory effects are observed when the GABA/Gly synaptic frequency is below 50 Hz (B3). This effect is not observed when  $E_{GABAAR} = -60$  mV (B4) or is almost absent in the WT-like MN with  $E_{GABAAR} = -50$  mV.

The online version of this article includes the following figure supplement(s) for figure 6:

Figure supplement 1. Simulated E17.5 WT-like and E17.5 SOD-like MNs.

Figure supplement 2. Firing activity and synaptic inputs recorded from E17.5 MNs during fictive locomotion.

set to  $-50$  mV (the value measured in biological SOD MNs), increasing the GABA/Gly  $\tau_{decay}$  from 20 ms to 25 ms drastically increased its inhibitory effect on the MN discharge (Figure 6): whereas a 71 Hz GABA/Gly synaptic event train with a  $\tau_{decay}$  of 20 ms slowed down the WT model MNs'

discharge from 12 Hz to 8–10 Hz, the same train totally blocked spike activity with a GABA/Gly  $\tau_{decay}$  of 25 ms (Figure 6A1–A2) and almost blocked it in a SOD MN (Figure 6B1–B2). We then repeated these simulations for a set of synaptic frequencies ranging from 0 Hz to 100 Hz for the two  $\tau_{decay}$  values (20 and 25 ms), with an  $E_{GABAAR}$  set at  $-50$  or  $-60$  mV for the WT (Figure 6A3–A4) and SOD MNs (Figure 6B3–B4). The value of  $E_{GABAAR}$  was determinant for the inhibitory effect of GABA/Gly events because in the WT-like MN, as in the SOD-like MN, the efficacy of the inhibitory train was much stronger when  $E_{GABAAR}$  was set to  $-60$  mV rather than  $-50$  mV. Indeed, with  $E_{GABAAR} = -60$  mV, a 15 Hz GABA/Gly event train totally blocked the discharge in both MN types (Figure 6A4–B4), with little or no difference occurring between the two ( $\tau_{decay}$  of 20 and 25 ms) event/firing rate curves. By contrast, the corresponding curves differed significantly when  $E_{GABAAR}$  was set to  $-50$  mV (Figure 6, compare A3 with B3).

Significantly, the morphology of the MNs also played a role in the inhibitory effect of the 71 Hz GABA/Gly train on their activity with a  $\tau_{decay}$  set to 20 ms: the inhibition was stronger in the WT-like MN (discharge reduction from 12.5 Hz to 7.33 Hz, Figure 6A3) than in the SOD-like MN (reduction from 12.5 Hz to only 9.83 Hz, Figure 6B3). The effect of morphology was also evident in the difference (frequency shift) between the two curves ( $\tau_{decay}$  of 20 and 25 ms) being more pronounced in the SOD- (17 Hz) than in the WT-like MN (14 Hz). A final influence of MN morphology was observed for a GABA/Gly synaptic frequency below 50 Hz: in the SOD-like MN with  $E_{GABAAR} = -50$  mV, the GABA/Gly synaptic trains produced excitatory effects (Figure 6B3), although these effects were much smaller (if at all) in the WT-like MN (Figure 6A3). This excitatory action of GABA/Gly synapses was not observed when  $E_{GABAAR} = -60$  mV (Figure 6A4–B4).

We chose a firing frequency of 12.5 Hz for the model MNs since this corresponded to the mean value measured during locomotor-like activity in E17 WT embryos (Figure 6—figure supplement 2A–B). Together our results from computer simulations thus indicate that an increase of  $\tau_{decay}$  from 20 to 25 ms may constitute a partial compensatory mechanism contributing to reinforcing the inhibitory strength of GABA/Gly synaptic events that are dramatically reduced in SOD-type MNs mainly because of their more depolarized  $E_{GABAAR}$  ( $-50$  mV instead of  $-60$  mV).

## Effect of slower decay time of GABA/Gly synaptic currents on locomotor rhythm

In a final step, we wished to assess the functional consequence of increasing  $\tau_{decay}$  during ongoing locomotor activity. To this end, a simplified computer simulation of two half-centers driving antagonistic MNs was employed (Figure 7A). Pacemaker activity was obtained using a simplified model (see Appendix 1) based on previous physiological observations on the fundamental role played by  $I_{NaP}$  and  $I_{KCa}$  in pacemaker activity (Tazerart *et al.*, 2008). Interestingly, increasing  $\tau_{decay}$  slowed-down the locomotor rhythm when  $E_{GABAAR}$  was set to  $-60$  mV (WT MN value) and  $g_{GABA/Gly}$  was set to 0.04 mS (Figure 7A1, A2). This slow-down of the locomotor rhythm was also observed when  $g_{GABA/Gly}$  was increased to 0.2 mS with  $E_{GABAAR} = -60$  mV (Figure 7B1). When  $E_{GABAAR}$  was set to  $-50$  mV with a  $g_{GABA/Gly}$  of 0.2 mS, increasing  $\tau_{decay}$  still slowed down the locomotor rhythm, but the effect was much smaller (Figure 7B2). This result was in agreement with our findings that the pharmacologically-evoked locomotor rhythm in SOD SCs was slower than in WT SCs (Figure 3B). Again, although this slight change in the locomotor rhythm observed in SOD SCs has likely no physiological consequences, it reveals one side effect of increasing  $\tau_{decay}$  of GABA/Gly synaptic events.

## Discussion

In the present study we show that fetal E17.5 SOD1<sup>G93A</sup> MNs express an impairment of chloride homeostasis that leads to a more depolarized reversal potential for GABA<sub>A</sub>R ( $E_{GABAAR}$ ), indicating that a very early inhibitory dysfunction may initiate the pathogenesis in ALS MNs as hypothesized by others (van Zundert *et al.*, 2012; Clark *et al.*, 2015). This could lead to a less efficient inhibitory input to MNs (Branchereau *et al.*, 2016), which in turn would be expected to affect locomotor coordination. However, this was not observed here, likely due to a compensatory prolongation of inhibitory synaptic events revealed in our study. Moreover, we found that the passive properties of E17.5 MNs (Rin and Cm) complied with previous observations (Martin *et al.*, 2013), in that Rin increased and Cm decreased in SOD MNs (Table 1), in accordance with a morphometric alteration (shorter dendritic length without changes at the soma level). Decreased capacitance and membrane

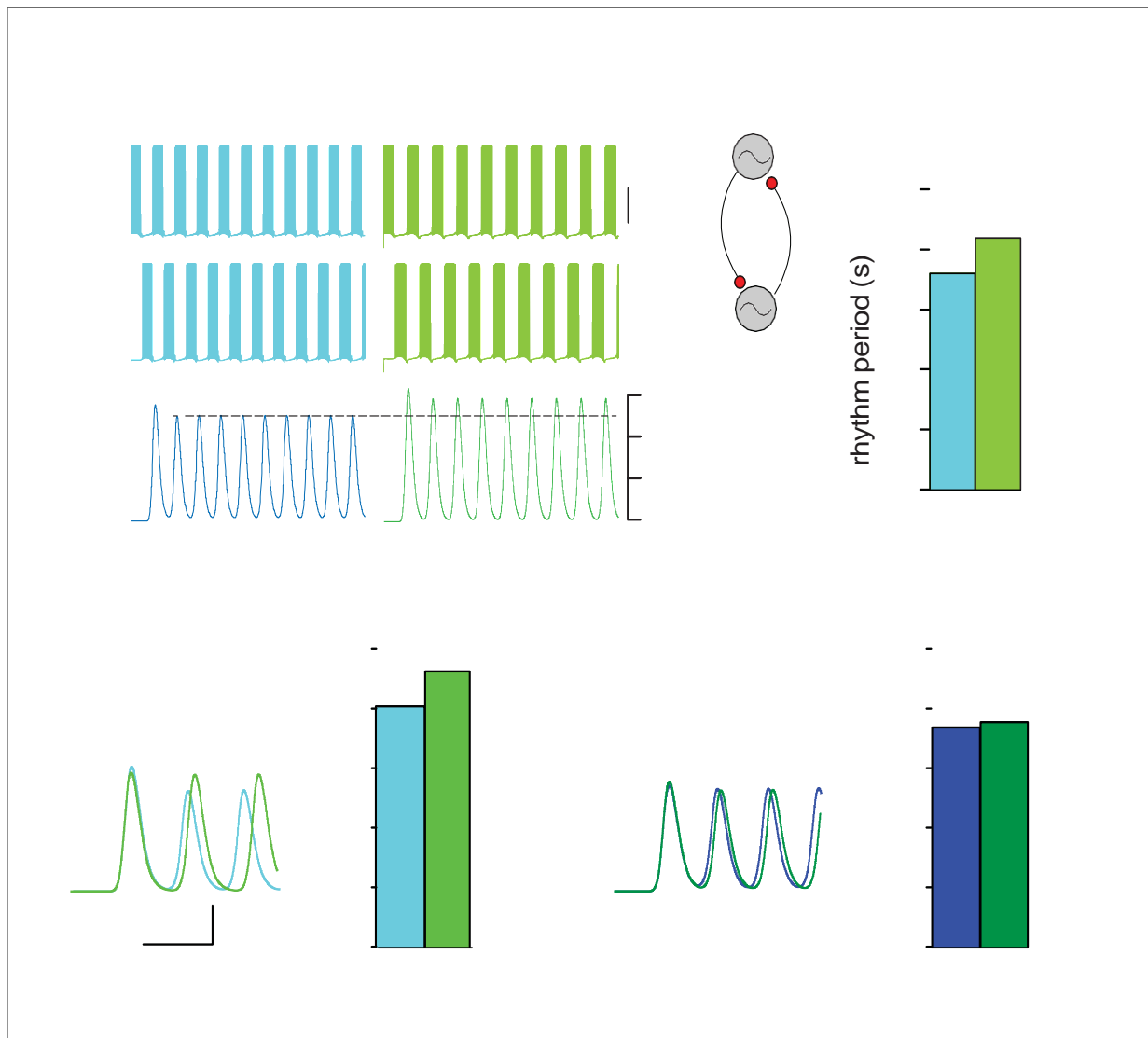


Figure 7. Functional consequence of increasing  $\tau_{decay}$  on locomotor activity. (A) Effect of  $\tau_{decay}$  on the locomotor rhythm when  $E_{GABAAR}$  ( $E_{Ci}$ ) is set to  $-60$  mV (A1-A2, B1) and  $-50$  mV (B2).

conductance were therefore not related to smaller size of E17.5 SOD mouse MNs. These findings therefore support the conclusion that fetal E17.5 SOD MNs are also hyperexcitable. The following will consider possible compensatory mechanisms that counteract the reduction in effective inhibitory input and the hyperexcitability of SOD MNs.

### The frequency and amplitude of inhibitory synaptic inputs are only weakly affected in fetal SOD MNs

In our study we show that frequency of inhibitory synaptic inputs is reduced in SOD MNs. This conclusion was supported by both physiological and anatomical observations. Firstly, SOD MNs displayed less frequent mIPSCs ( $\sim 6\%$ ) (Figure 4A2), which correlates with the finding that VIAAT/synaptophysin co-localization was diminished ( $\sim 23\%$ ) in these mice (Figure 5B3). Second, the amplitudes of the mIPSCs were slightly smaller in SOD1 MNs than in WT, especially for large events (Figure 4A3) and sIPSC events also exhibited this tendency (Figure 4B3). These main features of SOD IPSCs compared to WT are summarized in the schematic representation of Figure 8A1–A2.

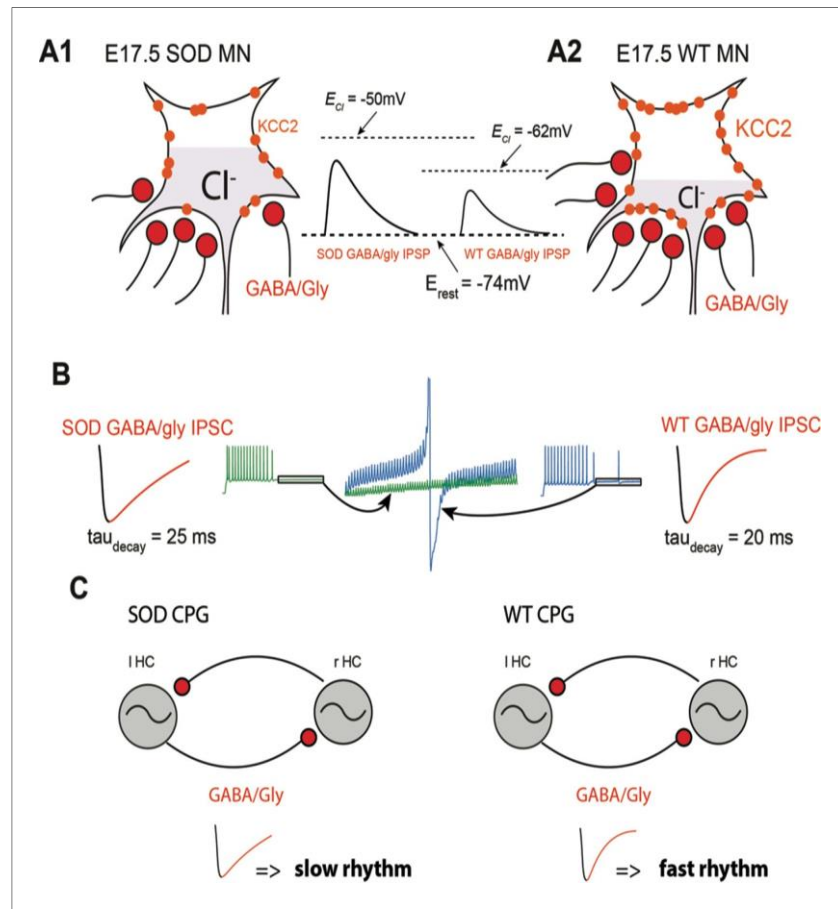


Figure 8. Summary. (A) Schematic drawing summarizing the altered inhibitory inputs (~25% reduction, see Figure 3B3) to fetal SOD MNs.  $[Cl^-]$  is higher in SOD MNs (A1) than in WT MNs (A2) because of a KCC2 downregulation, leading to an increased GABA/Gly-induced depolarizing effect (see insets). (B) Consequence of increasing  $\tau_{decay}$  on the GABA/gly inhibitory effect in SOD-like MNs. Due to an accumulation in the intracellular compartment,  $E_{GABAAR}$  exerts a strong depolarizing effect. A burst of spikes generated by MNs is hardly blocked by a barrage of GABA/gly events (see blue traces) when  $\tau_{decay}$  is set to 20 ms. Increasing  $\tau_{decay}$  to 25 ms allows a better summation of the shunting component of the depolarizing GABA/gly post-synaptic event leading to a better clamp of  $E_m$  towards  $E_{GABAAR}$  and to the blockade of MN discharge (see green traces). (C) Impact of a larger  $\tau_{decay}$  in SOD MNs on the frequency of the locomotor rhythm.

The reduced degree of synaptic input to mouse prenatal SOD MNs assessed by VIAAT/synaptophysin staining is reminiscent of anatomical data from adult human ALS patients in which a reduction of synaptophysin was also identified (Ikemoto *et al.*, 2002). It cannot be explained by a reduced SOD MN size (i.e., smaller cells can host fewer synapses) because we have shown in a previous article that soma perimeters and soma surface of WT MNs and SOD MNs are comparable (Martin *et al.*, 2013). Even though the reduced degree of synaptic input might reflect a developmental delay in the maturation of SOD SCs compared to WT, data from the literature seems to indicate that this reduction persists with time. In fact, MNs cultured from other ALS patients were shown to progressively lose their synaptic activity (Devlin *et al.*, 2015), as was also shown in pre-symptomatic (P60-P120) adult SOD mice (Zang *et al.*, 2005).

The mixed GABA/Glycine IPSCs recorded in our study are likely to reflect a major contribution of GlyR because of the fast  $\tau_{decay}$  (Gao *et al.*, 2001; Muller *et al.*, 2006). Therefore, IPSCs, which were slightly reduced in amplitude in our recordings in SOD MNs, represent glycinergic events whereas GABAergic IPSCs amplitude remained unaffected. This hypothesis is supported by the fact that the ratio  $g_{GABAAR}/C_m$  measured in our perforated patch-clamp recordings did not differ

between SOD and WT MNs (Table 1). Interestingly, a reduction in amplitude of glycinergic synaptic events but not GABAergic events was described in SOD1<sup>G93A</sup> lumbar MNs maintained in culture (Chang and Martin, 2011). Less frequent and smaller amplitude IPSCs convey a reduced inhibitory drive onto prenatal SOD1 MNs. Measurements of IPSC amplitudes derived from CsCl medium-based whole-cell recordings in which  $E_{\text{GABAAR}}$  approached 0 mV. Therefore, WT and SOD MNs shared the same artificial driving force for chloride and so the observed reduction of IPSC amplitude in SOD MNs was likely to be related to a change in post-synaptic GlyR as described in cultured SOD1<sup>G93A</sup> MNs (Chang and Martin, 2011).

### A prolongation of inhibitory synaptic events in SOD MNs as a compensatory mechanism

Our data revealed a noticeable increase of  $\tau_{\text{decay}}$  in both SOD1 mIPSCs and sIPSCs. We found a mean  $\tau_{\text{decay}}$  of around 20-25 ms, which is in the same range as that previously described for mIPSCs during perinatal stages in rat lumbar MNs (Gao et al., 1998). Because a part of our study did not differentiate unequivocally between GABA<sub>A</sub>R-mediated versus GlyR-mediated mIPSCs, we pharmacologically dissected GABA<sub>A</sub>R-mediated versus GlyR-mediated mIPSCs. This confirmed that the mean  $\tau_{\text{decay}}$  is between  $\tau_{\text{decay}}$  of pure GABA<sub>A</sub>R-mediated mIPSCs and pure GlyR-mediated mIPSCs and that both types of mIPSCs exhibit a longer relaxation. Interestingly, GlyRs switch from immature homomeric  $\alpha 2$  GlyRs with slow decay kinetics of glycinergic mIPSCs to heteromeric GlyRs that include  $\alpha 1$ ,  $\alpha 3$  and  $\beta$  subunits with fast kinetics (Legendre, 2001; Raltschev et al., 2016). E17.5 SOD1 MNs may therefore exhibit a delayed development with a preponderance of homomeric  $\alpha 2$  GlyRs. However, this is unlikely to be the case, since most electrical properties measured from birth to postnatal day 12 in SOD1<sup>G93A</sup> MNs instead show an accelerated rate of maturation (Quinlan et al., 2011). During perinatal development of rat spinal MNs, GlyR-mediated mIPSCs become dominating over GABA<sub>A</sub>R-mediated mIPSCs (Gao et al., 2001). We also found a majority of pure GlyR-mediated mIPSCs and found the same ratio of pure GABA<sub>A</sub>R-mediated mIPSCs and pure GlyR-mediated mIPSCs in SOD and WT MNs, indicating similar prenatal developmental stage for both genotypes.

Considering that SOD SCs do not express a development delay compared to WT SCs from the same littermate, we questioned the origin of the prolonged  $\tau_{\text{decay}}$  in GABA<sub>A</sub>R- and GlyR-mediated mIPSCs, sIPSCs and eIPSCs. It has been demonstrated that high  $[\text{Cl}]_i$  slows down the decay of glycine- and GABA-mediated inhibitory synaptic events (Pitt et al., 2008; Houston et al., 2009), reducing the firing probability of Purkinje neurons (Houston et al., 2009). Interestingly, the structural basis of this effect was described as a direct effect of chloride ions acting in the pore of glycine and GABA channels (Moroni et al., 2011). Therefore the elevated  $[\text{Cl}]_i$  likely accounts for the prolonged relaxation of GABA/Gly IPSCs in SOD MNs. The increase in  $[\text{Cl}]_i$  affect GABA<sub>A</sub>R and GlyR and thus IPSCs duration (Pitt et al., 2008; Houston et al., 2009; Moroni et al., 2011). In P10 rat MNs a change from 10 mM  $[\text{Cl}]_i$  to 131 mM led to an increase in  $\tau_{\text{decay}}$  from 9.2 ms to 19.8 ms (Pitt et al., 2008). In P12 Purkinje cells a change from 10 mM  $[\text{Cl}]_i$  to 150 mM led to an increase in  $\tau_{\text{decay}}$  from 14 ms to 19.8 ms (Houston et al., 2009). Finally, in HEK-293 cells, a change from 10 mM  $[\text{Cl}]_i$  to 30 mM and then 131 mM led to an increase in  $\tau_{\text{decay}}$  from 9.6 ms to 12 ms and then 22 ms (Pitt et al., 2008). Even though our data highlight a more prolonged  $\tau_{\text{decay}}$  in SOD GABA<sub>A</sub>R/Gly IPSCs, we cannot directly link  $\tau_{\text{decay}}$  values to physiological  $[\text{Cl}]_i$  values, because  $\tau_{\text{decay}}$  values have been collected from CsCl recordings in which  $[\text{Cl}]_i$  was set as being elevated.

Impaired KCC2 expression or function is involved in a number of neurodevelopmental and neurological disorders (Doyon et al., 2016). We provide evidence that altered  $E_{\text{GABA}}$  in E17.5 SOD1<sup>G93A</sup> mouse embryo likely arises from down-regulation of KCC2 in the lumbar cord and lumbar MNs. Again this down-regulation of KCC2 is unlikely linked to the decrease in the size of the SOD MNs, that is smaller neurons have less volume of the cytosol and less surface of the membrane to host KCC2, because soma perimeters and surface of E17.5 WT MNs and SOD MNs were found as similar (Martin et al., 2013). KCC2 protein has been quantified at the soma level and proximal dendrites that are not affected in SOD1 MNs. Also KCC2 efficacy and  $E_{\text{GABA}}$  have been assessed at the soma level. SOD MNs do not have less volume to adjust and the lower efficacy of KCC2 in SOD MNs is not related to a change in MN size.

In hippocampal pyramidal neurons, NKCC1 up-regulation has been the proposed mechanism that drives transient perinatal GABA switch in rodent models of autism (Tyzio et al., 2014). However, our

data show that NKCC1 is unaltered in the E17.5 lumbar SCs. KCC2 down-regulation in the hippocampus delays postnatal GABA shift in oxytocin receptor knockout mouse model of autism (Leonzino *et al.*, 2016). More recent evidence shows that KCC2 down-regulation explains long-lasting effects of adolescent nicotine exposure (Thomas *et al.*, 2018). In ALS-vulnerable motoneurons of adult SOD1<sup>G93A</sup> mouse lumbar cord, a strong decrease of mRNA and protein expression levels was reported (Fuchs *et al.*, 2010). Thus, KCC2 is a likely molecular substrate underlying perinatal alteration of chloride homeostasis in the lumbar spinal cord.

It may be surprising to observe a  $\tau_{decay}$  more prolonged in SOD MNs when  $[Cl^-]_i$  is imposed (0 mV or  $-45$  mV). Indeed, when we imposed similar  $[Cl^-]_i$  in SOD and WT MNs, we expected a similar  $\tau_{decay}$  in SOD and WT. However, since our data clearly indicate a deficit in KCC2 efficacy in SOD MNs, the actual  $[Cl^-]_i$  may have been counteracted in WT MNs by the KCC2 protein more effectively than in SOD MNs. Therefore, we observed a longer relaxation of GABA<sub>A</sub>R-mediated/GlyR mediated mIPSCs, sIPSCs and VLF-evoked IPSCs in SOD MNs compared to WT.

Our first series of computer simulations demonstrated that increasing  $\tau_{decay}$  from 20 ms to 25 ms clearly potentiated the efficacy of GABA/glycine inhibition. With a  $\tau_{decay}$  of 20 ms, a 20 Hz barrage of inhibitory inputs totally blocks WT-like MN firing activity (12 Hz, i.e. locomotor firing frequency, with  $E_{Cl} = -60$  mV). In contrast, SOD-like MNs (with  $E_{Cl} = -50$  mV) required a  $\sim 90$  Hz inhibitory barrage to suppress their firing. Increasing  $\tau_{decay}$  to 25 ms significantly reduced the threshold cutting frequency to  $\sim 70$  Hz in SOD-like MNs. Those blocking frequencies are in agreement with GABA/glycinergic event frequencies encountered in lumbar spinal MNs during fictive locomotion ( $>100$  Hz) (Figure 6—figure supplement 2C, D). Increasing  $\tau_{decay}$  from 20 ms to 25 ms also leads to a higher capacity of shunting effect summation (Branchereau *et al.*, 2016). This is clearly visible in Figure 8B in which the increased shunting effect tends to maintain  $E_m$  towards  $E_{GABAAR}$  and prevents spike occurrence (compare green and blue traces).

Our second series of computer simulations demonstrate that increasing  $\tau_{decay}$  slowed-down the locomotor rhythm (Figure 7). This is in agreement with our findings that the pharmacologically-evoked locomotor rhythm in SOD SCs was slower than in WT SCs (Figure 3B). The effect of IPSCs  $\tau_{decay}$  on locomotor rhythm was only observed when  $E_{GABAAR}$  was set to  $-60$  mV in the interneurons of a central-pattern generator (CPG, half-centers) (Figure 7). To our knowledge, however, no  $E_{GABAAR}$  and  $g_{GABA/Gly}$  measurements have been obtained in the CPG interneurons of ALS mouse models. In their study of 2-3 week in vitro organotypic slice cultures of the spinal cord (from E12-E13), Medelin *et al.* (2016) suggested that the  $Cl^-$  reversal potential is similar in SOD1<sup>G93A</sup> and WT ventral interneurons, around  $-60$  mV. However, neither the excitatory versus inhibitory nature of the recorded interneurons, nor their relationship with CPG circuitry were reported in their study. Our computer model of locomotor rhythm was based on half-center interneurons without considering the output MNs. Therefore it may be argued that changes in IPSCs  $\tau_{decay}$  observed in spinal MNs has nothing to do with the spinal locomotor rhythm generator. However, a recent study clearly demonstrated that MNs participate to the rhythm generation in neonatal mouse (Falgairolle *et al.*, 2017). Therefore the effect of  $\tau_{decay}$  increase observed in SOD MNs could therefore impinge the locomotor rhythm frequency.

## Materials and methods

### Key resources table

Reagent type (species) or resource	Designation	Source or reference	Identifiers	Additional information
Strain ( <i>Mus musculus</i> )	B6SJL-Tg (SOD1*G93A)1Gur/J	The Jackson Laboratory	RRID:IMSR_JAX:002726	
Antibody	anti-KCC2 rabbit polyclonal	Millipore	Cat#07-432 RRID:AB_11213615	1:1000 (WB) 1:400 (IHC)
Antibody	anti-NKCC1 mouse monoclonal	Developmental Studies Hybridoma Bank	T4	1:400 (WB)

Continued on next page

## Continued

Reagent type (species) or resource	Designation	Source or reference	Identifiers	Additional information
Antibody	anti-VIAAT rabbit polyclonal	Provided by B. Gasnier, Paris Descartes University	VIAAT	1:1000 (IHC)
Antibody	anti-synaptophysin mouse monoclonal	Millipore Sigma	Clone SVP38 RRID:AB_2315393	1:500 (IHC)
Antibody	anti-FoxP1 rabbit polyclonal	Millipore Sigma	Cat#AB2277 RRID:AB_10631732	1:500 (IHC)
Antibody	goat anti-rabbit secondary antibody Alexa Fluor 546	Invitrogen	Cat#A-11035	1:500 (IHC)
Antibody	goat anti-mouse secondary antibody Alexa Fluor 647	Invitrogen	Cat#A-21235 RRID:AB_2535804	1:500 (IHC)
Antibody	Goat anti-Rabbit IgG-heavy and light chain cross-adsorbed Antibody HRP Conjugated	Euromedex	Cat#A120-201P	1:20000 (WB)
Antibody	Immun-Star GAM-HRP Conjugate	Bio-Rad	Cat#1705047	1:20000 (WB)
Commercial assay, kit	Qproteome Mammalian Protein Prep Kit	Qiagen	Cat#37901	
Chemical compound, drug	Phosphatase Inhibitor Cocktail 2	Millipore Sigma	Cat#P5726	
Commercial assay, kit	DC protein assay	Bio-Rad	Cat#5000113 Cat#5000114 Cat#5000115	
Commercial assay, kit	Mini-PROTEAN TGX Stain-Free Gels	Bio-Rad	Cat#4568034	
Chemical compound, drug	10x Tris/Glycine/SDS	Bio-Rad	Cat#1610732	
Commercial assay, kit	Precision Plus Protein All Blue Standards	Bio-Rad	Cat#1610373	
Commercial assay, kit	Trans-Blot Turbo Transfer Pack, nitrocellulose	Bio-Rad	Cat#1704158	
Chemical compound, drug	Clarity Western ECL, Substrate	Bio-Rad	Cat#1705060	
Chemical compound, drug	Tetrodotoxin (citrate free)	Latoxan Laboratory, France	Cat#L8503	0.2 mM
Chemical compound, drug	Kynurenic acid	Millipore Sigma	Cat#K3375	4 mM
Chemical compound, drug	Tubocurarine hydrochloride pentahydrate	Millipore Sigma	Cat#2379	10 mM
Chemical compound, drug	Dihydro- <i>b</i> -erythroidine hydrobromide	Bio-technie, France	Cat#2349/10	5 mM
Chemical compound, drug	Strychnine Hemisulfate salt	Millipore Sigma	Cat#S7001	3 mM
Chemical compound, drug	(2 <i>R</i> )-amino-5-phosphonovaleric acid (DL-AP5)	Bio-technie, France	Cat#0105/10	40 mM
Chemical compound, drug	6-cyano-7-nitroquin oxaline-2,3-dione (CNQX)	Bio-technie, France	Cat#0190/10	20 mM

Continued on next page

## Continued

Reagent type (species) or resource	Designation	Source or reference	Identifiers	Additional information
Chemical compound, drug	SR 95531 hydrobromide (GABAzine)	Bio-technie, France	Cat#1262/10	3 mM
Chemical compound, drug	bumetanide	Millipore Sigma	Cat#B3023	10 mM
Chemical compound, drug	VU0240551	Bio-technie, France	Cat#3888/10	10 mM
Chemical compound, drug	Isoguvacine hydrochloride	Bio-technie, France	Cat#0235/100	50 mM
Chemical compound, drug	Dopamine hydrochloride	Millipore Sigma	Cat#H8502	100 mM
Chemical compound, drug	Serotonin hydrochloride (5-HT)	Millipore Sigma	Cat#H9523	10 mM
Chemical compound, drug	N-Methyl-D-aspartic acid (NMDA)	Millipore Sigma	Cat#M3262	10 mM
Chemical compound, drug	Gramicidin from <i>Bacillus aneurinolyticus</i> ( <i>Bacillus brevis</i> )	Millipore Sigma	Cat#G5002	10-20 mgml <sup>-1</sup>
Software, algorithm	NEURON 7.3	NEURON	RRID:SCR_005393	

## Ethical considerations and mouse model

All procedures were carried out in accordance with the local ethics committee of the University of Bordeaux and European Committee Council directives. All efforts were made to minimize animal suffering and reduce the number of animals used. B6SJLTgN(SOD1-G93A)/1Gur/J mice expressing the human G93A Cu/Zn superoxide dismutase (SOD1) mutation (Gly93fi Ala substitution) were obtained from the Jackson Laboratory (<https://www.jax.org/strain/002726>). Heterozygous B6SJL-TgN(SOD1-G93A)/1 Gur/J (named SOD in this report) were maintained by crossing heterozygous transgene-positive male mice with B6SJL F1 hybrid females (Janvier labs, France). Gestation in SOD lasted for ~18.5 days, embryonic day 0.5 (E0.5) being defined as the day after the mating night. Experiments were performed on E17.5 fetuses, that is collected one day before their birth.

## Dissection and isolation of the embryonic spinal cord (SC)

Pregnant mice were sacrificed by cervical dislocation. A laparotomy was performed and the fetuses were removed after cutting the uterine muscle. Fetuses were removed from their individual embryonic sacs and transferred into cooled artificial cerebrospinal fluid (aCSF) oxygenated with a 95% O<sub>2</sub> and 5% CO<sub>2</sub> mixture. The composition of the latter was in mM: 114.5 NaCl, 3 KCl, 2 CaCl<sub>2</sub>·2H<sub>2</sub>O, 1 MgCl<sub>2</sub>·6H<sub>2</sub>O, 25 NaHCO<sub>3</sub>, 1 NaH<sub>2</sub>PO<sub>4</sub>·H<sub>2</sub>O, 25 D-Glucose, pH 7.4 and osmolarity 307 mosmol/kg H<sub>2</sub>O. Only fetuses that displayed active movements were chosen for experiments. The fetuses selected were then decapitated and the SC preparation was dissected out. Their tails were preserved for subsequent genotyping. An incision was performed on the ventral side of the lumbar cord (between the midline and ventral roots) at the level of lumbar 4-5 (L4-L5) ventral roots, which innervate the extensor muscles, in order to remove the meninges. This exposes the MNs and makes them accessible for the patch-clamp electrode (generally 1-2 MNs recorded in each SC). The SC preparation was placed in a recording chamber and continuously superfused (~1.5 mL·min<sup>-1</sup>) with oxygenated aCSF. All experiments were carried out at constant temperature (30°C). Experiments were performed blindly without knowing the genotype of the animals. Fetuses were genotyped at the Genotyping Platform at the Magendie Neurocentre (Bordeaux). The genotyping was performed by standard PCR from mice tail samples using established primers and a protocol as stated by the Jackson Laboratory.

## Protein extraction and western blotting (WB)

WB analysis was performed on whole E17.5 lumbar spinal cords. For protein extraction, 15 WT and 15 SOD mice, from four different litters, were used. Each of the 15 lumbar spinal cords were divided into three groups of five lumbar SCs, crushed (micro-potter, PP750ACD), and homogenized with mammalian lysis buffer (Qproteome Mammalian Protein Prep Kit, Qiagen) with a phosphatase inhibitor cocktail (Millipore Sigma). Homogenate was incubated (5 min at 4°C), centrifuged (10 min at 4°C to 14,000 RCF) to recover the supernatant from debris and stored 48 hr at –80°C. Total protein concentration in the supernatant solution was determined by the DC protein assay (Bio-Rad) using an iMark microplate reader (Bio-Rad). Briefly, colorimetric technique was used to measure color change proportional to total protein concentration. Based on a determined concentration of total protein, volume of a supernatant solution that contains a desired amount of total protein could be calculated. Then, samples were deposited at –80°C for future use. WB was performed by denaturing the sample at 100°C for 5 min and loading 20 mg of protein of each sample (3 wells of WT and 3 wells of SOD samples) in Mini-PROTEAN TGX Stain-Free Gels (Bio-Rad) with migration buffer (2.5 mM Tris, 19.2 mM Glycine, 0.01% SDS prepared from 10X Tris/Glycine/SDS (Bio-Rad). Molecular weight markers (Precision Plus Protein All Blue Standards, Bio-Rad) were used in each individual gel. Electrophoresis of the samples and MW markers was powered by electrophoresis power supply EPS 600 (Pharmacia Biothe, Sweden) device at 250V. In order to be able to visualize the total proteins (stain free), the gel was activated in ChemiDoc MP imaging system (Bio-Rad). The transfer from gel to mini format 0.2 mm nitrocellulose membrane pack (Bio-Rad) was made using Trans-Blot Turbo Transfer System (Bio-Rad). Once the transfer was confirmed with ChemiDoc MP imaging system, membrane was blocked with 5% milk in tris-buffered saline (Millipore Sigma) containing 2% Tween-20 (Millipore Sigma) (TBST) buffer for 1 hr on agitator (Heidolph, UNIMAX 1010, Germany), and then incubated with primary antibody at 4°C overnight. The primary antibodies used were rabbit polyclonal anti-KCC2 (1:1000, reference Millipore 07-432, Millipore Sigma) or mouse monoclonal anti-NKCC1 (1:400, reference T4 from Developmental Studies Hybridoma Bank, The University of Iowa, USA). The next day, membrane was washed 3-5 times using TBST and incubated with goat anti-rabbit or anti-mouse Horseradish Peroxidase (HRP) conjugated secondary antibody diluted to 1:20000 (Euro-medex or Bio-Rad) for 1.5 hr at room temperature. After 3-5 rinses in TBST, total proteins on the membrane were visualized using a ChemiDoc MP imaging system (Bio-Rad). Membrane was then incubated 5 min in Clarity western ECL substrate (Bio-Rad) and the KCC2 or NKCC1 protein was visualized using the ChemiDoc. Four rounds of WB were run from the same deposited WT and SOD spinal cord samples. The ~140 kDa KCC2 band and ~150 kDa NKCC1 were analyzed.

The stain-free staining of total proteins loaded was used as the normalization control to quantify the KCC2 or NKCC1 band. Quantification was performed using Image Lab (Bio-Rad). Data presented are normalized to mean values from WT samples.

## Immunohistochemistry

Immunohistochemistry was performed on frontal sections from lumbar SCs prepared as follows. The mice used were offspring of female Hb9-eGFP mice cross bred with SOD male mice. These mice express GFP in the dendrites and the soma of spinal MNs. The lumbar SC samples of SOD and WT embryos at E17.5 were fixed in 4% paraformaldehyde (PFA) for 2 hr at room temperature. They were rinsed three times with 0.1 M Phosphate Buffer Saline (PBS) and then cryoprotected in 15% sucrose for 24 hr, followed by 30% sucrose for another 24 hr. After placing them in Tissue-Tek (O.C. T. Compound, Sakura Finetek) and freezing, the samples were sliced using a Leica 3050 s Cryostat. Sections (20 μm thickness) were affixed on gelatinized slides and preserved at –25°C until their use. Each slide was rinsed three times with 0.1 M PBS, blocked with a medium containing 2% bovine serum albumin (BSA), then incubated for 48 hr with primary antibodies prepared in PBST (1% triton, BSA 0.2%). We processed the sections with an anti-synaptophysin antibody (1:500, mouse monoclonal, Clone SVP38, Millipore Sigma) coupled either with a rabbit polyclonal antibody directed against the vesicular inhibitory amino acid transporter (1:1000, VIAAT, antibody Provided by B. Gasnier, Paris Descartes University). VIAAT reflects the synaptic release of the GABA and glycine neurotransmitters (Dumoulin *et al.*, 1999). The rabbit polyclonal anti-FoxP1 antibody (1:500, AB2277, Millipore) was also used to assess the LMC identity of recorded MNs (Figure 1—figure supplement 1) (Dasen *et al.*, 2008). For KCC2 staining, we used the rabbit polyclonal anti-KCC2 antibody (1:400,

reference Millipore 07-432, Millipore Sigma). After three rinses, slides were incubated for 2 hr at room temperature with a goat anti-rabbit secondary antibody Alexa Fluor 546 (A-11035) and/or goat anti-mouse secondary antibody Alexa Fluor 647 (A-21235) (1:500, Invitrogen, France) and then rinsed with 0.1 M PBS. After rinsing, slides mounted with an anti-fade reagent (Fluoromount, Electron Microscopy Sciences) and stored at 4°C in obscurity until confocal observation.

### Confocal microscopy

Samples were visualized either in the laboratory with a BX51 Olympus Fluoview 500 confocal microscope or in the Bordeaux Imaging Center (BIC) with a SP5 Leica. Serial optical sections (thickness 0.2  $\mu$ m) were obtained using a x60 oil-immersion objective. Lasers were selected according to the wavelength required for visualization. The different transporters and proteins were visualized as spot aggregates. Spots were detected using the spot detector plugin in Icy version 1.8.1.0, a quantitative image analysis program (Institut Pasteur - CNRS UMR 3691). Spots were then quantified and the co-localization of synaptophysin with VIAAT was assessed in the marginal zone edging the MN soma location. The percentage of co-localization was calculated according to the surface of the synaptophysin positive area. The global and membrane KCC2 staining density was assessed using Image J. For the KCC2 membrane staining a specific macro, allowing to delineate the periphery of MNs and quantify the KCC2 staining density, was developed by Sébastien Marais from the BIC. Briefly, the contour of Hb9-eGFP MNs was manually outlined in order to build an area (five pixels on each side of the outline), in which KCC2 punctiform profiles were automatically detected. Density of KCC2 puncta was then calculated as the number of puncta relative to the outline area. Values are expressed as arbitrary unit (AU).

### Electrophysiological procedures and data analysis

Patch-clamp electrodes were constructed from thin-walled single filamented borosilicate glass (1.5 mm outer diameter, Harvard Apparatus, Les Ulis, France) using a two-stage vertical microelectrode puller (PP-830, Narishige, Tokyo, Japan). Patch electrode resistances ranged from 3 to 5 MW. All recordings were made with an Axon Multiclamp 700B amplifier (Molecular Devices, Sunnyvale, CA, USA). Data were low-pass filtered (2 kHz) and acquired at 20 kHz on a computer via an analog-to-digital converter (Digidata 1322A, Molecular Devices) and a data acquisition software (Clampex 10.3, Molecular Devices).

Motorized micromanipulators (Luigs and Neumann, Ratingen, Germany) were used to position the patch-clamp electrode on a visually identified MN using a CCD video camera (Zeiss Axiocam MR). Recorded MNs were located in the lateral column (*Figure 1—figure supplement 1*) and were identified by their pear-shaped cell bodies. Values of  $R_{in}$  and  $C_m$  also further confirmed the motoneuron identity of recorded neurons (*Martin et al., 2013*).

For the KCC2 efficacy assessment, the aCSF contained the following in mM: 127 NaCl, 6 KCl, 2 CaCl<sub>2</sub> 2H<sub>2</sub>O, 1 MgCl<sub>2</sub> 6H<sub>2</sub>O, 20 HEPES, 11 D-glucose, osmolarity 306 mosmol/kg H<sub>2</sub>O, oxygenated with 100% O<sub>2</sub>, pH adjusted to 7.4 with NaOH. The patch-clamp recording pipette was filled with the following in mM: 120 K-gluconate, 13 KCl, 1 CaCl<sub>2</sub> 2H<sub>2</sub>O, 10 mM HEPES, 5 CsCl, 1 TEACl, 10 mM Verapamil, 2 ATP Mg<sup>2+</sup>, 10 EGTA, pH = 7.4 adjusted with KOH. This led to a theoretical  $E_{Cl}$  of -49 mV. In order to challenge the KCC2 efficacy, MNs were voltage-clamped at -20 mV (above  $E_{Cl}$ ) while isoguvacine was applied during 40 s, inducing a massive influx of chloride ions. Actual  $E_{Cl}$  was measured by holding the voltage from -100 mV to 10 mV using a 1 s ramp protocol (*Figure 2C1*). Subtracting the ramp current obtained in the presence of isoguvacine to the control ramp current allowed to determine  $E_{Cl}$  (*Figure 2C1*).

For recordings of IPSCs, patch pipettes were filled with cesium chloride (CsCl) intracellular medium, the composition of which being (in mM): 130 CsCl, 4 MgCl<sub>2</sub>-6H<sub>2</sub>O, 10 HEPES, 10 EGTA, 4 ATP-2Na, 302 mosmol/kg H<sub>2</sub>O. The pH was adjusted to 7.4 with the addition of CsOH. The intracellular CsCl medium led to an  $E_{GABAAR}$  that approached 0 (2.89 mV), allowing a clear visualization of Cl<sup>-</sup>-dependent IPSCs. All synaptic events were recorded while holding the membrane potential of MNs at -70 mV.

In order to assess both Glu and GABA/Gly synaptic events in individual neurons (*Figure 6—figure supplement 2*), whole-cell patch-clamp recordings were conducted in voltage-clamp mode (holding membrane potential -45 mV). The intracellular medium was composed of (in mM): 130 KGLuconate,

5 NaCl, 1 CaCl<sub>2</sub>, 2H<sub>2</sub>O, 10 HEPES, 10 EGTA, and 2 MgATP, (284 mosmol/kg H<sub>2</sub>O) adjusted to pH 7.4 using 1M KOH.

For E<sub>GABAAR</sub> assessment, gramicidin perforated patch-clamp recordings were conducted. For perforation, a gramicidin (Millipore Sigma) stock solution was dissolved at 10 mg ml<sup>-1</sup> in DMSO (Millipore Sigma) and diluted to a final concentration of 10-20 mgml<sup>-1</sup> in the intracellular medium composed of (in mM): 130 KCl, 10 HEPES, 10 EGTA, and 2 MgATP, (284 mosmol/kg H<sub>2</sub>O) adjusted to pH 7.4 using 1M KOH. Gramicidin stock and diluted solutions were prepared <1 hr before each experiment. Pipette tips were filled with a filtered ~3 mL intracellular medium and subsequently back-filled with gramicidin solution. The GABA<sub>A</sub>R specific agonist isoguvacine (50 mM, Bio-Techne, France) was pressure ejected (~ 3 psi; 50 ms) via a puff pipette placed in the vicinity of motoneuron somata with a PicoSpritzer II (Parker Hannifin Corporation, Fairfield, NJ, USA) driven by a programmable Master 8 Stimulator/Pulse Generator (Master-8, A.M.P.I. Jerusalem, Israel). Isoguvacine applications were repeated at different membrane voltages, allowing to assessment of the reversal potential of evoked GABA<sub>A</sub>R-related currents. Measurements were corrected for liquid junction potentials (3.3 mV) calculated with the Clampex junction potential calculator. Using the Nernst equation, E<sub>GABAAR</sub> was calculated to be 1.5 mV. Thus, to confirm that the perforated-patch configuration had not ruptured during the experiment, repetitive E<sub>GABAAR</sub> tests were performed. Measurements leading to an E<sub>GABAAR</sub> close to 0 mV were considered as whole-cell recordings and cells were discarded. The Clampex membrane test was used to monitor the input resistance (R<sub>in</sub>) and membrane capacitance (C<sub>m</sub>): a -60 mV holding membrane potential and 5 mV steps (negative and positive, 40 ms duration) were chosen. The reversal potential for GABA<sub>A</sub>R (E<sub>GABAAR</sub>) was calculated by a linear fit (Prism seven from GraphPad Software Inc, USA). The  $\tau_{rise}$  (ms), and  $\tau_{decay}$  (ms) of IPSCs were determined using Spike 2 software version 7.15 (Cambridge Electronic Design, Cambridge, England) and by fitting a single exponential.

In order to elicit evoked IPSCs (eIPSCs) from MNs, a concentric bipolar wire stimulating electrode (FHC, USA) was placed on the ventro-lateral funiculus (VLF) in order to activate local inhibitory fibers. Single stimulations delivered to the VLF (duration 1 ms, intensity ranging 10-20 mA) were driven by a programmable Master 8 Stimulator/Pulse generator (Master-8, A.M.P.I. Jerusalem, Israel).

For extracellular recordings of locomotor-like activity, left and right lumbar ventral roots (at the level of L3 to L5) were recorded. Raw signals were collected with a high-gain AC amplifier (ISO-DAM8A-4 Bio-amplifier System, World Precision Instruments Ltd, Stevenage, UK). Filtered (cutoff frequency: 0.3-3 kHz) raw signals were integrated off-line and analyzed using Spike 2 software. Locomotor-like activity was elicited by applying a cocktail of 5-HT 10 mM, NMDA 10 mM and DA (100 mM) (5-HT/NMDA/DA). This cocktail has been previously established (Han *et al.*, 2007; Milan *et al.*, 2014) to evoke stable locomotor-like activity. Two 50 s representative episodes of strongly alternating locomotor-like activity (assessed by the Rayleigh's test) were analyzed in each WT and SOD experiment.

## Pharmacology

In gramicidin perforated experiments and in experiments performed for assessing the KCC2 efficacy, GABA<sub>A</sub>R responses were isolated by using a cocktail of drugs containing 0.2 mM tetrodotoxin (TTX, Latoxan Laboratory, France), 4 mM kynurenic acid (Millipore Sigma), 10 mM (+)-tubocurarine (Millipore Sigma), 5 mM Dihydro-*b*-erythroidine hydrobromide (DHbE, Bio-technne, France), and 3 mM strychnine (Millipore Sigma) that respectively blocked voltage-dependent Na<sup>+</sup> action potentials, and glutamate, cholinergic, and glycinergic input to MNs. In CsCl experiments, IPSCs were isolated pharmacologically using DL-AP5 40 mM ((2*R*)-amino-5-phosphonovaleric acid, Bio-technne, France) and CNQX 20 mM (6-cyano-7-nitroquinoxaline-2,3-dione, Bio-technne, France). mIPSCs were isolated in the presence of 0.2 mM TTX (Latoxan, France). GABA and glycine mIPSCs were isolated by adding 3 mM strychnine or 3 mM GABAzine (SR 95531 hydrobromide, Bio-technne, France), respectively. These blockers were added to the cocktail containing 0.2 mM TTX, 4 mM kynurenic acid, 10 mM (+)-tubocurarine and 5 mM DHbE. In experiments assessing the KCC2 efficacy, 10 mM bumetanide (Millipore Sigma) was applied to block NKCC1 and 10 mM VU0240551 (Bio-technne, France) (10 mM) to block KCC2. Serotonin (5-HT, 10 mM), dopamine (DA, 100 mM) and N-Methyl-D-aspartic acid (NMDA, 10 mM) were from Millipore Sigma.

## Membrane properties and data analysis

Data analysis was performed using Clampfit 10.6 (Axon Instruments), MiniAnalysis 6.0 or Spike 2. For synaptic event analysis, 100-200 s recording samples were selected from each MN. All selected synaptic events were concatenated for SOD versus WT MNs. After analysis, the information obtained included mean values for event amplitude (pA),  $\tau_{rise}$  (ms),  $\tau_{decay}$  (ms) as well as inter-event interval (IEI) (ms). The MN capacitance (Cm), membrane input resistance (Rin) and access resistance (Ra) were recorded immediately after establishing whole-cell patch-clamp. The membrane voltage was held at  $-70$  mV as this corresponds to the resting membrane potential of mice MNs at E17.5 (Delpy et al., 2008). As a result, all events appeared as downward events.

## Computer simulations

GABA/glycine synaptic events in E17.5 MNs were simulated using a multi-compartment neuron model that was elaborated with the NEURON 7.3 program (Hines and Carnevale, 1997). Two simulated neurons were constructed: an E17.5 WT-like MN and an E17.5 SOD-like MN (Figure 6—figure supplement 1). These canonical MNs, designed from the average topology of real E17.5 MNs, were built on models used in a previous study (Martin et al., 2013). Both MNs were virtually identical, with similar channels and morphologies, except for the terminal dendritic segments of the SOD-like MN that were 40% less in extent than the WT terminal segments (Martin et al., 2013). In each section (dendrites and axon), the number of segments was an odd number calculated according to the d-lambda rule (Hines and Carnevale, 2001; Carnevale and Hines, 2006). The following conductances were used: a passive leakage current ( $I_{leak}$ ), a transient K channel ( $I_A$ ), a voltage-dependent calcium-activated potassium channel ( $I_C$ ) also called  $I_{K(Ca)}$  (McLarnon et al., 1995; Gao and Ziskind-Conhaim, 1998) and a high-threshold calcium current ( $I_L$ ) (Walton and Fulton, 1986).  $I_{leak}$  was simulated in each MN section ( $I_{leak} = (E_{leak} - E) \cdot G_{leak}$ , with  $E_{leak} = -73$  mV and  $G_{leak} = 1/Rm$ ).  $Rm$ , the specific membrane resistance was set to  $21200 \text{ W.cm}^2$ , in order to obtain an input resistance of  $120 \text{ MW}$  in the WT MN.  $I_A$  was present in the axon initial segment (AIS), with  $G_{IA} = 0.0033 \text{ S.cm}^{-2}$ ;  $I_C$  was present in soma, with  $G_{IC} = 0.0025 \text{ S.cm}^{-2}$ .  $I_L$  was present in the soma, with  $G_{IL} = 8.10^{-5} \text{ S.cm}^{-2}$ . Each of the axon segments ( $n = 750$ ) was equipped with Na and K Hodgkin Huxley (HH) channels ( $G_{Na} = 0.012 \text{ S.cm}^{-2}$  and  $G_K = 0.0036 \text{ S.cm}^{-2}$ , respectively) used to generate spikes. The density of Na and K channels in the initial segment ( $G_{Na} = 0.5 \text{ S.cm}^{-2}$  and  $G_K = 0.15 \text{ S.cm}^{-2}$ ) were adjusted in order to obtain a spike threshold of  $-48$  mV for the WT MN (for more details see Appendix 1).

In addition, calcium dynamics (Blaustein, 1988) were added in the soma to reproduce calcium accumulation, diffusion and pumping (for more details see [Destexhe et al., 1993]). The parameters used in the intracellular calcium dynamics were:  $depth = 0.17 \text{ mm}$ ,  $\tau_{ur} = 1e^{10} \text{ ms}$ ,  $Ca_{inf} = 0.0002 \text{ mM}$ ,  $Kt = 0.00025 \text{ mM.ms}^{-1}$ ,  $Kd = 0.0001 \text{ mM}$ ,  $Ca_i = 2.4e^{-4} \text{ mM}$  and  $Ca_o = 3 \text{ mM}$ .

Inhibitory and excitatory synaptic inputs were inserted on the somatic MN compartment using two exponentials equations (one for rising phase and the other for decay phase). Depolarizing GABAergic/glycinergic post-synaptic current kinetics was set with  $\tau_{rise} = 0.3 \text{ ms}$  and  $\tau_{decay} = 15/20 \text{ ms}$  (for WT/SOD, respectively). Excitatory synaptic current kinetics was set with  $\tau_{rise} = 0.1 \text{ ms}$  and  $\tau_{decay} = 10 \text{ ms}$ . Equations concerning channel properties and GABA<sub>A</sub>R synaptic activation are summarized in the Appendix 1.

## Statistical analysis

GraphPad Prism 7 software was used to analyze all the data. The results are presented as means  $\pm$  the standard error of the mean (SEM) unless otherwise specified.  $n$  is the number of MNs used in the analysis and  $N$  the number of fetuses. Significance was determined as  $p < 0.05$  (\*),  $p < 0.01$  (\*\*),  $p < 0.001$  (\*\*\*) or  $p < 0.001$  (\*\*\*\*). The difference between the cumulative frequencies was analyzed using the Kolmogorov-Smirnov (K-S) test. The statistical differences between two data sets were assessed with the Mann Whitney test for non-parametric data.

## Acknowledgements

We thank Marie-Paule Algeo, Marie-Alix Derieppe and Nathalie Argenta for excellent technical assistance and animal breeding. A part of the microscopy was done in the Bordeaux Imaging Center, a

service unit of the CNRS-INSERM and Bordeaux University, member of the national infrastructure France Biomedicine. The help of Sébastien Marais is specifically acknowledged. This work was supported by funding from the 'Fédération pour la Recherche sur le Cerveau' (FRC) and the 'Association pour la recherche sur la Sclérose Latérale Amyotrophique et autres maladies du Motoneurone' (ARSLA).

---

## Additional information

### Funding

Funder	Author
Fédération pour la Recherche sur le Cerveau	Pascal Branchereau
Association pour la Recherche sur la Sclérose Latérale Amyotrophique et autres Maladies du Motoneurone	Pascal Branchereau

The funders had no role in study design, data collection and interpretation, or the decision to submit the work for publication

### Author contributions

Pascal Branchereau, Conceptualization, Data curation, Formal analysis, Supervision, Funding acquisition, Validation, Investigation, Visualization, Methodology, Project administration; Elodie Martin, William Cazenave, Fara Hodeib, Amandine Lauphié, Urvashi Dalvi, Hongmei Zhu, Formal analysis, Investigation; Anne-Emilie Allain, Conceptualization, Formal analysis, Investigation; Laura Supiot, Data curation, Formal analysis; Daniel Cattaert, Conceptualization, Data curation, Software, Formal analysis, Supervision, Validation, Investigation, Visualization, Methodology

### Author ORCIDs

Pascal Branchereau  <https://orcid.org/0000-0003-3972-8229>

### Ethics

Animal experimentation: All procedures were carried out in accordance with the local ethics committee of the University of Bordeaux (Saisine SOD1G093A - APAFiS #19366) and European Committee Council directives. All efforts were made to minimize animal suffering and reduce the number of animals used.

### Decision letter and Author response

Decision letter <https://doi.org/10.7554/eLife.51402.sa1>

Author response <https://doi.org/10.7554/eLife.51402.sa2>

---

## Additional files

### Supplementary files

Transparent reporting form

### Data availability

All data generated or analysed during this study are included in the manuscript and supporting files.

## References

Alger BE, Nicoll RA. 1982. Pharmacological evidence for two kinds of GABA receptor on rat hippocampal pyramidal cells studied *in vitro*. *The Journal of Physiology* 328:125-141. DOI: <https://doi.org/10.1113/jphysiol.1982.sp014256>, PMID: 7131310

- Amendola J, Durand J. 2008. Morphological differences between wild-type and transgenic superoxide dismutase 1 lumbar motoneurons in postnatal mice. *The Journal of Comparative Neurology* 511:329-341. DOI: <https://doi.org/10.1002/cne.21818>, PMID: 18803237
- Avossa D, Grandolfo M, Mazzarol F, Zatta M, Ballerini L. 2006. Early signs of motoneuron vulnerability in a disease model system: characterization of transverse slice cultures of spinal cord isolated from embryonic ALS mice. *Neuroscience* 138:1179-1194. DOI: <https://doi.org/10.1016/j.neuroscience.2005.12.009>, PMID: 16442737
- Blaustein MP. 1988. Calcium transport and buffering in neurons. *Trends in Neurosciences* 11:438-443. DOI: [https://doi.org/10.1016/0166-2236\(88\)90195-6](https://doi.org/10.1016/0166-2236(88)90195-6), PMID: 2469161
- Bories C, Amendola J, Lamotte d'Incamps B, Durand J. 2007. Early electrophysiological abnormalities in lumbar motoneurons in a transgenic mouse model of amyotrophic lateral sclerosis. *European Journal of Neuroscience* 25:451-459. DOI: <https://doi.org/10.1111/j.1460-9568.2007.05306.x>, PMID: 17284186
- Bormann J, Hamill OP, Sakmann B. 1987. Mechanism of anion permeation through channels gated by glycine and gamma-aminobutyric acid in mouse cultured spinal neurones. *The Journal of Physiology* 385:243-286. DOI: <https://doi.org/10.1113/jphysiol.1987.sp016493>, PMID: 2443667
- Bosco DA, Morfini G, Karabacak NM, Song Y, Gros-Louis F, Pasinelli P, Goolsby H, Fontaine BA, Lemay N, McKenna-Yasek D, Frosch MP, Agar JN, Julien JP, Brady ST, Brown RH. 2010. Wild-type and mutant SOD1 share an aberrant conformation and a common pathogenic pathway in ALS. *Nature Neuroscience* 13:1396-1403. DOI: <https://doi.org/10.1038/nn.2660>, PMID: 20953194
- Branchereau P, Morin D, Bonnot A, Ballion B, Chapron J, Viala D. 2000. Development of lumbar rhythmic networks: from embryonic to neonate locomotor-like patterns in the mouse. *Brain Research Bulletin* 53:711-718. DOI: [https://doi.org/10.1016/S0361-9230\(00\)00403-2](https://doi.org/10.1016/S0361-9230(00)00403-2), PMID: 11165805
- Branchereau P, Cattaert D, Delpy A, Allain AE, Martin E, Meyrand P. 2016. Depolarizing GABA/glycine synaptic events switch from excitation to inhibition during frequency increases. *Scientific Reports* 6:21753. DOI: <https://doi.org/10.1038/srep21753>, PMID: 26912194
- Carnevale NT, Hines ML. 2006. *The NEURON Book*. Cambridge: Cambridge University Press.
- Chang Q, Martin LJ. 2011. Glycine receptor channels in spinal motoneurons are abnormal in a transgenic mouse model of amyotrophic lateral sclerosis. *Journal of Neuroscience* 31:2815-2827. DOI: <https://doi.org/10.1523/JNEUROSCI.2475-10.2011>, PMID: 21414903
- Chang Q, Martin LJ. 2016. Voltage-gated calcium channels are abnormal in cultured spinal motoneurons in the G93A-SOD1 transgenic mouse model of ALS. *Neurobiology of Disease* 93:78-95. DOI: <https://doi.org/10.1016/j.nbd.2016.04.009>, PMID: 27151771
- Clark R, Blizzard C, Dickson T. 2015. Inhibitory dysfunction in amyotrophic lateral sclerosis: future therapeutic opportunities. *Neurodegenerative Disease Management* 5:511-525. DOI: <https://doi.org/10.2217/nmt.15.49>, PMID: 26619150
- Dasen JS, De Camilli A, Wang B, Tucker PW, Jessell TM. 2008. Hox repertoires for motor neuron diversity and connectivity gated by a single accessory factor, FoxP1. *Cell* 134:304-316. DOI: <https://doi.org/10.1016/j.cell.2008.06.019>, PMID: 18662545
- Delpy A, Allain A-E, Meyrand P, Branchereau P. 2008. NKCC1 cotransporter inactivation underlies embryonic development of chloride-mediated inhibition in mouse spinal motoneuron. *The Journal of Physiology* 586:1059-1075. DOI: <https://doi.org/10.1113/jphysiol.2007.146993>
- Destexhe A, Babloyantz A, Sejnowski TJ. 1993. Ionic mechanisms for intrinsic slow oscillations in thalamic relay neurons. *Biophysical Journal* 65:1538-1552. DOI: [https://doi.org/10.1016/S0006-3495\(93\)81190-1](https://doi.org/10.1016/S0006-3495(93)81190-1), PMID: 8274647
- Devlin AC, Burr K, Boroah S, Foster JD, Cleary EM, Geti I, Vallier L, Shaw CE, Chandran S, Miles GB. 2015. Human iPSC-derived motoneurons harbouring TARDBP or C9ORF72 ALS mutations are dysfunctional despite maintaining viability. *Nature Communications* 6:5999. DOI: <https://doi.org/10.1038/ncomms6999>, PMID: 25580746
- Doyon N, Vinay L, Prescott SA, De Koninck Y. 2016. Chloride regulation: a dynamic equilibrium crucial for synaptic inhibition. *Neuron* 89:1157-1172. DOI: <https://doi.org/10.1016/j.neuron.2016.02.030>, PMID: 26985723
- Dumoulin A, Rostaing P, Bedet C, Le'vi S, Isambert MF, Henry JP, Triller A, Gasnier B. 1999. Presence of the vesicular inhibitory amino acid transporter in GABAergic and glycinergic synaptic terminal boutons. *Journal of Cell Science* 112:811-823. PMID: 10036231
- Eisen A, Kiernan M, Mitsumoto H, Swash M. 2014. Amyotrophic lateral sclerosis: a long preclinical period? *Journal of Neurology, Neurosurgery & Psychiatry* 85:1232-1238. DOI: <https://doi.org/10.1136/jnnp-2013-307135>
- Falgairolle M, Puhl JG, Pujala A, Liu W, O'Donovan MJ. 2017. Motoneurons regulate the central pattern generator during drug-induced locomotor-like activity in the neonatal mouse. *eLife* 6:e26622. DOI: <https://doi.org/10.7554/eLife.26622>, PMID: 28671548
- Filipchuk AA, Durand J. 2012. Postnatal dendritic development in lumbar motoneurons in mutant superoxide dismutase 1 mouse model of amyotrophic lateral sclerosis. *Neuroscience* 209:144-154. DOI: <https://doi.org/10.1016/j.neuroscience.2012.01.046>, PMID: 22387111
- Fogarty MJ. 2018. Driven to decay: excitability and synaptic abnormalities in amyotrophic lateral sclerosis. *Brain Research Bulletin* 140:318-333. DOI: <https://doi.org/10.1016/j.brainresbull.2018.05.023>, PMID: 29870780
- Fuchs A, Ringer C, Bilkei-Gorzo A, Weihe E, Roeper J, Schu"tz B. 2010. Downregulation of the potassium chloride cotransporter KCC2 in vulnerable motoneurons in the SOD1-G93A mouse model of amyotrophic lateral

- sclerosis. *Journal of Neuropathology & Experimental Neurology* 69:1057-1070. DOI: <https://doi.org/10.1097/NEN.0b013e3181f4dcef>, PMID: 20838240
- Gao BX, Cheng G, Ziskind-Conhaim L. 1998. Development of spontaneous synaptic transmission in the rat spinal cord. *Journal of Neurophysiology* 79:2277-2287. DOI: <https://doi.org/10.1152/jn.1998.79.5.2277>, PMID: 9582204
- Gao BX, Stricker C, Ziskind-Conhaim L. 2001. Transition from GABAergic to glycinergic synaptic transmission in newly formed spinal networks. *Journal of Neurophysiology* 86:492-502. DOI: <https://doi.org/10.1152/jn.2001.86.1.492>, PMID: 11431527
- Gao BX, Ziskind-Conhaim L. 1995. Development of glycine- and GABA-gated currents in rat spinal motoneurons. *Journal of Neurophysiology* 74:113-121. DOI: <https://doi.org/10.1152/jn.1995.74.1.113>, PMID: 7472315
- Gao BX, Ziskind-Conhaim L. 1998. Development of ionic currents underlying changes in action potential waveforms in rat spinal motoneurons. *Journal of Neurophysiology* 80:3047-3061. DOI: <https://doi.org/10.1152/jn.1998.80.6.3047>, PMID: 9862905
- Gulledge AT, Stuart GJ. 2003. Excitatory actions of GABA in the cortex. *Neuron* 37:299-309. DOI: [https://doi.org/10.1016/S0896-6273\(02\)01146-7](https://doi.org/10.1016/S0896-6273(02)01146-7), PMID: 12546824
- Han P, Nakanishi ST, Tran MA, Whelan PJ. 2007. Dopaminergic modulation of spinal neuronal excitability. *Journal of Neuroscience* 27:13192-13204. DOI: <https://doi.org/10.1523/JNEUROSCI.1279-07.2007>, PMID: 18045913
- Hines ML, Carnevale NT. 1997. The NEURON simulation environment. *Neural Computation* 9:1179-1209. DOI: <https://doi.org/10.1162/neco.1997.9.6.1179>, PMID: 9248061
- Hines ML, Carnevale NT. 2001. NEURON: a tool for neuroscientists. *The Neuroscientist* 7:123-135. DOI: <https://doi.org/10.1177/107385840100700207>, PMID: 11496923
- Houston CM, Bright DP, Sivilotti LG, Beato M, Smart TG. 2009. Intracellular chloride ions regulate the time course of GABA-mediated inhibitory synaptic transmission. *Journal of Neuroscience* 29:10416-10423. DOI: <https://doi.org/10.1523/JNEUROSCI.1670-09.2009>, PMID: 19692617
- Ikemoto A, Nakamura S, Akiguchi I, Hirano A. 2002. Differential expression between synaptic vesicle proteins and presynaptic plasma membrane proteins in the anterior horn of amyotrophic lateral sclerosis. *Acta Neuropathologica* 103:179-187. DOI: <https://doi.org/10.1007/s004010100449>, PMID: 11810185
- Kuo JJ, Schonewille M, Siddique T, Schults AN, Fu R, Baer PR, Anelli R, Heckman CJ, Kroese AB. 2004. Hyperexcitability of cultured spinal motoneurons from presymptomatic ALS mice. *Journal of Neurophysiology* 91:571-575. DOI: <https://doi.org/10.1152/jn.00665.2003>, PMID: 14523070
- Kuo JJ, Siddique T, Fu R, Heckman CJ. 2005. Increased persistent Na<sup>+</sup> current and its effect on excitability in motoneurons cultured from mutant SOD1 mice. *The Journal of Physiology* 563:843-854. DOI: <https://doi.org/10.1113/jphysiol.2004.074138>, PMID: 15649979
- Legendre P. 2001. The glycinergic inhibitory synapse. *Cellular and Molecular Life Sciences* 58:760-793. DOI: <https://doi.org/10.1007/PL00000899>, PMID: 11437237
- Leonzino M, Busnelli M, Antonucci F, Verderio C, Mazzanti M, Chini B. 2016. The timing of the Excitatory-to-Inhibitory GABA switch is regulated by the oxytocin receptor via KCC2. *Cell Reports* 15:96-103. DOI: <https://doi.org/10.1016/j.celrep.2016.03.013>, PMID: 27052180
- Leroy F, Lamotte d'Incamps B, Imhoff-Manuel RD, Zytnicki D. 2014. Early intrinsic hyperexcitability does not contribute to motoneuron degeneration in amyotrophic lateral sclerosis. *eLife* 3:e04046. DOI: <https://doi.org/10.7554/eLife.04046>, PMID: 25313866
- Logroscino G, Traynor BJ, Hardiman O, Chio A, Mitchell D, Swingler RJ, Millul A, Benn E, Beghi E, for EURALS. 2010. Incidence of amyotrophic lateral sclerosis in Europe. *Journal of Neurology, Neurosurgery & Psychiatry* 81:385-390. DOI: <https://doi.org/10.1136/jnnp.2009.183525>
- Martin E, Cazenave W, Cattaert D, Branchereau P. 2013. Embryonic alteration of motoneuronal morphology induces hyperexcitability in the mouse model of amyotrophic lateral sclerosis. *Neurobiology of Disease* 54:116-126. DOI: <https://doi.org/10.1016/j.nbd.2013.02.011>, PMID: 23466698
- McLarnon JG, Kim SU, Michikawa M, Xu R. 1995. Properties of inward and outward potassium currents in cultured mouse motoneurons. *Neuroscience* 64:139-151. DOI: [https://doi.org/10.1016/0306-4522\(95\)90396-0](https://doi.org/10.1016/0306-4522(95)90396-0)
- Medelin M, Rancic V, Cellot G, Laishram J, Veeraraghavan P, Rossi C, Muzio L, Sivilotti L, Ballerini L. 2016. Altered development in GABA co-release shapes glycinergic synaptic currents in cultured spinal slices of the SOD1(G93A) mouse model of amyotrophic lateral sclerosis. *The Journal of Physiology* 594:3827-3840. DOI: <https://doi.org/10.1113/JP272382>, PMID: 27098371
- Michelson HB, Wong RK. 1991. Excitatory synaptic responses mediated by GABA receptors in the Hippocampus. *Science* 253:1420-1423. DOI: <https://doi.org/10.1126/science.1654594>, PMID: 1654594
- Milan L, Barrière G, De Deurwaerdère P, Cazalets JR, Bertrand SS. 2014. Monoaminergic control of spinal locomotor networks in SOD1G93A newborn mice. *Frontiers in Neural Circuits* 8:77. DOI: <https://doi.org/10.3389/fncir.2014.00077>, PMID: 25071458
- Milan L, Courtand G, Carroit L, Masmejean F, Barrière G, Cazalets JR, Garret M, Bertrand SS. 2015. Age-Related changes in pre- and postsynaptic partners of the cholinergic C-Boutons in Wild-Type and SOD1G93A lumbar motoneurons. *PLOS ONE* 10:e0135525. DOI: <https://doi.org/10.1371/journal.pone.0135525>, PMID: 26305672
- Misgeld U, Wagner A, Ohno T. 1982. Depolarizing IPSPs and depolarization by GABA of rat neostriatum cells in vitro. *Experimental Brain Research* 45:108-114. DOI: <https://doi.org/10.1007/BF00235769>, PMID: 7056316
- Moroni M, Biro I, Giugliano M, Vijayan R, Biggin PC, Beato M, Sivilotti LG. 2011. Chloride ions in the pore of glycine and GABA channels shape the time course and voltage dependence of agonist currents. *Journal of Neuroscience* 31:14095-14106. DOI: <https://doi.org/10.1523/JNEUROSCI.1985-11.2011>, PMID: 21976494

- Muller E, Le Corronc H, Triller A, Legendre P. 2006. Developmental dissociation of presynaptic inhibitory neurotransmitter and postsynaptic receptor clustering in the hypoglossal nucleus. *Molecular and Cellular Neuroscience* 32:254-273. DOI: <https://doi.org/10.1016/j.mcn.2006.04.007>, PMID: 16765056
- Pambo-Pambo A, Durand J, Gueritaud JP. 2009. Early excitability changes in lumbar motoneurons of transgenic SOD1G85R and SOD1G(93A-Low) mice. *Journal of Neurophysiology* 102:3627-3642. DOI: <https://doi.org/10.1152/jn.00482.2009>, PMID: 19828728
- Paré B, Lehmann M, Beaudin M, Nordström U, Saikali S, Julien JP, Gilthorpe JD, Marklund SL, Cashman NR, Andersen PM, Forsberg K, Dupré N, Gould P, Brännström T, Gros-Louis F. 2018. Misfolded SOD1 pathology in sporadic amyotrophic lateral sclerosis. *Scientific Reports* 8:14223. DOI: <https://doi.org/10.1038/s41598-018-31773-z>, PMID: 30242181
- Payne JA, Stevenson TJ, Donaldson LF. 1996. Molecular characterization of a putative K-Cl cotransporter in rat brain A neuronal-specific isoform. *The Journal of Biological Chemistry* 271:16245-16252. DOI: <https://doi.org/10.1074/jbc.271.27.16245>, PMID: 8663311
- Pitt SJ, Sivilotti LG, Beato M. 2008. High intracellular chloride slows the decay of glycinergic currents. *Journal of Neuroscience* 28:11454-11467. DOI: <https://doi.org/10.1523/JNEUROSCI.3890-08.2008>, PMID: 18987182
- Quinlan KA, Schuster JE, Fu R, Siddique T, Heckman CJ. 2011. Altered postnatal maturation of electrical properties in spinal motoneurons in a mouse model of amyotrophic lateral sclerosis. *The Journal of Physiology* 589:2245-2260. DOI: <https://doi.org/10.1113/jphysiol.2010.200659>, PMID: 21486770
- Raltshev C, Hetsch F, Winkelmann A, Meier JC, Semtner M. 2016. Electrophysiological Signature of Homomeric and Heteromeric Glycine Receptor Channels. *Journal of Biological Chemistry* 291:18030-18040. DOI: <https://doi.org/10.1074/jbc.M116.735084>
- Ramirez-Jarquín UN, Lazo-Gómez R, Tovar-Y-Romo LB, Tapia R. 2014. Spinal inhibitory circuits and their role in motor neuron degeneration. *Neuropharmacology* 82:101-107. DOI: <https://doi.org/10.1016/j.neuropharm.2013.10.003>, PMID: 24157492
- Ramírez-Jarquín UN, Tapia R. 2018. Excitatory and inhibitory neuronal circuits in the spinal cord and their role in the control of motor neuron function and degeneration. *ACS Chemical Neuroscience* 9:211-216. DOI: <https://doi.org/10.1021/acscchemneuro.7b00503>, PMID: 29350907
- Rivera C, Voipio J, Payne JA, Ruusuvaara E, Lahtinen H, Lamsa K, Pirvola U, Saarna M, Kaila K. 1999. The K<sup>+</sup>/Cl<sup>-</sup> co-transporter KCC2 renders GABA hyperpolarizing during neuronal maturation. *Nature* 397:251-255. DOI: <https://doi.org/10.1038/16697>, PMID: 9930699
- Russell JM. 2000. Sodium-potassium-chloride cotransport. *Physiological Reviews* 80:211-276. DOI: <https://doi.org/10.1152/physrev.2000.80.1.211>, PMID: 10617769
- Song I, Savtchenko L, Semyanov A. 2011. Tonic excitation or inhibition is set by GABA(A) conductance in hippocampal interneurons. *Nature Communications* 2:376. DOI: <https://doi.org/10.1038/ncomms1377>, PMID: 21730957
- Stacey WC, Durand DM. 2000. Stochastic resonance improves signal detection in hippocampal CA1 neurons. *Journal of Neurophysiology* 83:1394-1402. DOI: <https://doi.org/10.1152/jn.2000.83.3.1394>, PMID: 10712466
- Staley KJ, Mody I. 1992. Shunting of excitatory input to dentate gyrus granule cells by a depolarizing GABA<sub>A</sub> receptor-mediated postsynaptic conductance. *Journal of Neurophysiology* 68:197-212. DOI: <https://doi.org/10.1152/jn.1992.68.1.197>, PMID: 1381418
- Tazerart S, Vinay L, Brocard F. 2008. The persistent sodium current generates pacemaker activities in the central pattern generator for locomotion and regulates the locomotor rhythm. *Journal of Neuroscience* 28:8577-8589. DOI: <https://doi.org/10.1523/JNEUROSCI.1437-08.2008>, PMID: 18716217
- Thomas AM, Ostroumov A, Kimmey BA, Taormina MB, Holden WM, Kim K, Brown-Mangum T, Dani JA. 2018. Adolescent nicotine exposure alters GABA<sub>AA</sub> Receptor Signaling in the Ventral Tegmental Area and Increases Adult Ethanol Self-Administration. *Cell Reports* 23:68-77. DOI: <https://doi.org/10.1016/j.celrep.2018.03.030>, PMID: 29617674
- Tyzio R, Nardou R, Ferrari DC, Tsintsadze T, Shahrokhi A, Eftekhari S, Khalilov I, Tsintsadze V, Brouchoud C, Chazal G, Lemonnier E, Lozovaya N, Burnashev N, Ben-Ari Y. 2014. Oxytocin-mediated GABA inhibition during delivery attenuates autism pathogenesis in rodent offspring. *Science* 343:675-679. DOI: <https://doi.org/10.1126/science.1247190>, PMID: 24503856
- Van Damme P, Robberecht W, Van Den Bosch L. 2017. Modelling amyotrophic lateral sclerosis: progress and possibilities. *Disease Models & Mechanisms* 10:537-549. DOI: <https://doi.org/10.1242/dmm.029058>, PMID: 28468939
- Van den Bos MAJ, Higashihara M, Geevasinga N, Menon P, Kiernan MC, Vucic S. 2018. Imbalance of cortical facilitatory and inhibitory circuits underlies hyperexcitability in ALS. *Neurology* 91:e1669-e1676. DOI: <https://doi.org/10.1212/WNL.0000000000006438>, PMID: 30282772
- van Zundert B, Peuscher MH, Hynynen M, Chen A, Neve RL, Brown RH, Constantine-Paton M, Bellingham MC. 2008. Neonatal neuronal circuitry shows hyperexcitable disturbance in a mouse model of the adult-onset neurodegenerative disease amyotrophic lateral sclerosis. *Journal of Neuroscience* 28:10864-10874. DOI: <https://doi.org/10.1523/JNEUROSCI.1340-08.2008>, PMID: 18945894
- van Zundert B, Izaurieta P, Fritz E, Alvarez FJ. 2012. Early pathogenesis in the adult-onset neurodegenerative disease amyotrophic lateral sclerosis. *Journal of Cellular Biochemistry* 113:3301-3312. DOI: <https://doi.org/10.1002/jcb.24234>, PMID: 22740507
- Walton K, Fulton BP. 1986. Ionic mechanisms underlying the firing properties of rat neonatal motoneurons studied *in vitro*. *Neuroscience* 19:669-683. DOI: [https://doi.org/10.1016/0306-4522\(86\)90291-5](https://doi.org/10.1016/0306-4522(86)90291-5)

Zang DW, Lopes EC, Cheema SS. 2005. Loss of synaptophysin-positive boutons on lumbar motor neurons innervating the medial gastrocnemius muscle of the SOD1G93A G1H transgenic mouse model of ALS. *Journal of Neuroscience Research* 79:694-699. DOI: <https://doi.org/10.1002/jnr.20379>, PMID: 15668955

## **CHAPTER 2 RESULTS – PAPER 2**

# Excitatory action of low frequency depolarizing GABA/glycine synaptic events is favored in prenatal spinal SOD1<sup>G93A</sup> motoneurons

Hongmei Zhu, Urvashi Dalvi, William Cazenave, Daniel Cattaert and Pascal Branchereau  
Univ. Bordeaux, CNRS, INCIA, UMR 5287, F-33000 Bordeaux, France

## \*For correspondence:

Pascal Branchereau, PhD  
Institut de Neurosciences Cognitives et Intégratives d'Aquitaine (INCIA)  
Université de Bordeaux, CNRS, UMR 5287  
Zone nord - bâtiment 2ab - 2<sup>ème</sup> étage  
BP 22  
146 rue Léo Saignat  
33076 BORDEAUX Cedex  
E-mail: [pascal.branchereau@u-bordeaux.fr](mailto:pascal.branchereau@u-bordeaux.fr)

## Abbreviated title:

Early alteration in low frequency dGSPs integration in fetal SOD motoneuron

## Keywords:

ALS disease; SOD1G93A mouse; inhibitory synaptic events; synaptic integration; GABA/glycine; patch-clamp; modelling; spinal cord; spinal lumbar motoneuron

## Number of pages:

35

## Figures and tables:

6 Figures, 7 tables, 2 Supplementary figures

## Number of words:

- Abstract: 249  
- Introduction: 858  
- Discussion: 1653

## Declaration of interest:

None

## Acknowledgements:

H.Z. was granted by the China scholarship Council (CSC). We thank Nathalie Argenta for excellent technical assistance and animal breeding. The help of Gilles Courtand for image analyses is acknowledged. We finally warmly thank the "Association pour la recherche sur la Sclérose Latérale Amyotrophique et autres maladies du Motoneurone" (ARSLA), as well as AFM-Téléthon for their financial support. This study received financial support from the French government in the framework of the University of Bordeaux's IdEx "Investments for the Future" program / GPR BRAIN\_2030.

## Abstract

Prenatal E17.5 spinal motoneurons (MNs) of the SOD1<sup>G93A</sup> mouse model of amyotrophic lateral sclerosis (ALS) exhibit an altered chloride homeostasis. At this prenatal stage, MNs receive depolarizing GABAergic/glycinergic postsynaptic potentials (dGPSPs). Here, using a functional electrophysiological design, we assessed *ex vivo* the physiological effect of dGPSPs barrages on the repetitive firing ability of SOD1<sup>G93A</sup> vs WT E17.5 MNs. Chloride equilibrium (ECI) was set below spike threshold and dGPSPs were evoked by electrical stimulations of different frequencies. Two types of dGPSPs responses were obtained in WT MNs based on dGPSPs frequency: dual response that is excitation at low frequencies but inhibition at high frequencies, and pure inhibition response at all dGPSPs frequencies. Dual responses were specific to high Rin and the pure inhibition responses to low Rin. SOD1<sup>G93A</sup> MNs exhibited 3 types of dGPSP responses: Inhibition, Dual responses, but also pure Excitation whatever the Rin value. Most SOD1<sup>G93A</sup> MNs were overexcited. Simulation showed that pure excitation could be obtained in SOD-like MNs by moving away GABA/glycine input from cell body to dendrites. MNs reconstructions highlighted a distinct morphology between the two WT clusters: longer and more complex dendrites in low-Rin group, while shorter and simpler dendrites in high-Rin group. These morphological features were also observed in SOD1<sup>G93A</sup> clusters. Quantitative analysis of inhibitory synapses revealed SOD1<sup>G93A</sup> MNs receive lower-dense VIAAT perisomatic inputs. In conclusion, low Rin SOD1<sup>G93A</sup> MNs - putative fast ALS vulnerable - are therefore lacking Inhibition at fetal stage, reinforcing the early improper construction of ALS spinal motor networks.

## Highlights

- Prenatal (E17.5) spinal SOD1<sup>G93A</sup> MNs exhibit more excitatory actions by low-frequency electrically evoked-dGPSPs than WT MNs.

- At late embryonic stage, stimulation by dGPSPs allows functional and morphological identification of two types of spinal MNs located in the lateral motor column: low-Rin (the dominant population) and high-Rin WT MNs.
- Low Rin WT MNs are preferentially inhibited by dGPSPs stimulation unlike SOD1<sup>G93A</sup> MNs
- dGPSP effects do not correlate with morphology (and Rin) in SOD1<sup>G93A</sup> MNs
- Simulation show that moving away GABA/glycine input from cell body to dendrites favors excitatory effect of dGPSPs
- The density of perisomatic VIAAT terminals in SOD1<sup>G93A</sup> MNs is lower compared to WT MNs.
- Low Rin SOD1<sup>G93A</sup> MNs - putative fast ALS vulnerable - lack Inhibition at fetal stage

## Introduction

Amyotrophic Lateral Sclerosis (ALS) is an incurable fatal neurodegenerative disease characterized by gradual degeneration of motoneurons (MNs) located in brainstem and spinal cord as well as pyramidal motor neurons located in primary motor cortex ([M. C. Kiernan et al., 2011](#)). Despite decades of efforts, the disease mechanisms are still largely unknown, resulting in conspicuous absence of any treatment. Most of the ALS cases are sporadic, meaning random with unknown etiology, but the remaining 10% cases are familial (fALS), where the disease is transmitted in families usually with dominant inheritance traits ([Taylor et al., 2016](#)). The SOD1<sup>G93A</sup> transgenic mouse line is the most widely studied mouse model of ALS, with mice carrying the mutated human SOD1 gene (Gly93→Ala substitution) ([M. E. Gurney, Pu, Chiu, Dal Canto, et al., 1994](#)) and developing many pathological hallmarks and clinical symptoms similar to ALS patients ([Tu et al., 1996](#)). Using this transgenic ALS mouse model, we previously found that spinal SOD1<sup>G93A</sup> MNs are hyperexcitable at the embryonic day (E) (17.5) because of a shorter dendritic tree leading to elevated input resistance ([Martin et al., 2013](#)). Hyperexcitability of cultured mouse E12-E14 SOD1<sup>G93A</sup> MNs ([J. J. Kuo et al., 2004](#)) and MNs derived from ALS patients carrying mutations in the SOD1, C9orf72, FUS and TARDBP genes have also been described ([B. J. Wainger et al., 2014](#)) ([A. C. Devlin et al.,](#)

2015) ([Burley et al., 2022](#)), highlighting motoneuronal hyperexcitability as a possible contributor to the pathology of ALS disease.

In SOD1<sup>G93A</sup> mice, E17.5 is the day before birth. At this prenatal stage, the locomotor networks become functional and it is possible to evoke alternated locomotor-like activities from *ex-vivo* brainstem-spinal cord preparations ([Branchereau et al., 2019](#)), indicating that inhibitory commissural connections are likely functional ([Branchereau et al., 2000a](#)). However, at E17.5 GABA and glycine effects on lumbar spinal MNs are not hyperpolarizing but evoke depolarizing GABAergic/glycinergic post synaptic potentials (dGPSPs), which have mixed inhibitory (shunting) and excitatory (depolarizing) components ([Branchereau et al., 2016](#)).

Converging lines of evidence highlight alterations of the inhibitory system ([Ramirez-Jarquin et al., 2014](#)) ([Clark et al., 2015b](#)) ([Van den Bos et al., 2018](#)), with a perinatal time-window of vulnerability ([Kiernan et al., 2019](#)) ([Eisen et al., 2014a](#)), among the numerous potential causative links in ALS associated dysfunction and degeneration. In this line of evidence, we found that the inhibitory system is altered as early as E17.5 in SOD1<sup>G93A</sup> MNs that exhibit a reversal equilibrium for chloride ions ECl 10mV more depolarized relative to littermate wild-type (WT) MNs (ECl being -50mV and -60mV in SOD and WT, respectively) ([Branchereau et al., 2019](#)). At high-frequency stimulations, dGPSPs are inhibitory because of gCl summation ([Branchereau et al., 2016](#)) but evidence from computer modelling approach performed on E17.5 MN models indicated that low-frequency (< 50Hz) dGPSPs could be excitatory in SOD-like MNs but not in WT-like MNs with similar ECl ([Branchereau et al., 2019](#)). However, we did not study the effect of dGPSPs on the repetitive firing ability of real E17.5 lumbar MNs that drive the contraction of muscle fibers and are the final pathway ([Manuel et al., 2011](#)). Are these results the same under physiological conditions? Does the same mechanism operate in a real MN? In addition, the relationship between morphological

alterations and dGPSPs effects on real E17.5 lumbar MNs was not studied. We address these issues here in three ways. First, we performed *ex-vivo* electrophysiological experiments using whole-cell patch-clamp recordings from WT and SOD1<sup>G93A</sup> fetal E17.5 mouse lumbar spinal MNs. ECI was imposed and physiological dGPSPs were evoked by activating local pharmacologically isolated GABA/glycine fibers with ventro-lateral funiculus (VLF) electrical stimulations. The effect of dGPSPs was assessed on the firing of MNs elicited by intracellular injection of current. Our results confirmed dual effects of dGPSPs on MN firing frequency, i.e., excitatory effect at low dGPSPs frequency and inhibitory at high frequency (Dual MNs), and showed that dGPSPs are also able to exert pure inhibitory effects at low frequency (Inhibited MNs). SOD MNs were mainly Dual MNs whatever their Rin whereas the majority of WT MNs - having low Rin - were Inhibited MNs, remaining with high Rin were Dual WT MNs. Second, we examined whether morphology could interpret the different dGPSPs responses in SOD1<sup>G93A</sup> and WT MNs by morphometric analysis of neurobiotin-injected recorded MNs. MNs reconstructions revealed that the morphology is highly associated with Rin in both WT and SOD1<sup>G93A</sup> MNs. Morphometric results showed that dual WT MNs displayed decreased total dendritic area and the trend of reduced dendritic trees, which is linked to high Rm. However, SOD1<sup>G93A</sup> MNs can have dual or inhibited responses whatever their morphology. Given that morphology could not interpret the different dGPSPs-evoked responses in SOD1<sup>G93A</sup> MNs, we proposed that GABA/glycine synaptic integration may be a potential cause. Then we simulated the different synapse integration on SOD MNs by using NEURON simulation. The simulation results revealed that less amount of inhibitory synapse on SOD-like MNs soma can induce more excitatory action of evoked dGPSPs before switching to inhibition. Interestingly, pure excitation could be obtained in SOD-like MNs by moving away the inhibitory input from the cell body to distal dendrites (~100  $\mu$ m). It indicates that the intergration way of dGPSP synapse may play the major role in dGPSPs

responses of SOD1<sup>G93A</sup> MNs. Third, from the molecular level by quantification analysis of synaptic VIAAT density, we verified that less abundant of synaptic and non-synaptic VIAAT on SOD1<sup>G93A</sup> MNs soma and proximal dendrites could induce more excitatory action of evoked dGPSPs before switching to inhibition, compared to WT MNs. Taken together, our data show that low density and location of GABA/glycine synaptic inputs on MNs favor excitatory effects of dGPSP trains in fetal SOD1<sup>G93A</sup> MNs, highlighting the early dysfunction of the GABA/glycine inhibitory system in the SOD1<sup>G93A</sup> mouse strain of ALS disease.

## Results

### SOD lumbar MNs are more excited by low frequency dGPSPs

Using simulation made on E17.5 WT-like MNs, we previously found that repetitive dGPSPs, delivered to the MN soma, were able to totally block the ongoing MN discharge when reaching a cut-off frequency (*Branchereau et al., 2019*). Interestingly, similar simulations made on E17.5 SOD-like MNs exhibiting shorter dendritic trees (*Martin et al., 2013*) revealed that such repetitive dGPSPs were also able to exert an excitatory effect on the ongoing MN discharge when occurring at low frequency before switching to full inhibitory effect at higher frequency (cut-off frequency) (*Branchereau et al., 2019*). Here, we initially sought to verify whether this excitatory effect was found in real prenatal SOD1<sup>G93A</sup> MNs. To answer this question, we used whole-cell patch-clamp recordings from lumbar E17.5 MNs - total 71 MNs (N = 39 litters, *table 1*) located in the lateral column (*Branchereau et al., 2019*) - in which ECl was set to -57.5 mV, i.e., in the range of the recorded physiological E<sub>GABAAR</sub> in E17.5 MNs (*Branchereau et al., 2019*). SOD or WT genotype was not known at the moment of the recording. MNs were depolarized by injecting through the recording patch-clamp pipette, in current-clamp mode, a positive current in order to elicit a tonic firing (~20 Hz, *Figure 1A-C*) during 5 s while dGPSPs were evoked at different frequencies thanks to

electrical stimulations of the ventral lateral funiculus (VLF) in the presence of glutamate, cholinergic and serotonergic blockers. As illustrated on [Figure 1](#), three types of dGPSPs effects were found: dGPSPs excitatory effect at low frequency but also at high frequency - up to 200 Hz (termed Excited MNs, [Figure 1A](#)), dGPSPs excitatory effect at low frequency switching to inhibitory effect above 50 Hz (termed Dual MNs [Figure 1B](#)) and dGPSPs inhibitory effects at low and high frequencies (between 10 Hz to 200 Hz) (termed Inhibited MNs [Figure 1C](#)). Genotyping revealed that ~60% of the WT MNs (19/32, 7 female and 8 male MNs, N = 11 litters) were inhibited while the remaining ~40% (13/32, 7 female and 6 male MNs, N = 13) were Dual MNs. Interestingly, it also revealed that excited MNs were exclusively SOD MNs (n=7, 3 female and 4 male MNs, N = 7), those latter corresponding to ~18% of the SOD MNs (7/39), most of the remaining SOD MNs being dual (~54%, n = 21, 8 female and 13 male MNs, N = 16) or inhibited (~28%, n = 11, 7 female and 4 male MNs, N = 10) ([Figure 1D](#)) (\*\*\*\* p < 0.0001, Chi-square test). Therefore, if our electrophysiological data did not confirm the exclusivity of dual dGPSPs effect in SOD MNs because some WT MNs could also be dual, it showed that fetal E17.5 SOD MNs were more excited by low frequency repetitive dGPSP than WT MNs from the same littermate, some of them being unable to switch to inhibition when dGPSPs frequency was above 40 Hz. This propensity to be excited by low frequency repetitive dGPSPs was not due to the resting membrane potential ( $E_{Rest}$ ), spike amplitude (Spike Amp.), spike width, difference between spike threshold and membrane potential ( $V_{thr}-V_r$ ) of MNs that were similar values between WT Dual, WT Inhibited, SOD Dual, SOD Inhibited and SOD Excited MNs ([table 1](#)). It was not due to the initial MN firing frequency of MNs since this latter was not significantly different between the five groups ([Figure 1E1](#)) ([table 1](#)). For each experiment, VLF intensity was adjusted in order to evoked dGPSPs with amplitude corresponding to spontaneous dGPSPs (see upper traces in [Figures 1A-C](#)). We found that the VLF intensity was significantly higher (p<0.0001,

Mann Whitney test) in SOD MNs ( $14.8 \pm 1.1 \mu\text{A}$ ,  $n = 39$ ) compared to WT MNs ( $8.3 \pm 1.0 \mu\text{A}$ ,  $n = 32$ ) (Figure 1E2, see table 1 for individual comparisons). Even though theoretical ECl was set to  $-57.5\text{mV}$ , the actual ECl was measured for each MN by assessing, in voltage-clamp mode, the reversal potential of single VLF-evoked IPSCs (Figures 1F1-F2). We did not find any significant difference between the five groups (Figures 1F3) (table 1). The slope of I/V curves performed for assessing actual ECl gives the IPSC conductance (gIPSC) that was divided by the membrane capacitance (gIPSC/Cm). No statistical differences were found between WT and SOD MNs groups (Figures 1F4) (table 1), indicating equal contribution of GABA<sub>A</sub>/glycine receptors when the VLF intensity was adjusted to obtain comparable dGPSPs (or IPSCs).

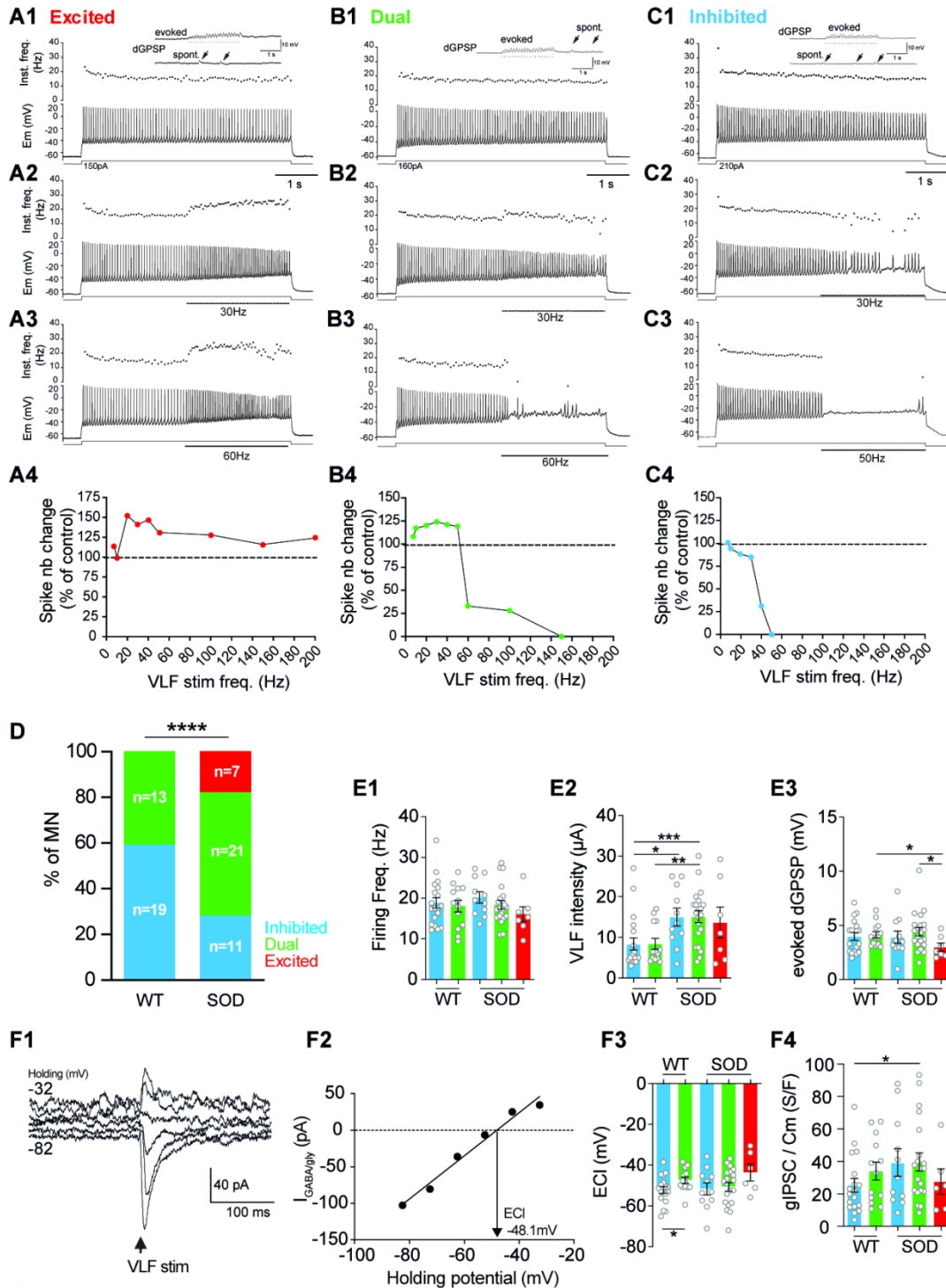


**Figure 1: Differential effects of dGSPS on E17.5 MN spiking activity.** (A1) Representative current-clamp traces of a lumbar E17.5 spinal MN - lateral motor column - exhibiting a constant firing when depolarized by a positive square pulse (150pA). The upper graph shows the instantaneous spiking frequency whereas the upper traces (right corner) depict evoked and spontaneous dGSPS with similar amplitude. (A2) On the same MN, a 30 Hz VLF stimulation, activating specifically local GABA/glycine fibers (see Methods), increases the MN firing frequency. (A3) A 60 Hz VLF stimulation induces a further MN firing frequency. (A4) Quantification of the change in MN firing frequency (spike number change, % of control) for VLF stimulations between 7.5 Hz to 200 Hz. Note that VLF stimulation always evoke an increase in firing frequency so the MN was considered as being excited. (B) Similar traces for another representative E17.5 MN showing an excitation (increase of spike frequency) (B2) at 30 Hz VLF frequency switching to inhibition at 60 Hz (B3). The graph of the spike number change shows that the switch occurs between 50 Hz and 60 Hz for this MN that is therefore considered as being dual. (C) A third representative fetal MN shows partial inhibition of its firing activity when receiving dGSPS at

the frequency of 30 Hz, switching to full inhibition at the frequency of 50 Hz). This type of fetal MN is named inhibited. **(D)** Distribution of excited, dual and inhibited MNs in WT and SOD E17.5 MNs from the same littermate. Note that excited MNs are exclusively SOD MNs and that WT MNs are mainly inhibited. \*\*\*\*  $p < 0.0001$ , Chi-square test. **(E1)** Control firing frequency of inhibited (blue bar) and dual (green bar) WT, and inhibited (blue bar), dual (green bar) and excited (red bar) SOD MNs. Note the similar firing frequency (no statistical differences, Mann Whitney tests). **(E2)** VLF intensity ( $\mu\text{A}$ ) used to elicit alike dGPSPs in every MN. Note the lower values in WT MNs compared to SOD MNs. \*  $p < 0.05$ , \*\*  $p < 0.01$ , \*\*\*  $p < 0.001$ , Mann Whitney test. **(E3)** Amplitudes of VLF-evoked dGPSP are comparable between groups, except in excited SOD MNs that exhibit reduced size evoked dGPSPs. \*  $p < 0.05$ , Mann Whitney test. **(F1)** Voltage-clamp traces showing the VLF-induced (single stimulation, arrow) current that upward for more positive holding potential and downward for negative ones. **(F2)**  $I_{\text{GABA/gly}}$  currents expressed as a function of the holding potential allowing to assess the actual ECl value ( $-48.1$  mV). **(F3)** Actual ECl values in WT and SOD MNs groups. Note the more hyperpolarized ECl values in inhibited WT MNs. \*  $p < 0.05$ , Mann Whitney test. **(F4)** gIPSC / Cm values are similar in WT and SOD MNs groups.

**Table 1.** Physiological values measured in lumbar E17.5 spinal MNs

MN sub-group	WT Inhibited	WT Dual	SOD Inhibited	SOD Dual	SOD Excited
Number of MNs	n=19	n=13	n=11	n=21	n=7
Female MNs	n=11	n=7	n=7	n=8	n=3
Male MNs	n=8	n=6	n=4	n=13	n=4
Number of litters	N=11	N=13	N=10	N=16	N=7
$E_{\text{Rest}}$ (mV)	$-74.2 \pm 1.1$	$-74.9 \pm 1.4$	$-75.5 \pm 1.4$	$-76.8 \pm 0.8$	$-77.8 \pm 1.4$
Rin	$82.0 \pm 5.7$	$128.7 \pm 15.7$	$143.3 \pm 21.1$	$119.8 \pm 9.9$	$153.1 \pm 26.6$
$C_m$ (M $\Omega$ )	$171.9 \pm 13.2^*$	$122.3 \pm 10.3$	$130.5 \pm 10.9$	$129.4 \pm 8.9$	$124.1 \pm 9.9$
Rheobase (pA)	$246.8 \pm 29.5$	$199.5 \pm 45.1$	$173.8 \pm 28.4$	$201.2 \pm 26.6$	$202.0 \pm 79.0$
SpNbCh30 (%)	$34.9 \pm 9.5^{**}$	$101.6 \pm 8.2$	$65.7 \pm 9.5^{**}$	$97.6 \pm 6.1^{***}$	$121.3 \pm 3.5^{****}$
Spike Amp. (mV)	$50.2 \pm 1.4$	$49.0 \pm 2.0$	$48.1 \pm 1.6$	$52.8 \pm 1.4$	$54.6 \pm 2.7$
Spike Width (ms)	$1.5 \pm 0.06$	$1.4 \pm 0.04$	$1.7 \pm 0.12$	$1.4 \pm 0.06$	$1.4 \pm 0.08$
$V_{\text{thr-Vr}}$ (mV)	$28.5 \pm 1.4$	$31.2 \pm 2.2$	$30.5 \pm 1.9$	$31.6 \pm 1.4$	$31.8 \pm 1.0$
Firing Freq (Hz)	$18.8 \pm 1.2$	$18.0 \pm 1.4$	$20.1 \pm 1.3$	$18.3 \pm 1.0$	$16.0 \pm 1.8$
VLF Intensity ( $\mu\text{A}$ )	$8.3 \pm 1.5^{**}$	$8.4 \pm 1.3$	$15.0 \pm 2.1$	$15.1 \pm 1.4$	$13.6 \pm 3.8$
Evoked dGPSP Amp. (mV)	$3.9 \pm 0.3$ (18)	$4.1 \pm 0.2$	$3.9 \pm 0.5$	$4.4 \pm 0.3$	$3.0 \pm 0.3$
ECl (mV)	$-52.1 \pm 1.6$ (18)	$-47.4 \pm 1.5$	$-51.6 \pm 2.9$	$-50.6 \pm 2.0$ (20)	$-43.6 \pm 4.1$ (6)
gIPSC (nS)	$4.0 \pm 0.5$ (18)	$3.8 \pm 0.6$	$4.6 \pm 0.8$	$4.6 \pm 0.6$ (20)	$3.2 \pm 1.0$ (6)
gIPSC/Cm (nS/pF)	$25.3 \pm 4.2$ (18)	$34.1 \pm 5.5$	$39.3 \pm 8.4$	$39.6 \pm 5.5$ (20)	$27.6 \pm 7.8$ (6)

Values in parenthesis are number of MNs when not corresponding values mentioned above.  $E_{\text{Rest}}$ : ns. Rin: ns.  $C_m$ : \*between WT Inh and WT Dual. Rheobase: ns. SpNbCh30: \*\*between WT Inh and WT Dual, \*\*\*between SOD Dual and WT inh, \*\*\*\*between SOD Exc and WT Inh, \*\*between SOD Inh and SOD Exc. Spike Amp.: ns. Spike Width: ns.  $V_{\text{thr-Vr}}$ : ns. Firing Freq.: ns. VLF Intensity: \*\*between WT Inh and SOD Dual. Evoked dGPSP Amp.: ns. ECl: ns. gIPSC: ns. gIPSC/Cm: ns. ns = not significant; \*  $p < 0.05$ ; \*\*  $p < 0.01$ ; \*\*\*\*  $p < 0.0001$ . Kruskal-Wallis test followed by Dunn's multiple comparisons test.

## **Principal Component Analysis (PCA) of the three groups of responses in SOD MNs and two groups of responses in WT MNs**

As described above, depending on their response to VLF stimulation, E17.5 MNs were classified into Excited (MN excited at all tested VLF stimulation frequencies), Dual (MNs excited at low VLF frequencies and then inhibited when increasing VLF stimulation frequency), and Inhibited (MN that were exclusively inhibited by VLF discharges). Five non correlated parameters were used to characterize those responses: percentage of variation of the number of spikes produced by the MN during the one second VLF stimulation at 30 Hz, compared to control spiking discharge - same time (SpNbCH30); MN input resistance ( $R_{in}$ ); Rheobase; Voltage difference between threshold potential for spikes and membrane potential ( $V_{thr}-V_r$ ); Spike width (SpkWdth). The first parameter corresponded to the cut VLF frequency at which dSPSPs were either excitatory or inhibitory, whereas the remaining four parameters discriminating mouse P6-10 delayed MNs from immediate MNs, likely F-type MNs and S-type MNs, respectively ([Leroy et al., 2014](#)).

The result of the PCA is shown in [figures 2A](#) for WT MNs and [figures 2B](#) for SOD MNs. Contribution of variables to the first and second component ([table 3](#) and [table 4](#)) indicates that the first component of the PCA (horizontal axis) mostly represented Rheobase,  $R_{in}$  and Spike Width (in red) in both SOD and WT. However, spike width (SpkWdth) was also determinant in first component for in SOD MNs but not for WT MNs. Using a similar method, the second component was interpreted as representing the change in MN discharge (number of spikes during VLF stimulation at 30 Hz expressed as % of the control: SpNbCh30), and the spike width (in green).

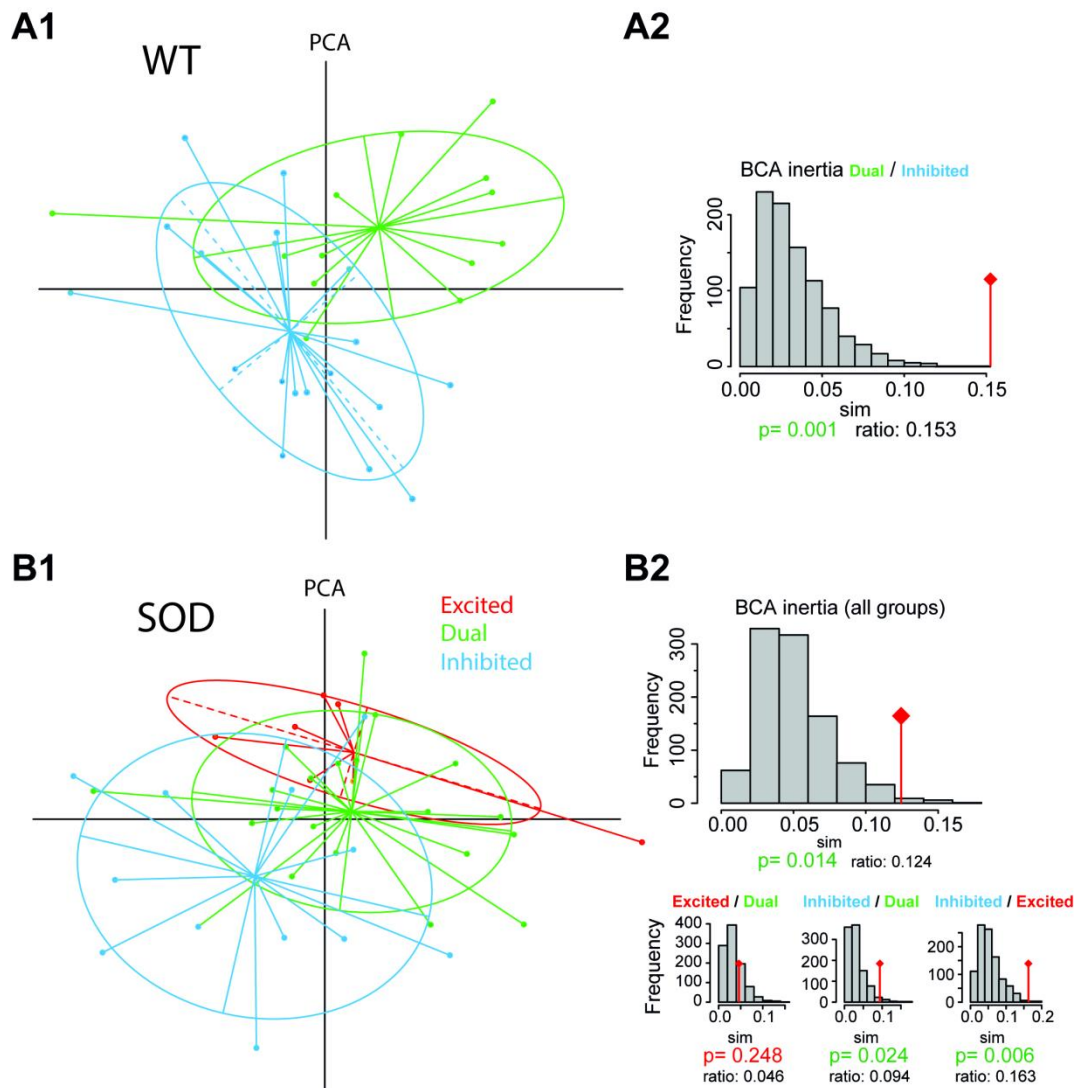


**Figure 2: Principal Component Analysis (PCA) of groups of MNs made on the basis of their d-responses to VLF inhibitory stimulation. (A)** In SOD MNs, three groups of MNs were tested: Excited, Dual and Inhibited (see text of explanations). PCA is presented in (A1); Results of Montecarlo tests to simulate 1000 inertia (see histograms) (A2). Real inertia value is presented as a red vertical line. *P*-value was then calculated as the ratio of the number of simulations in which the simulated inertia was larger than the real inertia to the total number of runs. The top histogram represents the inertia calculated for all groups. The three smaller histograms represent inertias calculated for pairs of groups. **(B)** In WT PCA was made for the two groups Dual and Inhibited (B1); the Montecarlo test indicates that these two groups are significantly different (B2). Between-Class Analysis (BCA).

**Table 3. SOD MNs: Contributions to PCA 1st and 2nd Components variance**

	Comp1	Comp2
SpNbCh30	1421	4177*
Rin	2797*	1294
Rheobase	3190*	1044
Vthr_Vr	504	1343
SpkWidth	2088*	2142*
mean	2000	2000

**Table 4.** WT MNs: Contributions to PCA 1st and 2nd Components variance

	Comp1	Comp2
SpNbCh30	403	4494*
Rin	4142*	402
Rheobase	4480*	40
Vthr_Vr	274	1816
SpkWidth	700	3248*
mean	1999.8	2000

In order to estimate whether the probability groups were distinct, separation between pairs of groups was evaluated by calculating the inertia, which was defined as the ratio of the between-group variance to the global variance. The statistical significance of inertia for group separation was estimated using a Monte Carlo permutation test (1000 runs) (see methods). For WT MNs, the Dual group was significantly different from the Inhibited group ( $p=0.001$ , figures 2A2 and table 5). For SOD MNs, Excited and Dual groups were not found statistically different ( $p = 0.213$ ), while Inhibited were statistically different from Dual ( $p=0.023$ ) and Excited ( $p=0.013$ ) (see histograms of simulated inertia in figures 2B2 and table 5). Therefore, in the following, Dual and Excited were grouped.

**Table 5.** p values from Montecarlo test after PCA

Groups	SOD MNs		WT MNs
	Excited	Dual	Dual
Dual	0.213		
Inhibited	0.013	0.023	0.001

### Low input resistance SOD MNs are not specifically inhibited

We previously showed that SOD E17.5 spinal lumbar MNs have higher input resistance (Rin) than WT MNs from the same littermate (*Martin et al., 2013; Branchereau et al., 2019*). Interestingly, our present set of data revealed a similar finding: Rin was  $101.0 \pm 8.2 \text{ M}\Omega$  ( $n = 32$ , 18 female and 14 male MNs,  $N = 24$ ) for WT MNs and  $132.4 \pm 9.3 \text{ M}\Omega$  ( $n = 39$ , 18

female and 21 male MNs, N = 33) for SOD MNs ( $p < 0.05$ , Mann Whitney test) (Figure 3A1). Rheobase - the minimum current injection to elicit a spiking activity - was lower in SOD MNs ( $193.9 \pm 21.0$  pA, n = 39) compared to WT MNs ( $227.6 \pm 25.3$  pA, n = 32) ( $p < 0.05$ , Mann Whitney test), in agreement with higher Rin values (Figure 3A2). The between groups analysis (Kruskal-Wallis test followed by Dunn's comparisons test) showed that Rin of WT Inhibited MNs was significantly reduced when compared to Rin of Dual and Inhibited SOD MNs (Figure 3B) and a similar trend was found when compared to Rin of Dual WT MNs, even though not significant ( $p = 0.0534$ ). Plots of rheobase according to Rin values revealed an expected relationship for WT and SOD MNs, i.e., MNs with low Rin express a high rheobase and *vice versa* (Figures 3C1-C2). But it also revealed that most Rin values were below 100 M $\Omega$  for Inhibited MNs (Figure 3C1), which was not the case in SOD MNs that were Dual or Inhibited whatever Rin values (Figure 3C2). The percentage of Inhibited MNs with Rin below 100 m $\Omega$  was ~90% (2/19) in WT and only 45% in SOD (5/11) (\*\*\*\*  $p < 0.0001$ , Chi-square test) (figure 3C3).

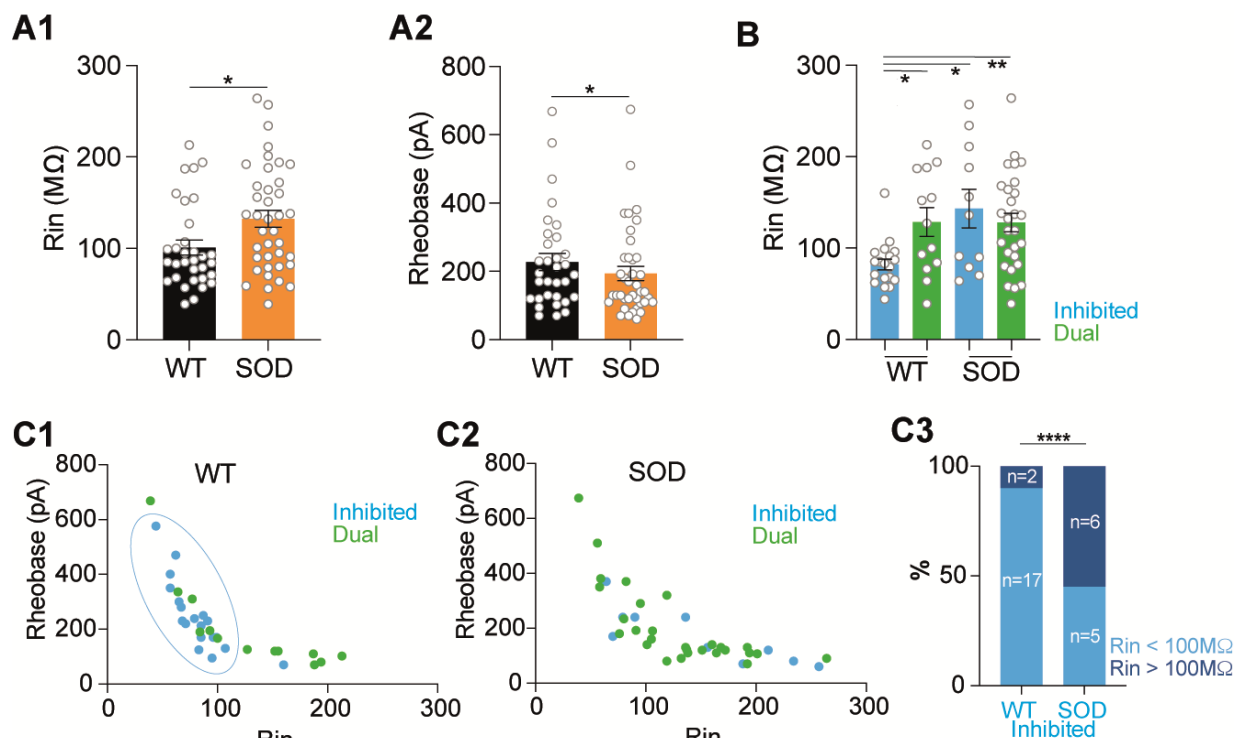


**Figure 3: WT Inhibited MNs are low Rin but not SOD MNs.** (A1) SOD MNs have lessened Rin value compared to WT MNs from the same littermate. (A2) Rheobase is low in SOD MNs that are more excitable. \*  $p < 0.05$ , Mann Whitney test. (B) Rin is low exclusively in WT inhibited MNs. \*  $p < 0.05$ , \*  $p < 0.01$ , Mann Whitney test. (C) Rheobase values are inversely proportional to Rin value in WT and SOD MNs. Unlike SOD MNs (C2), most inhibited WT MNs are  $< 100 \text{ M}\Omega$  (C1). (C3) Percentage of inhibited MN  $< 100 \text{ M}\Omega$  (bright blue) in both genotypes. \*\*\*  $p < 0.0001$ , Chi-square test.

### **dGPSP effects in SOD MNs firing activity do not correlate with morphology**

In an attempt to verify whether Dual (Excited / Inhibited) MNs exhibited altered dendritic tree as expected in our working hypothesis, some recorded MNs tested for electrophysiology were neurobiotin-injected and reconstructed (figure 4). Dendrogram were performed and morphometric parameters collected. Eight WT MNs (N =7) and 11 SOD MNs (N =10) were encompassed in the present study. In our 2013 paper (Martin *et al.*, 2013) we have shown that morphometric parameters of E17.5 MNs correlated with their measured Rin, MNs with shorter dendrites having higher Rin and *vice versa*. Therefore, in order to probe whether such relationship also exist in the present study, reconstructed MNs were grouped according to their high (H) Rin ( $>100 \text{ m}\Omega$ ) or low (L) Rin ( $<100 \text{ m}\Omega$ ). As illustrated in table 6 the total dendritic length ( $\Sigma_{\text{Len}}$ ) was lower in WT H Rin MNs ( $2408 \pm 379 \mu\text{m}$ ) compared to WT L Rin MNs ( $3433 \pm 458 \mu\text{m}$ ), the difference between the two groups being not different likely because only 3 H Rin WT MNs were considered. A similar trend was found for the mean length of the terminal dendritic segment ( $\text{Mean}_{\text{Len term}}$ ), mean length of the intermediate dendritic segment ( $\text{Mean}_{\text{Len interm}}$ ) and total dendritic volume ( $\Sigma_{\text{volume}}$ ). The total dendritic area ( $\Sigma_{\text{area}}$ ) was significantly lower in WT H Rin MNs ( $6838 \pm 1417 \mu\text{m}$ ) compared to WT L Rin MNs ( $10335 \pm 1069 \mu\text{m}$ ) (table 6).  $\Sigma_{\text{Len}}$  was significantly lessened in SOD H Rin MNs ( $2653 \pm 460 \mu\text{m}$ ) compared to WT L Rin MNs ( $4417 \pm 313 \mu\text{m}$ ) and similar trend was obtained for other considered morphometric parameters (table 6). Interestingly, WT H Rin were Dual MNs (in green in table 6) and WT L Rin were Inhibited MNs (in blue in table 6) whereas Dual MNs and Inhibited MNs were found in SOD H Rin and SOD L Rin (table 6), indicating that

dGPSP effects in SOD MNs firing activity were not closely correlated to morphology (and Rin) (see also [figures 3C2-C3](#)), unlike in WT MNs.

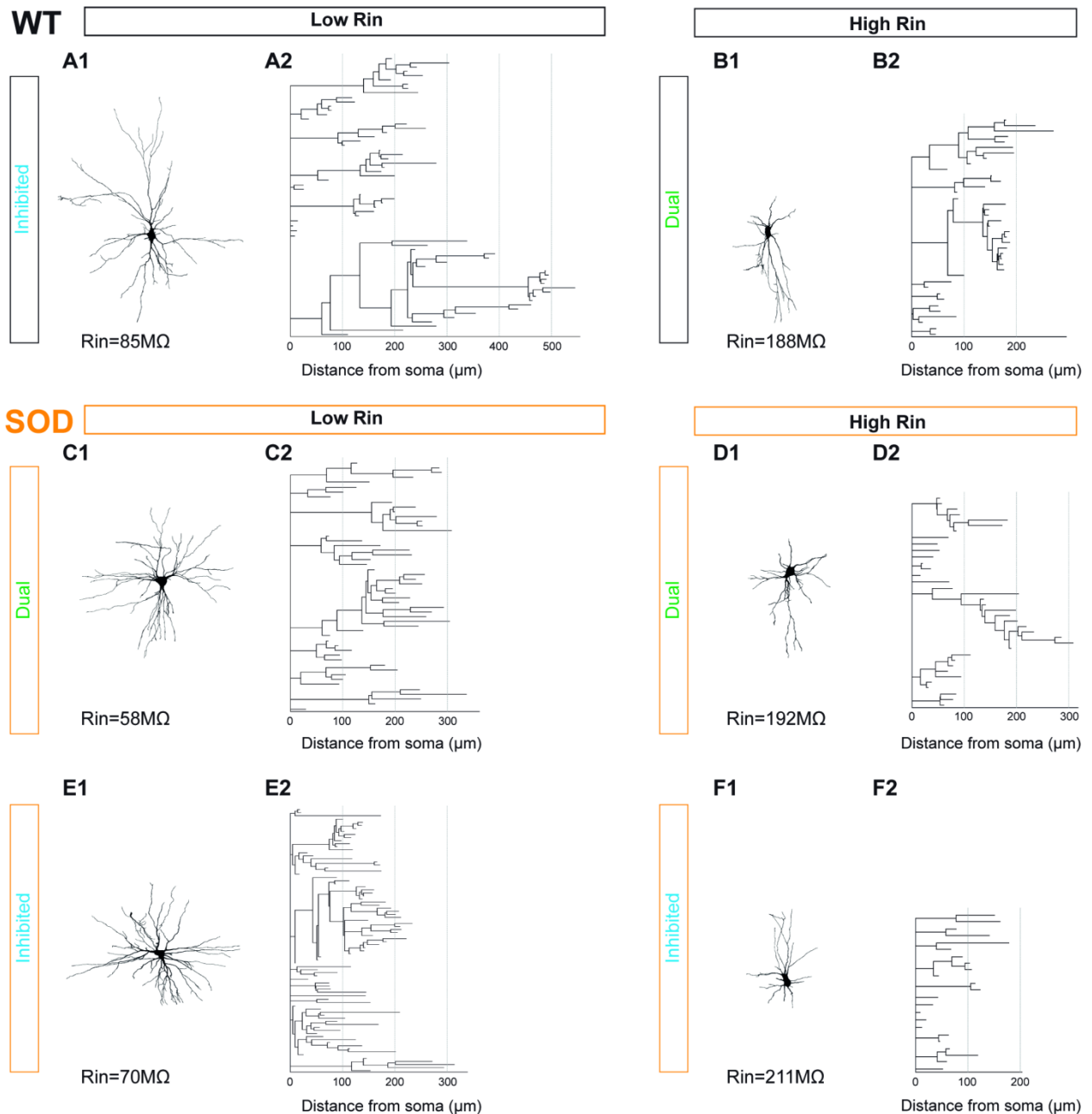


**Figure 4: Morphological analysis of low Rin vs high Rin E17.5 MNs.** (A-B) Representative 3D reconstruction (A1) and dendrogram (A2) of a Low Rin WT MN (MN#4 in Tables 6 and 7) and High Rin MN (B1-B2) (MN#1 in Tables 6 and 7), previously recorded and filled with neurobiotin. Note the short dendritic tree of High Rin MN. Low Rin WT MN is Inhibited MN whereas High Rin WT MN is Dual one. (C-D) 3D reconstruction (C1-D1) and dendrogram (C2-D2) of two Dual SOD MNs. (E-F) 3D reconstruction (E1-F1) and dendrogram (E2-F2) of two Inhibited SOD MNs. Dual and Inhibited SOD MNs may be Low or High Rin (MN#9 and MN#5 in Tables 6 and 7). Reconstructions were made from x40 high magnification confocal acquisitions (0.2  $\mu\text{m}$  in Z). Rin value for each illustrated MN is given below the 3D reconstruction image.

**Table 6.** Rin and dendritic morphometric parameter.

		Rin	Mean <sub>Len term</sub>	Mean <sub>Len interm</sub>	$\Sigma_{Len}$	$\Sigma_{Area}$	$\Sigma_{Volume}$	
	Group	(M $\Omega$ )	( $\mu\text{m}$ )	( $\mu\text{m}$ )	( $\mu\text{m}$ )	( $\mu\text{m}^2$ )	( $\mu\text{m}^3$ )	
<b>WT</b>								
	MN1	H Rin	188	124.55	112.03	1656.08	4090.22	978.39
	MN2	H Rin	155	152.73	181.24	2824.56	8814.96	2903.26
	MN3	H Rin	187	96.21	176.51	2743.15	7610.29	1991.05
	<b>Mean WT</b>	<b>H Rin</b>	<b>176.7</b>	<b>124.5</b>	<b>156.6</b>	<b>2408</b>	<b>6838.00</b>	<b>1958.00</b>
	<b>SEM</b>		<b>10.84</b>	<b>16.32</b>	<b>22.32</b>	<b>376.7</b>	<b>1417.00</b>	<b>555.90</b>
	MN4	L Rin	85	164.21	273.34	3719.74	9043.98	2115.35
	MN5	L Rin	99	448.03	298.49	5076.68	14579.9	4396.22
	MN6	L Rin	87	252.07	221.71	3094.78	9368.69	2934.65
	MN7	L Rin	65	188.16	209.35	2761.36	8979.47	2820.47
	MN8	L Rin	95	130.18	172.61	2510.09	9703.52	4106.88
	<b>Mean WT</b>	<b>L Rin</b>	<b>86.2</b>	<b>236.5</b>	<b>235.1</b>	<b>3433</b>	<b>10335.00</b>	<b>3275.00</b>
	<b>SEM</b>		<b>5.886</b>	<b>56.5</b>	<b>22.61</b>	<b>458.3</b>	<b>1069.00</b>	<b>425.20</b>
	P		0.0357	0.0714	0.1429	0.2500	0.0357	0.1429
	Sign		*	ns	ns	ns	*	ns
<b>SOD</b>								
	MN1	H Rin	105	204.30	187.97	3955.28	10715.30	3110.49
	MN2	H Rin	119	144.87	191.78	2117.87	4922.91	1387.94
	MN3	H Rin	168	325.13	281.12	3356.41	10379.10	3561.50
	MN4	H Rin	192	97.78	109.26	1621.91	5183.74	1617.13
	MN5	H Rin	211	60.41	68.67	1266.00	3192.48	776.19
	MN6	H Rin	257	183.90	146.98	3603.44	9840.53	2681.77
	<b>Mean SOD</b>	<b>H Rin</b>	<b>175.3</b>	<b>169.4</b>	<b>164.3</b>	<b>2653</b>	<b>7372.00</b>	<b>2189.00</b>
	<b>SEM</b>		<b>23.38</b>	<b>37.99</b>	<b>30.24</b>	<b>460.7</b>	<b>1349.00</b>	<b>445.00</b>
	MN7	L Rin	58	253.75	202.52	3903.86	9251.66	2355.83
	MN8	L Rin	82	226.62	209.35	4813.01	12275.40	3198.43
	MN9	L Rin	70	284.93	174.23	4243.14	12564.50	3957.78
	MN10	L Rin	90	220.69	212.86	3704.70	9030.16	2432.64
	MN11	L Rin	64	202.28	264.89	5418.15	11675.00	2561.46
	<b>Mean SOD</b>	<b>L Rin</b>	<b>72.8</b>	<b>237.7</b>	<b>212.8</b>	<b>4417</b>	<b>10959</b>	<b>2901.00</b>
	<b>SEM</b>		<b>5.851</b>	<b>14.41</b>	<b>14.69</b>	<b>313.1</b>	<b>756.9</b>	<b>303.10</b>
	P		0.0043	0.1255	0.1775	0.0173	0.1255	0.4286
	Sign		**	ns	ns	*	ns	ns

Abbreviations: Rin = input resistance, Mean<sub>Len term</sub> = mean length of the terminal dendritic segment; Mean<sub>Len interm</sub> = mean length of the intermediate dendritic segment;  $\Sigma_{Len}$  = total dendritic length,  $\Sigma_{area}$  = total dendritic area;  $\Sigma_{volume}$  = total dendritic volume. H Rin = high Rin; L Rin = low Rin. Sign indicates the level of significance in Mann Whitney test: ns = not significant; \* p < 0.05; \*\* p < 0.01. Blue values are Inhibited MNs whereas green values correspond to Dual MNs.

Somatic morphometric parameters were compared between reconstructed WT and SOD MNs. We found that the soma area measured in transversal plane ( $A_{trans}$ ), the soma area ( $A_{soma}$ ), the soma volume ( $V_{soma}$ ) as well as the minimum feret of the soma ( $F_{min}$ ) were significantly higher in SOD MNs relative to age-matched WT MNs (table 7). As a whole, somatic parameters showed that E17.5 SOD lumbar spinal MNs exhibited bigger soma that WT MNs from the same littermate.

**Table 7.** somatic morphometric parameter.

	$P_{\text{soma}}$ ( $\mu\text{m}$ )	$A_{\text{trans}}$ ( $\mu\text{m}^2$ )	$A_{\text{soma}}$ ( $\mu\text{m}^2$ )	$V_{\text{soma}}$ ( $\mu\text{m}^3$ )	$F_{\text{max}}$ ( $\mu\text{m}$ )	$F_{\text{min}}$ ( $\mu\text{m}$ )
<b>WT</b>						
MN1	80	251.45	410.67	1027.75	26.79	4.99
MN2	75.99	326.24	514.19	1223.51	27.17	8.23
MN3	78.68	159.41	406.11	822.66	31.07	3.42
MN4	93.61	342.82	406.91	1104.42	34.18	1.87
MN5	96.09	395.75	451.51	1269.31	37.16	5.77
MN6	89.73	299.48	265.27	750.97	25.83	1.72
MN7	69.32	235	412.35	985.72	24.25	4.99
MN8	68.63	282.3	1014.4	2599.08	23.56	2.18
<b>Mean WT</b>	<b>81.51</b>	<b>286.6</b>	<b>485.2</b>	<b>1223,00</b>	<b>28.75</b>	<b>4.146</b>
<b>SEM</b>	<b>3.736</b>	<b>25.67</b>	<b>79.47</b>	<b>206.5</b>	<b>1.73</b>	<b>0.804</b>
<b>SOD<sup>G93A</sup></b>						
MN1	77.66	376.13	452.95	1626.96	26.98	5.93
MN2	91.08	414.8	788.1	2811.67	34.76	4.99
MN3	79.71	356.25	682.87	1865.6	27.79	8.93
MN4	89.3	406.2	1479.95	4339.01	32.37	6.34
MN5	84.18	338.85	807.17	2512.49	32.88	6.61
MN6	77.14	352.91	587.87	1715.04	28.16	8.17
MN7	98.82	393.79	857.85	2823.09	26.06	8.27
MN8	94.1	418.32	561.87	1581.88	34.28	3.74
MN9	77.5	333.88	716.26	2149.42	26.38	8.83
MN10	85.49	334.93	421.6	1094.74	25.47	6.14
MN11	68.37	269.74	553.22	1623.83	22.94	5.15
<b>Mean SOD<sup>G93A</sup></b>	<b>83.94</b>	<b>363.3</b>	<b>719.1</b>	<b>2195,00</b>	<b>28.92</b>	<b>6.645</b>
<b>SEM</b>	<b>2.687</b>	<b>13.41</b>	<b>87.43</b>	<b>270.5</b>	<b>1.2</b>	<b>0.5155</b>
P	0.7168	0.0157	0.0091	0.005	0.778	0.0119
Sign	ns	*	**	**	ns	*

Abbreviations:  $P_{\text{soma}}$  = soma perimeter;  $A_{\text{trans}}$  = soma area measured in transversal plane;  $A_{\text{soma}}$  = soma area;  $V_{\text{soma}}$  = soma volume,  $F_{\text{max}}$  = maximum feret of the soma;  $F_{\text{min}}$  = minimum feret of the soma. Sign indicates the level of significance in Mann Whitney test: ns = not significant; \*  $p < 0.05$ ; \*\*  $p < 0.01$ .

### Estimation of effects of ECI, distal dendritic length, soma diameter and synapse position on dGPSP burst effects by simulations

In a previous work, we have used simulations to show how ECI interact with  $V_{\text{rest}}$  and other parameters (morphology, synaptic conductance etc.) of MNs in order to produce mixed inhibitory and excitatory responses in single PSPs (*Branchereau et al., 2016*). Here, we addressed more precisely this question using the same protocol as used in physiological experiments. Basically, the MN received a continuous amount of constant current in order to produce a stable 12 Hz discharge (*figure 5A2*). On this basal activity, a train of dGPSPs was elicited (GABA/glycine inputs) at a range of frequencies from 0.2 to 300 Hz. When ECI was

around -50 mV, a small variation of ECl could produce opposite effects. For example, in a WT MN, when ECl was set to -47.4 mV (as in experiments) a 20 Hz fiber stimulation of GABAergic/glycinergic neurons (GABA/glycine stimulation) evoked an excitatory response that increased with frequency up to 166 Hz and then decreased and became inhibitory for GABA/glycine stimulation frequency > 300 Hz (figure 5A1, red symbols, illustrated until 200 Hz). A modest decrease of ECl (to -52.1 mV) led to a total absence of excitatory effect from 20 Hz. The MN discharge was even totally blocked at GABA/glycine stimulation frequency = 50 Hz (and above) (figure 5A1, blue symbols; figure 5A2).

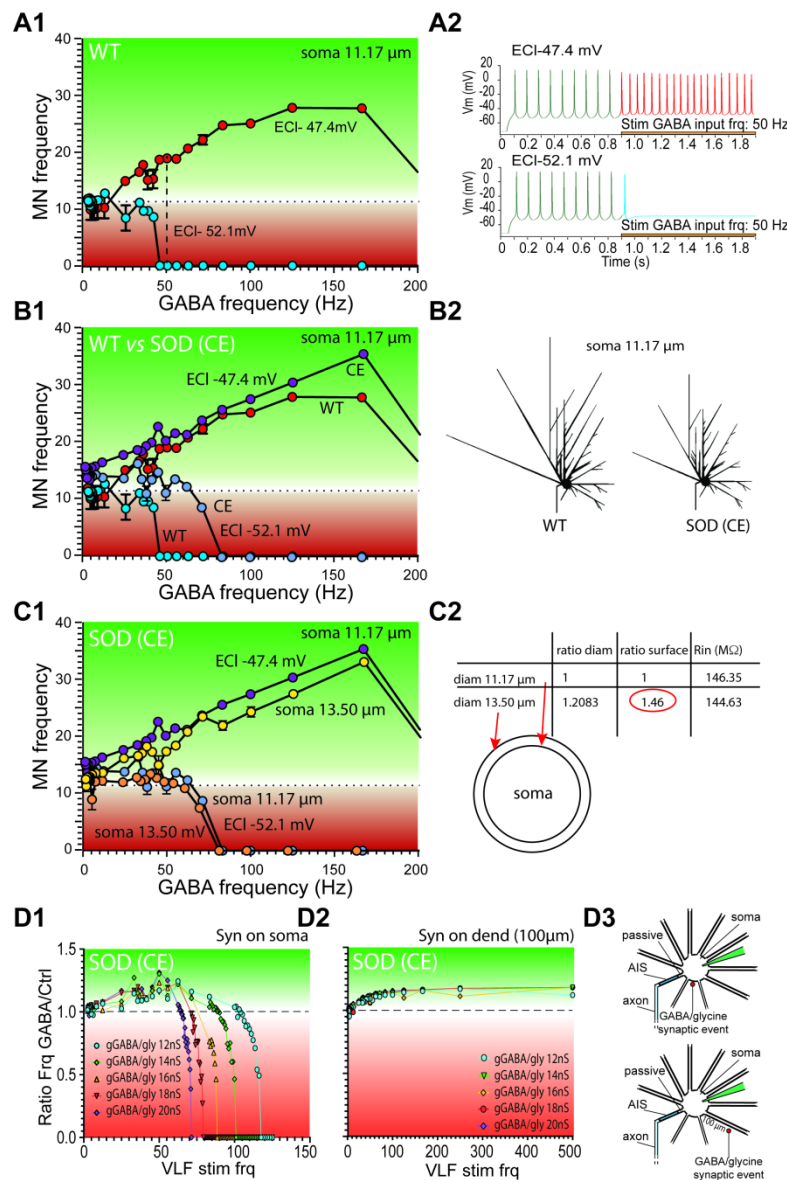


**Figure 5: Simulation of the effects of ECl, distal dendritic length, soma diameter, synapse position on DGPSP burst. (A)** Comparison of effect of two ECl values: -47.4 mV (red circles) and -52.1 mV (light blue

circles) (A1) for a WT MN (see methods for characteristics of WT and CE MNs). Two raw data are presented to illustrate the procedure (A2). A constant current is injected in the MN (200 pA) so that MN discharge is around 12 Hz. GABA synapse stimulation starts at  $t = 900$  ms. (B) Comparison of the responses presented in A for WT MNs, with CE MNs (40% decrease of distal dendrites length, see methods) B1: Simulation results; B2 Shape of dendritic trees of WT and CE MNs. (C) Comparison of the effect of increasing soma membrane area by 146% in CE MNs for two ECl values (-47.4 mV and -52.1 mV). C1: Simulation results; c2: illustration of the change in MN diameter. (D) Comparison of the effect of GABA synapse stimulation with two GABA synapse location: on soma (D1) and 100 $\mu$ m away from soma on a dendrite (D2). D3: illustration of the geometric disposition. Default soma diameter was 11.17 $\mu$ m (A1, B1, D1).

By comparison, the effect of dendrite length was less prominent (figure 5B1-B2). In this new simulation, we used WT-like MNs and SOD-like MNs. SOD-like MNs had the same characteristics as WT-like MNs except for terminal dendrites that were 40% shorter than that of the WT model as observed in SOD MNs (Martin *et al.*, 2013). These SOD model MNs were therefore called “cut ends” - CE MNs. This reduced length of their terminal dendrites increased their input resistance. Interestingly, this morphological change increased the excitability of these CE MNs in such a way that, at low GABA/glycine stimulation frequency (< 50 Hz), CE MNs presented an excitatory response for ECl values of -47.4 mV and -52.1 mV (figure 5B1), transforming the previously inhibited response (light blue trace as in figure 5A1) into a dual response (dark blue trace, figure 5B1). For CE MNs, with ECl = -52.1 mV, this response turned into an inhibition for GABA/glycine stimulation frequency > 70 Hz (dark blue trace, figure 5B1), while with ECl = -47.4 mV, excitatory response to GABA/glycine stimulation was larger than for WT MNs.

In the same manner, increasing the diameter had very modest effect on MN response to GABA/glycine stimulation (figure 5C1). In this new simulation, we increased the soma membrane area by a factor 1.46 (as values observed in some SOD MNs compared to WT MNs, see Results). Therefore, two types of CE MNs were modeled (soma diameter of 11.17 $\mu$ m and 13.50 $\mu$ m, respectively, figure 5C2). This CE MNs with increased soma diameter were slightly less excitable than previous CE MNs, but presented roughly the same characteristic response to GABA/glycine stimulation, with a dual response present when ECl = -52.1 mV (figure 5C1).

In the last series of simulations, we aimed at illustrating the effect of dGPSP synapse position on the response of SOD MNs to GABA/glycine stimulation (figure 5D1-D3). And this effect was estimated for various dGPSP synapse conductance. dGPSP synapse was moved from soma ( $x=0\mu\text{m}$ ) to a proximal dendrite at  $x = 100\mu\text{m}$  from soma (figure 5D3). This modest displacement had tremendous consequences on the effect of dGPSP trains. Whereas a dGPSP synapse in soma position ( $x=0\mu\text{m}$ ) induced a mixed excitatory response (at low GABA/glycine stimulation frequencies) and inhibitory response (at high stimulation frequencies) (figure 5D1) whatever the dGPSP conductance (12-20 nS), only excitatory responses were elicited by dGPSP trains when the dGPSP synapse was on the dendrite ( $x = 100 \mu\text{m}$ , figure 5D2).

### **SOD MNs exhibit less inhibitory inputs**

Our simulation data suggest that SOD MNs lack GABA/glycine terminals on the soma compartment. Therefore, some neurobiotin-injected MNs (in blue in figure 6) were processed for VIAAT immunostaining to detect presynaptic GABA/glycine terminals (in green) on soma and proximal dendrites of MNs and gephyrin (in red), the GABA<sub>A</sub>/glycine receptors anchoring protein. We found that a reduced VIAAT staining on the cytoplasmic membrane of SOD MN somata (figure 6A), relative to age-matched WT MNs (figure 6B). This was confirmed by a quantitative analysis of global VIAAT (figure 6C1) both on soma and proximal dendrite:  $97.23 \pm 2.68 / 100 \mu\text{m}$  for WT vs  $66.04 \pm 3.44 / 100 \mu\text{m}$  for SOD MN soma,  $90.49 \pm 1.78 / 100 \mu\text{m}$  for WT vs  $70.03 \pm 1.79 / 100 \mu\text{m}$  for SOD proximal dendrite. Synaptic VIAAT (co-localizing with gephyrin) (figure 6C2) also pointed out a reduction in SOD MNs compared to WT littermates:  $17.80 \pm 2.12 / 100 \mu\text{m}$  for WT vs  $12.05 \pm 2.11 / 100 \mu\text{m}$  for SOD MN soma,  $23.75 \pm 1.54 / 100 \mu\text{m}$  for WT vs  $17.51 \pm 1.41 / 100 \mu\text{m}$  for SOD proximal dendrite. Similar change on soma membrane and proximal dendrite membrane is in

agreement with the literature. Indeed, the density of GAD65/67 immunoreactive synaptic boutons has been described in neonatal rat MNs as being similar when analyzed on soma and on dendrites located up to 100 $\mu$ m away from the soma (*Jean-Xavier et al., 2007*). Here, the proximal dendrite length that was analyzed was  $28.5 \pm 0.8 \mu\text{m}$  and  $24.6 \pm 0.7 \mu\text{m}$ , for WT and SOD MNs respectively. The synaptic coverage diminished for the most distal dendrites (200-250  $\mu\text{m}$ ). In order to verify whether the lowered VIAAT innervation of SOD MNs, compared to WT littermate MNs, could impact the motoneuronal network, we analyzed the synaptic GABA/glycine activity in SOD vs WT MNs. Interestingly, we found that the frequency of GABA/glycine synaptic events - see [figures 6D](#) for representative traces and [figures 6E](#) for related analysis - was lessened in SOD E17.5 MNs compared to WT MNs ([figure 6F1](#)) ( $5.44 \pm 0.39 \text{ Hz}$  for WT MNs and  $4.33 \pm 0.27 \text{ Hz}$  for SOD MNs), without any change in amplitude ([figure 6F2](#)) ( $0.43 \pm 0.02 \text{ Hz}$  for WT and  $0.45 \pm 0.01 \text{ Hz}$  for SOD).

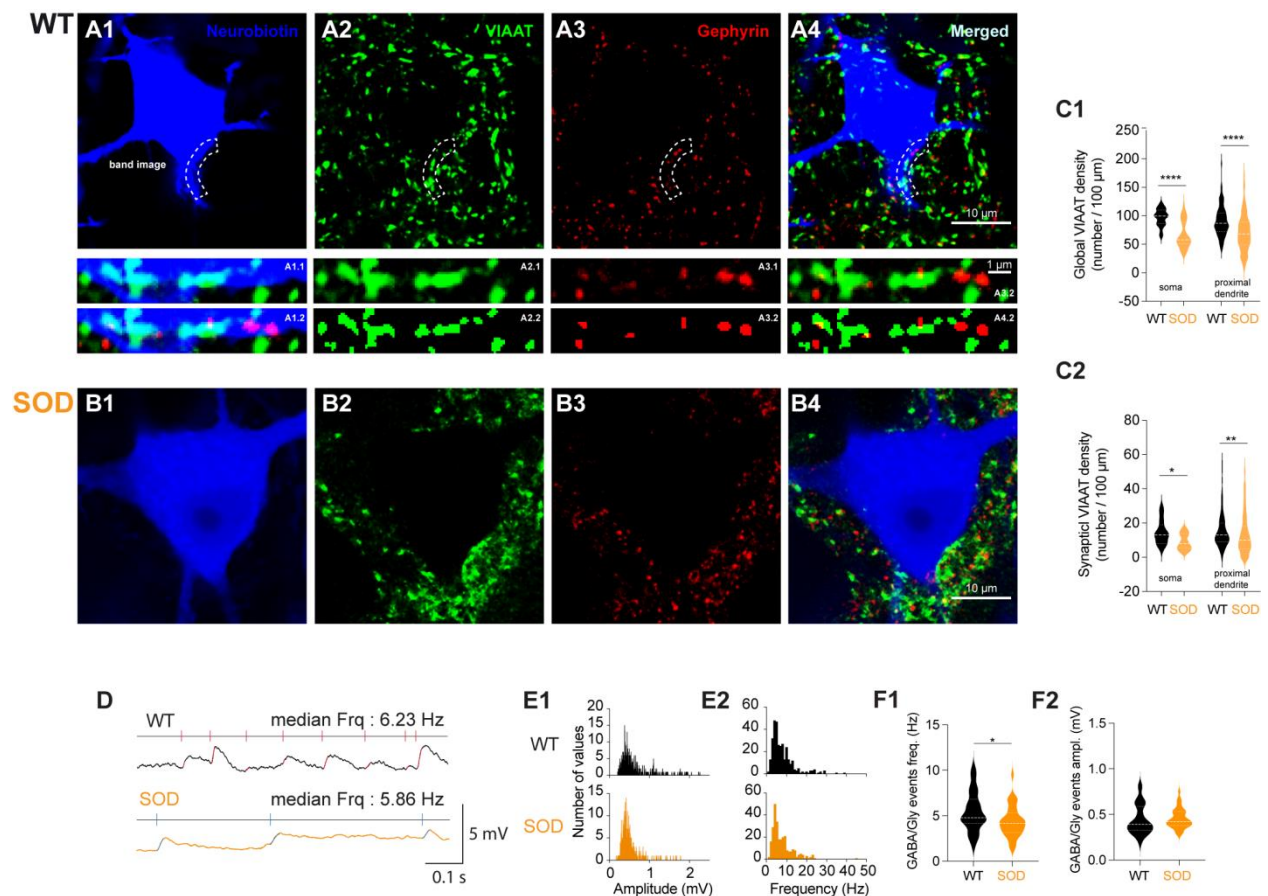


**Figure 6: SOD MNs lack VIAAT terminals on soma and proximal dendrite.** (A-B) Confocal images (x63) of neurobiotin-injected soma (blue), VIAAT (green), gephyrin (red), and merged of a E17.5 WT MN (A panels) and SOD MN (B panels). An example of a band image analysis is given for the WT MN as row images (A1.1-A2.1-A3.1-A4.1) and detected particles (see A1.2-A2.2-A3.2-A4.2). (C1) Global VIAAT density on soma and proximal dendrite, expressed as number / 100  $\mu\text{m}$ . (C2) Synaptic VIAAT density on soma and proximal dendrite (number / 100  $\mu\text{m}$ ). (D) Representative raw traces from a WT and SOD MN illustrating the detection of GABA/glycine synaptic events. (E) Corresponding amplitude (E1) and frequency (E2) analysis. (F) GABA/glycine events frequency (F1) and amplitude (F2) in WT and SOD MNs. Quartiles and median are indicated in the violon plots as white dotted and hatched lines, respectively.

## Discussion

We have investigated the effect of dGPSPs occurring at various frequencies on the firing of fetal E17.5 lumbar spinal MNs from the SOD1<sup>G93A</sup> ALS mouse model compared to WT MNs from same littermates. We have disclosed two types of MNs: Dual MNs exhibiting increase MN firing (excitation) of at dGPSP frequency < 50Hz and decrease MN firing (inhibition) at frequency > 50Hz), and an Inhibited MNs showing decrease MN firing (inhibition) at all dGPSP frequencies. We have found that 60% of the WT MNs were Inhibited MNs exhibiting Rin < 100 M $\Omega$  whereas 72% of SOD MNs were Dual MNs, without any relationship with their Rin value. A reduced density of GABA/glycine terminals on the soma of SOD MNs accounted for the propensity of SOD MNs to be excited by dGPSPs occurring at low frequency.

### What mean the different subtype of fetal MNs?

We previously described that prenatal E17.5 lumbar spinal MNs for the SOD1<sup>G93A</sup> ALS mouse model are hyperexcitable because of shorter dendrites and exhibit higher Rin compared to WT MNs from the same littermate ([Martin et al., 2013](#)). Our present data, collected from similar fetal MNs located in the lateral motor column ([Branchereau et al., 2019](#)), confirm the high Rin in SOD MNs but also show some SOD MNs with low Rin and extended dendritic tree ([figures 4C-E](#)). Similarly, some fetal WT MNs are high Rin and exhibit short dendrites ([figures 4B](#)). Does this correspond to two types of MNs? Leroy and

colleagues have shown, in post-natal (P) 6-10 days (P6-P10) SOD1<sup>G93A</sup>, that only S-type (innervating the slow-contracting muscle fibers)  $\alpha$  MNs displayed intrinsic hyperexcitability and shrunk dendritic tree, the excitability of F-type (innervating the fast-contracting muscle fibers)  $\alpha$  MNs being unchanged ([Leroy et al., 2014](#)). Similarly, Venugopal and collaborators found in P8-P12 SOD1<sup>G93A</sup> trigeminal MNs that predicted fast SOD MNs showed hyperexcitable shifts marked by reduced rheobase and increased input resistance whereas predicted slow SOD MNs did not present significant alterations in these properties when compared to WT littermate MNs ([Venugopal et al., 2015](#)). Leroy and colleagues described an immediate firing in S-type MNs and a delayed firing in F-type MNs. S-type were identified as expressing the estrogen-related receptor  $\beta$  (Err $\beta$ ) but not the matrix metalloproteinase-9 (MMP9), whereas most of the F-type were enriched with MMP9 ([Leroy et al., 2014](#)) and Err $\beta$  negative ([Leroy et al., 2014](#)). MMP-9 is not expressed by embryonic MNs and is first detected in the spinal cord around P5 ([Kaplan et al., 2014](#)). We have tried to detect MMP-9 in neurobiotin-injected fetal MNs but could not detect any staining. We also checked the immediate vs delayed firing when MNs were depolarized at threshold with a 5s long depolarizing pulse and could only detect immediate firing. In addition, voltage difference between threshold potential for spikes and membrane potential (V<sub>thr</sub>-V<sub>r</sub>) and spike width (SpkWdth) did not differ between E17.5 MNs ([table 1](#)) unlike P6-10 MNs ([Leroy et al., 2014](#)). However, even though it is difficult to conclude about the identity of our recorded fetal MNs, low Rin (< 100 M $\Omega$ ) WT MNs, inhibited by dGSPs, likely correspond to future F-type MNs. Their morphology complies with this described in WT MNs in our previous study ([Martin et al., 2013](#)). Interestingly, our data highlight a more hyperpolarized actual ECl in low Rin WT Inhibited MNs compared to high Rin WT Dual MNs ([figure 1F3](#)), suggesting a higher efficacy of KCC2. However, the protocol used in the present study was not a KCC2

challenging protocol and did not reveal any main difference in actual ECI values between WT and SOD MNs as previously described ([Branchereau et al., 2019](#)).

### **Motoneuronal properties**

Our data did not highlight any differences in MN  $E_{Rest}$ , spike amplitude and spike width between E17.5 SOD1<sup>G93A</sup> and WT littermate mice. No difference in  $E_{Rest}$  and action potential shape was also reported in between G93A and control MNs from spinal cord slices cultured during 3 weeks starting at E12-14 days ([J. J. Kuo et al., 2004](#)). P6-10 SOD1<sup>G93A</sup> spinal MNs also did not show any change in  $E_{Rest}$ , spike amplitude and spike width ([Leroy et al., 2014](#)) whereas  $E_{Rest}$  of P30-P60 SOD1<sup>G93A</sup> spinal MNs is 10 mV more hyperpolarized than WT littermate MNs, this difference in  $E_{Rest}$  becoming undetected at P90-P120 ([Huh et al., 2021](#)). This hyperpolarization of MN  $E_{Rest}$  that was not detected at early and late stages was described as a cellular adjustment useful to compensate an increase in the persistent inward current (PIC) ([Huh et al., 2021](#)). Interestingly, the authors described an overall pattern of oscillations across the lifespan of the SOD1<sup>G93A</sup> ALS mouse model, with the PIC oscillations tending to increase excitability but the conductance and  $E_{Rest}$  oscillations tending to reduce it ([Huh et al., 2021](#)).

### **Prenatal SOD motoneurons receive less VIAAT-positive inputs**

Our result show that fetal SOD MNs can be Dual or Inhibited MNs whatever their  $R_{in}$  and morphology, unlike WT MNs from the littermates. What could explain this surprising result? If we consider that Inhibited low  $R_{in}$  WT MNs are future F-type (innervating the fast-contracting muscle fibers)  $\alpha$  MNs that start getting mature at E17.5, then we may consider that the spinal cord from the SOD1<sup>G93A</sup> strain matures less rapidly than littermate WT spinal cords, i.e., the developmental sequence of the lumbar motoneuronal network (decrease of the

MN Rin, increase of the MN Cm (*A. Delpy et al., 2008*), increase of the synaptic input onto MNs (*Scain et al., 2010*)), is delayed. Another explanation is that the lack of GABA/glycine impedes the occurrence of Inhibited low Rin SOD MNs. We have shown that increasing gGABA/glycine favors dGPSPs inhibition occurring on SOD MN soma (*figures 5D1*). The role of gGABA/glycine (gCl) in the dual effect of dGPSPs was also demonstrated in a previous study where we found that increasing gCl favors inhibition either during a single dGPSP or during trains in which gCl summates (*Branchereau et al., 2016*). Our immunohistochemical data indicate a lower density of VIAAT staining on MN somata and proximal dendrites from the SOD1<sup>G93A</sup> strain compared to WT littermate MNs. Consequently, VLF stimulation activate less GABA/glycine inputs, lowering the shunting (inhibitory effect) of dGPSPs. Our physiological data show that we had to increase the VLF intensity in SOD preparations to obtain evoked single dGPSPs of similar size than WT preparation (*figures 1E2*), in agreement to anatomical data highlighting lower density of VIAAT-positive terminals on SOD MNs. A reduction of inhibitory synapse was not found in SOD1<sup>G93A</sup> E12.5 spinal cords maintained in culture during 14 days but rather an increase was described (higher ratio inhibitory/excitatory synapses) (*Avossa et al., 2006*). However, in a recent study, Allodi and collaborators have shown that F-type MNs from P45 SOD1<sup>G93A</sup> mice lose inhibitory glycinergic connections before S-type MNs (*Allodi et al., 2021*). A major reduction of inhibitory synapse densities (gephyrin puncta) in the ventral horn of the SOD1<sup>G93A</sup> slow mutant was also described at early stages of disease (P50) (*S. Saxena et al., 2013*). Our previous data show that VIAAT positive terminals are less abundant in the marginal zone edging the E17.5 MN soma location (*Branchereau et al., 2019*). Here, we found a reduction of VIAAT density (global and synaptic) on soma of SOD MNs, relative to age-matched WT. In addition, as in our previous study (*Branchereau et al., 2019*), we found a reduction in the frequency of GABA/glycine synaptic events, in SOD MNs corroborating the reduction of

synaptic VIAAT density. This highlights the selective reduction of GABA/glycine inputs on MN cell bodies that likely accounts for the lack of inhibitory effect of dGPSPs barrages in prenatal SOD<sup>G93A</sup> MNs and for the reduction in the frequency of GABA/glycine synaptic events in SOD MNs. This selective reduction of GABA/glycine inputs may start occurring around birth and may strengthen over time in adult. Therefore, even if we did not analyze the lack of VIAAT staining on F-type vs S-type MNs (because of lack of specific markers at fetal stages, see above), we may hypothesize that it reflects an early reduction of GABA/glycine terminals on F-type MNs that are low Rin neurons.

### **Somatic morphometric parameters**

Our morphometric analysis has uncovered an increase in SOD MNs soma size compared to WT littermates. This was not evidenced in our previous morphometric analysis performed on E17.5 SOD1<sup>G93A</sup> mice ([Martin et al., 2013](#)), as in other studies done on postnatal (P6-10) SOD1<sup>G93A</sup> mice ([Leroy et al., 2014](#)) or P3-9 SOD<sup>G85R</sup> mice ([Amendola et al., 2008](#); [Filipchuk et al., 2012](#)). Interestingly, such an increase in SOD MNs soma was described in a comprehensive study performed on large sample size of immunolabelled P10 SOD1<sup>G93A</sup> MNs, specifically in F-type  $\alpha$  MNs, ([Dukkipati et al., 2018](#)). A larger sample size was also considered in the study performed by Shoenfeld and collaborators who observed an increase in the soma size of P30 SOD1<sup>G93A</sup> MNs ([Shoenfeld et al., 2014](#)). Maybe we focused more on future F-type MNs in the present study compared to Martin and collaborators ([Martin et al., 2013](#)).

### **Effect of recurring dGPSPs on MN firing: a complex equation**

The present study highlights the effect of recurring dGPSPs on the repetitive firing ability of E17.5 lumbar MNs that drive the contraction of muscle fibers and are the final physiological

pathway (*Manuel et al., 2011*). We show that the excitatory action of low frequency dGPSPs is favored in SOD1<sup>G93A</sup> MNs and we explain this alteration by a lower density and location of GABA/glycine synaptic inputs on SOD MNs compared to WT MNs. Simulations also indicate that morphological changes in SOD MNs - shorter dendritic tree - favor the excitatory action (*Figures 5B*). Additional parameters are governing the effect of repetitive dGPSPs on MN firing. ECl value clearly controls this effect and a slight hyperpolarization of ECl is able to switch the effect from pure excitation to pure inhibition (*Figures 5A*). A shorter decay time of dGPSPs favors their excitatory effect on MN firing as we previously described (*Branchereau et al., 2019*) because it leads to higher capacity of shunting effect summation (*Branchereau et al., 2016*). The decay of dGPSPs is closely dependent on  $[Cl^-]_i$  (*Pitt et al., 2008a*) (*Houston et al., 2009a*) because of a direct effect of chloride ions acting in the pore of glycine and GABA channels (*Moroni et al., 2011a*). Here,  $[Cl^-]_i$  was set as similar in SOD and WT MNs, hence the decay time of dGPSPs was maintained as similar in all recorded MNs. We have previously shown that E17.5 SOD1<sup>G93A</sup> MNs exhibit dGPSPs with an increased decay time compared to WT littermate MNs (*Branchereau et al., 2019*) and this change could compensate the more depolarized ECl value found in SOD MNs. In physiological conditions, this compensatory change may limit the over-excitatory action of repetitive dGPSPs in SOD MNs demonstrated in the present study. It is however likely that the lack of inhibitory GABA/Gly inputs on SOD MNs and their morphological alteration (*Martin et al., 2013*) make them vulnerable MNs.

## Limitations of the study

In the present study, we did not analyze the lack of VIAAT staining on F-type vs S-type MNs because of lack of specific markers at fetal stages (see Discussion part). Therefore, we could not address if any specific early reduction of GABA/glycine terminals on F-type MNs exists

at prenatal stage. We also did not look at GABA<sub>A</sub>R and GlyR on spinal MNs. A decrease of surface postsynaptic GlyR on SOD1<sup>G93A</sup> MNs maintained in culture from E12.5 during 12-16 days has been described ([Q. Chang et al., 2011](#)). A possible reduction of GlyR on SOD MNs may also account for the higher excitability of dGPSPs in our experiments. Finally, the main limitation of our study is based on the fact that MNs were recorded in whole-cell configuration with similar ECl values. As physiological ECl is 10 mV more depolarized in E17.5 SOD1<sup>G93A</sup> MNs compared to WT littermate MNs ([Branchereau et al., 2019](#)), it would have been better to test the effect of dGPSPs barrages on the MN spiking activity using perforated patch-clamp recordings that preserve physiological ECl.

## Materials and Methods

### **Ethical considerations and mouse model**

All procedures were carried out in accordance with the local ethics committee of the University of Bordeaux and the UE Directive 2010/63. In order to apply the 3Rs rule, all efforts were made to curtail animal suffering and reduce the number of animals used. B6SJL-Tg(SOD1\*G93A)1Gur/J mice expressing the human G93A Cu/Zn superoxide dismutase (SOD1) mutation (Gly93→ Ala substitution) were obtained from the Jackson Laboratory (<https://www.jax.org/strain/002726>). Heterozygous B6SJL-Tg(SOD1\*G93A)1Gur/J (named SOD in this manuscript) were maintained by crossing heterozygous transgene-positive male mice with B6SJL F1 hybrid females (Janvier labs, France). Gestation in SOD lasted for ~18.5 days, embryonic day 0.5 (E0.5) being defined as the day after the mating night. Experiments were performed on E17.5 fetuses of either sex, collected one day before their birth.

## **Dissection and isolation of the embryonic brainstem-spinal cord preparation**

Pregnant mice were sacrificed by cervical dislocation. The fetuses were removed from the mother using the surgical procedure of laparotomy and transferred into cold artificial cerebrospinal fluid (aCSF) (6–8°C), oxygenated with 95% O<sub>2</sub> and 5% CO<sub>2</sub> mixture. The aCSF was composed of the following components (in mM): 114.5 NaCl, 3 KCl, 2 CaCl<sub>2</sub>·2H<sub>2</sub>O, 1 MgCl<sub>2</sub>·6H<sub>2</sub>O, 25 NaHCO<sub>3</sub>, 1 NaH<sub>2</sub>PO<sub>4</sub>·H<sub>2</sub>O, and 11 D-glucose, with a pH of 7.4 and osmolarity 307 mosmol/kg H<sub>2</sub>O. Fetuses were chosen randomly, decapitated and the brainstem-spinal cord preparation was dissected out in oxygenated cold aCSF. The suprasegmental transection was done under the binocular microscope at the level of the r1 alar plate (<https://developingmouse.brain-map.org/static/atlas>). The brainstem was not detached in order to keep intact descending inputs that already reach the lumbar spinal cord at E17.5, such as serotonergic (*Rajaofetra et al., 1989*; *Ballion et al., 2002*) and noradrenergic (*Rajaofetra et al., 1992*) fibers. Meninges were removed all along the brainstem - spinal cord after opening the spinal cord dorsally (open-book preparation) . This procedure allowed easy access to lumbar MNs for the patch-clamp electrode. The preparation was then positioned in a recording chamber with the ventral side up, maintained open under a nylon mesh and superfused (~1.5mL.min<sup>-1</sup>) with oxygenated aCSF. All experiments were carried out at constant temperature (30°C) (Temperature controller V, Luigs & Neumann, Ratingen, Germany). Experiments were performed blindly without knowing the genotype of the animals. We recorded only 1-2 MNs from each brainstem-spinal cord preparation. Fetuses were genotyped at the genotyping platform (Magendie Neurocentre, Bordeaux). Genotyping was performed by standard PCR from mice tail samples using primers stated in a protocol from the Jackson Laboratory (<https://www.jax.org/Protocol?stockNumber=002726&protocolID=29082>).

## **Immunohistochemistry**

Immunohistochemistry was performed as follows. MNs were recorded with patch pipettes filled with 0.4% (wt/vol) Neurobiotin (CliniSciences, Montrouge, France) diluted in the intracellular medium (see below). After recording sessions, whole brainstem-SC preparations (SOD or WT embryos) were fixed in 4% paraformaldehyde (PFA) prepared with 0.1 M PB (wt/vol) for 2h at room temperature. They were rinsed three times with 0.1 M Phosphate Buffer Saline (PBS), blocked with a blocking buffer containing 2 % (wt/vol) bovine serum albumin (BSA) and 0.5% PBST [0.5% Triton X-100 in 0.1M PBS (vol/vol)], followed by incubation with primary antibody and streptavidin-Cy3 (1:400, Invitrogen) diluted in incubating solution made with 0.1 M PBS containing 0.1% Triton X-100 (Sigma) and 0.2% BSA (Sigma, St Louis, MO, USA) for 48h at 4 °C. We processed brainstem-SC preparations with an anti-gephyrin antibody (1:400, mouse monoclonal, mAb7a (GlyR7a), Synaptic Systems GmbH, Germany), coupled with a rabbit antibody directed against the vesicular inhibitory amino acid transporter (VIAAT, 1:1000, antibody Provided by B. Gasnier, Institut de Biologie Physico-chimique, Paris). Gephyrin is the GABA<sub>A</sub>/glycine receptors anchoring protein ([Meyer et al., 1995](#)) whereas VIAAT reflects the synaptic release of the GABA and glycine neurotransmitters ([A. Dumoulin et al., 1999](#)). The brainstem-SC preparations were thereafter washed four times for 20 min, incubated with secondary antibody conjugated to Alexa Fluor488 goat anti-rabbit IgG(H + L) (1/500, Invitrogen, France) for 2 h, at room temperature, abundantly rinsed in 0.1 M PBS, and finally mounted with an anti-fade reagent (Fluoromount, Electron Microscopy Sciences, CliniSciences, France) and stored at 4°C in obscurity until confocal observation.

## **Confocal microscopy and neuron reconstruction**

Fluorescent images were acquired with a Zeiss LSM 900 confocal microscope, with a 63× oil-immersion objective (NA 1.40) and optical section thickness was set at 300 nm; and images were acquired at 16-bit depth. Acquisition parameters were adjusted to maintain fluorescence intensity from target structures below saturation and above zero values; Imaging parameters were kept constant across preparations and genotypes. Confocal stacks were acquired with 10–15 optical sections for each MN. Preparations displaying staining artifacts and uneven staining or bad neurobiotin injection were not considered for imaging. Immunostaining and imaging were performed in batches that included 1-3 samples per experimental day. Gephyrin and VIAAT immunostaining were visualized as spot aggregates. Spots aggregates were detected using an Image J macro, allowing to delineate the periphery of MNs and quantify the VIAAT immunopositive density. The macro was developed by Gilles Courtand, Research Engineer at INCIA lab. MNs were identified by Neurobiotin-positive staining, which allows defining the cellular contour and establishing the spatial orientation of synaptic structures. The presynaptic structures located on the cytoplasmic membrane and its close proximity (a 20-pixel wide band image) are considered to belong to the identified MN, whereas those located away from the cytoplasmic membrane are considered to belong to other structures or cells and were excluded from the analysis. Based on the Nyquist criterion and our confocal acquisition parameters (1 pixel= 0.099 μm), the area of the smallest VIAAT-positive spot is 0.0518μm<sup>2</sup> [0.099μm\*2.3 in X and Y direction=(0.099μm\*2.3)<sup>2</sup> = 0.0518μm<sup>2</sup>]. The FIJI macro therefore defined VIAAT-positive terminals as area of their immunostained spots greater than 0.0518 μm<sup>2</sup>. We used the FIJI macro to define a synapse as a colocalized region (at least 10% overlap) between the staining of presynaptic VIAAT-positive boutons and staining of postsynaptic Gephyrin spots. Spots were then quantified on the cytoplasmic membrane - and its close proximity - of MN somata and proximal dendrites by analyzing five

consecutive optical sections. The global and synaptic density of VIAAT was then assessed. The VIAAT density was calculated by dividing the total number of VIAAT by total length of their selected band image. Three to six proximal dendrites (dendritic length < 50µm) per MN and two side of each dendrites were quantified.

Three-dimensional (3D) reconstruction of patch-clamp recorded WT and SOD MNs were performed with a *NeuroLucida* confocal module (MBF Bioscience Inc., Williston, VT, USA). Morphometric parameters, characterizing morphologic and topologic features of MN dendritic arborization and cell body, were harvested with the *NeuroLucida Explorer* software package (MBF Bioscience Inc) (see [table 2](#)).

### **Electrophysiological procedures and data analysis**

Patch-clamp electrodes were constructed from thin-walled single filamented borosilicate glass (1.5 mm outer diameter, Harvard Apparatus, Les Ulis, France) using a two-stage vertical microelectrode puller (PP-830, Narishige, Tokyo, Japan). Patch electrode resistances ranged from 4 to 6 MΩ. All recordings were made with an Axon Multiclamp 700B amplifier (Molecular Devices, Sunnyvale, CA, USA). Data were low-pass filtered (2 kHz) and acquired at 20 kHz on a computer *via* an analog-to-digital converter (Digidata 1322A, Molecular Devices) and a data acquisition software (Clampex 10.7, Molecular Devices).

Motorized micromanipulators (Luigs & Neumann) were used to position the patch-clamp electrode on a visually identified MN using a CCD video camera (Carl Zeiss Axiocam MRm). All recorded MNs were located in the lateral column ([Branchereau et al., 2019](#)) and were identified by their pear-shaped cell bodies. Values of Rin and Cm also further confirmed the motoneuron identity of recorded neurons ([Martin et al., 2013](#)).

Evoked dGPSPs from MNs were elicited using a concentric bipolar wire stimulating electrode (FHC, USA) positioned on the ventro-lateral funiculus (VLF), rostral to the

recording electrode, in order to activate local inhibitory fibers that are pharmacologically isolated (see pharmacology below) (Figure S1). Monophasic single stimulations delivered to the VLF (duration 1ms, intensity ranging 3-30  $\mu$ A) were driven by a programmable Master 8 Stimulator/Pulse generator (Master-8, A.M.P.I. Jerusalem, Israel).

$E_{GABA_A/glyR}$ , considered as  $E_{Cl}$  because of the low  $HCO_3^-$  conductance of  $GABA_A/glycineR$  in embryonic spinal MNs (J. Bormann *et al.*, 1987), was set to -45mV (-57.5mV after correction of the junction potential, see below), which was in the range of the recorded physiological  $E_{GABAAR}$  in E17.5 MNs (Branchereau *et al.*, 2019). Intracellular medium composed (in mM) was the following: 115 K gluconate, 5 NaCl, 15 KCl, 1 CaCl<sub>2</sub>, 2H<sub>2</sub>O, 10 HEPES, 10 EGTA, and 2 MgATP, (297 mosmol/kg H<sub>2</sub>O) adjusted to pH 7.4 using 1M KOH. Measurements were corrected for liquid junction potentials (12.5 mV) calculated with the Clampex junction potential calculator. Actual  $E_{Cl}$  was measured by assessing the reversal membrane potential of evoked IPSCs (eIPSCs) elicited by a single VLF stimulation (local inhibitory fibers activation) at different membrane voltages (Figure 1F1). See Figure S2 for the specificity of  $GABA_A/GlyR$  activation. The reversal potential was calculated by a linear fit (Prism 9 from GraphPad Software Inc., USA) (Figure 1F2).

Clampex (10.7, Molecular Devices) membrane test was used to monitor the passive properties of a neuron, namely, membrane resistance ( $R_{in}$ ), access resistance ( $R_a$ ) and membrane capacitance ( $C_m$ ). Only neurons with resting membrane potential more hyperpolarized than -50mV (value not corrected for the junction potential) were used for recording. Rheobase was recorded as the minimum current pulse injected to elicit an action potential. Intracellular stimulation intensity was adjusted for each recording to evoke a train of action potentials at ~20Hz (Figure 1E1), the duration of which was set to 5 seconds. The intensity of VLF stimulation was adjusted in order to elicit synaptic events equivalent to spontaneous ones observed in MNs (Figure 1A-C, upper traces). Nine VLF frequencies were

selected from previous simulation data: 7.5Hz, 10Hz, 20Hz, 30Hz, 40Hz, 50Hz, 100Hz, 150Hz and 200Hz. The duration of VLF was kept as 2.5 s for all the experiments, occurring 2.5 s after MN spiking activity (Figure 1A-C). The recording protocol consisted of one control bursts (intracellular stimulation of cell to produce a train of spikes), followed by one test burst (intracellular stimulation accompanied by VLF stimulation after 2.5 s). The spike number change (% of control) was assessed during 1 s by comparing spike number during VLF stimulation to spike number in the preceding control, at the same time. The inter-burst duration was retained as ~40 s. This frequency discharge protocol was recorded in current-clamp mode and analyzed using a Spike 2 V7 script developed by D.C. whereas actual ECl from each MNs were assessed using from voltage-clamp recordings analyzed using Clampfit 10.7 (Axon Instruments).

### **Pharmacology**

In whole-cell patch-clamp experiments, GABA<sub>A</sub>R/GlyR responses were isolated by using a cocktail of pharmacological drugs containing 4mM kynurenic acid (Bio-technie, France), 5μM dihydro-beta erythroidine, that respectively blocked glutamate and cholinergic input to MNs. Two serotonin (5-HT) receptors blockers methysergide (10 μM) and ketanserine (10 μM) were also applied to prevent any 5-HT release from descending fibers that are already dense in the VLF (Ballion *et al.*, 2002). Gabazine 3 μM (SR-95531, Bio-technie, France) and strychnine 3 μM (Sigma-Aldrich Chimie SARL, France) were used to verify that our VLF stimulation specifically elicited GABA<sub>A</sub>R- and GlyR-related synaptic events (Figure S2).

### **Membrane properties and data analysis**

Data analysis was performed using Clampfit 10.7 (Axon Instruments) and Spike 2 V7 (Cambridge Electronic Design Ltd). For synaptic event analysis, representative 1-2 min

recording samples were selected from each MN. The MN capacitance ( $C_m$ ), membrane input resistance ( $R_{in}$ ) and access resistance ( $R_a$ ) were recorded immediately after establishing whole-cell patch-clamp.

### Computer simulations

GABA/glycine synaptic events in E17.5 MNs were simulated using a multi-compartment neuron model that was elaborated with the NEURON 7.3 program ([Hines et al., 1997](#)). Two simulated neurons were constructed: an E17.5 WT-like MN and an E17.5 SOD-like MN ([figure 5B2](#)). These canonical MNs, designed from the average topology of real E17.5 MNs, were built on models used in a previous study. Both MNs were virtually identical, with similar channels and morphologies, except for the terminal dendritic segments of the SOD-like MN that were 40% less in extent than the WT terminal segments ([Martin et al., 2013](#)). In each section (dendrites and axon), the number of segments was an odd number calculated according to the d-lambda rule ([Hines et al., 2001](#)) ([Carnevale et al., 2006](#)). The following conductances were used: a passive leakage current ( $I_{leak}$ ), a transient K channel ( $I_A$ ), a voltage-dependent calcium-activated potassium channel ( $I_C$ ) also called  $I_{K(Ca)}$  ([McLarnon et al., 1995](#)) ([B. X. Gao et al., 1998](#)) and a high-threshold calcium current ( $I_L$ ) ([Walton et al., 1986](#)).  $I_{leak}$  was simulated in each MN section ( $I_{leak} = (E_{leak} - E) \cdot G_{leak}$ , with  $E_{leak} = -73$  mV and  $G_{leak} = 1/R_m$ ).  $R_m$ , the specific membrane resistance was set to  $21200 \Omega \cdot cm^2$ , in order to obtain an input resistance  $R_{in}$  of  $120 M\Omega$  in the WT MN.  $I_A$  was present in the axon initial segment (AIS), with  $G_{IA} = 0.0005 S \cdot cm^{-2}$ ;  $I_C$  was present in soma, with  $G_{IC} = 0.0035 S \cdot cm^{-2}$ .  $I_L$  was present in the soma, with  $G_{IL} = 9 \cdot 10^{-5} S \cdot cm^{-2}$ . Each of the axon segments ( $n = 750$ ) was equipped with Na and K Hodgkin Huxley (HH) channels ( $G_{Na} = 0.012 S \cdot cm^{-2}$  and  $G_K = 0.0036 S \cdot cm^{-2}$ , respectively) used to generate spikes. The density of Na and K channels in the

initial segment ( $G_{Na} = 0.5 \text{ S.cm}^{-2}$  and  $G_K = 0.15 \text{ S.cm}^{-2}$ ) were adjusted in order to obtain a spike threshold of -48 mV.

In addition, calcium dynamics ([Blaustein, 1988](#)) were added in the soma to reproduce calcium accumulation, diffusion and pumping (for more details see ([Destexhe et al., 1993](#))). The parameters used in the intracellular calcium dynamics were: depth = 0.17 mm,  $\tau_f = 10^{10}$  ms,  $Ca_{inf} = 0.0002 \text{ mM}$ ,  $Kt = 0.00025 \text{ mM.ms}^{-1}$ ,  $Kd = 0.0001 \text{ mM}$ ,  $Ca_i = 2.4 \times 10^{-4} \text{ mM}$  and  $Ca_o = 3 \text{ mM}$ .

Inhibitory synaptic inputs were inserted on the somatic MN compartment using two-exponentials equations (one for rising phase and the other for decay phase). Depolarizing GABAergic/glycinergic post-synaptic current kinetics was set with  $\tau_{rise} = 0.3 \text{ ms}$  and  $\tau_{decay} = 20 \text{ ms}$ . More details about equations for channel properties and synaptic activation can be found in ([Martin et al., 2013](#)) and ([Branchereau et al., 2019](#)).

### Principal component analysis (PCA)

Principal component analysis was performed using R software (Ade4 package) based on the behavioral variables described in [table 2](#). In a first step, the contribution of each variable to the variance in the first and second components of the PCA was calculated ([tables 2-3](#)). Only the variables whose contribution to the variance of a given component was larger than the mean contribution of all variables to that component (i.e., #2000) were considered (see \*).

**Table 2.** Variables used for PCA

Variables	Definition	Measurement	Range
SpNbCh30	% of change in number of spikes during VLF stimulation 30 Hz	%	0-150
Rin	Input resistance	MΩ	113 to 264
Rheobase	Threshold current	pA	60 to 510
Vthr-Vr	Threshold Mb potential – resting membrane potential	pA	21 to 43
Spike Width	Mid amplitude spike width	ms	1 to 2.25

### **Statistical analysis**

GraphPad Prism 9 software was used to analyze all the data. The results are presented as means  $\pm$  the standard error of the mean (SEM) unless otherwise specified.  $n$  is the number of MNs used in the analysis and  $N$  the number of fetuses. Significance was determined as  $p < 0.05$  (\*),  $p < 0.01$  (\*\*),  $p < 0.001$  (\*\*\*) or  $p < 0.0001$  (\*\*\*\*). The statistical differences between two data sets were assessed with the Mann Whitney test for non-parametric data. Kruskal-Wallis test values are also given in table 1.

## Supplementary figures

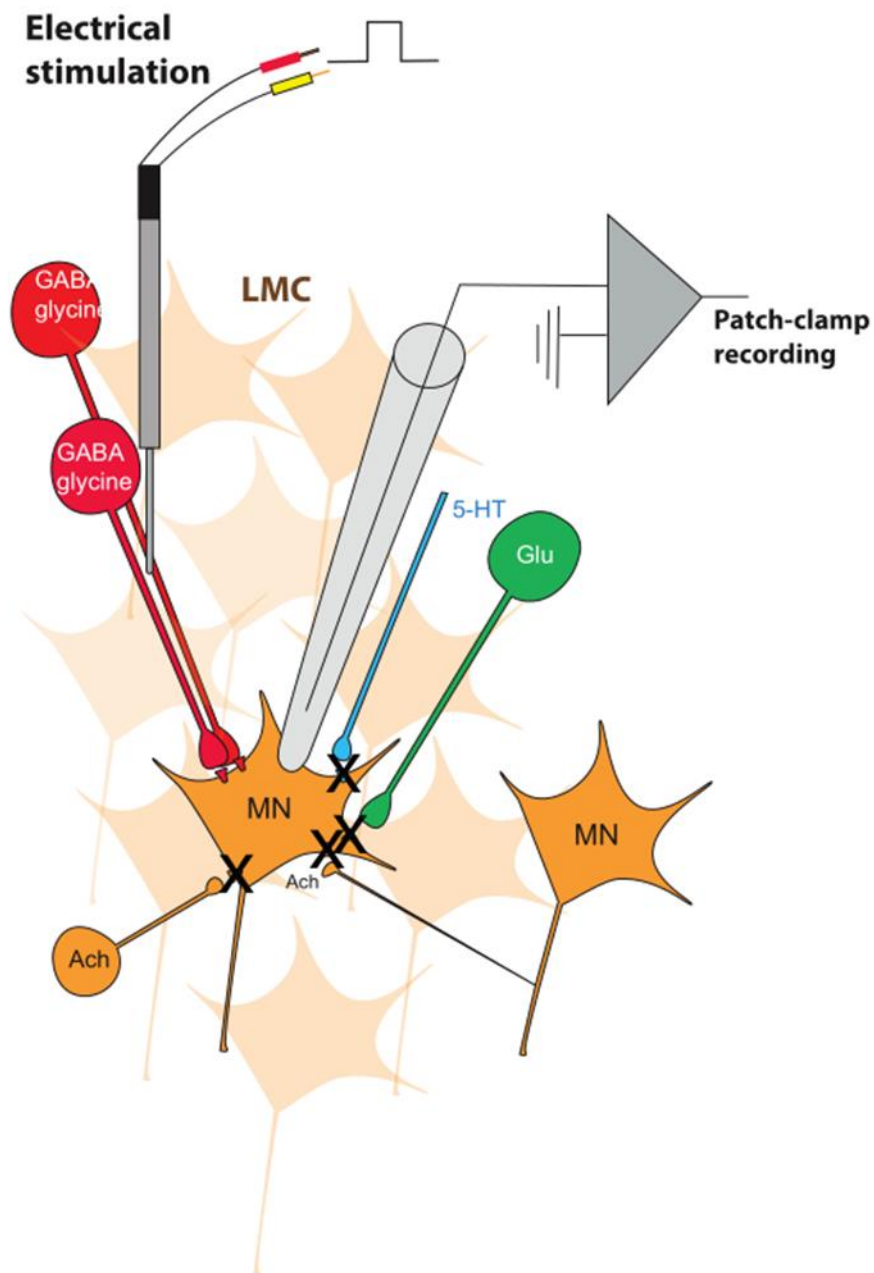


**Figure S1: E17.5 MN recording paradigm.** MN, located in the lateral motor column (LMC), was recorded in whole-cell configuration in the presence of the following drugs dissolved in the aCSF: kynurenic acid (4 mM, blocks glutamate receptors), dihydro-beta erythroidine (5  $\mu$ M, blocks cholinergic receptors), methysergide (10  $\mu$ M) and ketanserin (10  $\mu$ M) that block the serotonergic system. Synaptic activation of the GABAAR/GlyR was elicited thanks to electrical stimulation of local inhibitory fibers using a concentric bipolar wire stimulating electrode positioned on the ventro-lateral funiculus (VLF), rostral to the recording electrode.

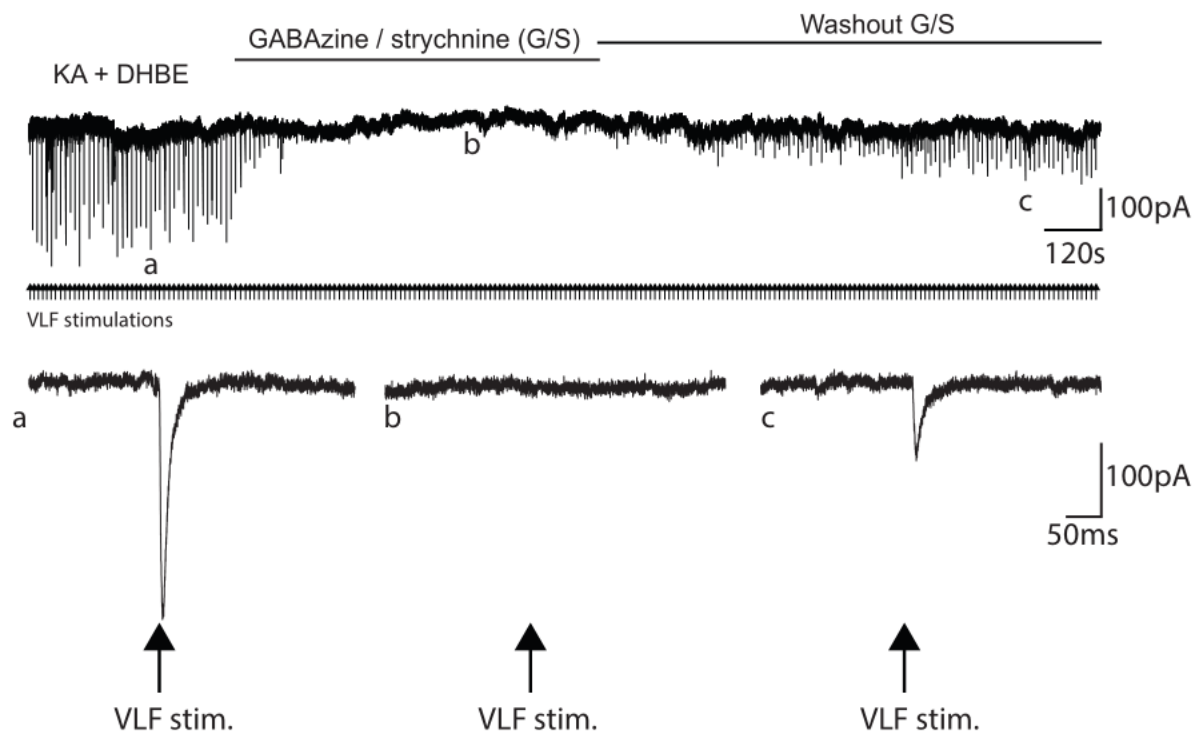


**Figure S2: VLF stimulation selectively activates GABAAR/GlyR.** The downward synaptic current evoked by a single stimulation of the VLF (**a**) is fully blocked by a bath application of Gabazine (G, 3  $\mu$ M) / strychnine (S, 3  $\mu$ M) (G/S) (**b**), this blockade being partially reversible when Gabazine and strychnine (G/S) are washout (**c**). Kynurenic acid (KA, 4 mM) and dihydro-beta erythroidine (DHBE, 5  $\mu$ M) are applied all along the experiment. The recorded MN was voltage-clamped at -70 mV.

## Author Contributions

Abbreviations: Hongmei Zhu (H.Z.), Urvashi Dalvi (U.D.), William Cazenave (W.C.), Daniel Cattaert (D.C.) and Pascal Branchereau (P.B.). H.Z., U. D. and P.B. performed electrophysiological experiments and analyses. In addition, P.B. conceived the experiments and wrote the manuscript. H.Z. performed immunohistochemistry, confocal imaging and amended the manuscript. D.C. performed some analyses, the computer simulations and amended the manuscript.

## Additional Information

Competing financial interests: The authors declare no competing financial interests.

## References

- Alexander, G. M., et al., 2004. Effect of transgene copy number on survival in the G93A SOD1 transgenic mouse model of ALS. *Brain Res Mol Brain Res.* 130, 7-15.
- Allodi, I., et al., 2021. Locomotor deficits in a mouse model of ALS are paralleled by loss of V1-interneuron connections onto fast motor neurons. *Nat Commun.* 12, 3251.
- Amendola, J., Durand, J., 2008. Morphological differences between wild-type and transgenic superoxide dismutase 1 lumbar motoneurons in postnatal mice. *J Comp Neurol.* 511, 329-41.
- Ballion, B., et al., 2002. Ontogeny of descending serotonergic innervation and evidence for intraspinal 5-HT neurons in the mouse spinal cord. *Brain Res Dev Brain Res.* 137, 81-8.
- Blaustein, M. P., 1988. Calcium transport and buffering in neurons. *Trends Neurosci.* 11, 438-43.
- Bormann, J., et al., 1987. Mechanism of anion permeation through channels gated by glycine and gamma-aminobutyric acid in mouse cultured spinal neurones. *J Physiol.* 385, 243-86.
- Branchereau, P., et al., 2016. Depolarizing GABA/glycine synaptic events switch from excitation to inhibition during frequency increases. *Sci Rep.* 6, 21753.
- Branchereau, P., et al., 2019. Relaxation of synaptic inhibitory events as a compensatory mechanism in fetal SOD spinal motor networks. *Elife.* 8.
- Burley, S., et al., 2022. Hyperexcitability in young iPSC-derived C9ORF72 mutant motor neurons is associated with increased intracellular calcium release. *Sci Rep.* 12, 7378.
- Carnevale, N. T., Hines, M. L., 2006. *The NEURON Book.* Cambridge University Press, Cambridge, UK.
- Clark, R., et al., 2015. Inhibitory dysfunction in amyotrophic lateral sclerosis: future therapeutic opportunities. *Neurodegener Dis Manag.* 5, 511-25.
- Delpy, A., et al., 2008. NKCC1 cotransporter inactivation underlies embryonic development of chloride-mediated inhibition in mouse spinal motoneuron. *J Physiol.* 586, 1059-75.
- Destexhe, A., et al., 1993. Ionic mechanisms for intrinsic slow oscillations in thalamic relay neurons. *Biophys J.* 65, 1538-52.
- Devlin, A. C., et al., 2015. Human iPSC-derived motoneurons harbouring TARDBP or C9ORF72 ALS mutations are dysfunctional despite maintaining viability. *Nat Commun.* 6, 5999.
- Dukkipati, S. S., et al., 2018. The vulnerability of spinal motoneurons and soma size plasticity in a mouse model of amyotrophic lateral sclerosis. *J Physiol.* 596, 1723-1745.
- Dumoulin, A., et al., 1999. Presence of the vesicular inhibitory amino acid transporter in GABAergic and glycinergic synaptic terminal boutons. *J Cell Sci.* 112 ( Pt 6), 811-23.
- Eisen, A., et al., 2014. Amyotrophic lateral sclerosis: a long preclinical period? *J Neurol Neurosurg Psychiatry.* 85, 1232-8.
- Filipchuk, A. A., Durand, J., 2012. Postnatal dendritic development in lumbar motoneurons in mutant superoxide dismutase 1 mouse model of amyotrophic lateral sclerosis. *Neuroscience.* 209, 144-54.
- Gao, B. X., Ziskind-Conhaim, L., 1998. Development of ionic currents underlying changes in action potential waveforms in rat spinal motoneurons. *J Neurophysiol.* 80, 3047-61.
- Glykys, J., et al., 2017. Chloride Dysregulation, Seizures, and Cerebral Edema: A Relationship with Therapeutic Potential. *Trends Neurosci.* 40, 276-294.
- Gurney, M. E., et al., 1994. Motor neuron degeneration in mice that express a human Cu,Zn superoxide dismutase mutation. *Science.* 264, 1772-5.

- Hines, M. L., Carnevale, N. T., 1997. The NEURON simulation environment. *Neural Comput.* 9, 1179-209.
- Hines, M. L., Carnevale, N. T., 2001. NEURON: a tool for neuroscientists. *Neuroscientist.* 7, 123-35.
- Jean-Xavier, C., et al., 2007. Dual personality of GABA/glycine-mediated depolarizations in immature spinal cord. *Proc Natl Acad Sci U S A.* 104, 11477-82.
- Kaplan, A., et al., 2014. Neuronal matrix metalloproteinase-9 is a determinant of selective neurodegeneration. *Neuron.* 81, 333-48.
- Kiernan, M. C., et al., 2011. Amyotrophic lateral sclerosis. *Lancet.* 377, 942-55.
- Kiernan, M. C., et al., 2019. Amyotrophic lateral sclerosis: Origins traced to impaired balance between neural excitation and inhibition in the neonatal period. *Muscle Nerve.* 60, 232-235.
- Kuo, J. J., et al., 2004. Hyperexcitability of cultured spinal motoneurons from presymptomatic ALS mice. *J Neurophysiol.* 91, 571-5.
- Leroy, F., et al., 2014. Early intrinsic hyperexcitability does not contribute to motoneuron degeneration in amyotrophic lateral sclerosis. *Elife.* 3.
- Martin, E., et al., 2013. Embryonic alteration of motoneuronal morphology induces hyperexcitability in the mouse model of amyotrophic lateral sclerosis. *Neurobiol Dis.* 54, 116-26.
- McLarnon, J. G., et al., 1995. Properties of inward and outward potassium currents in cultured mouse motoneurons. *Neuroscience.* 64, 139-51.
- Meyer, G., et al., 1995. Identification of a gephyrin binding motif on the glycine receptor beta subunit. *Neuron.* 15, 563-72.
- Rivera, C., et al., 1999. The K<sup>+</sup>/Cl<sup>-</sup> co-transporter KCC2 renders GABA hyperpolarizing during neuronal maturation. *Nature.* 397, 251-5.
- Russell, J. M., 2000. Sodium-potassium-chloride cotransport. *Physiol Rev.* 80, 211-76.
- Saxena, S., et al., 2013. Neuroprotection through excitability and mTOR required in ALS motoneurons to delay disease and extend survival. *Neuron.* 80, 80-96.
- Scain, A. L., et al., 2010. Glycine release from radial cells modulates the spontaneous activity and its propagation during early spinal cord development. *J Neurosci.* 30, 390-403.
- Shoenfeld, L., et al., 2014. Soma size and Cav1.3 channel expression in vulnerable and resistant motoneuron populations of the SOD1G93A mouse model of ALS. *Physiol Rep.* 2.
- Staley, K. J., Mody, I., 1992. Shunting of excitatory input to dentate gyrus granule cells by a depolarizing GABA<sub>A</sub> receptor-mediated postsynaptic conductance. *J Neurophysiol.* 68, 197-212.
- Taylor, J. P., et al., 2016. Decoding ALS: from genes to mechanism. *Nature.* 539, 197-206.
- Tu, P. H., et al., 1996. Transgenic mice carrying a human mutant superoxide dismutase transgene develop neuronal cytoskeletal pathology resembling human amyotrophic lateral sclerosis lesions. *Proc Natl Acad Sci U S A.* 93, 3155-60.
- Van Damme, P., et al., 2017. Modelling amyotrophic lateral sclerosis: progress and possibilities. *Dis Model Mech.* 10, 537-549.
- Van den Bos, M. A. J., et al., 2018. Imbalance of cortical facilitatory and inhibitory circuits underlies hyperexcitability in ALS. *Neurology.* 91, e1669-e1676.
- Venugopal, S., et al., 2015. Homeostatic dysregulation in membrane properties of masticatory motoneurons compared with oculomotor neurons in a mouse model for amyotrophic lateral sclerosis. *J Neurosci.* 35, 707-20.
- Wainger, B. J., et al., 2014. Intrinsic membrane hyperexcitability of amyotrophic lateral sclerosis patient-derived motor neurons. *Cell Rep.* 7, 1-11.

Walton, K., Fulton, B., 1986. Ionic mechanisms underlying the firing properties of rat neonatal motoneurons studied *in vitro*. *Neuroscience*. 19, 669-683.

## CHAPTER 3 DISCUSSION

### i. How $\text{Cl}^-$ Homeostasis Affects Synaptic Inhibition efficacy of GABA/glycine inhibition in prenatal $\text{SOD}^{\text{G93A}}$ MNs. ( *Article1* )

Efficacy of synaptic inhibition depends on multiple, dynamically interacting mechanisms implicated in chloride homeostasis, including  $\text{GABA}_{\text{A}}$ R-mediated  $\text{Cl}^-$  flux, longitudinal diffusion within dendrites and the soma, and Cation-chloride cotransporters (CCCs) activity. (*N. Doyon et al., 2011*). Chloride homeostasis is a critical determinant of the strength and robustness of inhibition mediated by  $\text{GABA}_{\text{A}}$  and glycine receptors ( $\text{GABA}_{\text{A}}$ Rs and GlyRs). Synaptic inhibition in central neurons is mediated by the neurotransmitter  $\gamma$ -aminobutyric acid (GABA) and glycine (Gly) through the activation of ionic channels of  $\text{GABA}_{\text{A}}$ Rs and GlyRs, respectively (*H. U. Zeilhofer et al., 2012; Fritschy et al., 2014*). These receptors show high permeability to chloride ( $\text{Cl}^-$ ) and low permeability to bicarbonate ( $\text{HCO}_3^-$ ) (*Kaila et al., 1993*). Therefore, the strength of inhibition critically depends upon the intracellular concentration of  $\text{Cl}^-$  ( $[\text{Cl}^-]_i$ ), which determines the reversal potential for  $\text{GABA}_{\text{A}}$ R- and GlyR-mediated currents ( $E_{\text{GABAAR/GlyR}}$ ). Adult neurons in the healthy nervous system express low levels of the cation-cotransporter NKCC1 ( $\text{Cl}^-$  importer) and high levels of KCC2 ( $\text{Cl}^-$  exporter), this latter extrudes  $\text{Cl}^-$  out of the cells. This assures low  $[\text{Cl}^-]_i$  and a  $\text{Cl}^-$  electrochemical gradient that mediates  $\text{Cl}^-$  inflow after opening of the  $\text{GABA}_{\text{A}}$ R/GlyR by binding of the inhibitory neurotransmitter GABA/Glycine.  $E_{\text{GABAAR/GlyR}}$  is thus set below the resting potential near the  $\text{Cl}^-$  equilibrium ( $E_{\text{Cl}}$ ). It follows that  $\text{Cl}^-$  produces a net hyperpolarization of the membrane and an inhibitory action. However, GABAergic neurotransmission predominate in developing neurons (*Allain et al., 2011*), so  $\text{Cl}^-$  ions are mainly involved in  $\text{GABA}_{\text{A}}$ R currents in fetal MNs (i.e.,  $E_{\text{GABAAR}} = E_{\text{Cl}}$ ). In fetal mouse lumbar spinal MNs,  $E_{\text{GABAAR}}$  is very depolarizing above the spike threshold that induces strong excitatory action at early developmental stages (E13.5-E15.5) whereas drops significantly below spike threshold at late embryonic stages (E16.5-E18.5) (*Alain Delpy et al., 2008*). Besides, our lab previously found that at E17.5 fictive alternate locomotor activity may be elicited by 5-HT bath application (*Branchereau et al., 2000b*). This implies that at E17.5 the lumbar spinal networks may express a left-right coordination, indicating the presence of inhibitions between ipsi- and contra-lateral sides. Interestingly, during the E16.5-E18.5 period, the mouse spinal motoneurons still exhibit depolarizing  $E_{\text{Cl}}$  ( $E_{\text{Cl}}$  above the resting membrane potential but largely below the spike threshold), so such inhibitions between ipsi- and contra-

lateral sides may be caused by shunting effects of GABA/Glycine inputs ([Alain Delpy et al., 2008](#)). This shunting inhibition is a form of postsynaptic potential inhibition owing to an increase of the postsynaptic membrane conductance due to the sustained activation of GABA<sub>A</sub> receptors and the opening of ion channels, and always present independently of the effect of depolarizing or hyperpolarizing GABA ([Kurbatova et al., 2016](#)). My thesis works expect to examine whether molecular and/or cellular mechanisms affecting chloride homeostasis are responsible for hyperexcitability in E17.5 SOD1<sup>G93A</sup> MNs, which is possibly due to shunting inhibition or inhibition *via* excitatory effects upon inhibitory interneurons. However, the specific roles of these two types - indirect synaptic inhibition and shunting inhibition - of GABA/Glycine inhibition in E17.5 SOD1<sup>G93A</sup> MNs, which are involved in cellular hyperexcitability, is not fully examined.

This thesis aimed to investigate the chloride-related inhibitory system in lumbar spinal motor networks underlying the modulation of hyperexcitability in the SOD1<sup>G93A</sup> mouse model of ALS disease at early stage. We first investigated the changes in physiological [Cl<sup>-</sup>]<sub>i</sub> or ECl values by perforated patch-clamp recording. Our study revealed that prenatal E17.5 SOD1<sup>G93A</sup> MNs express an impairment of chloride homeostasis that leads to a 10 mV more depolarized ECl, indicating that a very early inhibitory dysfunction may initiate the pathogenesis in ALS MNs as hypothesized by others ([van Zundert et al., 2012](#); [Clark et al., 2015a](#)). This could lead to a less efficient inhibitory inputs to MNs ([Branchereau et al., 2016](#)), which in turn would be expected to affect locomotor coordination. Moreover, we found that the passive properties (R<sub>in</sub> and C<sub>m</sub>) of E17.5 MNs are consistent with previous observations ([Martin et al., 2013](#)), in that R<sub>in</sub> was increased and C<sub>m</sub> decreased in SOD1<sup>G93A</sup> MNs, in accordance with a morphometric alteration exhibiting shorter dendritic length but no changes at the soma level. Decreased capacitance and membrane conductance were thus not related to smaller size of MNs in E17.5 SOD<sup>G93A</sup> mice. These findings therefore support the conclusion that prenatal E17.5 SOD<sup>G93A</sup> MNs are also hyperexcitable. The following will consider possible compensatory mechanisms that counteract the reduction in effective inhibitory input and the hyperexcitability of SOD<sup>G93A</sup> MNs.

#### **□ The frequency and amplitude of inhibitory synaptic inputs are only weakly affected in fetal SOD MNs.**

We showed that SOD<sup>G93A</sup> MNs have a decreased GABA/Glycine inhibition, reflected by smaller amplitude and less frequent mIPSCs and sIPSC. This conclusion was supported by both physiological and anatomical observations. According to the functional criteria, the

frequency of IPSCs events is thought to represent pre-synaptic release mechanism whereas the amplitude is indicative of post-synaptic receptor function (*Frerking et al., 1997*). First, SOD<sup>G93A</sup> MNs displayed less frequent mIPSCs (~6%), which correlates with diminished (~23%) inhibitory synaptic inputs (VIAAT/synaptophysin co-localization). Similarly, SOD<sup>G93A</sup> MNs also exhibited less frequent sIPSC (~13%). Second, the amplitudes of the mIPSCs were slightly smaller in SOD<sup>G93A</sup> MNs than that in WT, especially for large events, and sIPSC events also exhibited this tendency. The reduced degree of synaptic input to mouse prenatal SOD<sup>G93A</sup> MNs assessed by VIAAT/synaptophysin staining is reminiscent of anatomical data from adult human ALS patients in which a reduction of synaptophysin was also identified (*Ikemoto et al., 2002*). It cannot be explained by a reduced SOD<sup>G93A</sup> MN size (i.e., smaller cells can host fewer synapses) because we have shown in a previous article that soma perimeters and soma surface of WT MNs and SOD<sup>G93A</sup> MNs are comparable (*Martin et al., 2013*). Even though the reduced degree of synaptic input might reflect a developmental delay in the maturation of SOD<sup>G93A</sup> cords compared to WT, data from the literature seems to indicate that this reduction persists with time. In fact, MNs cultured from other ALS patients were shown to progressively lose their synaptic activity (*A.-C. Devlin et al., 2015*), as was also shown in surviving  $\alpha$ - and  $\gamma$ -MNs from symptomatic (P90-120) adult SOD<sup>G93A</sup> mice (*Zang et al., 2005*)

The mixed GABA/Glycine IPSCs recorded in our study are likely to reflect a major contribution of GlyR because of the fast  $\tau_{\text{decay}}$  (*B.-X. Gao et al., 2001; Muller et al., 2006*). Therefore, IPSCs, which were slightly reduced in amplitude in our recordings in SOD<sup>G93A</sup> MNs, represent glycinergic events whereas GABAergic IPSCs amplitude remained unaffected. This hypothesis is supported by the fact that the ratio  $\text{gGABA}_A\text{R}/\text{Cm}$  measured by using perforated patch-clamp recordings under physiological conditions did not differ between SOD<sup>G93A</sup> and WT MNs. Interestingly, a reduction in amplitude of glycinergic synaptic events but not GABAergic events was described in SOD<sup>G93A</sup> lumbar MNs maintained in culture (*Q. Chang et al., 2011*). Less frequent and smaller amplitude IPSCs convey a reduced inhibitory drive onto prenatal SOD<sup>G93A</sup> MNs. Measurements of IPSC amplitudes derived from CsCl medium-based whole-cell recordings in which  $E_{\text{GABAAR}}$  approached 0 mV. Therefore, WT and SOD<sup>G93A</sup> MNs shared the same artificial driving force for chloride and so the observed reduction of IPSC amplitude in SOD<sup>G93A</sup> MNs was likely to be related to a decrease of surface post-synaptic GlyR clusters in cultured SOD<sup>G93A</sup> MNs (*Q. Chang et al., 2011*). However, in the present study, since no GlyR staining was performed, we cannot determine

whether reduction of IPSC amplitude is attributable to a reduction in the number of channels clustered at postsynaptic sites.

Our findings indicate that there are two possibilities that could underlie the deficits in GABA/glycine inhibition. It could result from a decreased GABA/Glycine release from pre-synaptic terminals as indicated by a reduced frequency for IPSCs events and a reduction in the number of pre-synaptic GABAergic/glycinergic inputs, and also a modification in glycinergic synaptic transmission as evidenced by decreased mIPSCs amplitude and a possible reduction in number of post-synaptic GlyRs channels number (i.e., size of GlyRs clusters) by excluding the involvement of GABA<sub>A</sub>Rs. As a result, inhibitory insufficiency induced hyperexcitability of E17.5 SOD<sup>G93A</sup> MNs.

#### □ A prolongation of inhibitory synaptic events in SOD MNs as a compensatory mechanism.

Another key property can be extracted or analyzed from post-synaptic GABA/Gly IPSCs events: the kinetics changes representing how fast (time course) cells can respond to inputs. Our data revealed a noticeable increase of  $\tau_{\text{decay}}$  in both SOD<sup>G93A</sup> mIPSCs and sIPSCs. We found a mean  $\tau_{\text{decay}}$  of around 20–25 ms, which is in the same range as that previously described for mIPSCs during perinatal stages in rat lumbar MNs (*B.-X. Gao et al., 1998*). Because a part of our study did not differentiate unequivocally between GABA<sub>A</sub>R-mediated versus GlyR-mediated mIPSCs, we pharmacologically dissected GABA<sub>A</sub>R-mediated *versus* GlyR-mediated mIPSCs. This confirmed that the mean  $\tau_{\text{decay}}$  is between  $\tau_{\text{decay}}$  of pure GABA<sub>A</sub>R-mediated mIPSCs and pure GlyR-mediated mIPSCs and that both types of mIPSCs exhibit a longer relaxation. Interestingly, GlyRs switch from immature homomeric  $\alpha 2$  GlyRs with slow decay kinetics of glycinergic mIPSCs to heteromeric GlyRs that include  $\alpha 1$ ,  $\alpha 3$  and  $\beta$  subunits with fast kinetics (*Legendre, 2001b; Raltshev et al., 2016*). E17.5 SOD1<sup>G93A</sup> MNs may therefore exhibit a delayed development with a preponderance of homomeric  $\alpha 2$  GlyRs. However, this is unlikely to be the case, since most electrical properties measured from birth to postnatal day 12 in SOD1<sup>G93A</sup> MNs instead show an accelerated rate of maturation (*Quinlan et al., 2011*). During perinatal development of rat spinal MNs, GlyR-mediated mIPSCs become dominating over GABA<sub>A</sub>R-mediated mIPSCs (*B.-X. Gao et al., 2001*). We also found a majority of pure GlyR-mediated mIPSCs and found the same ratio of pure GABA<sub>A</sub>R-mediated mIPSCs and pure GlyR-mediated mIPSCs in SOD1<sup>G93A</sup> and WT MNs, indicating similar prenatal developmental stage for both genotypes.

Considering that SOD spinal cords do not express a development delay compared to WT cords from the same littermate, we questioned the origin of the prolonged  $\tau_{\text{decay}}$  in GABA<sub>A</sub>R- and GlyR-mediated mIPSCs, sIPSCs and eIPSCs. It has been demonstrated that high  $[\text{Cl}^-]_i$  slows down the decay of glycine- and GABA-mediated inhibitory synaptic events (*Pitt et al., 2008b; Houston et al., 2009b*), reducing the firing probability of Purkinje neurons (*Houston et al., 2009b*). Interestingly, the structural basis of this effect was described as a direct effect of chloride ions acting in the pore of glycine and GABA channels (*Moroni et al., 2011b*). Therefore, the elevated  $[\text{Cl}^-]_i$  likely accounts for the prolonged relaxation of GABA/Gly IPSCs in SOD1<sup>G93A</sup> MNs. The increase in  $[\text{Cl}^-]_i$  affect GABA<sub>A</sub>R and GlyR and thus IPSCs duration (*Pitt et al., 2008b; Houston et al., 2009b; Moroni et al., 2011b*). In P10 rat MNs a change from 10 mM  $[\text{Cl}^-]_i$  to 131 mM led to an increase in  $\tau_{\text{decay}}$  from 9.2 ms to 19.8 ms (*Pitt et al., 2008b*). In P12 Purkinje cells a change from 10 mM  $[\text{Cl}^-]_i$  to 150 mM led to an increase in  $\tau_{\text{decay}}$  from 14 ms to 19.8 ms (*Houston et al., 2009b*). Finally, in HEK-293 cells, a change from 10 mM  $[\text{Cl}^-]_i$  to 30 mM and then 131 mM led to an increase in  $\tau_{\text{decay}}$  from 9.6 ms to 12 ms and then 22 ms (*Pitt et al., 2008b*). Even though our data highlight a more prolonged  $\tau_{\text{decay}}$  in SOD1<sup>G93A</sup> GABA<sub>A</sub>R/GlyR IPSCs, we cannot directly link  $\tau_{\text{decay}}$  values to physiological  $[\text{Cl}^-]_i$  values, because  $\tau_{\text{decay}}$  values have been collected from CsCl recordings in which  $[\text{Cl}^-]_i$  was set as being elevated.

#### □ Molecular mechanisms modulating the elevated $[\text{Cl}^-]_i$ in SOD1<sup>G93A</sup> MNs.

##### Which Cl<sup>-</sup> transporter raised or upregulated the $[\text{Cl}^-]_i$ in E17.5 SOD1<sup>G93A</sup> MNs?

The intracellular Cl<sup>-</sup> concentration ( $[\text{Cl}^-]_i$ ) is mainly regulated by the action of two Cl<sup>-</sup> transport proteins: NKCC1 (Cl<sup>-</sup> importer) and KCC2 (Cl<sup>-</sup> excluder). To determine the molecular mechanisms underlying the elevated  $[\text{Cl}^-]_i$  that prolonged  $\tau_{\text{decay}}$  in E17.5 SOD1<sup>G93A</sup> MNs, we examined whether the dissipation of elevated  $[\text{Cl}^-]_i$  was mediated by activation of neuronal KCC2 (*Payne et al., 1996; Rivera et al., 1999*), which is expressed at early stages in the embryonic spinal cords (*Alain Delpy et al., 2008*). Impaired KCC2 expression or function is involved in a number of neurodevelopmental and neurological disorders (*Nicolas Doyon et al., 2016*). We therefore quantified the KCC2 protein express and provide evidence that altered  $E_{\text{GABAAR}}$  in E17.5 SOD1<sup>G93A</sup> mouse embryo likely arises from down-regulation of KCC2 in the lumbar cord and the membrane of lumbar MNs. This down-regulation of KCC2 was unlikely linked to the decrease in the size of the SOD<sup>G93A</sup> MNs, namely, smaller neurons have less volume of the cytosol and less surface of the membrane to

host KCC2, because soma perimeters and surface of E17.5 WT MNs and SOD1<sup>G93A</sup> MNs were found to be similar (Martin *et al.*, 2013). Also, KCC2 efficacy and  $E_{\text{GABAR}}$  have been assessed at the soma level. SOD<sup>G93A</sup> MNs do not have less volume to adjust and the lower efficacy of KCC2 in SOD<sup>G93A</sup> MNs is not related to a change in MN size. This suggests that upstream molecules of KCC2 probably regulate the efficacy of KCC2.

In hippocampal pyramidal neurons, NKCC1 up-regulation has been the proposed mechanism that drives transient perinatal GABA switch in rodent models of autism (Tyzio *et al.*, 2014). However, our data show that NKCC1 is unaltered in the E17.5 lumbar spinal cords. KCC2 down-regulation in the hippocampus delays postnatal GABA shift in oxytocin receptor knockout mouse model of autism (Leonzino *et al.*, 2016). More recent evidence shows that KCC2 down-regulation explains long-lasting effects of adolescent nicotine exposure (A. M. Thomas *et al.*, 2018). In ALS-vulnerable motoneurons of adult SOD1<sup>G93A</sup> mouse lumbar cord, a strong decrease of mRNA and protein expression levels was reported (Fuchs *et al.*, 2010). Thus, KCC2 is a likely molecular substrate underlying perinatal alteration of chloride homeostasis in the lumbar spinal cord.

### Lower efficacy of KCC2 raised the physiological $[\text{Cl}^-]_i$ of E17.5 SOD1<sup>G93A</sup> MNs.

It may be surprising to observe a  $\tau_{\text{decay}}$  more prolonged in SOD<sup>G93A</sup> MNs when ECl was imposed at 0 mV (to visualize the Cl<sup>-</sup>-dependent IPSCs) or at -45 mV. Owing to the similar ECl values that are experimentally imposed in SOD<sup>G93A</sup> and WT MNs, theoretical  $[\text{Cl}^-]_i$  values of SOD<sup>G93A</sup> and WT MNs are also similar. Calculated from the Nernst equation, we therefore expected a similar  $\tau_{\text{decay}}$  in SOD<sup>G93A</sup> and WT MNs. However, since our data clearly indicated a deficit in KCC2 efficacy in SOD<sup>G93A</sup> MNs, the physiological  $[\text{Cl}^-]_i$  may have been counteracted by a higher KCC2 efficacy in WT MNs compared to SOD<sup>G93A</sup> MNs. Therefore, we observed a longer relaxation of GABA<sub>A</sub>R/GlyR-mediated mIPSCs and sIPSCs as well as VLF-evoked IPSCs in SOD<sup>G93A</sup> MNs compared to WT littermate MNs.

Our first series of computer simulations demonstrated that increasing  $\tau_{\text{decay}}$  from 20 ms to 25 ms clearly potentiated the efficacy of GABA/glycine inhibition. With a  $\tau_{\text{decay}}$  of 20 ms, a 20 Hz barrage of inhibitory inputs totally blocked WT-like MN firing activity (12 Hz, locomotor firing frequency, with ECl = -60mV). In contrast, SOD-like MNs (with ECl = -50mV) required a ~ 90 Hz inhibitory barrage to suppress their firing. Increasing  $\tau_{\text{decay}}$  to 25 ms significantly reduced the threshold cutting frequency to ~70 Hz in SOD-like MNs. Those blocking frequencies are in agreement with GABA/glycinergic event frequencies encountered

in lumbar spinal MNs during fictive locomotion (>100 Hz). Increasing  $\tau_{\text{decay}}$  from 20 ms to 25 ms also led to a higher capacity of shunting effect summation ([Branchereau et al., 2016](#)).

Our second series of computer simulations demonstrate that increasing  $\tau_{\text{decay}}$  slowed-down the locomotor rhythm. This was in agreement with our findings showing that the pharmacologically-evoked locomotor rhythm in SOD spinal cords was slower than in WT. The effect of IPSCs  $\tau_{\text{decay}}$  on locomotor rhythm was only observed when  $E_{\text{GABAAR}}$  was set to -60 mV in the interneurons of a central-pattern generator (CPG, half-centers). To our knowledge, however, no  $E_{\text{GABAAR}}$  and gGABA/Gly measurements have been obtained in the CPG interneurons of ALS mouse models. In their study of 2–3 weeks *in vitro* organotypic slice cultures of the spinal cord (from E12- E13), Medelin et al. (2016) suggested that the ECl is similar in SOD<sup>G93A</sup> and WT ventral interneurons, around -60 mV. However, neither the excitatory versus inhibitory nature of the recorded interneurons, nor their relationship with CPG circuitry were reported in their study. Our computer model of locomotor rhythm was based on half-center interneurons without considering the output MNs. Therefore, it may be argued that changes in IPSCs  $\tau_{\text{decay}}$  observed in spinal MNs has nothing to do with the spinal locomotor rhythm generator. However, a recent study clearly demonstrated that MNs participate to the rhythm generation in neonatal mouse ([Falgairolle et al., 2017](#)). Therefore, the effect of  $\tau_{\text{decay}}$  increase observed in SOD<sup>G93A</sup> MNs could therefore impinge the locomotor rhythm frequency. This change in the kinetics of GABA<sub>A</sub>R/GlyR- mediated IPSC might be due to a prolonged the opening duration of GABA<sub>A</sub>R/GlyR, thereby maximizing shunting inhibition or making inhibition more efficient, (even if  $E_{\text{GABAAR}}$  is depolarized), as reported in Kurbatova's study ([Kurbatova et al., 2016](#)).

To summarize ([Figure 39](#)), we found that E17.5 SOD<sup>G93A</sup> MNs are hyperexcitable due to depolarized ECl and weakening of GABA<sub>A</sub>R/GlyR-mediated inhibition, which is mediated by a rise in  $[\text{Cl}^-]_i$  through downregulation of the principal neuronal potassium–chloride cotransporter KCC2 and the reduction of GABA/glycine inputs. The rise in  $[\text{Cl}^-]_i$  is sufficient to make MNs hyperexcitable, but the potentiating the shunting inhibition of GABA/Glycine inputs by increasing the  $\tau_{\text{decay}}$  of GABA/Gly IPSCs to compensate the reduction in effective inhibitory inputs, resulting in a normal locomotor coordination. The GABA/Glycine inhibition of E17.5 SOD<sup>G93A</sup> MNs produce decreased GABA<sub>A</sub>R/GlyR-mediated inhibition (less frequent and smaller amplitude IPSCs) and enhancement of shunting inhibition (longer  $\tau_{\text{decay}}$ ) by distinct mechanisms, suggesting that maintenance of neuronal inhibition depends not only on the frequency and peak amplitude of IPSCs, but also on their time course. This

slower or longer  $\tau_{\text{decay}}$  could be attributable to expression of synaptic GlyR channels with slower kinetic properties, which was likely a consequence of altered channels gating efficacy (opening and closing rates). GABAergic/glycinergic disinhibition and depolarized  $E_{\text{Cl}}$  together renders ALS neuronal networks hyperexcitability that is susceptible to spasticity leading to important disabling complications of manual dexterity and gait, and propose KCC2 as a therapeutic target.

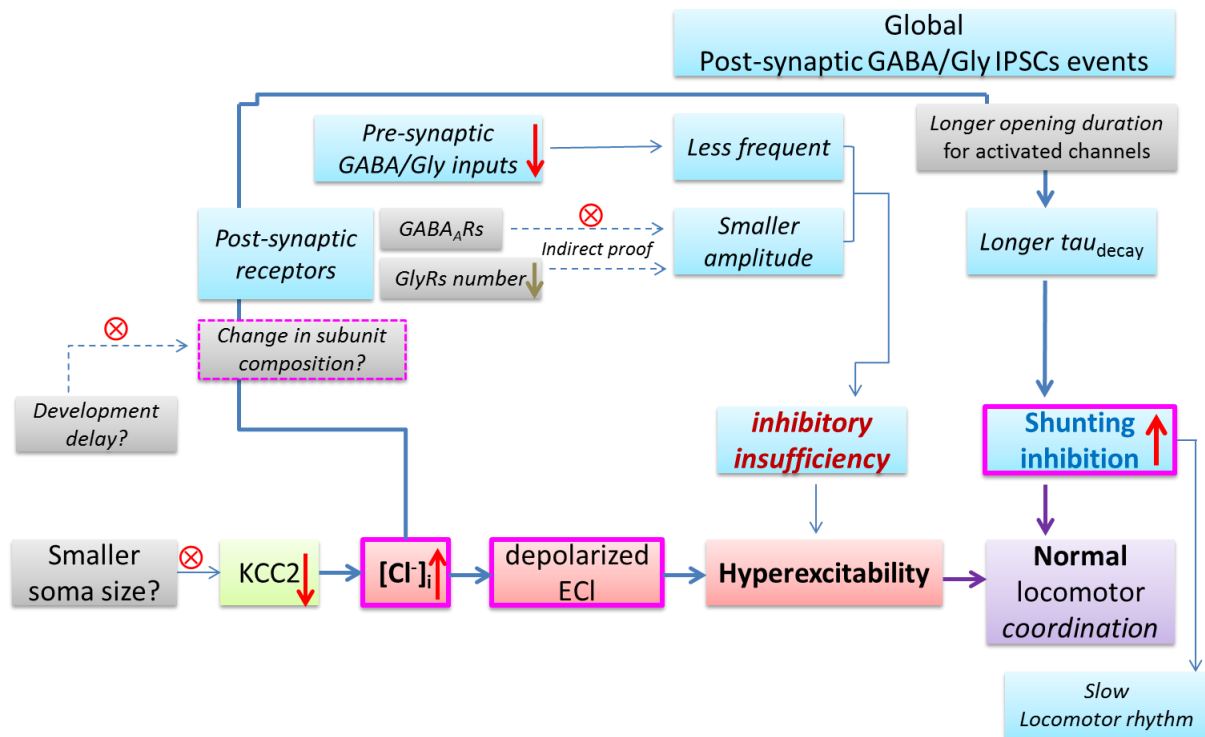


**Figure 39. Summary diagram of the mechanisms involved in  $\text{Cl}^-$  homeostasis regulating cellular hyperexcitability and affecting the synaptic inhibition efficacy of GABA/glycine in prenatal  $\text{SOD}^{\text{G93A}}$  MNs.** The solid line represents direct evidence proven by experimental data, while the dashed lines and boxes represent indirect evidence or possible interpretations mentioned in the discussion section. The circles with crosses represent excluded causal evidence. Neuronal  $\text{Cl}^-$  homeostasis ( $[\text{Cl}^-]_i$ ) as an intracellular messenger may modulate the expression of GABA<sub>A</sub>R/GlyR and subunit composition as well as control channel gating efficacy.

ii. **How do multiple factors such as morphology, inhibitory GABA/glycine synaptic inputs and  $E_{\text{Cl}}$  integrate in a physiological condition to regulate the hyperexcitability of prenatal  $\text{SOD}^{\text{G93A}}$  MNs? (Article 2)**

We have further investigated the effect of dGPSPs occurring at various frequencies on the firing of fetal E17.5 lumbar spinal MNs from the  $\text{SOD1G93A}$  ALS mouse model compared to WT MNs from same littermates. We have disclosed two types of MNs: Dual MNs exhibiting increase MN firing (excitation) of at dGPSP frequency  $< 50\text{Hz}$  and decrease

MN firing (inhibition) at frequency > 50Hz), and an Inhibited MNs showing decrease MN firing (inhibition) at all dGPSP frequencies. We have found that 60% of the WT MNs were Inhibited MNs exhibiting  $R_{in} < 100 \text{ M}\Omega$  whereas 72% of SOD MNs were Dual MNs, without any relationship with their  $R_{in}$  value. A reduced density of GABA/glycine terminals on the soma of SOD MNs accounted for the propensity of SOD MNs to be excited by dGPSPs occurring at low frequency.

#### ❑ What mean the different subtypes of fetal MNs?

We previously described that prenatal E17.5 lumbar spinal MNs for the SOD1<sup>G93A</sup> ALS mouse model are hyperexcitable because of shorter dendrites and exhibit higher  $R_{in}$  compared to WT MNs from the same littermate ([Martin et al., 2013](#)). Our present data, collected from similar fetal MNs located in the lateral motor column, confirm the high  $R_{in}$  in SOD MNs but also show some SOD MNs with low  $R_{in}$  and extended dendritic tree. Similarly, some fetal WT MNs are high  $R_{in}$  and exhibit short dendrites. Does this correspond to two types of MNs? Leroy and colleagues have shown, in post-natal (P) 6-10 days (P6-P10) SOD1<sup>G93A</sup>, that only S-type (innervating the slow-contracting muscle fibers)  $\alpha$  MNs displayed intrinsic hyperexcitability and shrunk dendritic tree, the excitability of F-type (innervating the fast-contracting muscle fibers)  $\alpha$  MNs being unchanged ([Leroy et al., 2014](#)). Similarly, Venugopal and collaborators found in P8-P12 SOD1<sup>G93A</sup> trigeminal MNs that predicted fast SOD MNs showed hyperexcitable shifts marked by reduced rheobase and increased input resistance whereas predicted slow SOD MNs did not present significant alterations in these properties when compared to WT littermate MNs ([Venugopal et al., 2015](#)). Leroy and colleagues described an immediate firing in S-type MNs and a delayed firing in F-type MNs. S-type were identified as expressing the estrogen-related receptor  $\beta$  (Err $\beta$ ) but not the matrix metalloproteinase-9 (MMP9), whereas most of the F-type were enriched with MMP9 ([Leroy et al., 2014](#)) and Err $\beta$  negative ([Leroy et al., 2014](#)). MMP-9 is not expressed by embryonic MNs and is first detected in the spinal cord around P5 ([Kaplan et al., 2014](#)). We have tried to detect MMP-9 in neurobiotin-injected fetal MNs but could not detect any staining. We also checked the immediate vs delayed firing when MNs were depolarized at threshold with a 5s long depolarizing pulse and could only detect immediate firing. In addition, voltage difference between threshold potential for spikes and membrane potential ( $V_{thr}$ - $V_r$ ) and spike width (SpkWdth) did not differ between E17.5 MNs unlike P6-10 MNs ([Leroy et al., 2014](#)). However, even though it is difficult to conclude about the identity of our recorded fetal MNs,

low Rin ( $< 100 \text{ M}\Omega$ ) WT MNs, inhibited by dGPSPs, likely correspond to future F-type MNs. Their morphology complies with this described in WT MNs in our previous study ([Martin et al., 2013](#)). Interestingly, our data highlight a more hyperpolarized actual ECl in low Rin WT Inhibited MNs compared to high Rin WT Dual MNs, suggesting a higher efficacy of KCC2. However, the protocol used in the present study was not a KCC2 challenging protocol and did not reveal any main difference in actual ECl values between WT and SOD MNs as previously described ([Branchereau et al., 2019](#)).

#### □ SOD motoneurons receive less VIAAT-positive inputs

Our result show that fetal SOD MNs can be Dual or Inhibited MNs whatever their Rin and morphology, unlike WT MNs from the littermates. What could explain this surprising result? If we consider that Inhibited low Rin WT MNs are future F-type (innervating the fast-contracting muscle fibers)  $\alpha$  MNs that start getting mature at E17.5, then we may consider that the spinal cord from the SOD1<sup>G93A</sup> strain matures less rapidly than littermate WT spinal cords, i.e., the developmental sequence of the lumbar motoneural network (decrease of the MN Rin, increase of the MN Cm ([A. Delpy et al., 2008](#)), increase of the synaptic input onto MNs ([Scain et al., 2010](#))), is delayed. Another explanation is that the lack of GABA/glycine impedes the occurrence of Inhibited low Rin SOD MNs. We have shown that increasing gGABA/glycine favors dGPSPs inhibition occurring on SOD MN soma. The role of gGABA/glycine (gCl) in the dual effect of dGPSPs was also demonstrated in a previous study where we found that increasing gCl favors inhibition either during a single dGPSP or during trains in which gCl summates ([Branchereau et al., 2016](#)). Our immunohistochemical data indicate a lower density of VIAAT staining on MN somata from the SOD1<sup>G93A</sup> strain compared to WT littermate MNs. Consequently, VLF stimulation activate less GABA/glycine inputs, lowering the shunting (inhibitory effect) of dGPSPs. Our data show that we had to increase the VLF intensity in SOD preparations to obtain evoked single dGPSPs of similar size than WT preparation, in agreement to anatomical data highlighting lower density of VIAAT positive terminals on SOD MNs. Interestingly, in a recent study Allodi and collaborators have shown that F-type MNs from P45 SOD1<sup>G93A</sup> mice lose inhibitory glycinergic connections before S-type MNs ([Allodi et al., 2021](#)). A major reduction of inhibitory synapse densities (gephyrin puncta) in the ventral horn of the SOD1<sup>G93A</sup> slow mutant was also described at early stages of disease (P50) ([S. Saxena et al., 2013](#)). Our previous data show that VIAAT positive terminals are less abundant in the marginal zone edging the E17.5 MN soma location ([Branchereau et al., 2019](#)). Here we found a reduction

of VIAAT density (global and synaptic) on soma of SOD MNs, relative to age-matched WT. In addition, as in our previous study ([Branchereau et al., 2019](#)), we found a reduction in the frequency of GABA/glycine synaptic events, in SOD MNs corroborating the reduction of synaptic VIAAT density. Therefore, even if we did not analyze the lack of VIAAT staining on F-type vs S-type MNs (because of lack of specific markers at fetal stages, see above), we may hypothesize that it reflects an early reduction of GABA/glycine terminals on F-type MNs that are low Rin neurons.

#### □ Somatic morphometric parameters

Our morphometric analysis has uncovered an increase in SOD MNs soma size compared to WT littermates. This was not evidenced in our previous morphometric analysis performed on E17.5 SOD1<sup>G93A</sup> mice ([Martin et al., 2013](#)), as in other studies done on postnatal (P6-10) SOD1<sup>G93A</sup> mice ([Leroy et al., 2014](#)) or P3-9 SOD<sup>G85R</sup> mice ([Amendola et al., 2008](#); [Filipchuk et al., 2012](#)). Interestingly, such an increase in SOD MNs soma was described in a comprehensive study performed on large sample size of immunolabelled P10 SOD1<sup>G93A</sup> MNs, specifically in F-type  $\alpha$  MNs, ([Dukkipati et al., 2018](#)). A larger sample size was also considered in the study performed by Shoenfeld and collaborators who observed an increase in the soma size of P30 SOD1<sup>G93A</sup> MNs ([Shoenfeld et al., 2014](#)). Maybe we focused more on future F-type MNs in the present study compared to Martin and collaborators ([Martin et al., 2013](#)).

### iii. How does inhibition alteration evolve during the disease progression in the SOD1<sup>G93A</sup> mouse ?

Given our findings in this thesis and studies by Chang and Martin pointing out that spinal SOD<sup>G93A</sup> MNs in ALS exhibit deficient inhibition as early as the prenatal stage, this insufficient synaptic inhibition leads to neuronal hyperexcitability due to reduced surface postsynaptic GlyRs in spinal SOD1<sup>G93A</sup> MNs cultured from E12-E14 embryos ([Q. Chang et al., 2011](#)) and *ex-vivo* lumbar E17.5 SOD<sup>G93A</sup> MNs (indirect evidence) ([Branchereau et al., 2019](#)). We thus would like to know how this (glycinergic) inhibitory insufficiency evolved during the progression of ALS disease. Moreover, other studies also show that SOD1<sup>G93A</sup> transgenic ALS mice develop an age-related loss of glycinergic innervation of MNs starting from 8-week old ([Q. Chang et al., 2009b](#)) and P45 days (F-type  $\alpha$ -MNs) ([Allodi et al., 2021](#)), whereas GABAergic innervation is unaffected ([Q. Chang et al., 2009b](#)). However, these

findings focus only on changes in global inhibition, which may derive from a process of degeneration involving Renshaw cells and/or neural networks. To further explore, we expect to identify the specific inhibitory pathways or cell substrates involved in glycinergic inhibitory deficits.

Glycinergic neurons appear during development in the vertebrate central nervous system (CNS) from embryonic E12.5 day on the somata of ventral horn cells in the spinal cord, followed by cells in the dorsal horn one day later (*Allain et al., 2006; Chalphin et al., 2010*). In spinal cord, GlyRs are expressed in the ventral and dorsal horns (*Baer et al., 2009*). During the maturation of ventral inhibitory synapses, important are developing interneurons (e.g., Ia IN, V2b, Renshaw cells), which possess diverse roles in shaping locomotor patterns. These interneurons are assigned to perform reciprocal (Ia inhibitory neurons), feedback (Renshaw cells), and feedforward (presynaptic sensory) inhibition (*Siembab et al., 2010*). Renshaw cell is the only interneuron in the spinal ventral horn that receives afferents directly from collateral axons of the MN and mediates recurrent inhibition back to the MN themselves, through the co-released inhibitory neurotransmitters of glycine and GABA (*B. Renshaw, 1946; Eccles et al., 1961; A. J. Todd et al., 1990; Schneider et al., 1992; F. J. Alvarez et al., 2007; Q. Chang et al., 2009b; F. J. Alvarez et al., 2013*). Individual Renshaw cell receives inputs from particular motor pools and spreads its inhibitory output to the same MNs, their synergists (i.e., motor pools exerting a similar action on the same joint), and sometimes selected motor pools across joints (*Eccles et al., 1961*). The recurrent inhibition thus may act as a variable gain regulator at the motoneuronal level. Renshaw inhibition dysfunction or even Renshaw cell loss has been attributed to the cause of the MNs degeneration in pathological conditions such as ALS (*Fornai et al., 2008; Pasquali et al., 2009*).

My thesis therefore also performed another project, in collaboration with Dr. Marco Beato from University College London (UCL), to investigate whether recurrent inhibition deficits occur in juvenile SOD<sup>G93A</sup> ALS MNs, which could be linked to a reduction in the size of the postsynaptic GlyRs clusters. Beato's lab examined the recurrent inhibition at ~P21 in SOD<sup>G93A</sup> MNs and littermate WT MNs and we investigated the expression of functional GlyRs forming postsynaptic receptor aggregates (i.e., size of GlyRs clusters) on ChAT-positive  $\alpha$ -MNs through immunostaining of coronal cryosections from PFA-fixed spinal cords. We confirmed the postsynaptic GlyRs by their colocalization with presynaptic glycinergic terminals GlyT2 with 10% overlap. Electrophysiological results from Beato's lab revealed that recurrent inhibition was preferentially reduced in large MNs (F-type MNs) from SOD<sup>G93A</sup> mice (**Figure 40**). Their Bayesian quantal analysis disclosed that quantal size was

reduced at Renshaw-motoneuron contacts, suggesting the possibility of some postsynaptic impairment at RC-MN synapses. Beato's lab recording of glycinergic miniature IPSCs (mIPSCs) from MNs revealed that the amplitude of the mIPSCs was smaller in SOD<sup>G93A</sup> MNs. Their data therefore indicated that the size of postsynaptic GlyRs clusters could be smaller in SOD<sup>G93A</sup> MNs compared to WT littermate MNs (*Lim et al., 1999*).

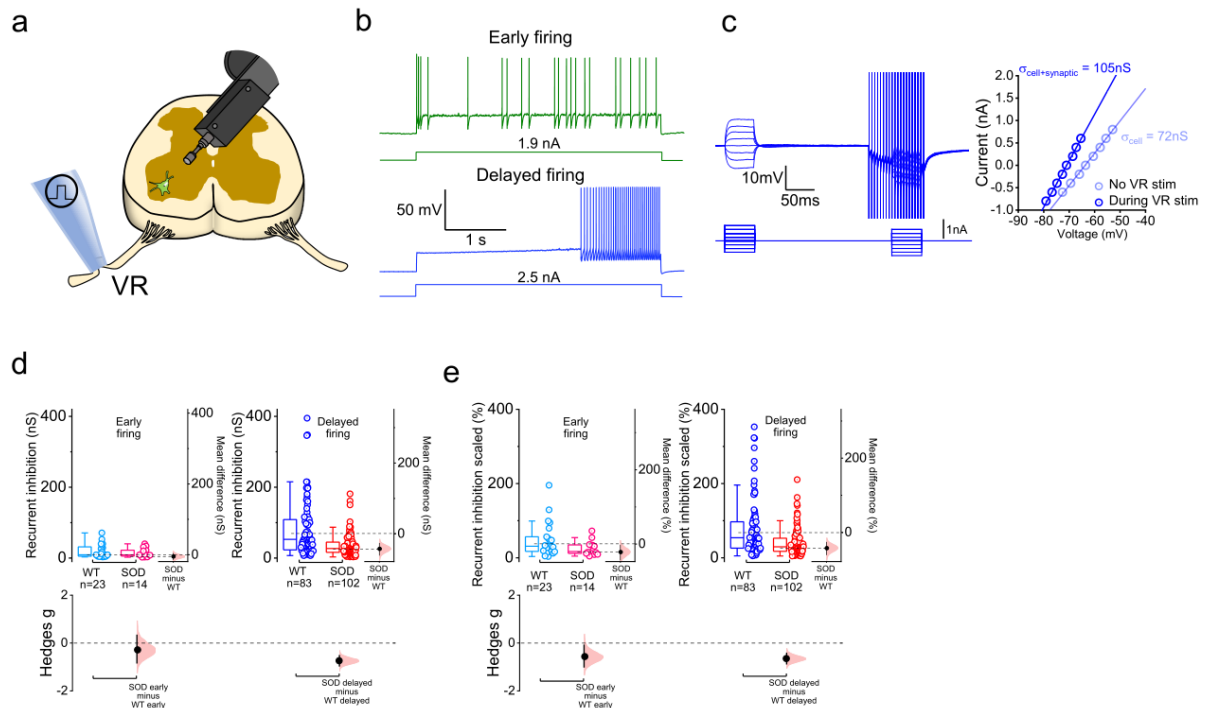


**Figure 40. Recurrent inhibition is preferentially reduced in delayed firing motoneurons from SOD1G93A mice.** (a) Schematic of the 350µm thick oblique spinal cord preparation used in this study, with patch-clamp recording electrode and suction electrode used for ventral root (VR) stimulation. (b) Representation of early (top) and delayed (bottom) firing profiles observed in lumbar motoneurons. (c) Left figure represents the voltage response to different current injections before and during 200Hz VR stimulation used to elicit recurrent inhibition (by evoking a series of IPSPs that reach a steady-state voltage) for WT and SOD1G93A early and delayed firing motoneurons; Plots on the right show respective current-frequency relationships before (light blue) and during (dark blue) VR stimulation that were used to estimate the conductance of recurrent inhibition. Group data for (d) absolute and (e) scaled recurrent inhibition for early and delayed firing motoneurons shown as estimation plots with bootstrapped mean difference aligned and bootstrapped Hedges g effect sizes.

However, our anatomical results, in terms of quantitative analysis of ChAT-positive  $\alpha$ -MNs with big cell body (Feret's diameter  $>40 \mu\text{m}$ , corresponding to F-type MNs), show no statistical difference in the size of postsynaptic GlyRs clusters between WT and SOD<sup>G93A</sup> MNs (Figure 41).

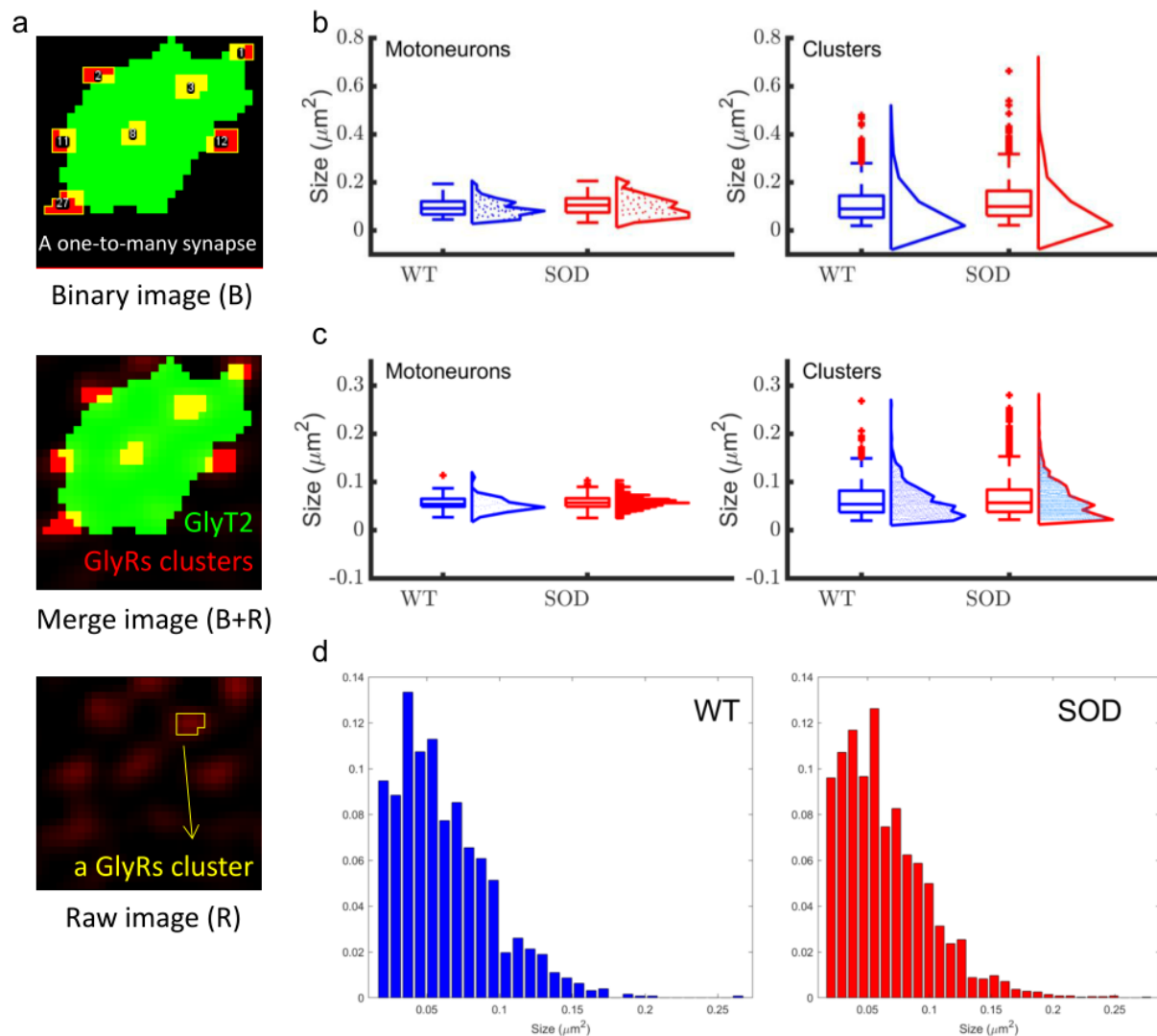


**Figure 41. Alterations in size of the postsynaptic GlyRs clusters onto Fast MNs.** (a) Example of multiple Glycine receptors (GlyRs) clustering in a presynaptic GlyT2+ terminal. Bottom image is a raw image from the membrane of GlyR immunostained MN located on lateral motor column of GlyT2-positive spinal cord. A spot highlighted in yellow in bottom image is used to show how properly the macro detects the size of the GlyRs cluster also represent the median size of  $0.051\mu\text{m}^2$  measured by Fiji. The top image is a binary image generated after running the macro. The middle image composites the raw and its corresponding binary image, for observing the effect of macros detected GlyRs spots. (b) Sum area of all clusters, apposed to a presynaptic GlyT2-positive (GlyT2+) terminal on each motoneuron (left) and individual clusters (right). (c) The size or area of each single GlyRs cluster colocalized to a presynaptic GlyT2+ terminal on each motoneuron (left) and individual clusters (right). (d) Distribution of all synaptic GlyRs clusters. The experiment was conducted on four (in b) and five (in c and d) WT and two (in b) and four ((in c and d) SOD<sup>G93A</sup> (SOD) mice at ~P21. All data were not statistically different between WT and SOD MNs. (Note: Bottom image in Figure 40a was extracted from an analyzed band image in the Annex.)

Although we did not obtain the expected experimental results, the size measurements of GlyRs clusters that we obtained are in agreement with those recently described by Maynard et al. 2021 (Maynard, 2021) (Figure 42). We propose the following possible reasons for the negative experimental results obtained for size measurements of postsynaptic GlyRs clusters:

1) We did not use specific biomarker to identify presynaptic glycinergic terminals from Renshaw cells (En1 and calbindin D28K (*Sapir et al., 2004*)), GlyT2+ presynaptic terminals representing the global inhibitory inputs. 2) anatomical results of spinal cord tissues perfused with PFA via the heart do not accurately reflect the dynamic changes in the size of synaptic GlyRs clusters under physiological conditions of ventral root stimulation given in electrophysiological experiments.

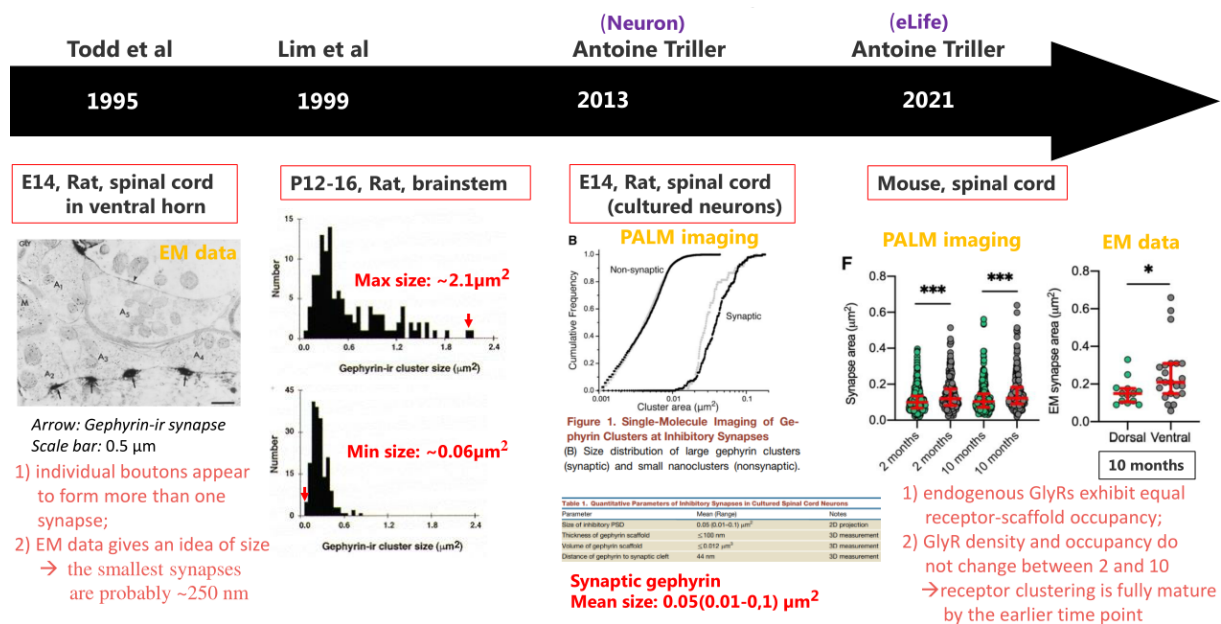


**Figure 42. A summary of size measurements of GlyRs clusters on rodent spinal MNs.**

(a) The nervous system is a dynamic structure causing structural modification including the possibility of reorganizing the neuronal membrane, the topography and translocation of transmitter receptors and ionic channels in neuronal membrane is susceptible to modulation under physiological conditions (*Poo, 1985*). Recording recurrent inhibition need to stimulate ventral roots in order to activate local recurrent inhibitory circuit. Functional GlyRs therefore cluster or aggregate towards the GABA/Glycine release sites where functional glycinergic synapse between Renshaw cells and MNs are formed. As a result, the size of synaptic GlyRs clusters in the physiological state would be larger than those obtained at the immunohistochemical level because GlyRs on motoneuronal membranes lose their mobility or translocation after PFA fixation process. (b) In the ventral horn of the spinal cord, not all MNs can form a recurrent inhibitory circuit with Renshaw cells (*see Figure 9 in this thesis introduction*) (*Bikoff et al., 2016*), which may lead to some “fake-recurrent inhibition” MNs (i.e., MNs without axonal collateral branches) being analyzed and their data being pooled into the anatomical data, contributing to dilute valid results. 3) Resolution limitation of ZEISS

Confocal microscope (LSM900). The distribution of cluster sizes for WT and SOD (Figure 41d) exhibit that slight excess of small cluster near the resolution limit in SOD MNs. There is a sharp cutoff at the level of the resolution (minimum cluster size detectable,  $0.02\mu\text{m}^2$ ), but if we were to fit both distributions, the size distribution could be shifted to the left, beyond the resolution limits. We thus may miss more “below resolution” SOD clusters than WT.

To conclude, if it's true that there was a change in GlyR cluster size due to the SOD mutation, we think that the technical issue is now the limiting factor and the reduced GlyRs clusters in SOD are more likely to be small-size clusters below  $0.02\mu\text{m}^2$ . To capture such small clusters, we would not be able to see it without using high-grade equipment with super resolution. Moreover, it is hard to estimate to what extent these small-size clusters are reduced in SOD, so it is possible that they are so small that they are reduced directly to complete disappearance. In this case, it is worth trying to analyze the density of receptors on the cell membrane from the images acquired with super-resolution instruments. Last but not least, it will be more worthwhile to conduct immunostaining of GlyRs on the recorded MNs after completion of electrophysiological recordings, because the localization (or clustering) of GlyRs can be dynamically modulated during electrophysiological recordings under each VR stimulation for recruiting different (amount of) MNs to Renshaw cells leading to the presence of the convergence of variable MNs onto each Renshaw cell (Figure 43). More MNs converge to Renshaw cell, and more GlyRs on motoneuronal membrane cluster towards the GABA/Glycine release sites from Renshaw cells with strong efficacy. Therefore, I would say the hypothesis is that GlyRs clusters are reduced in SOD, which under physiological conditions is more likely to occur in functional large-size clusters.

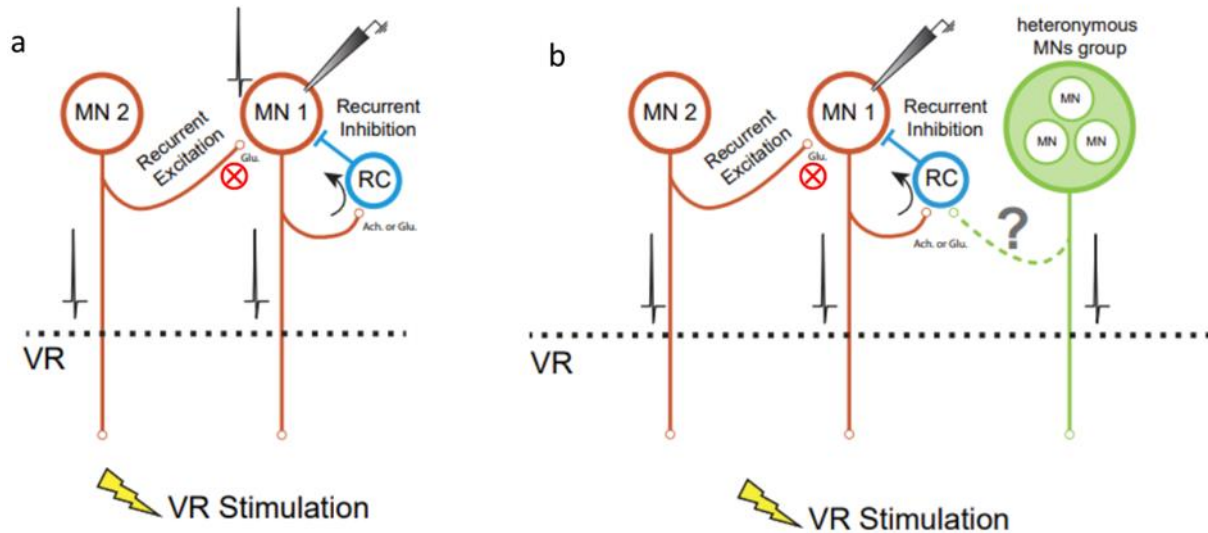


**Figure 43. Schematic drawing of recorded MN receiving recurrent inhibition from the Renshaw cell but with variable glycinergic input efficacy under physiological conditions. (a)** Stimulated single motoneuron (MN) connected Renshaw cell (RC) to recurrent inhibition back to same MN. **(b)** synergistic heteronymous motoneuron pools connected Renshaw cells can vary glycinergic input efficacy feedback to the recorded MN. (synergistic homonymous motoneuron pools converged onto Renshaw cells is not shown here). *Recurrent excitation was obtained in the presence of D-2-amino-5-phosphonopentanoic acid (APV, 50  $\mu$ M), 1,2,3,4-tetrahydrobenzo(f) quinoxaline-7-sulphonamide (NBQX, 3 $\mu$ M) and gabazine (3 $\mu$ M) in order to isolate the contribution of glycinergic inputs to motoneurons derived from Renshaw cells.*

#### iv. Limitations

MNs have a remarkably high diversity in classes and subclasses, and significantly different molecular, morphological, and functional properties. However, specific molecular biomarkers and electrophysiological signatures are lacking at the fetal stage. (For Article 2)

## CHAPTER 4 PERSPECTIVES

Among the most-studied adult-onset neurodegenerative diseases, ALS is recognized as one of the most severe neurodegenerative diseases characterized by relentlessly progressive muscle weakness, eventual paralysis, and death typically within 2-5 years of symptom onset. Great efforts have been made in search for effective therapies for ALS throughout the years. Based on the promising results in preclinical cellular and animal models, hundreds of agents have been proposed as candidates for ALS treatment. However, clinical trials have predominantly come to disappointing results in humans. Several obstacles are implicated in the failure of translation from bench to bedside in the field of ALS treatment.

First, the inadequacy of ALS models is considered as an important reason for failed clinical trials. At the preclinical level, genetically modified rodents carrying fALS mutations remain the most widely used models. However, they do not fully recapitulate the complete pathophysiological and phenotypic spectrum present in ALS patients. ALS is caused by defects in different interacting pathways that culminate in a large network. The relative extent to which each of these mechanisms contributes to the overall pathobiology of ALS has not been fully ascertained, making it difficult to discriminate initiating factors from secondary consequences and target the primary processes underlying ALS. A more comprehensive understanding of ALS pathogenic mechanisms will allow for advances in treatment.

Second, the lack of presymptomatic biomarkers and the delay in clinical diagnosis have significantly limited the therapeutic potential of putative disease-modifying drugs. It is now increasingly accepted that by the time patients fulfil the diagnostic criteria for ALS, a considerable disease burden has already occurred in the long presymptomatic phase. The timing of application of potentially neuroprotective interventions is fundamental for increasing the chance of success. The results of treatment that was started much in advance with respect to the onset of symptoms in animal models should be considered as indicative of success in humans. Presymptomatic diagnosis and clinical trials of early therapeutic intervention in fALS patients identified to carry ALS-related gene mutations are strongly recommended in the future. Also, potential biomarkers that allow early intervention to improve therapeutic outcomes of ALS are anticipated in the near future.

There is an urgent need to develop novel disease-modifying therapeutics to slow the disease progression and extend the lifespan of ALS patients. Since emerging evidence has supported the notion that dysregulation of autophagy is critical for the pathogenesis of ALS, the autophagic signal pathway may be a potential therapeutic target. Furthermore, studies elucidating the genotype–phenotype correlations in ALS patients in recent years have laid ground for individualized, gene-specific therapeutic approaches. The results of these studies advance our understanding of ALS and boost our hope that disease progression can be curbed in the future.

To date, most studies of ALS pathogenesis have focused on symptomatic adult stages, and there are no cures for ALS. Disease-modifying therapies for ALS remain restricted to two drugs, riluzole and edaravone. However, results from the clinical trials have suggested greater benefits for patients from riluzole treatment at early stage (less than 2 years) than later stage of their disease (i.e., more than 2 years) ([B. J. Traynor et al., 2003](#); [Zoing et al., 2006](#)). Thus, there is an urgent need to find some useful pathological hallmarks in the pre-symptomatic stage of ALS for early diagnosis and medical treatment in order to prolong the survival of patients and achieve better therapeutic outcomes. Evidence for ALS pathogenesis before symptomatic adult stages is growing. Deciphering the biology of pre-symptomatic or pre-manifest ALS relies on a clear conceptual framework for defining the earliest stages of disease.

Following to our lab previous finding, ALS may even start at developmental stage, because fetal E17.5 SOD<sup>G93A</sup> MNs showed a hyperexcitability in lumbar spinal cord associated with reduced terminal dendrite morphology and increased input resistance ([Martin et al., 2013](#)). My PhD thesis investigated hyperexcitability-related physiological abnormalities in SOD<sup>G93A</sup> spinal motoneuronal network at this prenatal stage, causative link to the motoneuronal vulnerability being Cl<sup>-</sup>-related inhibitory dysfunction. The work aimed at identifying some novel pathological hallmarks in pre-symptomatic stage of ALS and unravelling its the underlying cellular and molecular mechanisms. Finally, one of the most important results reveals that elevated [Cl<sup>-</sup>]<sub>i</sub> induced hyperexcitability of SODG93A MNs. We then investigated the molecular (Cl<sup>-</sup>-transporter of KCC2 and NKCC1) and cellular (Cl<sup>-</sup>-related inhibitory synapse) mechanisms that regulate this Cl<sup>-</sup> homeostasis alteration, showing an association with downregulation of Cl<sup>-</sup> excluder KCC2 and a reduction in GABAergic/glycinergic

inputs. Thus, my thesis work highlights the importance of Cl<sup>-</sup> homeostasis deficiency in the progression of ALS. Cl<sup>-</sup> homeostasis can be considered as a potential candidate pathological hallmark for ALS. Further work could also be conducted on: 1) decipher the upstream molecular mechanisms involved in the perinatal KCC2 deregulation; 2) investigate the alteration of Cl<sup>-</sup> homeostasis in other ALS mouse models (e.g., FUS, TDP43) at perinatal period (E17.5,P0,P2,P6); 3) rescue the KCC2 deficiency using the KCC2-T906A/T1007A knock-in mouse that exhibits a potentiated KCC2 activity (target KCC2 Protein); 4) identify whether KCC2 is differentially enriched in inhibitory glycinergic clusters (i.e., GlyRs) across development at two key postnatal stages (P20, P50) in SOD1<sup>G93A</sup> *versus* WT mice and in specific MN populations. This future work may provide us a better understanding of how Cl<sup>-</sup> homeostasis affects synaptic inhibition and the role in the progression of ALS.

# CHAPTER 5 List of publications and posters

## Publications

1. **Hongmei Zhu**, Urvashi Dalvi, William Cazenave, Daniel Cattaert and Pascal Branchereau. Excitatory action of low frequency depolarizing GABA/glycine synaptic events is favored in prenatal spinal SOD1<sup>G93A</sup> motoneurons. ***Submitted to Neurobiology of Disease***.
2. Pascal Branchereau, Elodie Martin, Anne-Emilie Allain, William Cazenave, Laura Supiot, Fara Hodeib, Amandine Laupénie, Urvashi Dalvi, **Hongmei Zhu**, Daniel Cattaert. Relaxation of synaptic inhibitory events as a compensatory mechanism in fetal SOD spinal motor networks. ***eLife, 2019, 8:e51402***.

## Conferences

1. **11<sup>th</sup> - 15<sup>th</sup> July 2020 - Glasgow, UK, FENS (Virtual Forum)**  
Dual effect of GABA/Glycine on fetal MNs of the SOD1<sup>G93A</sup> ALS mouse model:  
Do SOD1G93A MNs favor excitation?
2. **9<sup>th</sup> - 13<sup>th</sup> July 2022 - Paris, France, FENS (Onsite Forum)**  
Excitatory action of GABA/Glycine synaptic activity is favored in prenatal SOD1<sup>G93A</sup> MNs.

## Chapter 6 REFERENCES

- Abe, K., Itoyama, Y., Sobue, G., Tsuji, S., Aoki, M., Doyu, M., . . . Group, o. b. o. T. E. A. S. (2014). Confirmatory double-blind, parallel-group, placebo-controlled study of efficacy and safety of edaravone (MCI-186) in amyotrophic lateral sclerosis patients. *Amyotrophic Lateral Sclerosis and Frontotemporal Degeneration*, *15*(7-8), 610-617. doi: 10.3109/21678421.2014.959024
- Acevedo-Arozena, A., Kalmar, B., Essa, S., Ricketts, T., Joyce, P., Kent, R., . . . Fisher, E. M. C. (2011). A comprehensive assessment of the *SOD1G93A* low-copy transgenic mouse, which models human amyotrophic lateral sclerosis. *Disease Models & Mechanisms*, *4*(5), 686-700. doi: 10.1242/dmm.007237
- Acton, B. A., Mahadevan, V., Mercado, A., Uvarov, P., Ding, Y., Pressey, J., . . . Woodin, M. A. (2012). Hyperpolarizing GABAergic Transmission Requires the KCC2 C-Terminal ISO Domain. *Journal of Neuroscience*, *32*(25), 8746-8751. doi: 10.1523/JNEUROSCI.6089-11.2012
- Ahmad, S. S., Ahmad, K., Lee, E. J., Lee, Y.-H., & Choi, I. (2020). Implications of Insulin-Like Growth Factor-1 in Skeletal Muscle and Various Diseases. *Cells*, *9*(8), 1773. doi: 10.3390/cells9081773
- Al-Chalabi, A., & Hardiman, O. (2013). The epidemiology of ALS: a conspiracy of genes, environment and time. *Nature Reviews Neurology*, *9*(11), 617-628. doi: 10.1038/nrneurol.2013.203
- Al-Chalabi, A., van den Berg, L. H., & Veldink, J. (2017). Gene discovery in amyotrophic lateral sclerosis: implications for clinical management. *Nature Reviews Neurology*, *13*(2), 96-104. doi: 10.1038/nrneurol.2016.182
- Al-Mosawie, A., Wilson, J. M., & Brownstone, R. M. (2007). Heterogeneity of V2-derived interneurons in the adult mouse spinal cord. *Eur J Neurosci*, *26*(11), 3003-3015. doi: 10.1111/j.1460-9568.2007.05907.x
- Alaynick, W. A., Jessell, T. M., & Pfaff, S. L. (2011). SnapShot: Spinal Cord Development. *Cell*, *146*(1), 178-178.e171. doi: 10.1016/j.cell.2011.06.038
- Alexander, G. M., Erwin, K. L., Byers, N., Deitch, J. S., Augelli, B. J., Blankenhorn, E. P., & Heiman-Patterson, T. D. (2004). Effect of transgene copy number on survival in the G93A SOD1 transgenic mouse model of ALS. *Molecular Brain Research*, *130*(1-2), 7-15. doi: 10.1016/j.molbrainres.2004.07.002
- Allain, A. E., Bairi, A., Meyrand, P., & Branchereau, P. (2006). Expression of the glycinergic system during the course of embryonic development in the mouse spinal cord and its co-localization with GABA immunoreactivity. *J Comp Neurol*, *496*(6), 832-846. doi: 10.1002/cne.20967
- Allain, A. E., Le Corrionc, H., Delpy, A., Cazenave, W., Meyrand, P., Legendre, P., & Branchereau, P. (2011). Maturation of the GABAergic transmission in normal and pathologic motoneurons. *Neural Plast*, *2011*, 905624. doi: 10.1155/2011/905624
- Allan, D. W., & Greer, J. J. (1997a). Development of phrenic motoneuron morphology in the fetal rat. *The Journal of Comparative Neurology*, *382*(4), 469-479. doi: 10.1002/(SICI)1096-9861(19970616)382:4<469::AID-CNE4>3.0.CO;2-0
- Allan, D. W., & Greer, J. J. (1997b). Embryogenesis of the phrenic nerve and diaphragm in the fetal rat. *The Journal of Comparative Neurology*, *382*(4), 459-468. doi: 10.1002/(SICI)1096-9861(19970616)382:4<459::AID-CNE3>3.0.CO;2-1
- Allodi, I., Montanana-Rosell, R., Selvan, R., Low, P., & Kiehn, O. (2021). Locomotor deficits in a mouse model of ALS are paralleled by loss of V1-interneuron connections onto fast motor neurons. *Nat Commun*, *12*(1), 3251. doi: 10.1038/s41467-021-23224-7

- Alsultan, A. A., Waller, R., Heath, P. R., & Kirby, J. (2016). The genetics of amyotrophic lateral sclerosis: current insights. *Degener Neurol Neuromuscul Dis*, 6, 49-64. doi: 10.2147/DNND.S84956
- Alvarez, F. J., Benito-Gonzalez, A., & Siembab, V. C. (2013). Principles of interneuron development learned from Renshaw cells and the motoneuron recurrent inhibitory circuit. *Ann N Y Acad Sci*, 1279, 22-31. doi: 10.1111/nyas.12084
- Alvarez, F. J., Benito-Gonzalez, A., & Siembab, V. C. (2013). Principles of interneuron development learned from Renshaw cells and the motoneuron recurrent inhibitory circuit: Renshaw cell development. *Annals of the New York Academy of Sciences*, 1279(1), 22-31. doi: 10.1111/nyas.12084
- Alvarez, F. J., & Fyffe, R. E. (2007). The continuing case for the Renshaw cell. *J Physiol*, 584(Pt 1), 31-45. doi: 10.1113/jphysiol.2007.136200
- Alvarez, F. J., & Fyffe, R. E. W. (2007). The continuing case for the Renshaw cell: The continuing case for the Renshaw cell. *The Journal of Physiology*, 584(1), 31-45. doi: 10.1113/jphysiol.2007.136200
- Alvarez, F. J., Jonas, P. C., Sapir, T., Hartley, R., Berrocal, M. C., Geiman, E. J., . . . Goulding, M. (2005). Postnatal phenotype and localization of spinal cord V1 derived interneurons. *J Comp Neurol*, 493(2), 177-192. doi: 10.1002/cne.20711
- Amendola, J., & Durand, J. (2008). Morphological differences between wild-type and transgenic superoxide dismutase 1 lumbar motoneurons in postnatal mice. *J Comp Neurol*, 511(3), 329-341. doi: 10.1002/cne.21818
- Angelotti, T. P., & Macdonald, R. L. (1993). Assembly of GABAA receptor subunits: alpha 1 beta 1 and alpha 1 beta 1 gamma 2S subunits produce unique ion channels with dissimilar single-channel properties. *J Neurosci*, 13(4), 1429-1440.
- Annegers, J. F., Hauser, W. A., Coan, S. P., & Rocca, W. A. (1998). A Population-Based Study of Seizures after Traumatic Brain Injuries. *New England Journal of Medicine*, 338(1), 20-24. doi: 10.1056/NEJM199801013380104
- Aoki, K., Nakamura, T., Fujikawa, K., & Matsuda, M. (2005). Local phosphatidylinositol 3,4,5-trisphosphate accumulation recruits Vav2 and Vav3 to activate Rac1/Cdc42 and initiate neurite outgrowth in nerve growth factor-stimulated PC12 cells. *Mol Biol Cell*, 16(5), 2207-2217. doi: 10.1091/mbc.e04-10-0904
- Arai, T., Hasegawa, M., Akiyama, H., Ikeda, K., Nonaka, T., Mori, H., . . . Oda, T. (2006). TDP-43 is a component of ubiquitin-positive tau-negative inclusions in frontotemporal lobar degeneration and amyotrophic lateral sclerosis. *Biochemical and Biophysical Research Communications*, 351(3), 602-611. doi: 10.1016/j.bbrc.2006.10.093
- Arber, S. (2017). Organization and function of neuronal circuits controlling movement. *EMBO Molecular Medicine*, 9(3), 281-284. doi: 10.15252/emmm.201607226
- Ariel, M., & Daw, N. W. (1982). Pharmacological analysis of directionally sensitive rabbit retinal ganglion cells. *J Physiol*, 324, 161-185. doi: 10.1113/jphysiol.1982.sp014105
- Arundine, M., & Tymianski, M. (2003). Molecular mechanisms of calcium-dependent neurodegeneration in excitotoxicity. *Cell Calcium*, 34(4-5), 325-337. doi: 10.1016/S0143-4160(03)00141-6
- Attwell, D., Barbour, B., & Szatkowski, M. (1993). Nonvesicular release of neurotransmitter. *Neuron*, 11(3), 401-407. doi: 10.1016/0896-6273(93)90145-H
- Avossa, D., Grandolfo, M., Mazzarol, F., Zatta, M., & Ballerini, L. (2006). Early signs of motoneuron vulnerability in a disease model system: Characterization of transverse slice cultures of spinal cord isolated from embryonic ALS mice. *Neuroscience*, 138(4), 1179-1194. doi: 10.1016/j.neuroscience.2005.12.009
- Azpurua, J., & Eaton, B. A. (2015). Neuronal epigenetics and the aging synapse. *Frontiers in Cellular Neuroscience*, 9. doi: 10.3389/fncel.2015.00208

- Bae, J. R., & Kim, S. H. (2017). Synapses in neurodegenerative diseases. *BMB Rep*, 50(5), 237-246. doi: 10.5483/bmbrep.2017.50.5.038
- Bae, J. S., Simon, N. G., Menon, P., Vucic, S., & Kiernan, M. C. (2013). The Puzzling Case of Hyperexcitability in Amyotrophic Lateral Sclerosis. *Journal of Clinical Neurology*, 9(2), 65. doi: 10.3988/jcn.2013.9.2.65
- Baer, K., Waldvogel, H. J., Faull, R. L., & Rees, M. I. (2009). Localization of glycine receptors in the human forebrain, brainstem, and cervical spinal cord: an immunohistochemical review. *Front Mol Neurosci*, 2, 25. doi: 10.3389/neuro.02.025.2009
- Bakels, R., & Kernell, D. (1993). Average but not continuous speed match between motoneurons and muscle units of rat tibialis anterior. *Journal of Neurophysiology*, 70(4), 1300-1306. doi: 10.1152/jn.1993.70.4.1300
- Bakels, R., & Kernell, D. (1993). Matching between motoneurone and muscle unit properties in rat medial gastrocnemius. *The Journal of Physiology*, 463(1), 307-324. doi: 10.1113/jphysiol.1993.sp019596
- Ballion, B., Branchereau, P., Chapron, J., & Viala, D. (2002). Ontogeny of descending serotonergic innervation and evidence for intraspinal 5-HT neurons in the mouse spinal cord. *Brain Res Dev Brain Res*, 137(1), 81-88.
- Bathina, S., & Das, U. N. (2015). Brain-derived neurotrophic factor and its clinical implications. *Arch Med Sci*, 11(6), 1164-1178. doi: 10.5114/aoms.2015.56342
- Batra, R., & Lee, C. W. (2017). Mouse Models of C9orf72 Hexanucleotide Repeat Expansion in Amyotrophic Lateral Sclerosis/ Frontotemporal Dementia. *Frontiers in Cellular Neuroscience*, 11, 196. doi: 10.3389/fncel.2017.00196
- Becher, B., Spath, S., & Goverman, J. (2017). Cytokine networks in neuroinflammation. *Nature Reviews Immunology*, 17(1), 49-59. doi: 10.1038/nri.2016.123
- Beers, D. R., Henkel, J. S., Xiao, Q., Zhao, W., Wang, J., Yen, A. A., . . . Appel, S. H. (2006). Wild-type microglia extend survival in PU.1 knockout mice with familial amyotrophic lateral sclerosis. *Proceedings of the National Academy of Sciences*, 103(43), 16021-16026. doi: 10.1073/pnas.0607423103
- Bellardita, C., & Kiehn, O. (2015). Phenotypic characterization of speed-associated gait changes in mice reveals modular organization of locomotor networks. *Curr Biol*, 25(11), 1426-1436. doi: 10.1016/j.cub.2015.04.005
- Ben-Ari, Y. (2017). NKCC1 Chloride Importer Antagonists Attenuate Many Neurological and Psychiatric Disorders. *Trends Neurosci*, 40(9), 536-554. doi: 10.1016/j.tins.2017.07.001
- Ben-Ari, Y., Gaiarsa, J.-L., Tyzio, R., & Khazipov, R. (2007). GABA: A Pioneer Transmitter That Excites Immature Neurons and Generates Primitive Oscillations. *Physiological Reviews*, 87(4), 1215-1284. doi: 10.1152/physrev.00017.2006
- Ben-Ari, Y., Gaiarsa, J. L., Tyzio, R., & Khazipov, R. (2007). GABA: a pioneer transmitter that excites immature neurons and generates primitive oscillations. *Physiol Rev*, 87(4), 1215-1284. doi: 10.1152/physrev.00017.2006
- Ben-Ari, Y., Woodin, M. A., Sernagor, E., Cancedda, L., Vinay, L., Rivera, C., . . . Cherubini, E. (2012). Refuting the challenges of the developmental shift of polarity of GABA actions: GABA more exciting than ever! *Front Cell Neurosci*, 6, 35. doi: 10.3389/fncel.2012.00035
- Benarroch, E. E. (2013). Cation-chloride cotransporters in the nervous system: General features and clinical correlations. *Neurology*, 80(8), 756-763. doi: 10.1212/WNL.0b013e318283bb1c

- Bensimon, G., Lacomblez, L., & Meininger, V. (1994). A Controlled Trial of Riluzole in Amyotrophic Lateral Sclerosis. *New England Journal of Medicine*, 330(9), 585-591. doi: 10.1056/NEJM199403033300901
- Berg, E. M., Björnfors, E. R., Pallucchi, I., Picton, L. D., & El Manira, A. (2018). Principles Governing Locomotion in Vertebrates: Lessons From Zebrafish. *Frontiers in Neural Circuits*, 12, 73. doi: 10.3389/fncir.2018.00073
- Betley, J. N., Wright, C. V. E., Kawaguchi, Y., Erdélyi, F., Szabó, G., Jessell, T. M., & Kaltschmidt, J. A. (2009). Stringent Specificity in the Construction of a GABAergic Presynaptic Inhibitory Circuit. *Cell*, 139(1), 161-174. doi: 10.1016/j.cell.2009.08.027
- Bhumra, G. (2012). Co-release of GABA does not occur at glycinergic synapses onto lumbar motoneurons in juvenile mice. *Frontiers in Cellular Neuroscience*, 6. doi: 10.3389/fncel.2012.00008
- Bikoff, J. B., Gabitto, M. I., Rivard, A. F., Drobac, E., Machado, T. A., Miri, A., . . . Jessell, T. M. (2016). Spinal Inhibitory Interneuron Diversity Delineates Variant Motor Microcircuits. *Cell*, 165(1), 207-219. doi: 10.1016/j.cell.2016.01.027
- Blasco, H., Mavel, S., Corcia, P., & Gordon, P. H. (2014). The Glutamate Hypothesis in ALS: Pathophysiology and Drug Development. *Current Medicinal Chemistry*, 21(31), 3551-3575. doi: 10.2174/0929867321666140916120118
- Blaustein, M. P. (1988). Calcium transport and buffering in neurons. *Trends Neurosci*, 11(10), 438-443.
- Blizzard, C. A., Southam, K. A., Dawkins, E., Lewis, K. E., King, A. E., Clark, J. A., & Dickson, T. C. (2015). Identifying the primary site of pathogenesis in amyotrophic lateral sclerosis – vulnerability of lower motor neurons to proximal excitotoxicity. *Disease Models & Mechanisms*, 8(3), 215-224. doi: 10.1242/dmm.018606
- Boillée, S., Vande Velde, C., & Cleveland, Don W. (2006). ALS: A Disease of Motor Neurons and Their Nonneuronal Neighbors. *Neuron*, 52(1), 39-59. doi: 10.1016/j.neuron.2006.09.018
- Bollan, K., Robertson, L. A., Tang, H., & Connolly, C. N. (2003). Multiple assembly signals in gamma-aminobutyric acid (type A) receptor subunits combine to drive receptor construction and composition. *Biochem Soc Trans*, 31(Pt 4), 875-879. doi: 10.1042/bst0310875
- Bonfanti, E., Bonifacino, T., Raffaele, S., Milanese, M., Morgante, E., Bonanno, G., . . . Fumagalli, M. (2020). Abnormal Upregulation of GPR17 Receptor Contributes to Oligodendrocyte Dysfunction in SOD1 G93A Mice. *International Journal of Molecular Sciences*, 21(7), 2395. doi: 10.3390/ijms21072395
- Bories, C., Amendola, J., Lamotte d'Incamps, B., & Durand, J. (2007). Early electrophysiological abnormalities in lumbar motoneurons in a transgenic mouse model of amyotrophic lateral sclerosis. *European Journal of Neuroscience*, 25(2), 451-459. doi: 10.1111/j.1460-9568.2007.05306.x
- Bormann, J., Hamill, O. P., & Sakmann, B. (1987). Mechanism of anion permeation through channels gated by glycine and gamma-aminobutyric acid in mouse cultured spinal neurones. *J Physiol*, 385, 243-286.
- Bormann, J., Hamill, O. P., & Sakmann, B. (1987). Mechanism of anion permeation through channels gated by glycine and gamma-aminobutyric acid in mouse cultured spinal neurones. *The Journal of Physiology*, 385(1), 243-286. doi: 10.1113/jphysiol.1987.sp016493
- Bos, R., Harris-Warrick, R. M., Brocard, C., Demianenko, L. E., Manuel, M., Zytnicki, D., . . . Brocard, F. (2018). Kv1.2 Channels Promote Nonlinear Spiking Motoneurons for Powering Up Locomotion. *Cell Rep*, 22(12), 3315-3327. doi: 10.1016/j.celrep.2018.02.093

- Bostock, H., Sharief, M. K., Reid, G., & Murray, N. M. F. (1995). Axonal ion channel dysfunction in amyotrophic lateral sclerosis. *Brain*, *118*(1), 217-225. doi: 10.1093/brain/118.1.217
- Boston-Howes, W., Gibb, S. L., Williams, E. O., Pasinelli, P., Brown, R. H., & Trotti, D. (2006). Caspase-3 Cleaves and Inactivates the Glutamate Transporter EAAT2. *Journal of Biological Chemistry*, *281*(20), 14076-14084. doi: 10.1074/jbc.M600653200
- Boulenguez, P., Liabeuf, S., Bos, R., Bras, H., Jean-Xavier, C., Brocard, C., . . . Vinay, L. (2010). Down-regulation of the potassium-chloride cotransporter KCC2 contributes to spasticity after spinal cord injury. *Nature Medicine*, *16*(3), 302-307. doi: 10.1038/nm.2107
- Bowery, N. G., Hudson, A. L., & Price, G. W. (1987). GABAA and GABAB receptor site distribution in the rat central nervous system. *Neuroscience*, *20*(2), 365-383. doi: 10.1016/0306-4522(87)90098-4
- Bowling, A. C., & Beal, M. F. (1995). Bioenergetic and oxidative stress in neurodegenerative diseases. *Life Sciences*, *56*(14), 1151-1171. doi: 10.1016/0024-3205(95)00055-B
- Branchereau, P., Cattaert, D., Delpy, A., Allain, A. E., Martin, E., & Meyrand, P. (2016). Depolarizing GABA/glycine synaptic events switch from excitation to inhibition during frequency increases. *Sci Rep*, *6*, 21753. doi: 10.1038/srep21753
- Branchereau, P., Martin, E., Allain, A. E., Cazenave, W., Supiot, L., Hodeib, F., . . . Cattaert, D. (2019). Relaxation of synaptic inhibitory events as a compensatory mechanism in fetal SOD spinal motor networks. *Elife*, *8*. doi: 10.7554/eLife.51402
- Branchereau, P., Morin, D., Bonnot, A., Ballion, B., Chapron, J., & Viala, D. (2000a). Development of lumbar rhythmic networks: from embryonic to neonate locomotor-like patterns in the mouse. *Brain Res Bull*, *53*(5), 711-718.
- Branchereau, P., Morin, D., Bonnot, A., Ballion, B., Chapron, J., & Viala, D. (2000b). Development of lumbar rhythmic networks: from embryonic to neonate locomotor-like patterns in the mouse. *Brain Res Bull*, *53*(5), 711-718. doi: 10.1016/s0361-9230(00)00403-2
- Braz, B. Y., Wennagel, D., Ratie, L., de Souza, D. A. R., Deloulme, J. C., Barbier, E. L., . . . Humbert, S. (2022). Treating early postnatal circuit defect delays Huntington's disease onset and pathology in mice. *Science*, *377*(6613), eabq5011. doi: 10.1126/science.abq5011
- Breit, M., Stepniewski, M., Grein, S., Gottmann, P., Reinhardt, L., & Queisser, G. (2016). Anatomically Detailed and Large-Scale Simulations Studying Synapse Loss and Synchrony Using NeuroBox. *Front Neuroanat*, *10*, 8. doi: 10.3389/fnana.2016.00008
- Brettschneider, J., Del Tredici, K., Toledo, J. B., Robinson, J. L., Irwin, D. J., Grossman, M., . . . Trojanowski, J. Q. (2013). Stages of pTDP-43 pathology in amyotrophic lateral sclerosis: ALS Stages. *Annals of Neurology*, *74*(1), 20-38. doi: 10.1002/ana.23937
- Brickley, S. G., Cull-Candy, S. G., & Farrant, M. (1996). Development of a tonic form of synaptic inhibition in rat cerebellar granule cells resulting from persistent activation of GABAA receptors. *The Journal of Physiology*, *497*(3), 753-759. doi: 10.1113/jphysiol.1996.sp021806
- Britz, O., Zhang, J., Grossmann, K. S., Dyck, J., Kim, J. C., Dymecki, S., . . . Goulding, M. (2015). A genetically defined asymmetry underlies the inhibitory control of flexor-extensor locomotor movements. *Elife*, *4*. doi: 10.7554/eLife.04718
- Brooks, B. R., Miller, R. G., Swash, M., & Munsat, T. L. (2000). El Escorial revisited: Revised criteria for the diagnosis of amyotrophic lateral sclerosis. *Amyotrophic*

- Lateral Sclerosis and Other Motor Neuron Disorders*, 1(5), 293-299. doi: 10.1080/146608200300079536
- Brownstone, R. M., Bui, T. V., & Stifani, N. (2015). Spinal circuits for motor learning. *Current Opinion in Neurobiology*, 33, 166-173. doi: 10.1016/j.conb.2015.04.007
- Bruijn, L. I., Becher, M. W., Lee, M. K., Anderson, K. L., Jenkins, N. A., Copeland, N. G., . . . Cleveland, D. W. (1997). ALS-Linked SOD1 Mutant G85R Mediates Damage to Astrocytes and Promotes Rapidly Progressive Disease with SOD1-Containing Inclusions. *Neuron*, 18(2), 327-338. doi: 10.1016/S0896-6273(00)80272-X
- Bruijn, L. I., Houseweart, M. K., Kato, S., Anderson, K. L., Anderson, S. D., Ohama, E., . . . Cleveland, D. W. (1998). Aggregation and Motor Neuron Toxicity of an ALS-Linked SOD1 Mutant Independent from Wild-Type SOD1. *Science*, 281(5384), 1851-1854. doi: 10.1126/science.281.5384.1851
- Brundin, P., Melki, R., & Kopito, R. (2010). Prion-like transmission of protein aggregates in neurodegenerative diseases. *Nature Reviews Molecular Cell Biology*, 11(4), 301-307. doi: 10.1038/nrm2873
- Brunet, A., Stuart-Lopez, G., Burg, T., Scekcic-Zahirovic, J., & Rouaux, C. (2020). Cortical Circuit Dysfunction as a Potential Driver of Amyotrophic Lateral Sclerosis. *Frontiers in Neuroscience*, 14, 363. doi: 10.3389/fnins.2020.00363
- Bueker, E. D. (1944). DIFFERENTIATION OF THE LATERAL MOTOR COLUMN IN THE AVIAN SPINAL CORD. *Science*, 100(2591), 169-169. doi: 10.1126/science.100.2591.169
- Bui, T. V., Grande, G., & Rose, P. K. (2008). Relative Location of Inhibitory Synapses and Persistent Inward Currents Determines the Magnitude and Mode of Synaptic Amplification in Motoneurons. *Journal of Neurophysiology*, 99(2), 583-594. doi: 10.1152/jn.00718.2007
- Burden, S. J. (2002). Building the vertebrate neuromuscular synapse. *Journal of Neurobiology*, 53(4), 501-511. doi: 10.1002/neu.10137
- Burke, R. E., Levine, D. N., Tsairis, P., & Zajac, F. E. (1973). Physiological types and histochemical profiles in motor units of the cat gastrocnemius. *The Journal of Physiology*, 234(3), 723-748. doi: 10.1113/jphysiol.1973.sp010369
- Burke, R. E., Levine, D. N., Zajac, F. E., Tsairis, P., & Engel, W. K. (1971). Mammalian Motor Units: Physiological-Histochemical Correlation in Three Types in Cat Gastrocnemius. *Science*, 174(4010), 709-712. doi: 10.1126/science.174.4010.709
- Burley, S., Beccano-Kelly, D. A., Talbot, K., Llana, O. C., & Wade-Martins, R. (2022). Hyperexcitability in young iPSC-derived C9ORF72 mutant motor neurons is associated with increased intracellular calcium release. *Sci Rep*, 12(1), 7378. doi: 10.1038/s41598-022-09751-3
- Carnevale, N. T., & Hines, M. L. (2006). *The NEURON Book*: Cambridge University Press, Cambridge, UK.
- Castellano, C., Cestari, V., & Ciamei, A. (2001). NMDA Receptors and Learning and Memory Processes. *Current Drug Targets*, 2(3), 273-283. doi: 10.2174/1389450013348515
- Chalphin, A. V., & Saha, M. S. (2010). The specification of glycinergic neurons and the role of glycinergic transmission in development. *Front Mol Neurosci*, 3, 11. doi: 10.3389/fnmol.2010.00011
- Chang, Q., & Martin, L. J. (2009a). Glycinergic Innervation of Motoneurons Is Deficient in Amyotrophic Lateral Sclerosis Mice A Quantitative Confocal Analysis. *American Journal of Pathology*, 174(2), 574-585. doi: 10.2353/ajpath.2009.080557

- Chang, Q., & Martin, L. J. (2009b). Glycinergic innervation of motoneurons is deficient in amyotrophic lateral sclerosis mice: a quantitative confocal analysis. *Am J Pathol*, *174*(2), 574-585. doi: 10.2353/ajpath.2009.080557
- Chang, Q., & Martin, L. J. (2011). Glycine receptor channels in spinal motoneurons are abnormal in a transgenic mouse model of amyotrophic lateral sclerosis. *J Neurosci*, *31*(8), 2815-2827. doi: 10.1523/JNEUROSCI.2475-10.2011
- Chang, Q., & Martin, L. J. (2016). Voltage-gated calcium channels are abnormal in cultured spinal motoneurons in the G93A-SOD1 transgenic mouse model of ALS. *Neurobiology of Disease*, *93*, 78-95. doi: 10.1016/j.nbd.2016.04.009
- Charcot, J.-M. (1874). De la sclérose latérale amyotrophique. *Prog. Med*, *2*, 325-327, 341-342, 453-455.
- Charcot, J., & Joffroy, A. (1869). Deux cas d'atrophie musculaire progressive avec lesion de la substance grise et des faisceaux antero-latéraux de la moelle epiniere. *Arch. Physiol. Neurol. Pathol*, *2*, 744-754.
- Cheah, B. C., Vucic, S., Krishnan, A., & Kiernan, M. C. (2010). Riluzole, Neuroprotection and Amyotrophic Lateral Sclerosis. *Current Medicinal Chemistry*, *17*(18), 1942-1959. doi: 10.2174/092986710791163939
- Chiu, A. Y., Zhai, P., Dal Canto, M. C., Peters, T. M., Kwon, Y. W., Prattis, S. M., & Gurney, M. E. (1995). Age-Dependent Penetrance of Disease in a Transgenic Mouse Model of Familial Amyotrophic Lateral Sclerosis. *Molecular and Cellular Neuroscience*, *6*(4), 349-362. doi: 10.1006/mcne.1995.1027
- Clark, R., Blizzard, C., & Dickson, T. (2015a). <Clark et al.2015.Review\_Inhibitory dysfunction in amyotrophic lateral sclerosis- future therapeutic opportunities.pdf>. *Neurodegenerative Disease Management*.
- Clark, R., Blizzard, C., & Dickson, T. (2015b). Inhibitory dysfunction in amyotrophic lateral sclerosis: future therapeutic opportunities. *Neurodegener Dis Manag*, *5*(6), 511-525. doi: 10.2217/nmt.15.49
- Clement, A. M., Nguyen, M. D., Roberts, E. A., Garcia, M. L., Boillée, S., Rule, M., . . . Cleveland, D. W. (2003). Wild-Type Nonneuronal Cells Extend Survival of SOD1 Mutant Motor Neurons in ALS Mice. *Science*, *302*(5642), 113-117. doi: 10.1126/science.1086071
- Close, R. (1967). Properties of motor units in fast and slow skeletal muscles of the rat. *The Journal of Physiology*, *193*(1), 45-55. doi: 10.1113/jphysiol.1967.sp008342
- Cohen-Cory, S. (2002). The Developing Synapse: Construction and Modulation of Synaptic Structures and Circuits. *Science*, *298*(5594), 770-776. doi: 10.1126/science.1075510
- Cohen, I., Navarro, V., Clemenceau, S., Baulac, M., & Miles, R. (2002). On the Origin of Interictal Activity in Human Temporal Lobe Epilepsy in Vitro. *Science*, *298*(5597), 1418-1421. doi: 10.1126/science.1076510
- Condon, K., Silberstein, L., Blau, H. M., & Thompson, W. J. (1990). Development of muscle fiber types in the prenatal rat hindlimb. *Dev Biol*, *138*(2), 256-274. doi: 10.1016/0012-1606(90)90196-p
- Coull, J. A. M., Boudreau, D., Bachand, K., Prescott, S. A., Nault, F., Sîk, A., . . . Koninck, Y. D. (2003). Trans-synaptic shift in anion gradient in spinal lamina I neurons as a mechanism of neuropathic pain. *Nature*, *424*(6951), 938-942. doi: 10.1038/nature01868
- Cramer, S. W., Baggott, C., Cain, J., Tilghman, J., Allcock, B., Miranpuri, G., . . . Resnick, D. (2008). The role of cation-dependent chloride transporters in neuropathic pain following spinal cord injury. *Mol Pain*, *4*, 36. doi: 10.1186/1744-8069-4-36
- Crociara, P., Chieppa, M. N., Vallino Costassa, E., Berrone, E., Gallo, M., Lo Faro, M., . . . Corona, C. (2019). Motor neuron degeneration, severe myopathy and TDP-43 increase

- in a transgenic pig model of SOD1-linked familiar ALS. *Neurobiology of Disease*, 124, 263-275. doi: 10.1016/j.nbd.2018.11.021
- Crone, S. A., Quinlan, K. A., Zagoraiou, L., Droho, S., Restrepo, C. E., Lundfald, L., . . . Sharma, K. (2008). Genetic ablation of V2a ipsilateral interneurons disrupts left-right locomotor coordination in mammalian spinal cord. *Neuron*, 60(1), 70-83. doi: 10.1016/j.neuron.2008.08.009
- Crozat, A., Aman, P., Mandahl, N., & Ron, D. (1993). Fusion of CHOP to a novel RNA-binding protein in human myxoid liposarcoma. *Nature*, 363(6430), 640-644. doi: 10.1038/363640a0
- Cutler, C. P., & Cramb, G. (2002). Two isoforms of the Na<sup>+</sup>/K<sup>+</sup>/2Cl<sup>-</sup> cotransporter are expressed in the European eel (*Anguilla anguilla*). *Biochimica et Biophysica Acta (BBA) - Biomembranes*, 1566(1-2), 92-103. doi: 10.1016/S0005-2736(02)00596-5
- Dadon-Nachum, M., Melamed, E., & Offen, D. (2011). The “Dying-Back” Phenomenon of Motor Neurons in ALS. *Journal of Molecular Neuroscience*, 43(3), 470-477. doi: 10.1007/s12031-010-9467-1
- Dang, Y.-H., Ma, X.-C., Zhang, J.-C., Ren, Q., Wu, J., Gao, C.-G., & Hashimoto, K. (2014). Targeting of NMDA Receptors in the Treatment of Major Depression. *Current Pharmaceutical Design*, 20(32), 5151-5159. doi: 10.2174/1381612819666140110120435
- Darman, R. B., & Forbush, B. (2002). A regulatory locus of phosphorylation in the N terminus of the Na-K-Cl cotransporter, NKCC1. *J Biol Chem*, 277(40), 37542-37550. doi: 10.1074/jbc.M206293200
- Dasen, J. S., & Jessell, T. M. (2009). Hox networks and the origins of motor neuron diversity. *Curr Top Dev Biol*, 88, 169-200. doi: 10.1016/S0070-2153(09)88006-X
- de Carvalho, M., & Swash, M. (2013). Fasciculation potentials and earliest changes in motor unit physiology in ALS. *Journal of Neurology, Neurosurgery & Psychiatry*, 84(9), 963-968. doi: 10.1136/jnnp-2012-304545
- De Vos, K. J., Chapman, A. L., Tennant, M. E., Manser, C., Tudor, E. L., Lau, K.-F., . . . Grierson, A. J. (2007). Familial amyotrophic lateral sclerosis-linked SOD1 mutants perturb fast axonal transport to reduce axonal mitochondria content. *Human Molecular Genetics*, 16(22), 2720-2728. doi: 10.1093/hmg/ddm226
- Deidda, G., Bozarth, I. F., & Cancedda, L. (2014). Modulation of GABAergic transmission in development and neurodevelopmental disorders: investigating physiology and pathology to gain therapeutic perspectives. *Frontiers in Cellular Neuroscience*, 8. doi: 10.3389/fncel.2014.00119
- Deken, S. L., Wang, D., & Quick, M. W. (2003). Plasma Membrane GABA Transporters Reside on Distinct Vesicles and Undergo Rapid Regulated Recycling. *The Journal of Neuroscience*, 23(5), 1563-1568. doi: 10.1523/JNEUROSCI.23-05-01563.2003
- Delgado-Lezama, R., Loeza-Alcocer, E., Andres, C., Aguilar, J., Guertin, P., & Felix, R. (2013). Extrasynaptic GABA<sub>A</sub> Receptors in the Brainstem and Spinal Cord: Structure and Function. *Current Pharmaceutical Design*, 19(24), 4485-4497. doi: 10.2174/1381612811319240013
- Delpire, E., & Mount, D. B. (2002). Human and murine phenotypes associated with defects in cation-chloride cotransport. *Annu Rev Physiol*, 64, 803-843. doi: 10.1146/annurev.physiol.64.081501.155847
- Delpy, A., Allain, A.-E., Meyrand, P., & Branchereau, P. (2008). NKCC1 cotransporter inactivation underlies embryonic development of chloride-mediated inhibition in mouse spinal motoneuron: Ontogeny of inhibition in mouse spinal networks. *The Journal of Physiology*, 586(4), 1059-1075. doi: 10.1113/jphysiol.2007.146993

- Delpy, A., Allain, A. E., Meyrand, P., & Branchereau, P. (2008). NKCC1 cotransporter inactivation underlies embryonic development of chloride-mediated inhibition in mouse spinal motoneuron. *J Physiol*, *586*(4), 1059-1075. doi: 10.1113/jphysiol.2007.146993
- Deneris, E. S., & Hobert, O. (2014). Maintenance of postmitotic neuronal cell identity. *Nature Neuroscience*, *17*(7), 899-907. doi: 10.1038/nn.3731
- Destexhe, A., Babloyantz, A., & Sejnowski, T. J. (1993). Ionic mechanisms for intrinsic slow oscillations in thalamic relay neurons. *Biophys J*, *65*(4), 1538-1552. doi: 10.1016/S0006-3495(93)81190-1
- Devlin, A.-C., Burr, K., Boroah, S., Foster, J. D., Cleary, E. M., Geti, I., . . . Miles, G. B. (2015). Human iPSC-derived motoneurons harbouring TARDBP or C9ORF72 ALS mutations are dysfunctional despite maintaining viability. *Nature Communications*, *6*(1), 5999. doi: 10.1038/ncomms6999
- Devlin, A. C., Burr, K., Boroah, S., Foster, J. D., Cleary, E. M., Geti, I., . . . Miles, G. B. (2015). Human iPSC-derived motoneurons harbouring TARDBP or C9ORF72 ALS mutations are dysfunctional despite maintaining viability. *Nat Commun*, *6*, 5999. doi: 10.1038/ncomms6999
- Dharmadasa, T., Henderson, R. D., Talman, P. S., Macdonell, R. A., Mathers, S., Schultz, D. W., . . . Kiernan, M. C. (2017). Motor neurone disease: progress and challenges. *Medical Journal of Australia*, *206*(8), 357-362. doi: 10.5694/mja16.01063
- Di Giorgio, F. P., Carrasco, M. A., Siao, M. C., Maniatis, T., & Eggan, K. (2007). Non-cell autonomous effect of glia on motor neurons in an embryonic stem cell-based ALS model. *Nature Neuroscience*, *10*(5), 608-614. doi: 10.1038/nn1885
- Doble, A. (1996). The pharmacology and mechanism of action of riluzole. *Neurology*, *47*(Issue 6, Supplement 4), 233S-241S. doi: 10.1212/WNL.47.6\_Suppl\_4.233S
- Dobrowolny, G., Aucello, M., Molinaro, M., & Musarò, A. (2008). Local expression of mIgf-1 modulates ubiquitin, caspase and CDK5 expression in skeletal muscle of an ALS mouse model. *Neurological Research*, *30*(2), 131-136. doi: 10.1179/174313208X281235
- Dobrowolny, G., Giacinti, C., Pelosi, L., Nicoletti, C., Winn, N., Barberi, L., . . . Musarò, A. (2005). Muscle expression of a local Igf-1 isoform protects motor neurons in an ALS mouse model. *Journal of Cell Biology*, *168*(2), 193-199. doi: 10.1083/jcb.200407021
- Dong, X., Shen, K., & Bülow, H. E. (2015). Intrinsic and Extrinsic Mechanisms of Dendritic Morphogenesis. *Annual Review of Physiology*, *77*(1), 271-300. doi: 10.1146/annurev-physiol-021014-071746
- Doyon, N., Prescott, S. A., Castonguay, A., Godin, A. G., Kroger, H., & De Koninck, Y. (2011). Efficacy of synaptic inhibition depends on multiple, dynamically interacting mechanisms implicated in chloride homeostasis. *PLoS Comput Biol*, *7*(9), e1002149. doi: 10.1371/journal.pcbi.1002149
- Doyon, N., Vinay, L., Prescott, Steven A., & De Koninck, Y. (2016). Chloride Regulation: A Dynamic Equilibrium Crucial for Synaptic Inhibition. *Neuron*, *89*(6), 1157-1172. doi: 10.1016/j.neuron.2016.02.030
- Du, L., Zhang, Y., Chen, Y., Zhu, J., Yang, Y., & Zhang, H. L. (2017). Role of Microglia in Neurological Disorders and Their Potentials as a Therapeutic Target. *Mol Neurobiol*, *54*(10), 7567-7584. doi: 10.1007/s12035-016-0245-0
- Dukkipati, S. S., Garrett, T. L., & Elbasiouny, S. M. (2018). The vulnerability of spinal motoneurons and soma size plasticity in a mouse model of amyotrophic lateral sclerosis. *J Physiol*, *596*(9), 1723-1745. doi: 10.1113/JP275498

- Dumoulin, A., Rostaing, P., Bedet, C., Levi, S., Isambert, M. F., Henry, J. P., . . . Gasnier, B. (1999). Presence of the vesicular inhibitory amino acid transporter in GABAergic and glycinergic synaptic terminal boutons. *J Cell Sci*, *112* ( Pt 6), 811-823.
- Dumoulin, A., Triller, A., & Dieudonné, S. (2001). IPSC Kinetics at Identified GABAergic and Mixed GABAergic and Glycinergic Synapses onto Cerebellar Golgi Cells. *The Journal of Neuroscience*, *21*(16), 6045-6057. doi: 10.1523/JNEUROSCI.21-16-06045.2001
- Dunlop, J., Beal McIlvain, H., She, Y., & Howland, D. S. (2003). Impaired Spinal Cord Glutamate Transport Capacity and Reduced Sensitivity to Riluzole in a Transgenic Superoxide Dismutase Mutant Rat Model of Amyotrophic Lateral Sclerosis. *The Journal of Neuroscience*, *23*(5), 1688-1696. doi: 10.1523/JNEUROSCI.23-05-01688.2003
- Dzhala, V. I., Talos, D. M., Sdrulla, D. A., Brumback, A. C., Mathews, G. C., Benke, T. A., . . . Staley, K. J. (2005). NKCC1 transporter facilitates seizures in the developing brain. *Nature Medicine*, *11*(11), 1205-1213. doi: 10.1038/nm1301
- Eccles, J. C., Eccles, R. M., Iggo, A., & Ito, M. (1961). Distribution of recurrent inhibition among motoneurons. *J Physiol*, *159*(3), 479-499. doi: 10.1113/jphysiol.1961.sp006822
- Eccles, J. C., Fatt, P., & Koketsu, K. (1954). Cholinergic and inhibitory synapses in a pathway from motor-axon collaterals to motoneurons. *The Journal of Physiology*, *126*(3), 524-562. doi: 10.1113/jphysiol.1954.sp005226
- Edstrom, L., & Kugelberg, E. (1968). Histochemical composition, distribution of fibres and fatiguability of single motor units. Anterior tibial muscle of the rat. *Journal of Neurology, Neurosurgery & Psychiatry*, *31*(5), 424-433. doi: 10.1136/jnnp.31.5.424
- Eisen, A., Braak, H., Del Tredici, K., Lemon, R., Ludolph, A. C., & Kiernan, M. C. (2017). Cortical influences drive amyotrophic lateral sclerosis. *Journal of Neurology, Neurosurgery & Psychiatry*, *88*(11), 917-924. doi: 10.1136/jnnp-2017-315573
- Eisen, A., Kiernan, M., Mitsumoto, H., & Swash, M. (2014a). Amyotrophic lateral sclerosis: a long preclinical period? *J Neurol Neurosurg Psychiatry*, *85*(11), 1232-1238. doi: 10.1136/jnnp-2013-307135
- Eisen, A., Kiernan, M., Mitsumoto, H., & Swash, M. (2014b). Amyotrophic lateral sclerosis: a long preclinical period? *Journal of Neurology, Neurosurgery & Psychiatry*, *85*(11), 1232-1238. doi: 10.1136/jnnp-2013-307135
- Eisen, A., Kim, S., & Pant, B. (1992). Amyotrophic lateral sclerosis (ALS): A phylogenetic disease of the corticomotoneuron? *Muscle & Nerve*, *15*(2), 219-224. doi: 10.1002/mus.880150215
- Ellgaard, L., & Frickel, E.-M. (2003). Calnexin, Calreticulin, and ERp57: Teammates in Glycoprotein Folding. *Cell Biochemistry and Biophysics*, *39*(3), 223-248. doi: 10.1385/CBB:39:3:223
- Ensini, M., Tsuchida, T. N., Belting, H. G., & Jessell, T. M. (1998). The control of rostrocaudal pattern in the developing spinal cord: specification of motor neuron subtype identity is initiated by signals from paraxial mesoderm. *Development*, *125*(6), 969-982. doi: 10.1242/dev.125.6.969
- Escartin, C., Galea, E., Lakatos, A., O'Callaghan, J. P., Petzold, G. C., Serrano-Pozo, A., . . . Verkhratsky, A. (2021). Reactive astrocyte nomenclature, definitions, and future directions. *Nat Neurosci*, *24*(3), 312-325. doi: 10.1038/s41593-020-00783-4
- Falgairolle, M., Puhl, J. G., Pujala, A., Liu, W., & O'Donovan, M. J. (2017). Motoneurons regulate the central pattern generator during drug-induced locomotor-like activity in the neonatal mouse. *eLife*, *6*, e26622. doi: 10.7554/eLife.26622

- Farrant, M., & Kaila, K. (2007). The cellular, molecular and ionic basis of GABA(A) receptor signalling. *Prog Brain Res*, *160*, 59-87. doi: 10.1016/S0079-6123(06)60005-8
- Farrant, M., & Nusser, Z. (2005). Variations on an inhibitory theme: phasic and tonic activation of GABAA receptors. *Nature Reviews Neuroscience*, *6*(3), 215-229. doi: 10.1038/nrn1625
- Feeney, S. J., McKelvie, P. A., Austin, L., Jean-Francois, M. J., Kapsa, R., Tombs, S. M., & Byrne, E. (2001). Presymptomatic motor neuron loss and reactive astrogliosis in the SOD1 mouse model of amyotrophic lateral sclerosis. *Muscle Nerve*, *24*(11), 1510-1519. doi: 10.1002/mus.1176
- Fetcho, J. R. (1987). A review of the organization and evolution of motoneurons innervating the axial musculature of vertebrates. *Brain Research Reviews*, *12*(3), 243-280. doi: 10.1016/0165-0173(87)90001-4
- Filipchuk, A. A., & Durand, J. (2012). Postnatal dendritic development in lumbar motoneurons in mutant superoxide dismutase 1 mouse model of amyotrophic lateral sclerosis. *Neuroscience*, *209*, 144-154. doi: 10.1016/j.neuroscience.2012.01.046
- Fischer, L. R., Culver, D. G., Tennant, P., Davis, A. A., Wang, M., Castellano-Sanchez, A., . . . Glass, J. D. (2004). Amyotrophic lateral sclerosis is a distal axonopathy: evidence in mice and man. *Experimental Neurology*, *185*(2), 232-240. doi: 10.1016/j.expneurol.2003.10.004
- Flint, A. C., Liu, X., & Kriegstein, A. R. (1998). Nonsynaptic Glycine Receptor Activation during Early Neocortical Development. *Neuron*, *20*(1), 43-53. doi: 10.1016/S0896-6273(00)80433-X
- Fogarty, M. (2019). Amyotrophic lateral sclerosis as a synaptopathy. *Neural Regeneration Research*, *14*(2), 189. doi: 10.4103/1673-5374.244782
- Fogarty, M. J., Noakes, P. G., & Bellingham, M. C. (2015). Motor Cortex Layer V Pyramidal Neurons Exhibit Dendritic Regression, Spine Loss, and Increased Synaptic Excitation in the Presymptomatic hSOD1<sup>G93A</sup> Mouse Model of Amyotrophic Lateral Sclerosis. *The Journal of Neuroscience*, *35*(2), 643-647. doi: 10.1523/JNEUROSCI.3483-14.2015
- Fornai, F., Longone, P., Cafaro, L., Katsiuchenka, O., Ferrucci, M., Manca, M. L., . . . Paparelli, A. (2008). Lithium delays progression of amyotrophic lateral sclerosis. *Proc Natl Acad Sci U S A*, *105*(6), 2052-2057. doi: 10.1073/pnas.0708022105
- Francius, C., & Clotman, F. (2010). Dynamic expression of the Onecut transcription factors HNF-6, OC-2 and OC-3 during spinal motor neuron development. *Neuroscience*, *165*(1), 116-129. doi: 10.1016/j.neuroscience.2009.09.076
- Francius, C., & Clotman, F. (2013). Generating spinal motor neuron diversity: a long quest for neuronal identity. *Cell Mol Life Sci*, *71*(5), 813-829. doi: 10.1007/s00018-013-1398-x
- Francius, C., Harris, A., Rucchin, V., Hendricks, T. J., Stam, F. J., Barber, M., . . . Clotman, F. (2013). Identification of multiple subsets of ventral interneurons and differential distribution along the rostrocaudal axis of the developing spinal cord. *PLoS One*, *8*(8), e70325. doi: 10.1371/journal.pone.0070325
- Fray, A. E., Ince, P. G., Banner, S. J., Milton, I. D., Usher, P. A., Cookson, M. R., & Shaw, P. J. (1998). The expression of the glial glutamate transporter protein EAAT2 in motor neuron disease: an immunohistochemical study: EAAT2 expression in motor neuron disease. *European Journal of Neuroscience*, *10*(8), 2481-2489. doi: 10.1046/j.1460-9568.1998.00273.x
- Frerking, M., Borges, S., & Wilson, M. (1997). Are some minis multiquantal? *J Neurophysiol*, *78*(3), 1293-1304. doi: 10.1152/jn.1997.78.3.1293

- Frey, D., Schneider, C., Xu, L., Borg, J., Spooren, W., & Caroni, P. (2000). Early and Selective Loss of Neuromuscular Synapse Subtypes with Low Sprouting Competence in Motoneuron Diseases. *The Journal of Neuroscience*, *20*(7), 2534-2542. doi: 10.1523/JNEUROSCI.20-07-02534.2000
- Friese, A., Kaltschmidt, J. A., Ladle, D. R., Sigrist, M., Jessell, T. M., & Arber, S. (2009). Gamma and alpha motor neurons distinguished by expression of transcription factor *Err3*. *Proceedings of the National Academy of Sciences*, *106*(32), 13588-13593. doi: 10.1073/pnas.0906809106
- Fritschy, J. M., & Panzanelli, P. (2014). GABAA receptors and plasticity of inhibitory neurotransmission in the central nervous system. *Eur J Neurosci*, *39*(11), 1845-1865. doi: 10.1111/ejn.12534
- Fuchs, A., Ringer, C., Bilkei-Gorzo, A., Weihe, E., Roeper, J., & Schütz, B. (2010). Downregulation of the Potassium Chloride Cotransporter KCC2 in Vulnerable Motoneurons in the SOD1-G93A Mouse Model of Amyotrophic Lateral Sclerosis. *Journal of Neuropathology & Experimental Neurology*, *69*(10), 1057-1070. doi: 10.1097/NEN.0b013e3181f4dcef
- Fyffe, R. E. (1991). Spatial distribution of recurrent inhibitory synapses on spinal motoneurons in the cat. *Journal of Neurophysiology*, *65*(5), 1134-1149. doi: 10.1152/jn.1991.65.5.1134
- Galeffi, F. (2004). Changes in Intracellular Chloride after Oxygen-Glucose Deprivation of the Adult Hippocampal Slice: Effect of Diazepam. *Journal of Neuroscience*, *24*(18), 4478-4488. doi: 10.1523/JNEUROSCI.0755-04.2004
- Gamba, G. (2005). Molecular Physiology and Pathophysiology of Electroneutral Cation-Chloride Cotransporters. *Physiological Reviews*, *85*(2), 423-493. doi: 10.1152/physrev.00011.2004
- Gao, B.-X., Cheng, G., & Ziskind-Conhaim, L. (1998). Development of Spontaneous Synaptic Transmission in the Rat Spinal Cord. *Journal of Neurophysiology*, *79*(5), 2277-2287. doi: 10.1152/jn.1998.79.5.2277
- Gao, B.-X., Stricker, C., & Ziskind-Conhaim, L. (2001). Transition From GABAergic to Glycinergic Synaptic Transmission in Newly Formed Spinal Networks. *Journal of Neurophysiology*, *86*(1), 492-502. doi: 10.1152/jn.2001.86.1.492
- Gao, B. X., & Ziskind-Conhaim, L. (1995). Development of glycine- and GABA-gated currents in rat spinal motoneurons. *Journal of Neurophysiology*, *74*(1), 113-121. doi: 10.1152/jn.1995.74.1.113
- Gao, B. X., & Ziskind-Conhaim, L. (1998). Development of ionic currents underlying changes in action potential waveforms in rat spinal motoneurons. *J Neurophysiol*, *80*(6), 3047-3061. doi: 10.1152/jn.1998.80.6.3047
- Gardiner, P. F. (1993). Physiological properties of motoneurons innervating different muscle unit types in rat gastrocnemius. *Journal of Neurophysiology*, *69*(4), 1160-1170. doi: 10.1152/jn.1993.69.4.1160
- Garifulina, A., Friesacher, T., Stadler, M., Zangerl-Plessl, E. M., Ernst, M., Stary-Weinzinger, A., . . . Hering, S. (2022). beta subunits of GABAA receptors form proton-gated chloride channels: Insights into the molecular basis. *Commun Biol*, *5*(1), 784. doi: 10.1038/s42003-022-03720-2
- Garofalo, S., Coccozza, G., Bernardini, G., Savage, J., Raspa, M., Aronica, E., . . . Limatola, C. (2022). Blocking immune cell infiltration of the central nervous system to tame Neuroinflammation in Amyotrophic lateral sclerosis. *Brain Behav Immun*, *105*, 1-14. doi: 10.1016/j.bbi.2022.06.004

- Gatto, R. G., Li, W., & Magin, R. L. (2018). Diffusion tensor imaging identifies presymptomatic axonal degeneration in the spinal cord of ALS mice. *Brain Research*, 1679, 45-52. doi: 10.1016/j.brainres.2017.11.017
- Gatto, R. G., Mustafi, S. M., Amin, M. Y., Mareci, T. H., Wu, Y. C., & Magin, R. L. (2018). Neurite orientation dispersion and density imaging can detect presymptomatic axonal degeneration in the spinal cord of ALS mice. *Funct Neurol*, 33(3), 155-163.
- Ge, S., Goh, E. L. K., Sailor, K. A., Kitabatake, Y., Ming, G.-l., & Song, H. (2006). GABA regulates synaptic integration of newly generated neurons in the adult brain. *Nature*, 439(7076), 589-593. doi: 10.1038/nature04404
- Geevasinga, N., Howells, J., Menon, P., van den Bos, M., Shibuya, K., Matamala, J. M., . . . Vucic, S. (2019). Amyotrophic lateral sclerosis diagnostic index: Toward a personalized diagnosis of ALS. *Neurology*, 92(6), e536-e547. doi: 10.1212/WNL.00000000000006876
- Geevasinga, N., Menon, P., Özdinler, P. H., Kiernan, M. C., & Vucic, S. (2016). Pathophysiological and diagnostic implications of cortical dysfunction in ALS. *Nature Reviews Neurology*, 12(11), 651-661. doi: 10.1038/nrneurol.2016.140
- Geloso, M. C., Corvino, V., Marchese, E., Serrano, A., Michetti, F., & D'Ambrosi, N. (2017). The Dual Role of Microglia in ALS: Mechanisms and Therapeutic Approaches. *Frontiers in Aging Neuroscience*, 9, 242. doi: 10.3389/fnagi.2017.00242
- Gillingwater, T. H., & Wishart, T. M. (2013). Mechanisms underlying synaptic vulnerability and degeneration in neurodegenerative disease: Mechanisms of synapse degeneration. *Neuropathology and Applied Neurobiology*, 39(4), 320-334. doi: 10.1111/nan.12014
- Glickfeld, L. L., Roberts, J. D., Somogyi, P., & Scanziani, M. (2009). Interneurons hyperpolarize pyramidal cells along their entire somatodendritic axis. *Nat Neurosci*, 12(1), 21-23. doi: 10.1038/nn.2230
- Glover, J. C. (2000). Development of Specific Connectivity Between Premotor Neurons and Motoneurons in the Brain Stem and Spinal Cord. *Physiological Reviews*, 80(2), 615-647. doi: 10.1152/physrev.2000.80.2.615
- Glykys, J., Dzhala, V., Egawa, K., Balena, T., Saponjian, Y., Kuchibhotla, K. V., . . . Staley, K. J. (2014). <+Glykys et al. Science2014\_localImpermantAnions.pdf>. *Science*.
- Glykys, J., Dzhala, V., Egawa, K., Kahle, K. T., Delpire, E., & Staley, K. (2017). Chloride Dysregulation, Seizures, and Cerebral Edema: A Relationship with Therapeutic Potential. *Trends in Neurosciences*, 40(5), 276-294. doi: 10.1016/j.tins.2017.03.006
- Gonzalez-Forero, D., & Alvarez, F. J. (2005). Differential postnatal maturation of GABAA, glycine receptor, and mixed synaptic currents in Renshaw cells and ventral spinal interneurons. *J Neurosci*, 25(8), 2010-2023. doi: 10.1523/JNEUROSCI.2383-04.2005
- Gosgnach, S. (2022). Synaptic connectivity amongst components of the locomotor central pattern generator. *Front Neural Circuits*, 16, 1076766. doi: 10.3389/fncir.2022.1076766
- Gosgnach, S., Lanuza, G. M., Butt, S. J., Saueressig, H., Zhang, Y., Velasquez, T., . . . Goulding, M. (2006). V1 spinal neurons regulate the speed of vertebrate locomotor outputs. *Nature*, 440(7081), 215-219. doi: 10.1038/nature04545
- Goubert, E., Altwater, M., Rovira, M. N., Khalilov, I., Mazzarino, M., Sebastiani, A., . . . Pellegrino, C. (2019). Bumetanide Prevents Brain Trauma-Induced Depressive-Like Behavior. *Front Mol Neurosci*, 12, 12. doi: 10.3389/fnmol.2019.00012
- Goulding, M. (2009). Circuits controlling vertebrate locomotion: moving in a new direction. *Nat Rev Neurosci*, 10(7), 507-518. doi: 10.1038/nrn2608
- Gravel, M., Béland, L.-C., Soucy, G., Abdelhamid, E., Rahimian, R., Gravel, C., & Kriz, J. (2016). IL-10 Controls Early Microglial Phenotypes and Disease Onset in ALS

- Caused by Misfolded Superoxide Dismutase 1. *The Journal of Neuroscience*, 36(3), 1031-1048. doi: 10.1523/JNEUROSCI.0854-15.2016
- Gunes, Z. I., Kan, V. W. Y., Ye, X., & Liebscher, S. (2020). Exciting Complexity: The Role of Motor Circuit Elements in ALS Pathophysiology. *Frontiers in Neuroscience*, 14, 573. doi: 10.3389/fnins.2020.00573
- Gurney, M. E. (1997). The use of transgenic mouse models of amyotrophic lateral sclerosis in preclinical drug studies. *Journal of the Neurological Sciences*, 152, s67-s73. doi: 10.1016/S0022-510X(97)00247-5
- Gurney, M. E., Pu, H., Chiu, A. Y., Dal Canto, M. C., Polchow, C. Y., Alexander, D. D., . . . et al. (1994). Motor neuron degeneration in mice that express a human Cu,Zn superoxide dismutase mutation. *Science*, 264(5166), 1772-1775. doi: 10.1126/science.8209258
- Gurney, M. E., Pu, H. F., Chiu, A. Y., Dalcanto, M. C., Polchow, C. Y., Alexander, D. D., . . . Siddique, T. (1994). Motor-Neuron Degeneration in Mice That Express a Human Cu,Zn Superoxide-Dismutase Mutation. *Science*, 264(5166), 1772-1775. doi: DOI 10.1126/science.8209258
- Gustafson, M. P., Staff, N. P., Bornschlegl, S., Butler, G. W., Maas, M. L., Kazamel, M., . . . Dietz, A. B. (2017). Comprehensive immune profiling reveals substantial immune system alterations in a subset of patients with amyotrophic lateral sclerosis. *PLOS ONE*, 12(7), e0182002. doi: 10.1371/journal.pone.0182002
- Gutman, C. R., Ajmera, M. K., & Hollyday, M. (1993). Organization of motor pools supplying axial muscles in the chicken. *Brain Research*, 609(1-2), 129-136. doi: 10.1016/0006-8993(93)90865-K
- Hadzipasic, M., Tahvildari, B., Nagy, M., Bian, M., Horwich, A. L., & McCormick, D. A. (2014). Selective degeneration of a physiological subtype of spinal motor neuron in mice with SOD1-linked ALS. *Proceedings of the National Academy of Sciences*, 111(47), 16883-16888. doi: 10.1073/pnas.1419497111
- Hamann, M., Rossi, D. J., & Attwell, D. (2002). Tonic and spillover inhibition of granule cells control information flow through cerebellar cortex. *Neuron*, 33(4), 625-633. doi: 10.1016/s0896-6273(02)00593-7
- Hao, J., Wang, X. D., Dan, Y., Poo, M. M., & Zhang, X. H. (2009). An arithmetic rule for spatial summation of excitatory and inhibitory inputs in pyramidal neurons. *Proc Natl Acad Sci U S A*, 106(51), 21906-21911. doi: 10.1073/pnas.0912022106
- Hao, Z., Liu, L., Tao, Z., Wang, R., Ren, H., Sun, H., . . . Wang, G. (2019). Motor dysfunction and neurodegeneration in a C9orf72 mouse line expressing poly-PR. *Nat Commun*, 10(1), 2906. doi: 10.1038/s41467-019-10956-w
- Harikrishnareddy, D., Misra, S., Upadhyay, S., Modi, M., & Medhi, B. (2015). Roots to start research in amyotrophic lateral sclerosis: molecular pathways and novel therapeutics for future. *Rev Neurosci*, 26(2), 161-181. doi: 10.1515/revneuro-2014-0057
- Hartmann, A. M., & Nothwang, H. G. (2014). Molecular and evolutionary insights into the structural organization of cation chloride cotransporters. *Front Cell Neurosci*, 8, 470. doi: 10.3389/fncel.2014.00470
- Heath, P. R., & Shaw, P. J. (2002). Update on the glutamatergic neurotransmitter system and the role of excitotoxicity in amyotrophic lateral sclerosis. *Muscle & Nerve*, 26(4), 438-458. doi: 10.1002/mus.10186
- Heckman, C. J., & Enoka, R. M. (2012). Motor Unit. In R. Terjung (Ed.), *Comprehensive Physiology* (1 ed., pp. 2629-2682): Wiley.
- Hegedus, J., Putman, C. T., & Gordon, T. (2007). Time course of preferential motor unit loss in the SOD1G93A mouse model of amyotrophic lateral sclerosis. *Neurobiology of Disease*, 28(2), 154-164. doi: 10.1016/j.nbd.2007.07.003

- Henneman, E. (1957). Relation between Size of Neurons and Their Susceptibility to Discharge. *Science*, *126*(3287), 1345-1347. doi: 10.1126/science.126.3287.1345
- Henneman, E. (1985). The size-principle: a deterministic output emerges from a set of probabilistic connections. *Journal of Experimental Biology*, *115*(1), 105-112. doi: 10.1242/jeb.115.1.105
- Henstridge, C. M., Sideris, D. I., Carroll, E., Rotariu, S., Salomonsson, S., Tzioras, M., . . . Spires-Jones, T. L. (2018). Synapse loss in the prefrontal cortex is associated with cognitive decline in amyotrophic lateral sclerosis. *Acta Neuropathologica*, *135*(2), 213-226. doi: 10.1007/s00401-017-1797-4
- Herbst, R. (2020). MuSK function during health and disease. *Neuroscience Letters*, *716*, 134676. doi: 10.1016/j.neulet.2019.134676
- Hesser, B. A., Henschel, O., & Witzemann, V. (2006). Synapse disassembly and formation of new synapses in postnatal muscle upon conditional inactivation of MuSK. *Molecular and Cellular Neuroscience*, *31*(3), 470-480. doi: 10.1016/j.mcn.2005.10.020
- Heubl, M., Zhang, J., Pressey, J. C., Al Awabdh, S., Renner, M., Gomez-Castro, F., . . . Levi, S. (2017). GABA(A) receptor dependent synaptic inhibition rapidly tunes KCC2 activity via the Cl(-)-sensitive WNK1 kinase. *Nat Commun*, *8*(1), 1776. doi: 10.1038/s41467-017-01749-0
- Heubl, M., Zhang, J., Pressey, J. C., Al Awabdh, S., Renner, M., Gomez-Castro, F., . . . Lévi, S. (2017). GABAA receptor dependent synaptic inhibition rapidly tunes KCC2 activity via the Cl(-)-sensitive WNK1 kinase. *Nature Communications*, *8*(1), 1776. doi: 10.1038/s41467-017-01749-0
- Hevers, W., & Lüddens, H. (1998). The diversity of GABAA receptors: Pharmacological and electrophysiological properties of GABAA channel subtypes. *Molecular Neurobiology*, *18*(1), 35-86. doi: 10.1007/BF02741459
- Hinckley, C. A., Hartley, R., Wu, L., Todd, A., & Ziskind-Conhaim, L. (2005). Locomotor-like rhythms in a genetically distinct cluster of interneurons in the mammalian spinal cord. *J Neurophysiol*, *93*(3), 1439-1449. doi: 10.1152/jn.00647.2004
- Hines, M. L., & Carnevale, N. T. (1997). The NEURON simulation environment. *Neural Comput*, *9*(6), 1179-1209.
- Hines, M. L., & Carnevale, N. T. (2001). NEURON: a tool for neuroscientists. *Neuroscientist*, *7*(2), 123-135. doi: 10.1177/107385840100700207
- Hollyday, M., & Hamburger, V. (1977). An autoradiographic study of the formation of the lateral motor column in the chick embryo. *Brain Research*, *132*(2), 197-208. doi: 10.1016/0006-8993(77)90416-4
- Hollyday, M., & Jacobson, R. D. (1990). Location of motor pools innervating chick wing. *The Journal of Comparative Neurology*, *302*(3), 575-588. doi: 10.1002/cne.903020313
- Hooten, K. G., Beers, D. R., Zhao, W., & Appel, S. H. (2015). Protective and Toxic Neuroinflammation in Amyotrophic Lateral Sclerosis. *Neurotherapeutics*, *12*(2), 364-375. doi: 10.1007/s13311-014-0329-3
- Horn, S., Quasthoff, S., Grafe, P., Bostock, H., Renner, R., & Schrank, B. (1996). Abnormal axonal inward rectification in diabetic neuropathy. *Muscle & Nerve*, *19*(10), 1268-1275. doi: 10.1002/mus.880191002
- Hossaini, M., Cardona Cano, S., van Dis, V., Haasdijk, E. D., Hoogenraad, C. C., Holstege, J. C., & Jaarsma, D. (2011). Spinal inhibitory interneuron pathology follows motor neuron degeneration independent of glial mutant superoxide dismutase 1 expression in SOD1-ALS mice. *J Neuropathol Exp Neurol*, *70*(8), 662-677. doi: 10.1097/NEN.0b013e31822581ac

- Hossaini, M., French, P. J., & Holstege, J. C. (2007). Distribution of glycinergic neuronal somata in the rat spinal cord. *Brain Research*, 1142, 61-69. doi: 10.1016/j.brainres.2007.01.078
- Houston, C. M., Bright, D. P., Sivilotti, L. G., Beato, M., & Smart, T. G. (2009a). Intracellular chloride ions regulate the time course of GABA-mediated inhibitory synaptic transmission. *J Neurosci*, 29(33), 10416-10423. doi: 10.1523/JNEUROSCI.1670-09.2009
- Houston, C. M., Bright, D. P., Sivilotti, L. G., Beato, M., & Smart, T. G. (2009b). Intracellular Chloride Ions Regulate the Time Course of GABA-Mediated Inhibitory Synaptic Transmission. *Journal of Neuroscience*, 29(33), 10416-10423. doi: 10.1523/JNEUROSCI.1670-09.2009
- Howells, J., Matamala, J. M., Park, S. B., Garg, N., Vucic, S., Bostock, H., . . . Kiernan, M. C. (2018). *In vivo* evidence for reduced ion channel expression in motor axons of patients with amyotrophic lateral sclerosis: Reduced ion channel expression in amyotrophic lateral sclerosis. *The Journal of Physiology*, 596(22), 5379-5396. doi: 10.1113/JP276624
- Hughes, D. I., Mackie, M., Nagy, G. G., Riddell, J. S., Maxwell, D. J., Szabó, G., . . . Todd, A. J. (2005). P boutons in lamina IX of the rodent spinal cord express high levels of glutamic acid decarboxylase-65 and originate from cells in deep medial dorsal horn. *Proceedings of the National Academy of Sciences*, 102(25), 9038-9043. doi: 10.1073/pnas.0503646102
- Huh, S., Heckman, C. J., & Manuel, M. (2021). Time Course of Alterations in Adult Spinal Motoneuron Properties in the SOD1(G93A) Mouse Model of ALS. *eNeuro*, 8(2). doi: 10.1523/ENEURO.0378-20.2021
- Hultborn, H., Denton, M. E., Wienecke, J., & Nielsen, J. B. (2003). Variable amplification of synaptic input to cat spinal motoneurons by dendritic persistent inward current. *The Journal of Physiology*, 552(3), 945-952. doi: 10.1113/jphysiol.2003.050971
- Hultborn, H., Lindström, S., & Wigström, H. (1979). On the function of recurrent inhibition in the spinal cord. *Experimental Brain Research*, 37(2). doi: 10.1007/BF00237722
- Hung, C., & Chen, J. W. Y. (2012). Treatment of Post-Traumatic Epilepsy. *Current Treatment Options in Neurology*, 14(4), 293-306. doi: 10.1007/s11940-012-0178-5
- Hurtado, E., Cilleros, V., Nadal, L., Simo, A., Obis, T., Garcia, N., . . . Tomas, J. (2017). Muscle Contraction Regulates BDNF/TrkB Signaling to Modulate Synaptic Function through Presynaptic cPKC $\alpha$  and cPKC $\beta$ . *Front Mol Neurosci*, 10, 147. doi: 10.3389/fnmol.2017.00147
- Ikemoto, A., Akiguchi, I., Hirano, A., & Nakamura, S. (2002). Differential expression between synaptic vesicle proteins and presynaptic plasma membrane proteins in the anterior horn of amyotrophic lateral sclerosis. *Acta Neuropathologica*, 103(2), 179-187. doi: 10.1007/s004010100449
- Ishigaki, S., & Sobue, G. (2018). Importance of Functional Loss of FUS in FTL/ALS. *Front Mol Biosci*, 5, 44. doi: 10.3389/fmolb.2018.00044
- Jaarsma, D., Teuling, E., Haasdijk, E. D., De Zeeuw, C. I., & Hoogenraad, C. C. (2008). Neuron-Specific Expression of Mutant Superoxide Dismutase Is Sufficient to Induce Amyotrophic Lateral Sclerosis in Transgenic Mice. *Journal of Neuroscience*, 28(9), 2075-2088. doi: 10.1523/JNEUROSCI.5258-07.2008
- Jacobson, S., & Marcus, E. M. (2008). *Neuroanatomy for the Neuroscientist*. Boston, MA: Springer US.
- Jankowska, E. (2008). Spinal interneuronal networks in the cat: elementary components. *Brain Res Rev*, 57(1), 46-55. doi: 10.1016/j.brainresrev.2007.06.022

- Je, H. S., Yang, F., Ji, Y., Nagappan, G., Hempstead, B. L., & Lu, B. (2012). Role of pro-brain-derived neurotrophic factor (proBDNF) to mature BDNF conversion in activity-dependent competition at developing neuromuscular synapses. *Proc Natl Acad Sci U S A*, *109*(39), 15924-15929. doi: 10.1073/pnas.1207767109
- Jean-Xavier, C., Mentis, G. Z., O'Donovan, M. J., Cattaert, D., & Vinay, L. (2007). Dual personality of GABA/glycine-mediated depolarizations in immature spinal cord. *Proc Natl Acad Sci U S A*, *104*(27), 11477-11482. doi: 10.1073/pnas.0704832104
- Jean-Xavier, C., Pflieger, J. F., Liabeuf, S., & Vinay, L. (2006). Inhibitory postsynaptic potentials in lumbar motoneurons remain depolarizing after neonatal spinal cord transection in the rat. *J Neurophysiol*, *96*(5), 2274-2281. doi: 10.1152/jn.00328.2006
- Jentsch, T. J. (2016). VRACs and other ion channels and transporters in the regulation of cell volume and beyond. *Nature Reviews Molecular Cell Biology*, *17*(5), 293-307. doi: 10.1038/nrm.2016.29
- Jessell, T. M. (2000). Neuronal specification in the spinal cord: inductive signals and transcriptional codes. *Nature Reviews Genetics*, *1*(1), 20-29. doi: 10.1038/35049541
- Jha, M. K., Jo, M., Kim, J.-H., & Suk, K. (2019). Microglia-Astrocyte Crosstalk: An Intimate Molecular Conversation. *The Neuroscientist*, *25*(3), 227-240. doi: 10.1177/1073858418783959
- Jin, X., Huguenard, J. R., & Prince, D. A. (2005). Impaired Cl<sup>-</sup> Extrusion in Layer V Pyramidal Neurons of Chronically Injured Epileptogenic Neocortex. *Journal of Neurophysiology*, *93*(4), 2117-2126. doi: 10.1152/jn.00728.2004
- Jonas, P., Bischofberger, J., & Sandkühler, J. (1998). Corelease of Two Fast Neurotransmitters at a Central Synapse. *Science*, *281*(5375), 419-424. doi: 10.1126/science.281.5375.419
- Jones, M. V., & Westbrook, G. L. (1995). Desensitized states prolong GABAA channel responses to brief agonist pulses. *Neuron*, *15*(1), 181-191. doi: 10.1016/0896-6273(95)90075-6
- Jones, S. M., & Palmer, M. J. (2009). Activation of the tonic GABAC receptor current in retinal bipolar cell terminals by nonvesicular GABA release. *J Neurophysiol*, *102*(2), 691-699. doi: 10.1152/jn.00285.2009
- Jonsson, P. A., Graffmo, K. S., Brännström, T., Nilsson, P., Andersen, P. M., & Marklund, S. L. (2006). Motor Neuron Disease in Mice Expressing the Wild Type-Like D90A Mutant Superoxide Dismutase-1. *Journal of Neuropathology and Experimental Neurology*, *65*(12), 1126-1136. doi: 10.1097/01.jnen.0000248545.36046.3c
- Joyce, N. C., & Carter, G. T. (2013). Electrodiagnosis in Persons With Amyotrophic Lateral Sclerosis. *PM&R*, *5*, S89-S95. doi: 10.1016/j.pmrj.2013.03.020
- Kabashi, E., Valdmanis, P. N., Dion, P., Spiegelman, D., McConkey, B. J., Vande Velde, C., . . . Rouleau, G. A. (2008). TARDBP mutations in individuals with sporadic and familial amyotrophic lateral sclerosis. *Nat Genet*, *40*(5), 572-574. doi: 10.1038/ng.132
- Kahle, K. T., Staley, K. J., Nahed, B. V., Gamba, G., Hebert, S. C., Lifton, R. P., & Mount, D. B. (2008). Roles of the cation-chloride cotransporters in neurological disease. *Nat Clin Pract Neurol*, *4*(9), 490-503. doi: 10.1038/ncpneuro0883
- Kaila, K., Voipio, J., Paalasmaa, P., Pasternack, M., & Deisz, R. A. (1993). The role of bicarbonate in GABAA receptor-mediated IPSPs of rat neocortical neurones. *J Physiol*, *464*, 273-289. doi: 10.1113/jphysiol.1993.sp019634
- Kanai, K., Kuwabara, S., Misawa, S., Tamura, N., Ogawara, K., Nakata, M., . . . Bostock, H. (2006). Altered axonal excitability properties in amyotrophic lateral sclerosis: impaired potassium channel function related to disease stage. *Brain*, *129*(4), 953-962. doi: 10.1093/brain/aw1024

- Kaneda, M., Farrant, M., & Cull-Candy, S. G. (1995). Whole-cell and single-channel currents activated by GABA and glycine in granule cells of the rat cerebellum. *The Journal of Physiology*, *485*(2), 419-435. doi: 10.1113/jphysiol.1995.sp020739
- Kang, S. H., Li, Y., Fukaya, M., Lorenzini, I., Cleveland, D. W., Ostrow, L. W., . . . Bergles, D. E. (2013). Degeneration and impaired regeneration of gray matter oligodendrocytes in amyotrophic lateral sclerosis. *Nature Neuroscience*, *16*(5), 571-579. doi: 10.1038/nn.3357
- Kanning, K. C., Kaplan, A., & Henderson, C. E. (2010). Motor Neuron Diversity in Development and Disease. *Annual Review of Neuroscience*, *33*(1), 409-440. doi: 10.1146/annurev.neuro.051508.135722
- Kaplan, A., Spiller, K. J., Towne, C., Kanning, K. C., Choe, G. T., Geber, A., . . . Henderson, C. E. (2014). Neuronal matrix metalloproteinase-9 is a determinant of selective neurodegeneration. *Neuron*, *81*(2), 333-348. doi: 10.1016/j.neuron.2013.12.009
- Kaur, S. J., McKeown, S. R., & Rashid, S. (2016). Mutant SOD1 mediated pathogenesis of Amyotrophic Lateral Sclerosis. *Gene*, *577*(2), 109-118. doi: 10.1016/j.gene.2015.11.049
- Keon, M., Musrie, B., Dinger, M., Brennan, S. E., Santos, J., & Saksena, N. K. (2021). Destination Amyotrophic Lateral Sclerosis. *Front Neurol*, *12*, 596006. doi: 10.3389/fneur.2021.596006
- Kernell, D. (2006). *The Motoneurone and its Muscle Fibres*: Oxford University Press UK.
- Kiehn, O. (2011). Development and functional organization of spinal locomotor circuits. *Curr Opin Neurobiol*, *21*(1), 100-109. doi: 10.1016/j.conb.2010.09.004
- Kiehn, O. (2016). Decoding the organization of spinal circuits that control locomotion. *Nature Reviews Neuroscience*, *17*(4), 224-238. doi: 10.1038/nrn.2016.9
- Kiehn, O. (2016). Decoding the organization of spinal circuits that control locomotion. *Nat Rev Neurosci*, *17*(4), 224-238. doi: 10.1038/nrn.2016.9
- Kieran, D., Hafezparast, M., Bohnert, S., Dick, J. R. T., Martin, J., Schiavo, G., . . . Greensmith, L. (2005). A mutation in dynein rescues axonal transport defects and extends the life span of ALS mice. *Journal of Cell Biology*, *169*(4), 561-567. doi: 10.1083/jcb.200501085
- Kiernan, M. C., Vucic, S., Cheah, B. C., Turner, M. R., Eisen, A., Hardiman, O., . . . Zoing, M. C. (2011). Amyotrophic lateral sclerosis. *The Lancet*, *377*(9769), 942-955. doi: 10.1016/s0140-6736(10)61156-7
- Kiernan, M. C., Vucic, S., Cheah, B. C., Turner, M. R., Eisen, A., Hardiman, O., . . . Zoing, M. C. (2011). Amyotrophic lateral sclerosis. *Lancet*, *377*(9769), 942-955. doi: 10.1016/s0140-6736(10)61156-7
- Kiernan, M. C., Ziemann, U., & Eisen, A. (2019). Amyotrophic lateral sclerosis: Origins traced to impaired balance between neural excitation and inhibition in the neonatal period. *Muscle Nerve*, *60*(3), 232-235. doi: 10.1002/mus.26617
- King, A. E., Dickson, T. C., Blizzard, C. A., Foster, S. S., Chung, R. S., West, A. K., . . . Vickers, J. C. (2007). Excitotoxicity mediated by non-NMDA receptors causes distal axonopathy in long-term cultured spinal motor neurons: Excitotoxicity causes axonopathy in spinal neurons. *European Journal of Neuroscience*, *26*(8), 2151-2159. doi: 10.1111/j.1460-9568.2007.05845.x
- Kirsch, J. (2006). Glycinergic transmission. *Cell and Tissue Research*, *326*(2), 535-540. doi: 10.1007/s00441-006-0261-x
- Kjaerulff, O., & Kiehn, O. (1996). Distribution of networks generating and coordinating locomotor activity in the neonatal rat spinal cord in vitro: a lesion study. *J Neurosci*, *16*(18), 5777-5794. doi: 10.1523/JNEUROSCI.16-18-05777.1996

- Kneussel, M., & Betz, H. (2000). Clustering of inhibitory neurotransmitter receptors at developing postsynaptic sites: the membrane activation model. *Trends in Neurosciences*, 23(9), 429-435. doi: 10.1016/S0166-2236(00)01627-1
- Kong, X. C., Barzaghi, P., & Ruegg, M. A. (2004). Inhibition of synapse assembly in mammalian muscle *in vivo* by RNA interference. *EMBO reports*, 5(2), 183-188. doi: 10.1038/sj.embor.7400065
- Kostera-Pruszczyk, A., Niebroj-Dobosz, I., Emeryk-Szajewska, B., Karwańska, A., & Rowińska-Marcińska, K. (2002). Motor unit hyperexcitability in amyotrophic lateral sclerosis vs amino acids acting as neurotransmitters: Motor unit hyperexcitability and amino acids in ALS. *Acta Neurologica Scandinavica*, 106(1), 34-38. doi: 10.1034/j.1600-0404.2002.00149.x
- Kotak, V. C., Korada, S., Schwartz, I. R., & Sanes, D. H. (1998). A Developmental Shift from GABAergic to Glycinergic Transmission in the Central Auditory System. *The Journal of Neuroscience*, 18(12), 4646-4655. doi: 10.1523/JNEUROSCI.18-12-04646.1998
- Kuo, J. J., Schonewille, M., Siddique, T., Schults, A. N., Fu, R., Bar, P. R., . . . Kroese, A. B. (2004). Hyperexcitability of cultured spinal motoneurons from presymptomatic ALS mice. *J Neurophysiol*, 91(1), 571-575.
- Kuo, J. J., Schonewille, M., Siddique, T., Schults, A. N. A., Fu, R., Bär, P. R., . . . Kroese, A. B. A. (2004). Hyperexcitability of Cultured Spinal Motoneurons From Presymptomatic ALS Mice. *Journal of Neurophysiology*, 91(1), 571-575. doi: 10.1152/jn.00665.2003
- Kuo, J. J., Siddique, T., Fu, R., & Heckman, C. J. (2005). Increased persistent Na<sup>+</sup> current and its effect on excitability in motoneurons cultured from mutant SOD1 mice: Persistent Na<sup>+</sup> current in mutant SOD1 mice. *The Journal of Physiology*, 563(3), 843-854. doi: 10.1113/jphysiol.2004.074138
- Kurbatova, P., Wendling, F., Kaminska, A., Rosati, A., Nabbout, R., Guerrini, R., . . . Benquet, P. (2016). Dynamic changes of depolarizing GABA in a computational model of epileptogenic brain: Insight for Dravet syndrome. *Exp Neurol*, 283(Pt A), 57-72. doi: 10.1016/j.expneurol.2016.05.037
- Lagier-Tourenne, C., Polymenidou, M., & Cleveland, D. W. (2010). TDP-43 and FUS/TLS: emerging roles in RNA processing and neurodegeneration. *Hum Mol Genet*, 19(R1), R46-64. doi: 10.1093/hmg/ddq137
- Langosch, D., Thomas, L., & Betz, H. (1988). Conserved quaternary structure of ligand-gated ion channels: the postsynaptic glycine receptor is a pentamer. *Proceedings of the National Academy of Sciences*, 85(19), 7394-7398. doi: 10.1073/pnas.85.19.7394
- Lanuza, G. M., Gosgnach, S., Pierani, A., Jessell, T. M., & Goulding, M. (2004). Genetic identification of spinal interneurons that coordinate left-right locomotor activity necessary for walking movements. *Neuron*, 42(3), 375-386. doi: 10.1016/s0896-6273(04)00249-1
- Le, N. T. T., Chang, L., Kovlyagina, I., Georgiou, P., Safren, N., Braunstein, K. E., . . . Monteiro, M. J. (2016). Motor neuron disease, TDP-43 pathology, and memory deficits in mice expressing ALS-FTD-linked *UBQLN2* mutations. *Proceedings of the National Academy of Sciences*, 113(47). doi: 10.1073/pnas.1608432113
- Lee, J. D., Kumar, V., Fung, J. N. T., Ruitenber, M. J., Noakes, P. G., & Woodruff, T. M. (2017). Pharmacological inhibition of complement C5a-C5a<sub>1</sub> receptor signalling ameliorates disease pathology in the hSOD1<sup>G93A</sup> mouse model of amyotrophic lateral sclerosis: C5a<sub>1</sub> receptor antagonism is protective in ALS mice. *British Journal of Pharmacology*, 174(8), 689-699. doi: 10.1111/bph.13730
- Legendre, P. (2001a). The glycinergic inhibitory synapse. *Cell Mol Life Sci*, 58(5-6), 760-793. doi: 10.1007/pl00000899

- Legendre, P. (2001b). The glycinergic inhibitory synapse. *Cellular and Molecular Life Sciences*, 58(5), 760-793. doi: 10.1007/PL00000899
- Leonzino, M., Busnelli, M., Antonucci, F., Verderio, C., Mazzanti, M., & Chini, B. (2016). The Timing of the Excitatory-to-Inhibitory GABA Switch Is Regulated by the Oxytocin Receptor via KCC2. *Cell Reports*, 15(1), 96-103. doi: 10.1016/j.celrep.2016.03.013
- Lepeta, K., Lourenco, M. V., Schweitzer, B. C., Martino Adami, P. V., Banerjee, P., Catuara-Solarz, S., . . . Seidenbecher, C. (2016). Synaptopathies: synaptic dysfunction in neurological disorders - A review from students to students. *Journal of Neurochemistry*, 138(6), 785-805. doi: 10.1111/jnc.13713
- Lepore, E., Casola, I., Dobrowolny, G., & Musarò, A. (2019). Neuromuscular Junction as an Entity of Nerve-Muscle Communication. *Cells*, 8(8), 906. doi: 10.3390/cells8080906
- Leroy, F., Lamotte d'Incamps, B., Imhoff-Manuel, R. D., & Zytnicki, D. (2014). Early intrinsic hyperexcitability does not contribute to motoneuron degeneration in amyotrophic lateral sclerosis. *Elife*, 3. doi: 10.7554/eLife.04046
- Li, Y., Osuma, A., Correa, E., Okebalama, M. A., Dao, P., Gaylord, O., . . . Kratsios, P. (2020). Establishment and maintenance of motor neuron identity via temporal modularity in terminal selector function. *eLife*, 9, e59464. doi: 10.7554/eLife.59464
- Liao, B., Zhao, W., Beers, D. R., Henkel, J. S., & Appel, S. H. (2012). Transformation from a neuroprotective to a neurotoxic microglial phenotype in a mouse model of ALS. *Experimental Neurology*, 237(1), 147-152. doi: 10.1016/j.expneurol.2012.06.011
- Lim, R., Alvarez, F. J., & Walmsley, B. (1999). Quantal size is correlated with receptor cluster area at glycinergic synapses in the rat brainstem. *J Physiol*, 516 ( Pt 2)(Pt 2), 505-512. doi: 10.1111/j.1469-7793.1999.0505v.x
- Lin, C.-L. G., Bristol, L. A., Jin, L., Dykes-Hoberg, M., Crawford, T., Clawson, L., & Rothstein, J. D. (1998). Aberrant RNA Processing in a Neurodegenerative Disease: the Cause for Absent EAAT2, a Glutamate Transporter, in Amyotrophic Lateral Sclerosis. *Neuron*, 20(3), 589-602. doi: 10.1016/S0896-6273(00)80997-6
- Lino, M. M., Schneider, C., & Caroni, P. (2002). Accumulation of SOD1 mutants in postnatal motoneurons does not cause motoneuron pathology or motoneuron disease. *J Neurosci*, 22(12), 4825-4832.
- Loeffler, J. P., Picchiarelli, G., Dupuis, L., & Gonzalez De Aguilar, J. L. (2016). The Role of Skeletal Muscle in Amyotrophic Lateral Sclerosis. *Brain Pathology*, 26(2), 227-236. doi: 10.1111/bpa.12350
- Longinetti, E., & Fang, F. (2019). Epidemiology of amyotrophic lateral sclerosis: an update of recent literature. *Curr Opin Neurol*, 32(5), 771-776. doi: 10.1097/WCO.0000000000000730
- Löscher, W., Puskarjov, M., & Kaila, K. (2013). Cation-chloride cotransporters NKCC1 and KCC2 as potential targets for novel antiepileptic and antiepileptogenic treatments. *Neuropharmacology*, 69, 62-74. doi: 10.1016/j.neuropharm.2012.05.045
- Lundfald, L., Restrepo, C. E., Butt, S. J., Peng, C. Y., Droho, S., Endo, T., . . . Kiehn, O. (2007). Phenotype of V2-derived interneurons and their relationship to the axon guidance molecule EphA4 in the developing mouse spinal cord. *Eur J Neurosci*, 26(11), 2989-3002. doi: 10.1111/j.1460-9568.2007.05906.x
- Macdonald, R. L., & Botzolakis, E. J. (2009). GABAA Receptor Channels *Physiology and Pathology of Chloride Transporters and Channels in the Nervous System* (pp. 257-282): Elsevier.
- Macdonald, R. L., & Olsen, R. W. (1994). GABA<sub>A</sub> Receptor Channels. *Annual Review of Neuroscience*, 17(1), 569-602. doi: 10.1146/annurev.ne.17.030194.003033

- Mackenzie, I. R., Rademakers, R., & Neumann, M. (2010). TDP-43 and FUS in amyotrophic lateral sclerosis and frontotemporal dementia. *Lancet Neurol*, 9(10), 995-1007. doi: 10.1016/S1474-4422(10)70195-2
- Mackenzie, I. R. A., Bigio, E. H., Ince, P. G., Geser, F., Neumann, M., Cairns, N. J., . . . Trojanowski, J. Q. (2007). Pathological TDP-43 distinguishes sporadic amyotrophic lateral sclerosis from amyotrophic lateral sclerosis with SOD1 mutations. *Annals of Neurology*, 61(5), 427-434. doi: 10.1002/ana.21147
- Maconochie, D. J., Zempel, J. M., & Steinbach, J. H. (1994). How quickly can GABA<sub>A</sub> receptors open? *Neuron*, 12(1), 61-71. doi: 10.1016/0896-6273(94)90152-X
- Maisonpierre, P. C., Le Beau, M. M., Espinosa, R., 3rd, Ip, N. Y., Belluscio, L., de la Monte, S. M., . . . Yancopoulos, G. D. (1991). Human and rat brain-derived neurotrophic factor and neurotrophin-3: gene structures, distributions, and chromosomal localizations. *Genomics*, 10(3), 558-568. doi: 10.1016/0888-7543(91)90436-i
- Manuel, M., Iglesias, C., Donnet, M., Leroy, F., Heckman, C. J., & Zytnicki, D. (2009). Fast Kinetics, High-Frequency Oscillations, and Subprimary Firing Range in Adult Mouse Spinal Motoneurons. *Journal of Neuroscience*, 29(36), 11246-11256. doi: 10.1523/JNEUROSCI.3260-09.2009
- Manuel, M., & Zytnicki, D. (2011). Alpha, beta and gamma motoneurons: functional diversity in the motor system's final pathway. *J Integr Neurosci*, 10(3), 243-276. doi: 10.1142/S0219635211002786
- Maor-Nof, M., Shipony, Z., Lopez-Gonzalez, R., Nakayama, L., Zhang, Y. J., Couthouis, J., . . . Gitler, A. D. (2021). p53 is a central regulator driving neurodegeneration caused by C9orf72 poly(PR). *Cell*, 184(3), 689-708 e620. doi: 10.1016/j.cell.2020.12.025
- Martin, E., Cazenave, W., Cattaert, D., & Branchereau, P. (2013). Embryonic alteration of motoneuronal morphology induces hyperexcitability in the mouse model of amyotrophic lateral sclerosis. *Neurobiol Dis*, 54, 116-126. doi: 10.1016/j.nbd.2013.02.011
- Mathis, S., Couratier, P., Julian, A., Corcia, P., & Le Masson, G. (2017). Current view and perspectives in amyotrophic lateral sclerosis. *Neural Regeneration Research*, 12(2), 181. doi: 10.4103/1673-5374.200794
- Mattei, B., Schmied, A., Mazzocchio, R., Decchi, B., Rossi, A., & Vedel, J.-P. (2003). Pharmacologically induced enhancement of recurrent inhibition in humans: effects on motoneurone discharge patterns. *The Journal of Physiology*, 548(2), 615-629. doi: 10.1113/jphysiol.2002.033126
- Maynard, S. A. (2021). Identification of a stereotypic molecular arrangement of endogenous glycine receptors at spinal cord synapses.
- Mazzoni, E. O., Mahony, S., Peljto, M., Patel, T., Thornton, S. R., McCuine, S., . . . Wichterle, H. (2013). Saltatory remodeling of Hox chromatin in response to rostrocaudal patterning signals. *Nat Neurosci*, 16(9), 1191-1198. doi: 10.1038/nn.3490
- McCrea, D. A., & Rybak, I. A. (2008). Organization of mammalian locomotor rhythm and pattern generation. *Brain Res Rev*, 57(1), 134-146. doi: 10.1016/j.brainresrev.2007.08.006
- McGoldrick, P., Joyce, P. I., Fisher, E. M., & Greensmith, L. (2013). Rodent models of amyotrophic lateral sclerosis. *Biochim Biophys Acta*, 1832(9), 1421-1436. doi: 10.1016/j.bbadis.2013.03.012
- McKernan, R. M., & Whiting, P. J. (1996). Which GABA<sub>A</sub>-receptor subtypes really occur in the brain? *Trends in Neurosciences*, 19(4), 139-143. doi: 10.1016/S0166-2236(96)80023-3

- McLarnon, J. G., Kim, S. U., Michikawa, M., & Xu, R. (1995). Properties of inward and outward potassium currents in cultured mouse motoneurons. *Neuroscience*, *64*(1), 139-151.
- McNeill Alexander, R. (2002). Energetics and optimization of human walking and running: the 2000 Raymond Pearl memorial lecture. *Am J Hum Biol*, *14*(5), 641-648. doi: 10.1002/ajhb.10067
- Medelin, M., Rancic, V., Cellot, G., Laishram, J., Veeraraghavan, P., Rossi, C., . . . Ballerini, L. (2016). Altered development in GABA co-release shapes glycinergic synaptic currents in cultured spinal slices of the SOD1(G93A) mouse model of amyotrophic lateral sclerosis. *J Physiol*, *594*(13), 3827-3840. doi: 10.1113/JP272382
- Medina, I., Friedel, P., Rivera, C., Kahle, K. T., Kourdougli, N., Uvarov, P., & Pellegrino, C. (2014). Current view on the functional regulation of the neuronal K(+)-Cl(-) cotransporter KCC2. *Front Cell Neurosci*, *8*, 27. doi: 10.3389/fncel.2014.00027
- Meehan, C. F., Moldovan, M., Marklund, S. L., Graffmo, K. S., Nielsen, J. B., & Hultborn, H. (2010). Intrinsic properties of lumbar motor neurones in the adult G127insTGGG superoxide dismutase-1 mutant mouse in vivo: evidence for increased persistent inward currents: G127X SOD1 mice motor neurone properties in vivo. *Acta Physiologica*, *200*(4), 361-376. doi: 10.1111/j.1748-1716.2010.02188.x
- Meier, J., Juttner, R., Kirischuk, S., & Grantyn, R. (2002). Synaptic Anchoring of Glycine Receptors in Developing Collicular Neurons under Control of Metabotropic Glutamate Receptor Activity. *Molecular and Cellular Neuroscience*, *21*(2), 324-340. doi: 10.1006/mcne.2002.1161
- Meldrum, B. S. (2000). Glutamate as a Neurotransmitter in the Brain: Review of Physiology and Pathology. *The Journal of Nutrition*, *130*(4), 1007S-1015S. doi: 10.1093/jn/130.4.1007S
- Mendell, L. M., & Henneman, E. (1968). Terminals of Single Ia Fibers: Distribution within a Pool of 300 Homonymous Motor Neurons. *Science*, *160*(3823), 96-98. doi: 10.1126/science.160.3823.96
- Menon, P., Kiernan, M. C., & Vucic, S. (2015). Cortical hyperexcitability precedes lower motor neuron dysfunction in ALS. *Clinical Neurophysiology*, *126*(4), 803-809. doi: 10.1016/j.clinph.2014.04.023
- Meyer, G., Kirsch, J., Betz, H., & Langosch, D. (1995). Identification of a gephyrin binding motif on the glycine receptor beta subunit. *Neuron*, *15*(3), 563-572.
- Meyers, E. A., & Kessler, J. A. (2017). TGF-beta Family Signaling in Neural and Neuronal Differentiation, Development, and Function. *Cold Spring Harb Perspect Biol*, *9*(8). doi: 10.1101/cshperspect.a022244
- Milan, L. a., BarriÃre, G. g., De DeurwaerdÃre, P., Cazalets, J.-R., & Bertrand, S. S. (2014). Monoaminergic control of spinal locomotor networks in SOD1G93A newborn mice. *Frontiers in Neural Circuits*, *8*. doi: 10.3389/fncir.2014.00077
- Miller, K. E., Balbás, J. C., Benton, R. L., Lam, T. S., Edwards, K. M., Kriebel, R. M., & Schechter, R. (2012). Glutaminase Immunoreactivity and Enzyme Activity Is Increased in the Rat Dorsal Root Ganglion Following Peripheral Inflammation. *Pain Research and Treatment*, *2012*, 1-9. doi: 10.1155/2012/414697
- Mody, I., & Pearce, R. A. (2004). Diversity of inhibitory neurotransmission through GABAA receptors. *Trends in Neurosciences*, *27*(9), 569-575. doi: 10.1016/j.tins.2004.07.002
- Mogyoros, I. (1998). Strength-duration properties of sensory and motor axons in amyotrophic lateral sclerosis. *Brain*, *121*(5), 851-859. doi: 10.1093/brain/121.5.851
- Molinuevo, J. L., Lladó, A., & Rami, L. (2005). Memantine: Targeting glutamate excitotoxicity in Alzheimer's disease and other dementias. *American Journal of*

- Alzheimer's Disease & Other Dementias*, 20(2), 77-85. doi: 10.1177/153331750502000206
- Moore, Y. E., Deeb, T. Z., Chadchankar, H., Brandon, N. J., & Moss, S. J. (2018). Potentiating KCC2 activity is sufficient to limit the onset and severity of seizures. *Proc Natl Acad Sci U S A*, 115(40), 10166-10171. doi: 10.1073/pnas.1810134115
- Moroni, M., Biro, I., Giugliano, M., Vijayan, R., Biggin, P. C., Beato, M., & Sivilotti, L. G. (2011a). Chloride ions in the pore of glycine and GABA channels shape the time course and voltage dependence of agonist currents. *J Neurosci*, 31(40), 14095-14106. doi: 10.1523/JNEUROSCI.1985-11.2011
- Moroni, M., Biro, I., Giugliano, M., Vijayan, R., Biggin, P. C., Beato, M., & Sivilotti, L. G. (2011b). Chloride Ions in the Pore of Glycine and GABA Channels Shape the Time Course and Voltage Dependence of Agonist Currents. *Journal of Neuroscience*, 31(40), 14095-14106. doi: 10.1523/JNEUROSCI.1985-11.2011
- Mortensen, M., & Smart, T. G. (2006). Extrasynaptic  $\alpha\beta$  subunit GABA<sub>A</sub> receptors on rat hippocampal pyramidal neurons: Extrasynaptic GABA<sub>A</sub> receptor isoforms. *The Journal of Physiology*, 577(3), 841-856. doi: 10.1113/jphysiol.2006.117952
- Moustafa, Y. (2018). Gleason : A Rebirth. *American Journal of Psychiatry Residents' Journal*, 13(8), 11-11. doi: 10.1176/appi.ajp-rj.2018.130807
- Muller, E., Le-Corronc, H., & Legendre, P. (2008). Extrasynaptic and postsynaptic receptors in glycinergic and GABAergic neurotransmission: a division of labor? *Front Mol Neurosci*, 1, 3. doi: 10.3389/neuro.02.003.2008
- Muller, E., Le Corronc, H., Triller, A., & Legendre, P. (2006). Developmental dissociation of presynaptic inhibitory neurotransmitter and postsynaptic receptor clustering in the hypoglossal nucleus. *Molecular and Cellular Neuroscience*, 32(3), 254-273. doi: 10.1016/j.mcn.2006.04.007
- Muller, F. L., Liu, Y., Jernigan, A., Borchelt, D., Richardson, A., & Van Remmen, H. (2008). MnSOD deficiency has a differential effect on disease progression in two different ALS mutant mouse models. *Muscle & Nerve*, 38(3), 1173-1183. doi: 10.1002/mus.21049
- Murdock, B. J., Bender, D. E., Kashlan, S. R., Figueroa-Romero, C., Backus, C., Callaghan, B. C., . . . Feldman, E. L. (2016). Increased ratio of circulating neutrophils to monocytes in amyotrophic lateral sclerosis. *Neurology - Neuroimmunology Neuroinflammation*, 3(4), e242. doi: 10.1212/NXI.0000000000000242
- Murdock, B. J., Bender, D. E., Segal, B. M., & Feldman, E. L. (2015). The dual roles of immunity in ALS: Injury overrides protection. *Neurobiology of Disease*, 77, 1-12. doi: 10.1016/j.nbd.2015.02.017
- Murdock, B. J., Zhou, T., Kashlan, S. R., Little, R. J., Goutman, S. A., & Feldman, E. L. (2017). Correlation of Peripheral Immunity With Rapid Amyotrophic Lateral Sclerosis Progression. *JAMA Neurology*, 74(12), 1446. doi: 10.1001/jamaneurol.2017.2255
- Musaro, A., & Rosenthal, N. (2002). The Role of local Insulin-like Growth Factor-1 Isoforms in the Pathophysiology of Skeletal Muscle. *Current Genomics*, 3(3), 149-162. doi: 10.2174/1389202023350462
- Nabekura, J., Katsurabayashi, S., Kakazu, Y., Shibata, S., Matsubara, A., Jinno, S., . . . Ishibashi, H. (2004). Developmental switch from GABA to glycine release in single central synaptic terminals. *Nature Neuroscience*, 7(1), 17-23. doi: 10.1038/nn1170
- Nagai, M., Re, D. B., Nagata, T., Chalazonitis, A., Jessell, T. M., Wichterle, H., & Przedborski, S. (2007). Astrocytes expressing ALS-linked mutated SOD1 release factors selectively toxic to motor neurons. *Nature Neuroscience*, 10(5), 615-622. doi: 10.1038/nn1876

- Nagel, G., Peter, R. S., Rosenbohm, A., Koenig, W., Dupuis, L., Rothenbacher, D., & Ludolph, A. C. (2020). Association of Insulin-like Growth Factor 1 Concentrations with Risk for and Prognosis of Amyotrophic Lateral Sclerosis – Results from the ALS Registry Swabia. *Scientific Reports*, *10*(1), 736. doi: 10.1038/s41598-020-57744-x
- Nakata, M., Kuwabara, S., Kanai, K., Misawa, S., Tamura, N., Sawai, S., . . . Bostock, H. (2006). Distal excitability changes in motor axons in amyotrophic lateral sclerosis. *Clinical Neurophysiology*, *117*(7), 1444-1448. doi: 10.1016/j.clinph.2006.04.005
- Nerlich, J., Kuenzel, T., Keine, C., Korenic, A., Rubsamen, R., & Milenkovic, I. (2014). Dynamic Fidelity Control to the Central Auditory System: Synergistic Glycine/GABAergic Inhibition in the Cochlear Nucleus. *Journal of Neuroscience*, *34*(35), 11604-11620. doi: 10.1523/JNEUROSCI.0719-14.2014
- Neumann, M., Sampathu, D. M., Kwong, L. K., Truax, A. C., Micsenyi, M. C., Chou, T. T., . . . Lee, V. M.-Y. (2006). Ubiquitinated TDP-43 in Frontotemporal Lobar Degeneration and Amyotrophic Lateral Sclerosis. *Science*, *314*(5796), 130-133. doi: 10.1126/science.1134108
- Nicolopoulos-Stournaras, S., & Iles, J. F. (1983). Motor neuron columns in the lumbar spinal cord of the rat. *The Journal of Comparative Neurology*, *217*(1), 75-85. doi: 10.1002/cne.902170107
- Niebroj-Dobosz, I., Rafalowska, J., Fidzianska, A., Gadamski, R., & Grieb, P. (2007). Myelin composition of spinal cord in a model of amyotrophic lateral sclerosis (ALS) in SOD1<sup>G93A</sup> transgenic rats. *Folia Neuropathol*, *45*(4), 236-241.
- Nijssen, J., Comley, L. H., & Hedlund, E. (2017). Motor neuron vulnerability and resistance in amyotrophic lateral sclerosis. *Acta Neuropathologica*, *133*(6), 863-885. doi: 10.1007/s00401-017-1708-8
- Noga, B. R., Shefchyk, S. J., Jamal, J., & Jordan, L. M. (1987). The role of Renshaw cells in locomotion: antagonism of their excitation from motor axon collaterals with intravenous mecamylamine. *Experimental Brain Research*, *66*(1). doi: 10.1007/BF00236206
- O'Donnell-Ames, J. (2008). Hope loves company, Not misery! *Exceptional Parent*, *38*(7), 40.
- Obeidat, A. Z., Nardelli, P., Powers, R. K., & Cope, T. C. (2014). Modulation of motoneuron firing by recurrent inhibition in the adult rat in vivo. *Journal of Neurophysiology*, *112*(9), 2302-2315. doi: 10.1152/jn.00358.2014
- Ohgomori, T., Yamada, J., Takeuchi, H., Kadomatsu, K., & Jinno, S. (2016). Comparative morphometric analysis of microglia in the spinal cord of SOD1<sup>G93A</sup> transgenic mouse model of amyotrophic lateral sclerosis. *European Journal of Neuroscience*, *43*(10), 1340-1351. doi: 10.1111/ejn.13227
- Olsen, R. W., & Sieghart, W. (2009). GABA A receptors: subtypes provide diversity of function and pharmacology. *Neuropharmacology*, *56*(1), 141-148. doi: 10.1016/j.neuropharm.2008.07.045
- Olsen, R. W., & Tobin, A. J. (1990). Molecular biology of GABA<sub>A</sub> receptors. *The FASEB Journal*, *4*(5), 1469-1480. doi: 10.1096/fasebj.4.5.2155149
- Otis, T. S., De Koninck, Y., & Mody, I. (1994). Lasting potentiation of inhibition is associated with an increased number of gamma-aminobutyric acid type A receptors activated during miniature inhibitory postsynaptic currents. *Proceedings of the National Academy of Sciences*, *91*(16), 7698-7702. doi: 10.1073/pnas.91.16.7698
- Paez-Colasante, X., Figueroa-Romero, C., Sakowski, S. A., Goutman, S. A., & Feldman, E. L. (2015). Amyotrophic lateral sclerosis: mechanisms and therapeutics in the epigenomic era. *Nature Reviews Neurology*, *11*(5), 266-279. doi: 10.1038/nrneurol.2015.57

- Pambo-Pambo, A., Durand, J., & Gueritaud, J.-P. (2009). Early Excitability Changes in Lumbar Motoneurons of Transgenic SOD1<sup>G85R</sup> and SOD1<sup>G93A-Low</sup> Mice. *Journal of Neurophysiology*, *102*(6), 3627-3642. doi: 10.1152/jn.00482.2009
- Papp, E., Rivera, C., Kaila, K., & Freund, T. F. (2008). Relationship between neuronal vulnerability and potassium-chloride cotransporter 2 immunoreactivity in hippocampus following transient forebrain ischemia. *Neuroscience*, *154*(2), 677-689. doi: 10.1016/j.neuroscience.2008.03.072
- Parisi, C., Napoli, G., Pelegrin, P., & Volonté, C. (2016). M1 and M2 Functional Imprinting of Primary Microglia: Role of P2X7 Activation and miR-125b. *Mediators of Inflammation*, *2016*, 1-9. doi: 10.1155/2016/2989548
- Pasquali, L., Longone, P., Isidoro, C., Ruggieri, S., Paparelli, A., & Fornai, F. (2009). Autophagy, lithium, and amyotrophic lateral sclerosis. *Muscle Nerve*, *40*(2), 173-194. doi: 10.1002/mus.21423
- Payne, J. A., Rivera, C., Voipio, J., & Kaila, K. (2003). Cation-chloride co-transporters in neuronal communication, development and trauma. *Trends Neurosci*, *26*(4), 199-206. doi: 10.1016/S0166-2236(03)00068-7
- Payne, J. A., Rivera, C., Voipio, J., & Kaila, K. (2003). Cation-chloride co-transporters in neuronal communication, development and trauma. *Trends in Neurosciences*, *26*(4), 199-206. doi: 10.1016/S0166-2236(03)00068-7
- Payne, J. A., Stevenson, T. J., & Donaldson, L. F. (1996). Molecular Characterization of a Putative K-Cl Cotransporter in Rat Brain. *Journal of Biological Chemistry*, *271*(27), 16245-16252. doi: 10.1074/jbc.271.27.16245
- Peerboom, C., & Wierenga, C. J. (2021). The postnatal GABA shift: A developmental perspective. *Neuroscience & Biobehavioral Reviews*, *124*, 179-192. doi: 10.1016/j.neubiorev.2021.01.024
- Pérez-García, María J., & Burden, Steven J. (2012). Increasing MuSK Activity Delays Denervation and Improves Motor Function in ALS Mice. *Cell Reports*, *2*(3), 497-502. doi: 10.1016/j.celrep.2012.08.004
- Perrin, S. (2014). Preclinical research: Make mouse studies work. *Nature*, *507*(7493), 423-425. doi: 10.1038/507423a
- Pesiridis, G. S., Tripathy, K., Tanik, S., Trojanowski, J. Q., & Lee, V. M. (2011). A "two-hit" hypothesis for inclusion formation by carboxyl-terminal fragments of TDP-43 protein linked to RNA depletion and impaired microtubule-dependent transport. *J Biol Chem*, *286*(21), 18845-18855. doi: 10.1074/jbc.M111.231118
- Philips, T., & Robberecht, W. (2011). Neuroinflammation in amyotrophic lateral sclerosis: role of glial activation in motor neuron disease. *The Lancet Neurology*, *10*(3), 253-263. doi: 10.1016/S1474-4422(11)70015-1
- Philips, T., & Rothstein, J. D. (2015). Rodent Models of Amyotrophic Lateral Sclerosis. *Current Protocols in Pharmacology*, *69*(1). doi: 10.1002/0471141755.ph0567s69
- Pieri, M., Albo, F., Gaetti, C., Spalloni, A., Bengtson, C. P., Longone, P., . . . Zona, C. (2003). Altered excitability of motor neurons in a transgenic mouse model of familial amyotrophic lateral sclerosis. *Neuroscience Letters*, *351*(3), 153-156. doi: 10.1016/j.neulet.2003.07.010
- Piotrkiewicz, M., Kudina, L., Mierzejewska, J., & Hausmanowa - Petrusiewicz, I. (2008). Analysis of double discharges in amyotrophic lateral sclerosis. *Muscle & Nerve*, *38*(1), 845-854. doi: 10.1002/mus.20997
- Pisella, L. I., Gaiarsa, J. L., Diabira, D., Zhang, J., Khalilov, I., Duan, J., . . . Medina, I. (2019). Impaired regulation of KCC2 phosphorylation leads to neuronal network dysfunction and neurodevelopmental pathology. *Sci Signal*, *12*(603). doi: 10.1126/scisignal.aay0300

- Pitt, S. J., Sivilotti, L. G., & Beato, M. (2008a). High intracellular chloride slows the decay of glycinergic currents. *J Neurosci*, 28(45), 11454-11467. doi: 10.1523/JNEUROSCI.3890-08.2008
- Pitt, S. J., Sivilotti, L. G., & Beato, M. (2008b). High Intracellular Chloride Slows the Decay of Glycinergic Currents. *Journal of Neuroscience*, 28(45), 11454-11467. doi: 10.1523/JNEUROSCI.3890-08.2008
- Pizzarelli, R., & Cherubini, E. (2011). Alterations of GABAergic Signaling in Autism Spectrum Disorders. *Neural Plasticity*, 2011, 1-12. doi: 10.1155/2011/297153
- Plotkin, M. D., Snyder, E. Y., Hebert, S. C., & Delpire, E. (1997). Expression of the Na-K-2Cl cotransporter is developmentally regulated in postnatal rat brains: A possible mechanism underlying GABA's excitatory role in immature brain. *Journal of Neurobiology*, 33(6), 781-795. doi: 10.1002/(SICI)1097-4695(19971120)33:6<781::AID-NEU6>3.0.CO;2-5
- Pond, B. B., Berglund, K., Kuner, T., Feng, G., Augustine, G. J., & Schwartz-Bloom, R. D. (2006). The Chloride Transporter Na<sup>+</sup>-K<sup>+</sup>-Cl<sup>-</sup> Cotransporter Isoform-1 Contributes to Intracellular Chloride Increases after *In Vitro* Ischemia. *The Journal of Neuroscience*, 26(5), 1396-1406. doi: 10.1523/JNEUROSCI.1421-05.2006
- Poo, M. M. (1985). Mobility and localization of proteins in excitable membranes. *Annu Rev Neurosci*, 8, 369-406. doi: 10.1146/annurev.ne.08.030185.002101
- Pramatarova, A., Laganière, J., Roussel, J., Brisebois, K., & Rouleau, G. A. (2001). Neuron-Specific Expression of Mutant Superoxide Dismutase 1 in Transgenic Mice Does Not Lead to Motor Impairment. *The Journal of Neuroscience*, 21(10), 3369-3374. doi: 10.1523/JNEUROSCI.21-10-03369.2001
- Prasad, A., & Hollyday, M. (1991). Development and migration of avian sympathetic preganglionic neurons. *The Journal of Comparative Neurology*, 307(2), 237-258. doi: 10.1002/cne.903070207
- Pun, S., Santos, A. F., Saxena, S., Xu, L., & Caroni, P. (2006). Selective vulnerability and pruning of phasic motoneuron axons in motoneuron disease alleviated by CNTF. *Nature Neuroscience*, 9(3), 408-419. doi: 10.1038/nn1653
- Purves, D., Augustine, G. J., Fitzpatrick, D., Katz, L. C., LaMantia, A.-S., McNamara, J. O., & Williams, S. M. (2001). Damage to Descending Motor Pathways: The Upper Motor Neuron Syndrome. *Neuroscience*. 2nd edition.
- Quinlan, K. A., Schuster, J. E., Fu, R., Siddique, T., & Heckman, C. J. (2011). Altered postnatal maturation of electrical properties in spinal motoneurons in a mouse model of amyotrophic lateral sclerosis: Accelerated maturation of motoneurons in amyotrophic lateral sclerosis. *The Journal of Physiology*, 589(9), 2245-2260. doi: 10.1113/jphysiol.2010.200659
- Raffaele, S., Boccazzi, M., & Fumagalli, M. (2021). Oligodendrocyte Dysfunction in Amyotrophic Lateral Sclerosis: Mechanisms and Therapeutic Perspectives. *Cells*, 10(3), 565. doi: 10.3390/cells10030565
- Rahmati, N., Hoebeek, F. E., Peter, S., & De Zeeuw, C. I. (2018). Chloride Homeostasis in Neurons With Special Emphasis on the Olivocerebellar System: Differential Roles for Transporters and Channels. *Front Cell Neurosci*, 12, 101. doi: 10.3389/fncel.2018.00101
- Rajaofetra, N., Poulat, P., Marlier, L., Geffard, M., & Privat, A. (1992). Pre- and postnatal development of noradrenergic projections to the rat spinal cord: an immunocytochemical study. *Brain Res Dev Brain Res*, 67(2), 237-246. doi: 10.1016/0165-3806(92)90224-k
- Rajaofetra, N., Sandillon, F., Geffard, M., & Privat, A. (1989). Pre- and post-natal ontogeny of serotonergic projections to the rat spinal cord. *J Neurosci Res*, 22(3), 305-321.

- Raltshev, C., Hetsch, F., Winkelmann, A., Meier, J. C., & Semtner, M. (2016). Electrophysiological Signature of Homomeric and Heteromeric Glycine Receptor Channels. *Journal of Biological Chemistry*, 291(34), 18030-18040. doi: 10.1074/jbc.M116.735084
- Ramirez-Jarquín, U. N., Lazo-Gomez, R., Tovar, Y. R. L. B., & Tapia, R. (2014). Spinal inhibitory circuits and their role in motor neuron degeneration. *Neuropharmacology*, 82, 101-107. doi: 10.1016/j.neuropharm.2013.10.003
- Ramírez-Jarquín, U. N., & Tapia, R. (2018). Excitatory and Inhibitory Neuronal Circuits in the Spinal Cord and Their Role in the Control of Motor Neuron Function and Degeneration. *ACS Chemical Neuroscience*, 9(2), 211-216. doi: 10.1021/acscchemneuro.7b00503
- Rampon, C., Luppi, P. H., Fort, P., Peyron, C., & Jouvet, M. (1996). Distribution of glycine-immunoreactive cell bodies and fibers in the rat brain. *Neuroscience*, 75(3), 737-755. doi: 10.1016/0306-4522(96)00278-3
- Ransohoff, R. M. (2016). A polarizing question: do M1 and M2 microglia exist? *Nature Neuroscience*, 19(8), 987-991. doi: 10.1038/nn.4338
- Raoul, C., Estévez, A. G., Nishimune, H., Cleveland, D. W., deLapeyrière, O., Henderson, C. E., . . . Pettmann, B. (2002). Motoneuron Death Triggered by a Specific Pathway Downstream of Fas. *Neuron*, 35(6), 1067-1083. doi: 10.1016/S0896-6273(02)00905-4
- Ravits, J., Paul, P., & Jorg, C. (2007). Focality of upper and lower motor neuron degeneration at the clinical onset of ALS. *Neurology*, 68(19), 1571-1575. doi: 10.1212/01.wnl.0000260965.20021.47
- Ravits, J. M., & La Spada, A. R. (2009). ALS motor phenotype heterogeneity, focality, and spread: Deconstructing motor neuron degeneration. *Neurology*, 73(10), 805-811. doi: 10.1212/WNL.0b013e3181b6bbbd
- Raynor, E. M., & Shefner, J. M. (1994). Recurrent inhibition is decreased in patients with amyotrophic lateral sclerosis. *Neurology*, 44(11), 2148-2148. doi: 10.1212/WNL.44.11.2148
- Reaume, A. G., Elliott, J. L., Hoffman, E. K., Kowall, N. W., Ferrante, R. J., Siwek, D. R., . . . Snider, W. D. (1996). Motor neurons in Cu/Zn superoxide dismutase-deficient mice develop normally but exhibit enhanced cell death after axonal injury. *Nature Genetics*, 13(1), 43-47. doi: 10.1038/ng0596-43
- Renshaw, B. (1946). CENTRAL EFFECTS OF CENTRIPETAL IMPULSES IN AXONS OF SPINAL VENTRAL ROOTS. *Journal of Neurophysiology*, 9(3), 191-204. doi: 10.1152/jn.1946.9.3.191
- Renshaw, B. (1946). Central effects of centripetal impulses in axons of spinal ventral roots. *J Neurophysiol*, 9, 191-204. doi: 10.1152/jn.1946.9.3.191
- Renton, A. E., Chio, A., & Traynor, B. J. (2014). State of play in amyotrophic lateral sclerosis genetics. *Nat Neurosci*, 17(1), 17-23. doi: 10.1038/nn.3584
- Rima, M., Lattouf, Y., Abi Younes, M., Bullier, E., Legendre, P., Mangin, J. M., & Hong, E. (2020). Dynamic regulation of the cholinergic system in the spinal central nervous system. *Sci Rep*, 10(1), 15338. doi: 10.1038/s41598-020-72524-3
- Riolo, G., Ricci, C., De Angelis, N., Marzocchi, C., Guerrera, G., Borsellino, G., . . . Battistini, S. (2022). BDNF and Pro-BDNF in Amyotrophic Lateral Sclerosis: A New Perspective for Biomarkers of Neurodegeneration. *Brain Sci*, 12(5). doi: 10.3390/brainsci12050617
- Ripps, M. E., Huntley, G. W., Hof, P. R., Morrison, J. H., & Gordon, J. W. (1995). Transgenic mice expressing an altered murine superoxide dismutase gene provide an animal model of amyotrophic lateral sclerosis. *Proceedings of the National Academy of Sciences*, 92(3), 689-693. doi: 10.1073/pnas.92.3.689

- Rivera, C., Voipio, J., Payne, J. A., Ruusuvuori, E., Lahtinen, H., Lamsa, K., . . . Kaila, K. (1999). The K<sup>+</sup>/Cl<sup>-</sup> co-transporter KCC2 renders GABA hyperpolarizing during neuronal maturation. *Nature*, *397*(6716), 251-255. doi: 10.1038/16697
- Robberecht, W., & Philips, T. (2013). The changing scene of amyotrophic lateral sclerosis. *Nat Rev Neurosci*, *14*(4), 248-264. doi: 10.1038/nrn3430
- Rochat, C., Bernard-Marissal, N., & Schneider, B. L. (2016). Selective Vulnerability of Neuronal Subtypes in ALS: A Fertile Ground for the Identification of Therapeutic Targets. In H. Foyaca-Sibat & L. d. F. Ibañez-Valdés (Eds.), *Update on Amyotrophic Lateral Sclerosis*: InTech.
- Rodríguez Cruz, P. M., Cossins, J., Beeson, D., & Vincent, A. (2020). The Neuromuscular Junction in Health and Disease: Molecular Mechanisms Governing Synaptic Formation and Homeostasis. *Frontiers in Molecular Neuroscience*, *13*, 610964. doi: 10.3389/fnmol.2020.610964
- Romanes, G. J. (1951). The motor cell columns of the lumbo-sacral spinal cord of the cat. *The Journal of Comparative Neurology*, *94*(2), 313-363. doi: 10.1002/cne.900940209
- Romanes, G. J. (1964). The Motor Pools of the Spinal Cord *Progress in Brain Research* (Vol. 11, pp. 93-119): Elsevier.
- Rosen, D. R., Siddique, T., Patterson, D., Figlewicz, D. A., Sapp, P., Hentati, A., . . . Brown, R. H. (1993). Mutations in Cu/Zn superoxide dismutase gene are associated with familial amyotrophic lateral sclerosis. *Nature*, *362*(6415), 59-62. doi: 10.1038/362059a0
- Rothstein, J. D. (2017). Edaravone: A new drug approved for ALS. *Cell*, *171*(4), 725. doi: 10.1016/j.cell.2017.10.011
- Rothstein, J. D., Martin, L. J., & Kuncl, R. W. (1992). Decreased Glutamate Transport by the Brain and Spinal Cord in Amyotrophic Lateral Sclerosis. *New England Journal of Medicine*, *326*(22), 1464-1468. doi: 10.1056/NEJM199205283262204
- Rothstein, J. D., Van Kammen, M., Levey, A. I., Martin, L. J., & Kuncl, R. W. (1995). Selective loss of glial glutamate transporter GLT-1 in amyotrophic lateral sclerosis. *Annals of Neurology*, *38*(1), 73-84. doi: 10.1002/ana.410380114
- Rowland, L. P. (2001). How Amyotrophic Lateral Sclerosis Got Its Name: The Clinical-Pathologic Genius of Jean-Martin Charcot. *Archives of Neurology*, *58*(3). doi: 10.1001/archneur.58.3.512
- Rudomin, P. (2009). In search of lost presynaptic inhibition. *Exp Brain Res*, *196*(1), 139-151. doi: 10.1007/s00221-009-1758-9
- Ruffin, V. A., Salameh, A. I., Boron, W. F., & Parker, M. D. (2014). Intracellular pH regulation by acid-base transporters in mammalian neurons. *Frontiers in Physiology*, *5*. doi: 10.3389/fphys.2014.00043
- Rungta, Ravi L., Choi, Hyun B., Tyson, John R., Malik, A., Dissing-Olesen, L., Lin, Paulo J. C., . . . MacVicar, Brian A. (2015). The Cellular Mechanisms of Neuronal Swelling Underlying Cytotoxic Edema. *Cell*, *161*(3), 610-621. doi: 10.1016/j.cell.2015.03.029
- Russier, M., Carlier, E., Ankri, N., Fronzaroli, L., & Debanne, D. (2003). A -, T -, and H - type Currents Shape Intrinsic Firing of Developing Rat Abducens Motoneurons. *The Journal of Physiology*, *549*(1), 21-36. doi: 10.1113/jphysiol.2002.037069
- S, M., & TJ, B. (1981). The localization of the motoneurons supplying the hindlimb muscles of the mouse. *Philosophical Transactions of the Royal Society of London. B, Biological Sciences*, *293*(1069), 477-508. doi: 10.1098/rstb.1981.0082
- Sangan, P., Rajendran, V. M., Geibel, J. P., & Binder, H. J. (2002). Cloning and Expression of a Chloride-dependent Na<sup>+</sup>-H<sup>+</sup> Exchanger. *Journal of Biological Chemistry*, *277*(12), 9668-9675. doi: 10.1074/jbc.M110852200

- Sapir, T., Geiman, E. J., Wang, Z., Velasquez, T., Mitsui, S., Yoshihara, Y., . . . Goulding, M. (2004). Pax6 and engrailed 1 regulate two distinct aspects of renshaw cell development. *J Neurosci*, *24*(5), 1255-1264. doi: 10.1523/JNEUROSCI.3187-03.2004
- Sasaki, S., & Maruyama, S. (1994). Synapse loss in anterior horn neurons in amyotrophic lateral sclerosis. *Acta Neuropathologica*, *88*(3), 222-227. doi: 10.1007/BF00293397
- Saxena, S., Cabuy, E., & Caroni, P. (2009). A role for motoneuron subtype-selective ER stress in disease manifestations of FALS mice. *Nature Neuroscience*, *12*(5), 627-636. doi: 10.1038/nn.2297
- Saxena, S., Roselli, F., Singh, K., Leptien, K., Julien, J. P., Gros-Louis, F., & Caroni, P. (2013). Neuroprotection through excitability and mTOR required in ALS motoneurons to delay disease and extend survival. *Neuron*, *80*(1), 80-96. doi: 10.1016/j.neuron.2013.07.027
- Scain, A. L., Le Corronc, H., Allain, A. E., Muller, E., Rigo, J. M., Meyrand, P., . . . Legendre, P. (2010). Glycine release from radial cells modulates the spontaneous activity and its propagation during early spinal cord development. *J Neurosci*, *30*(1), 390-403. doi: 10.1523/JNEUROSCI.2115-09.2010
- Scamps, F., Aimond, F., Hilaire, C., & Raoul, C. (2021). Synaptic Transmission and Motoneuron Excitability Defects in Amyotrophic Lateral Sclerosis. In T. Araki (Ed.), *Amyotrophic Lateral Sclerosis*. Brisbane (AU).
- Schiaffino, S., Gorza, L., Pitton, G., Saggin, L., Ausoni, S., Sartore, S., & Lømo, T. (1988). Embryonic and neonatal myosin heavy chain in denervated and paralyzed rat skeletal muscle. *Developmental Biology*, *127*(1), 1-11. doi: 10.1016/0012-1606(88)90183-2
- Schiaffino, S., & Reggiani, C. (2011). Fiber Types in Mammalian Skeletal Muscles. *Physiological Reviews*, *91*(4), 1447-1531. doi: 10.1152/physrev.00031.2010
- Schinder, A. F., Olson, E. C., Spitzer, N. C., & Montal, M. (1996). Mitochondrial Dysfunction Is a Primary Event in Glutamate Neurotoxicity. *The Journal of Neuroscience*, *16*(19), 6125-6133. doi: 10.1523/JNEUROSCI.16-19-06125.1996
- Schmid, A., & Bülthoff, H. (1988). Using neuropharmacology to distinguish between excitatory and inhibitory movement detection mechanisms in the fly *Calliphora erythrocephala*. *Biol. Cybernetics* *59*, 71-80.
- Schneider, S. P., & Fyffe, R. E. (1992). Involvement of GABA and glycine in recurrent inhibition of spinal motoneurons. *J Neurophysiol*, *68*(2), 397-406. doi: 10.1152/jn.1992.68.2.397
- Scotter, E. L., Chen, H.-J., & Shaw, C. E. (2015). TDP-43 Proteinopathy and ALS: Insights into Disease Mechanisms and Therapeutic Targets. *Neurotherapeutics*, *12*(2), 352-363. doi: 10.1007/s13311-015-0338-x
- Sharma, A., Lyashchenko, A. K., Lu, L., Nasrabad, S. E., Elmaleh, M., Mendelsohn, M., . . . Shneider, N. A. (2016). ALS-associated mutant FUS induces selective motor neuron degeneration through toxic gain of function. *Nature Communications*, *7*(1), 10465. doi: 10.1038/ncomms10465
- Sharma, K., Leonard, A. E., Lettieri, K., & Pfaff, S. L. (2000). Genetic and epigenetic mechanisms contribute to motor neuron pathfinding. *Nature*, *406*(6795), 515-519. doi: 10.1038/35020078
- Shaw, P., & Eggett, C. J. (2000). Molecular factors underlying selective vulnerability of motor neurons to neurodegeneration in amyotrophic lateral sclerosis. *Journal of Neurology*, *247*(S1), I17-I27. doi: 10.1007/BF03161151
- Shaw, P. J., Forrest, V., Ince, P. G., Richardson, J. P., & Wastell, H. J. (1995). CSF and Plasma Amino Acid Levels in Motor Neuron Disease: Elevation of CSF Glutamate in a Subset of Patients. *Neurodegeneration*, *4*(2), 209-216. doi: 10.1006/neur.1995.0026

- Shefner, J. M., & Logigian, E. L. (1998). The mixed nerve silent period in normal subjects and patients with amyotrophic lateral sclerosis. *Electromyogr Clin Neurophysiol*, 38(8), 505-510.
- Shigenaga, Y., Moritani, M., Oh, S. J., Park, K. P., Paik, S. K., Bae, J. Y., . . . Bae, Y. C. (2005). The distribution of inhibitory and excitatory synapses on single, reconstructed jaw-opening motoneurons in the cat. *Neuroscience*, 133(2), 507-518. doi: 10.1016/j.neuroscience.2005.02.022
- Shoenfeld, L., Westenbroek, R. E., Fisher, E., Quinlan, K. A., Tysseling, V. M., Powers, R. K., . . . Binder, M. D. (2014). Soma size and Cav1.3 channel expression in vulnerable and resistant motoneuron populations of the SOD1G93A mouse model of ALS. *Physiol Rep*, 2(8). doi: 10.14814/phy2.12113
- Sibilla, S., & Ballerini, L. (2009). GABAergic and glycinergic interneuron expression during spinal cord development: dynamic interplay between inhibition and excitation in the control of ventral network outputs. *Prog Neurobiol*, 89(1), 46-60. doi: 10.1016/j.pneurobio.2009.06.001
- Siembab, V. C., Smith, C. A., Zagoraiou, L., Berrocal, M. C., Mentis, G. Z., & Alvarez, F. J. (2010). Target selection of proprioceptive and motor axon synapses on neonatal V1-derived Ia inhibitory interneurons and Renshaw cells. *J Comp Neurol*, 518(23), 4675-4701. doi: 10.1002/cne.22441
- Silayeva, L., Deeb, T. Z., Hines, R. M., Kelley, M. R., Munoz, M. B., Lee, H. H., . . . Moss, S. J. (2015). KCC2 activity is critical in limiting the onset and severity of status epilepticus. *Proc Natl Acad Sci U S A*, 112(11), 3523-3528. doi: 10.1073/pnas.1415126112
- Sillito, A. M. (1977). Inhibitory processes underlying the directional specificity of simple, complex and hypercomplex cells in the cat's visual cortex. *J Physiol*, 271(3), 699-720. doi: 10.1113/jphysiol.1977.sp012021
- Silverman, J. M., Fernando, S. M., Grad, L. I., Hill, A. F., Turner, B. J., Yerbury, J. J., & Cashman, N. R. (2016). Disease Mechanisms in ALS: Misfolded SOD1 Transferred Through Exosome-Dependent and Exosome-Independent Pathways. *Cellular and Molecular Neurobiology*, 36(3), 377-381. doi: 10.1007/s10571-015-0294-3
- Siucinska, E. (2019).  $\Gamma$ -Aminobutyric acid in adult brain: an update. *Behavioural Brain Research*, 376, 112224. doi: 10.1016/j.bbr.2019.112224
- Smith, J. (2015). The Luckiest Man: Errol Morris's *A Brief History of Time* and *The Pride of the Yankees*. *Quarterly Review of Film and Video*, 32(3), 193-207. doi: 10.1080/10509208.2013.811356
- Smith, C. L., & Hollyday, M. (1983). The development and postnatal organization of motor nuclei in the rat thoracic spinal cord. *The Journal of Comparative Neurology*, 220(1), 16-28. doi: 10.1002/cne.902200104
- Sofroniew, M. V., & Vinters, H. V. (2010). Astrocytes: biology and pathology. *Acta Neuropathologica*, 119(1), 7-35. doi: 10.1007/s00401-009-0619-8
- Sohn, E. (2017). Fundraising: The Ice Bucket Challenge delivers. *Nature*, 550(7676), S113-S114. doi: 10.1038/550S113a
- Song, A., Ashwell, K. W. S., & Tracey, D. J. (2000). Development of the rat phrenic nucleus and its connections with brainstem respiratory nuclei. *Anatomy and Embryology*, 202(2), 159-177. doi: 10.1007/s004290000096
- Song, Y.-H., Song, J. L., Delafontaine, P., & Godard, M. P. (2013). The therapeutic potential of IGF-I in skeletal muscle repair. *Trends in Endocrinology & Metabolism*, 24(6), 310-319. doi: 10.1016/j.tem.2013.03.004
- Soo, K. Y., Halloran, M., Sundaramoorthy, V., Parakh, S., Toth, R. P., Southam, K. A., . . . Atkin, J. D. (2015). Rab1-dependent ER-Golgi transport dysfunction is a common

- pathogenic mechanism in SOD1, TDP-43 and FUS-associated ALS. *Acta Neuropathologica*, 130(5), 679-697. doi: 10.1007/s00401-015-1468-2
- Southam, K. A., King, A. E., Blizzard, C. A., McCormack, G. H., & Dickson, T. C. (2013). Microfluidic primary culture model of the lower motor neuron-neuromuscular junction circuit. *J Neurosci Methods*, 218(2), 164-169. doi: 10.1016/j.jneumeth.2013.06.002
- Spalloni, A., & Longone, P. (2016). Cognitive impairment in amyotrophic lateral sclerosis, clues from the SOD1 mouse. *Neuroscience & Biobehavioral Reviews*, 60, 12-25. doi: 10.1016/j.neubiorev.2015.11.006
- Spike, R. C., Watt, C., Zafra, F., & Todd, A. J. (1997). An ultrastructural study of the glycine transporter GLYT2 and its association with glycine in the superficial laminae of the rat spinal dorsal horn. *Neuroscience*, 77(2), 543-551. doi: 10.1016/s0306-4522(96)00501-5
- Spiller, K. J., Cheung, C. J., Restrepo, C. R., Kwong, L. K., Stieber, A. M., Trojanowski, J. Q., & Lee, V. M.-Y. (2016). Selective Motor Neuron Resistance and Recovery in a New Inducible Mouse Model of TDP-43 Proteinopathy. *Journal of Neuroscience*, 36(29), 7707-7717. doi: 10.1523/JNEUROSCI.1457-16.2016
- Sreedharan, J., Blair, I. P., Tripathi, V. B., Hu, X., Vance, C., Rogelj, B., . . . Shaw, C. E. (2008). TDP-43 Mutations in Familial and Sporadic Amyotrophic Lateral Sclerosis. *Science*, 319(5870), 1668-1672. doi: 10.1126/science.1154584
- Sreedharan, J., Blair, I. P., Tripathi, V. B., Hu, X., Vance, C., Rogelj, B., . . . Shaw, C. E. (2008). TDP-43 mutations in familial and sporadic amyotrophic lateral sclerosis. *Science*, 319(5870), 1668-1672. doi: 10.1126/science.1154584
- Staley, K. J., Soldo, B. L., & Proctor, W. R. (1995). Ionic mechanisms of neuronal excitation by inhibitory GABAA receptors. *Science*, 269(5226), 977-981. doi: 10.1126/science.7638623
- Stephens, H. E., Felgoise, S., Young, J., & Simmons, Z. (2015). Multidisciplinary ALS clinics in the USA: A comparison of those who attend and those who do not. *Amyotrophic Lateral Sclerosis and Frontotemporal Degeneration*, 16(3-4), 196-201. doi: 10.3109/21678421.2014.994530
- Stifani, N. (2014). Motor neurons and the generation of spinal motor neuron diversity. *Frontiers in Cellular Neuroscience*, 8. doi: 10.3389/fncel.2014.00293
- Stil, A., Liabeuf, S., Jean-Xavier, C., Brocard, C., Viemari, J. C., & Vinay, L. (2009). Developmental up-regulation of the potassium-chloride cotransporter type 2 in the rat lumbar spinal cord. *Neuroscience*, 164(2), 809-821. doi: 10.1016/j.neuroscience.2009.08.035
- Stuart, D. G., & Hultborn, H. (2008). Thomas Graham Brown (1882--1965), Anders Lundberg (1920-), and the neural control of stepping. *Brain Res Rev*, 59(1), 74-95. doi: 10.1016/j.brainresrev.2008.06.001
- Suk, T. R., & Rousseaux, M. W. C. (2020). The role of TDP-43 mislocalization in amyotrophic lateral sclerosis. *Mol Neurodegener*, 15(1), 45. doi: 10.1186/s13024-020-00397-1
- Sunico, C. R., Domínguez, G., García-Verdugo, J. M., Osta, R., Montero, F., & Moreno-López, B. (2011). Reduction in the Motoneuron Inhibitory/Excitatory Synaptic Ratio in an Early-Symptomatic Mouse Model of Amyotrophic Lateral Sclerosis: Inhibitory Loss and Excitatory Gain in ALS. *Brain Pathology*, 21(1), 1-15. doi: 10.1111/j.1750-3639.2010.00417.x
- Swarup, V., Phaneuf, D., Dupré, N., Petri, S., Strong, M., Kriz, J., & Julien, J.-P. (2011). Deregulation of TDP-43 in amyotrophic lateral sclerosis triggers nuclear factor κB-

- mediated pathogenic pathways. *Journal of Experimental Medicine*, 208(12), 2429-2447. doi: 10.1084/jem.20111313
- Sweeney, L. B., Bikoff, J. B., Gabitto, M. I., Brenner-Morton, S., Baek, M., Yang, J. H., . . . Jessell, T. M. (2018). Origin and Segmental Diversity of Spinal Inhibitory Interneurons. *Neuron*, 97(2), 341-355 e343. doi: 10.1016/j.neuron.2017.12.029
- Takahashi, T., Momiyama, A., Hirai, K., Hishinuma, F., & Akagi, H. (1992). Functional correlation of fetal and adult forms of glycine receptors with developmental changes in inhibitory synaptic receptor channels. *Neuron*, 9(6), 1155-1161. doi: 10.1016/0896-6273(92)90073-M
- Takei, T., Confais, J., Tomatsu, S., Oya, T., & Seki, K. (2017). Neural basis for hand muscle synergies in the primate spinal cord. *Proc Natl Acad Sci U S A*, 114(32), 8643-8648. doi: 10.1073/pnas.1704328114
- Talpalari, A. E., Bouvier, J., Borgius, L., Fortin, G., Pierani, A., & Kiehn, O. (2013). Dual-mode operation of neuronal networks involved in left-right alternation. *Nature*, 500(7460), 85-88. doi: 10.1038/nature12286
- Tamura, N., Kuwabara, S., Misawa, S., Kanai, K., Nakata, M., Sawai, S., & Hattori, T. (2006). Increased nodal persistent Na<sup>+</sup> currents in human neuropathy and motor neuron disease estimated by latent addition. *Clinical Neurophysiology*, 117(11), 2451-2458. doi: 10.1016/j.clinph.2006.07.309
- Tan, R. H., Ke, Y. D., Ittner, L. M., & Halliday, G. M. (2017). ALS/FTLD: experimental models and reality. *Acta Neuropathol*, 133(2), 177-196. doi: 10.1007/s00401-016-1666-6
- Tang, Y., & Le, W. (2016). Differential Roles of M1 and M2 Microglia in Neurodegenerative Diseases. *Molecular Neurobiology*, 53(2), 1181-1194. doi: 10.1007/s12035-014-9070-5
- Taylor, J. P., Brown, R. H., Jr., & Cleveland, D. W. (2016). Decoding ALS: from genes to mechanism. *Nature*, 539(7628), 197-206. doi: 10.1038/nature20413
- Thaler, J. P., Koo, S. J., Kania, A., Lettieri, K., Andrews, S., Cox, C., . . . Pfaff, S. L. (2004). A postmitotic role for Isl-class LIM homeodomain proteins in the assignment of visceral spinal motor neuron identity. *Neuron*, 41(3), 337-350. doi: 10.1016/s0896-6273(04)00011-x
- Thomas, A. M., Ostroumov, A., Kimmey, B. A., Taormina, M. B., Holden, W. M., Kim, K., . . . Dani, J. A. (2018). Adolescent Nicotine Exposure Alters GABAA Receptor Signaling in the Ventral Tegmental Area and Increases Adult Ethanol Self-Administration. *Cell Reports*, 23(1), 68-77. doi: 10.1016/j.celrep.2018.03.030
- Thomas, R. C., & Wilson, V. J. (1965). Precise Localization of Renshaw Cells with a New Marking Technique. *Nature*, 206(4980), 211-213. doi: 10.1038/206211b0
- Todd, A. J., & Sullivan, A. C. (1990). Light microscope study of the coexistence of GABA-like and glycine-like immunoreactivities in the spinal cord of the rat. *J Comp Neurol*, 296(3), 496-505. doi: 10.1002/cne.902960312
- Todd, A. J., & Sullivan, A. C. (1990). Light microscope study of the coexistence of GABA-like and glycine-like immunoreactivities in the spinal cord of the rat. *The Journal of Comparative Neurology*, 296(3), 496-505. doi: 10.1002/cne.902960312
- Traynor, B. J., Alexander, M., Corr, B., Frost, E., & Hardiman, O. (2003). An outcome study of riluzole in amyotrophic lateral sclerosis--a population-based study in Ireland, 1996-2000. *J Neurol*, 250(4), 473-479. doi: 10.1007/s00415-003-1026-z
- Traynor, K. (2018). Federal right-to-try law aims to broaden access to investigational drugs. *American Journal of Health-System Pharmacy*, 75(15), 1085-1086. doi: 10.2146/news180048

- Tritsch, N. X., Granger, A. J., & Sabatini, B. L. (2016). Mechanisms and functions of GABA co-release. *Nat Rev Neurosci*, *17*(3), 139-145. doi: 10.1038/nrn.2015.21
- Tsuchida, T., Ensini, M., Morton, S. B., Baldassare, M., Edlund, T., Jessell, T. M., & Pfaff, S. L. (1994). Topographic organization of embryonic motor neurons defined by expression of LIM homeobox genes. *Cell*, *79*(6), 957-970. doi: 10.1016/0092-8674(94)90027-2
- Tu, P. H., Raju, P., Robinson, K. A., Gurney, M. E., Trojanowski, J. Q., & Lee, V. M. (1996). Transgenic mice carrying a human mutant superoxide dismutase transgene develop neuronal cytoskeletal pathology resembling human amyotrophic lateral sclerosis lesions. *Proc Natl Acad Sci U S A*, *93*(7), 3155-3160. doi: 10.1073/pnas.93.7.3155
- Turner, B., & Talbot, K. (2008). Transgenics, toxicity and therapeutics in rodent models of mutant SOD1-mediated familial ALS. *Progress in Neurobiology*, *85*(1), 94-134. doi: 10.1016/j.pneurobio.2008.01.001
- Turner, M. R., & Kiernan, M. C. (2012). Does interneuronal dysfunction contribute to neurodegeneration in amyotrophic lateral sclerosis? *Amyotrophic Lateral Sclerosis*, *13*(3), 245-250. doi: 10.3109/17482968.2011.636050
- Turner, M. R., & Swash, M. (2015). The expanding syndrome of amyotrophic lateral sclerosis: a clinical and molecular odyssey. *Journal of Neurology, Neurosurgery & Psychiatry*, *86*(6), 667-673. doi: 10.1136/jnnp-2014-308946
- Tyzio, R., Minlebaev, M., Rheims, S., Ivanov, A., Jorquera, I., Holmes, G. L., . . . Khazipov, R. (2008). Postnatal changes in somatic gamma-aminobutyric acid signalling in the rat hippocampus. *Eur J Neurosci*, *27*(10), 2515-2528. doi: 10.1111/j.1460-9568.2008.06234.x
- Tyzio, R., Nardou, R., Ferrari, D. C., Tsintsadze, T., Shahrokhi, A., Eftekhari, S., . . . Ben-Ari, Y. (2014). Oxytocin-mediated GABA inhibition during delivery attenuates autism pathogenesis in rodent offspring. *Science*, *343*(6171), 675-679. doi: 10.1126/science.1247190
- Udagawa, T., Fujioka, Y., Tanaka, M., Honda, D., Yokoi, S., Riku, Y., . . . Sobue, G. (2015). FUS regulates AMPA receptor function and FTL/ALS-associated behaviour via GluA1 mRNA stabilization. *Nature Communications*, *6*(1), 7098. doi: 10.1038/ncomms8098
- Ullah, M., Mansor, O., Ismail, Z. I. M., Kapitonova, M. Y., & Sirajudeen, K. N. S. (2007). Localization of the spinal nucleus of accessory nerve in rat: a horseradish peroxidase study. *Journal of Anatomy*, *210*(4), 428-438. doi: 10.1111/j.1469-7580.2007.00709.x
- Uvarov, P., Ludwig, A., Markkanen, M., Pruunsild, P., Kaila, K., Delpire, E., . . . Airaksinen, M. S. (2007). A novel N-terminal isoform of the neuron-specific K-Cl cotransporter KCC2. *J Biol Chem*, *282*(42), 30570-30576. doi: 10.1074/jbc.M705095200
- Vaaga, C. E., Borisovska, M., & Westbrook, G. L. (2014). Dual-transmitter neurons: functional implications of co-release and co-transmission. *Current Opinion in Neurobiology*, *29*, 25-32. doi: 10.1016/j.conb.2014.04.010
- Valeeva, G., Tressard, T., Mukhtarov, M., Baude, A., & Khazipov, R. (2016). An Optogenetic Approach for Investigation of Excitatory and Inhibitory Network GABA Actions in Mice Expressing Channelrhodopsin-2 in GABAergic Neurons. *J Neurosci*, *36*(22), 5961-5973. doi: 10.1523/JNEUROSCI.3482-15.2016
- Van Damme, P., Braeken, D., Callewaert, G., Robberecht, W., & Van Den Bosch, L. (2005). GluR2 deficiency accelerates motor neuron degeneration in a mouse model of amyotrophic lateral sclerosis. *J Neuropathol Exp Neurol*, *64*(7), 605-612. doi: 10.1097/01.jnen.0000171647.09589.07
- Van Deerlin, V. M., Leverenz, J. B., Bekris, L. M., Bird, T. D., Yuan, W., Elman, L. B., . . . Yu, C. E. (2008). TARDBP mutations in amyotrophic lateral sclerosis with TDP-43

- neuropathology: a genetic and histopathological analysis. *Lancet Neurol*, 7(5), 409-416. doi: 10.1016/S1474-4422(08)70071-1
- Van den Bos, M. A. J., Higashihara, M., Geevasinga, N., Menon, P., Kiernan, M. C., & Vucic, S. (2018). Imbalance of cortical facilitatory and inhibitory circuits underlies hyperexcitability in ALS. *Neurology*, 91(18), e1669-e1676. doi: 10.1212/WNL.00000000000006438
- van Zundert, B., Izaurieta, P., Fritz, E., & Alvarez, F. J. (2012). Early pathogenesis in the adult-onset neurodegenerative disease amyotrophic lateral sclerosis. *J Cell Biochem*, 113(11), 3301-3312. doi: 10.1002/jcb.24234
- van Zundert, B., Peuscher, M. H., Hynynen, M., Chen, A., Neve, R. L., Brown, R. H., . . . Bellingham, M. C. (2008). Neonatal Neuronal Circuitry Shows Hyperexcitable Disturbance in a Mouse Model of the Adult-Onset Neurodegenerative Disease Amyotrophic Lateral Sclerosis. *Journal of Neuroscience*, 28(43), 10864-10874. doi: 10.1523/JNEUROSCI.1340-08.2008
- Vanderhorst, V. G. J. M., & Holstege, G. (1997). Organization of lumbosacral motoneuronal cell groups innervating hindlimb, pelvic floor, and axial muscles in the cat. *The Journal of Comparative Neurology*, 382(1), 46-76. doi: 10.1002/(SICI)1096-9861(19970526)382:1<46::AID-CNE4>3.0.CO;2-K
- Vargas, M. R., Pehar, M., Cassina, P., Beckman, J. S., & Barbeito, L. (2006). Increased glutathione biosynthesis by Nrf2 activation in astrocytes prevents p75NTR-dependent motor neuron apoptosis: Astrocytic GSH and motor neuron apoptosis. *Journal of Neurochemistry*, 97(3), 687-696. doi: 10.1111/j.1471-4159.2006.03742.x
- Venugopal, S., Hsiao, C. F., Sonoda, T., Wiedau-Pazos, M., & Chandler, S. H. (2015). Homeostatic dysregulation in membrane properties of masticatory motoneurons compared with oculomotor neurons in a mouse model for amyotrophic lateral sclerosis. *J Neurosci*, 35(2), 707-720. doi: 10.1523/JNEUROSCI.1682-14.2015
- Verkhatsky, A., Parpura, V., Vardjan, N., & Zorec, R. (2019). Physiology of Astroglia. In A. Verkhatsky, M. S. Ho, R. Zorec & V. Parpura (Eds.), *Neuroglia in Neurodegenerative Diseases* (Vol. 1175, pp. 45-91). Singapore: Springer Singapore.
- Vermeer, S., Hoischen, A., Meijer, R. P. P., Gilissen, C., Neveling, K., Wieskamp, N., . . . Knoers, N. (2010). Targeted Next-Generation Sequencing of a 12.5 Mb Homozygous Region Reveals ANO10 Mutations in Patients with Autosomal-Recessive Cerebellar Ataxia. *The American Journal of Human Genetics*, 87(6), 813-819. doi: 10.1016/j.ajhg.2010.10.015
- Verstraelen, P., Van Dyck, M., Verschuuren, M., Kashikar, N. D., Nuydens, R., Timmermans, J. P., & De Vos, W. H. (2018). Image-Based Profiling of Synaptic Connectivity in Primary Neuronal Cell Culture. *Front Neurosci*, 12, 389. doi: 10.3389/fnins.2018.00389
- Virginio, C., & Cherubini, E. (1997). Glycine-activated whole cell and single channel currents in rat cerebellar granule cells in culture. *Developmental Brain Research*, 98(1), 30-40. doi: 10.1016/S0165-3806(96)00164-2
- von Bartheld, C. S., Bahney, J., & Herculano-Houzel, S. (2016). The search for true numbers of neurons and glial cells in the human brain: A review of 150 years of cell counting: Quantifying neurons and glia in human brain. *Journal of Comparative Neurology*, 524(18), 3865-3895. doi: 10.1002/cne.24040
- Vucic, S., & Kiernan, M. C. (2006). Axonal excitability properties in amyotrophic lateral sclerosis. *Clinical Neurophysiology*, 117(7), 1458-1466. doi: 10.1016/j.clinph.2006.04.016

- Vucic, S., & Kiernan, M. C. (2010). Upregulation of persistent sodium conductances in familial ALS. *Journal of Neurology, Neurosurgery & Psychiatry*, *81*(2), 222-227. doi: 10.1136/jnnp.2009.183079
- Vucic, S., Rothstein, J. D., & Kiernan, M. C. (2014). Advances in treating amyotrophic lateral sclerosis: insights from pathophysiological studies. *Trends in Neurosciences*, *37*(8), 433-442. doi: 10.1016/j.tins.2014.05.006
- Wainger, B. J., Kiskinis, E., Mellin, C., Wiskow, O., Han, S. S., Sandoe, J., . . . Woolf, C. J. (2014). Intrinsic membrane hyperexcitability of amyotrophic lateral sclerosis patient-derived motor neurons. *Cell Rep*, *7*(1), 1-11. doi: 10.1016/j.celrep.2014.03.019
- Wainger, Brian J., Kiskinis, E., Mellin, C., Wiskow, O., Han, Steve S. W., Sandoe, J., . . . Woolf, Clifford J. (2014). Intrinsic Membrane Hyperexcitability of Amyotrophic Lateral Sclerosis Patient-Derived Motor Neurons. *Cell Reports*, *7*(1), 1-11. doi: 10.1016/j.celrep.2014.03.019
- Walker, A. K., Spiller, K. J., Ge, G., Zheng, A., Xu, Y., Zhou, M., . . . Lee, V. M.-Y. (2015). Functional recovery in new mouse models of ALS/FTLD after clearance of pathological cytoplasmic TDP-43. *Acta Neuropathologica*, *130*(5), 643-660. doi: 10.1007/s00401-015-1460-x
- Walton, K., & Fulton, B. (1986). Ionic mechanisms underlying the firing properties of rat neonatal motoneurons studied *in vitro*. *Neuroscience*, *19*, 669-683.
- Ward, C. B., & Edmondson, D. R. (2015). The ALS Bucket Challenge: The good, the bad, and the money. *Journal of Critical Incidents*, *8*, 137-140.
- Watanabe, M., & Fukuda, A. (2015). Development and regulation of chloride homeostasis in the central nervous system. *Frontiers in Cellular Neuroscience*, *9*. doi: 10.3389/fncel.2015.00371
- Watanabe, M., Zhang, J., Mansuri, M. S., Duan, J., Karimy, J. K., Delpire, E., . . . Kahle, K. T. (2019). Developmentally regulated KCC2 phosphorylation is essential for dynamic GABA-mediated inhibition and survival. *Sci Signal*, *12*(603). doi: 10.1126/scisignal.aaw9315
- Webber, C. L., & Pleschka, K. (1976). Structural and functional characteristics of individual phrenic motoneurons. *Pflügers Archiv*, *364*(2), 113-121. doi: 10.1007/BF00585178
- Wenner, P., O'Donovan, M. J., & Matise, M. P. (2000). Topographical and physiological characterization of interneurons that express engrailed-1 in the embryonic chick spinal cord. *J Neurophysiol*, *84*(5), 2651-2657. doi: 10.1152/jn.2000.84.5.2651
- Wijesekera, L. C., & Nigel Leigh, P. (2009). Amyotrophic lateral sclerosis. *Orphanet Journal of Rare Diseases*, *4*(1), 3. doi: 10.1186/1750-1172-4-3
- Williamson, T. L., & Cleveland, D. W. (1999). Slowing of axonal transport is a very early event in the toxicity of ALS-linked SOD1 mutants to motor neurons. *Nature Neuroscience*, *2*(1), 50-56. doi: 10.1038/4553
- Willis, W. D. (1971). The case for the Renshaw cell. *Brain Behav Evol*, *4*(1), 5-52. doi: 10.1159/000125422
- Wilson, J., & Shaw, C. (2007). Late appearance of glutamate transporter defects in a murine model of ALS-parkinsonism dementia complex. *Neurochemistry International*, *50*(7-8), 1067-1077. doi: 10.1016/j.neuint.2006.09.017
- Windhorst, U. (1996). ON THE ROLE OF RECURRENT INHIBITORY FEEDBACK IN MOTOR CONTROL. *Progress in Neurobiology*, *49*(6), 517-587. doi: 10.1016/0301-0082(96)00023-8
- Wishart, T. M., Parson, S. H., & Gillingwater, T. H. (2006). Synaptic Vulnerability in Neurodegenerative Disease. *Journal of Neuropathology & Experimental Neurology*, *65*(8), 733-739. doi: 10.1097/01.jnen.0000228202.35163.c4

- Wolf, S. A., Boddeke, H. W. G. M., & Kettenmann, H. (2017). Microglia in Physiology and Disease. *Annual Review of Physiology*, 79(1), 619-643. doi: 10.1146/annurev-physiol-022516-034406
- Wong, P. C., Pardo, C. A., Borchelt, D. R., Lee, M. K., Copeland, N. G., Jenkins, N. A., . . . Price, D. L. (1995). An adverse property of a familial ALS-linked SOD1 mutation causes motor neuron disease characterized by vacuolar degeneration of mitochondria. *Neuron*, 14(6), 1105-1116. doi: 10.1016/0896-6273(95)90259-7
- Wu, C., & Sun, D. (2015). GABA receptors in brain development, function, and injury. *Metab Brain Dis*, 30(2), 367-379. doi: 10.1007/s11011-014-9560-1
- Xu, X., Shen, D., Gao, Y., Zhou, Q., Ni, Y., Meng, H., . . . Chen, S. (2021). A perspective on therapies for amyotrophic lateral sclerosis: can disease progression be curbed? *Transl Neurodegener*, 10(1), 29. doi: 10.1186/s40035-021-00250-5
- Xu, Z., Jung, C., Higgins, C., Levine, J., & Kong, J. (2004). Mitochondrial Degeneration in Amyotrophic Lateral Sclerosis. *Journal of Bioenergetics and Biomembranes*, 36(4), 395-399. doi: 10.1023/B:JOB.0000041774.12654.e1
- Yamada, J., Okabe, A., Toyoda, H., Kilb, W., Luhmann, H. J., & Fukuda, A. (2004). Cl<sup>-</sup> uptake promoting depolarizing GABA actions in immature rat neocortical neurones is mediated by NKCC1: NKCC-1 mediated Cl<sup>-</sup> uptake promoting depolarizing GABA actions. *The Journal of Physiology*, 557(3), 829-841. doi: 10.1113/jphysiol.2004.062471
- Yamanaka, K., Boillee, S., Roberts, E. A., Garcia, M. L., McAlonis-Downes, M., Mikse, O. R., . . . Goldstein, L. S. B. (2008). Mutant SOD1 in cell types other than motor neurons and oligodendrocytes accelerates onset of disease in ALS mice. *Proceedings of the National Academy of Sciences*, 105(21), 7594-7599. doi: 10.1073/pnas.0802556105
- Yamanaka, K., & Komine, O. (2018). The multi-dimensional roles of astrocytes in ALS. *Neuroscience Research*, 126, 31-38. doi: 10.1016/j.neures.2017.09.011
- Yang, H., Wang, G., Sun, H., Shu, R., Liu, T., Wang, C.-E., . . . Lai, L. (2014). Species-dependent neuropathology in transgenic SOD1 pigs. *Cell Research*, 24(4), 464-481. doi: 10.1038/cr.2014.25
- Yiangou, Y., Facer, P., Durrenberger, P., Chessell, I. P., Naylor, A., Bountra, C., . . . Anand, P. (2006). COX-2, CB2 and P2X7-immunoreactivities are increased in activated microglial cells/macrophages of multiple sclerosis and amyotrophic lateral sclerosis spinal cord. *BMC Neurology*, 6(1), 12. doi: 10.1186/1471-2377-6-12
- Yoshida, T., & Delafontaine, P. (2020). Mechanisms of IGF-1-Mediated Regulation of Skeletal Muscle Hypertrophy and Atrophy. *Cells*, 9(9), 1970. doi: 10.3390/cells9091970
- Zang, D. W., Lopes, E. C., & Cheema, S. S. (2005). Loss of synaptophysin-positive boutons on lumbar motor neurons innervating the medial gastrocnemius muscle of the SOD1G93A G1H transgenic mouse model of ALS. *J Neurosci Res*, 79(5), 694-699. doi: 10.1002/jnr.20379
- Zeilhofer, H. U., Benke, D., & Yevenes, G. E. (2012). Chronic pain states: pharmacological strategies to restore diminished inhibitory spinal pain control. *Annu Rev Pharmacol Toxicol*, 52, 111-133. doi: 10.1146/annurev-pharmtox-010611-134636
- Zeilhofer, H. U., Studler, B., Arabadzisz, D., Schweizer, C., Ahmadi, S., Layh, B., . . . Fritschy, J.-M. (2005). Glycinergic neurons expressing enhanced green fluorescent protein in bacterial artificial chromosome transgenic mice: Glycinergic Neurons Tagged with EGFP. *Journal of Comparative Neurology*, 482(2), 123-141. doi: 10.1002/cne.20349

- Zeineddine, R., & Yerbury, J. J. (2015). The role of macropinocytosis in the propagation of protein aggregation associated with neurodegenerative diseases. *Frontiers in Physiology*, 6. doi: 10.3389/fphys.2015.00277
- Zengel, J. E., Reid, S. A., Sypert, G. W., & Munson, J. B. (1985). Membrane electrical properties and prediction of motor-unit type of medial gastrocnemius motoneurons in the cat. *Journal of Neurophysiology*, 53(5), 1323-1344. doi: 10.1152/jn.1985.53.5.1323
- Zhang, J., Lanuza, G. M., Britz, O., Wang, Z., Siembab, V. C., Zhang, Y., . . . Goulding, M. (2014). V1 and v2b interneurons secure the alternating flexor-extensor motor activity mice require for limbed locomotion. *Neuron*, 82(1), 138-150. doi: 10.1016/j.neuron.2014.02.013
- Zhang, Y., Narayan, S., Geiman, E., Lanuza, G. M., Velasquez, T., Shanks, B., . . . Goulding, M. (2008). V3 spinal neurons establish a robust and balanced locomotor rhythm during walking. *Neuron*, 60(1), 84-96. doi: 10.1016/j.neuron.2008.09.027
- Zhao, P., Ignacio, S., Beattie, E. C., & Abood, M. E. (2008). Altered presymptomatic AMPA and cannabinoid receptor trafficking in motor neurons of ALS model mice: implications for excitotoxicity. *European Journal of Neuroscience*, 27(3), 572-579. doi: 10.1111/j.1460-9568.2008.06041.x
- Zhao, W., Beers, D. R., Henkel, J. S., Zhang, W., Urushitani, M., Julien, J.-P., & Appel, S. H. (2010). Extracellular mutant SOD1 induces microglial-mediated motoneuron injury. *Glia*, 58(2), 231-243. doi: 10.1002/glia.20919
- Zhao, W., Xie, W., Xiao, Q., Beers, D. R., & Appel, S. H. (2006). Protective effects of an anti-inflammatory cytokine, interleukin-4, on motoneuron toxicity induced by activated microglia. *Journal of Neurochemistry*, 99(4), 1176-1187. doi: 10.1111/j.1471-4159.2006.04172.x
- Zhong, G., Sharma, K., & Harris-Warrick, R. M. (2011). Frequency-dependent recruitment of V2a interneurons during fictive locomotion in the mouse spinal cord. *Nat Commun*, 2, 274. doi: 10.1038/ncomms1276
- Zhu, L., Lovinger, D., & Delpire, E. (2005). Cortical Neurons Lacking KCC2 Expression Show Impaired Regulation of Intracellular Chloride. *Journal of Neurophysiology*, 93(3), 1557-1568. doi: 10.1152/jn.00616.2004
- Ziskind-Conhaim, L. (1998). Physiological functions of GABA-induced depolarizations in the developing rat spinal cord. *Perspect Dev Neurobiol*, 5(2-3), 279-287.
- Zoing, M. C., Burke, D., Pamphlett, R., & Kiernan, M. C. (2006). Riluzole therapy for motor neurone disease: an early Australian experience (1996-2002). *J Clin Neurosci*, 13(1), 78-83. doi: 10.1016/j.jocn.2004.04.011
- Zoli, M. (1999). Volume transmission in the CNS and its relevance for neuropsychopharmacology. *Trends in Pharmacological Sciences*, 20(4), 142-150. doi: 10.1016/S0165-6147(99)01343-7
- Zwiegers, P., Lee, G., & Shaw, C. A. (2014). Reduction in hSOD1 copy number significantly impacts ALS phenotype presentation in G37R (line 29) mice: implications for the assessment of putative therapeutic agents. *Journal of Negative Results in BioMedicine*, 13(1), 14. doi: 10.1186/1477-5751-13-14

## ANNEX.

# Tutorial for measuring synaptic GlyR clusters size

### ➤ **software :**

- Fiji : <https://fiji.sc/>

!!! Require plugin **FeatureJ and Biovoxxel**

- Fiji macro: spot-SegmentationAndMeasure-3 developed by Gilles Courtand, IR INCIA.

### ➤ **Overall idea for 2D ANALYSIS (Area) of synaptic GlyR cluster size:**

-1. How to select appropriate band-images from a single plane confocal image of a ChAT-positive motoneuronal soma:

- ❖ **Do not select segments (Region of interest, ROI) of the MN soma that do not display clear staining such as segments that are damaged because of slicing problem or bad fixation processing**
- ❖ **Do not select ROI with interference signals** such as 1) *unclear GlyT2-boutons*, 2) *GlyR-ir spots* exhibiting abnormal size and/or brightness and **missing signals** such as *GlyR-ir without any presynaptic GlyT2-boutons*.

-2. How to detect pre-synaptic GlyT2 boutons and post-synaptic GlyR clusters using FIJI analysis?

- ❖ **The FIJI macro selects round or flattened GlyT2-eGFP boutons with a cross-sectional area greater than approximately  $0.2\mu\text{m}^2$**  (*Spike et al., 1997*) (*Q. Chang et al., 2009a*)

-3. How to perform a correct colocalization analysis of an **axosomatic synapse** where a GlyT2-bouton contacts its post-synaptic GlyR clusters on a ChAT+ MN soma:

- ❖ **The FIJI macro defines the synapse as a region of apparent colocalization (at least 30% overlap) between the staining of GlyT2-positive boutons and staining of postsynaptic GlyR clusters** (*Verstraelen et al., 2018*)

## ➤ Procedures:

### First part

Select a ROI which is a segment (band image) containing the intact soma membrane of large-size MNs ( $>40\mu\text{m}$ , Feret diameter) and unambiguous GlyR-ir spots and presynaptic GlyT2 terminals. The width of the segment (ROI) is set as 30 pixels in order to include GlyR-ir clusters apposed to GlyT2 boutons.

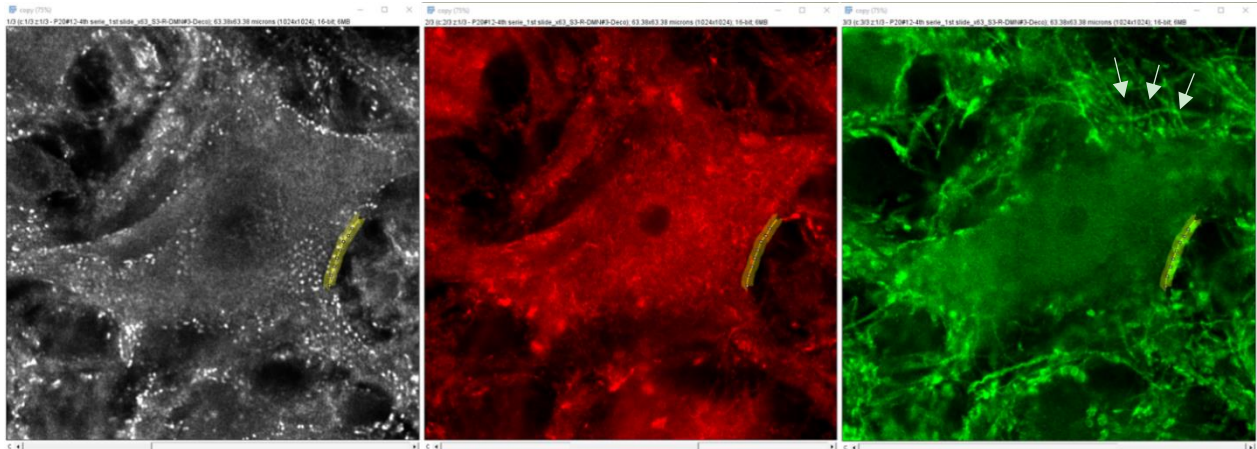
#### ✓ Notes on the selection criteria of band images

All soma segments of **ChAT-ir MN** with intact membrane (**red channel #2**) and its unambiguous **GlyR clusters** (**grey channel #1**) and co-localized **GlyT2-boutons** (**green channel #3**) were selected as band images.

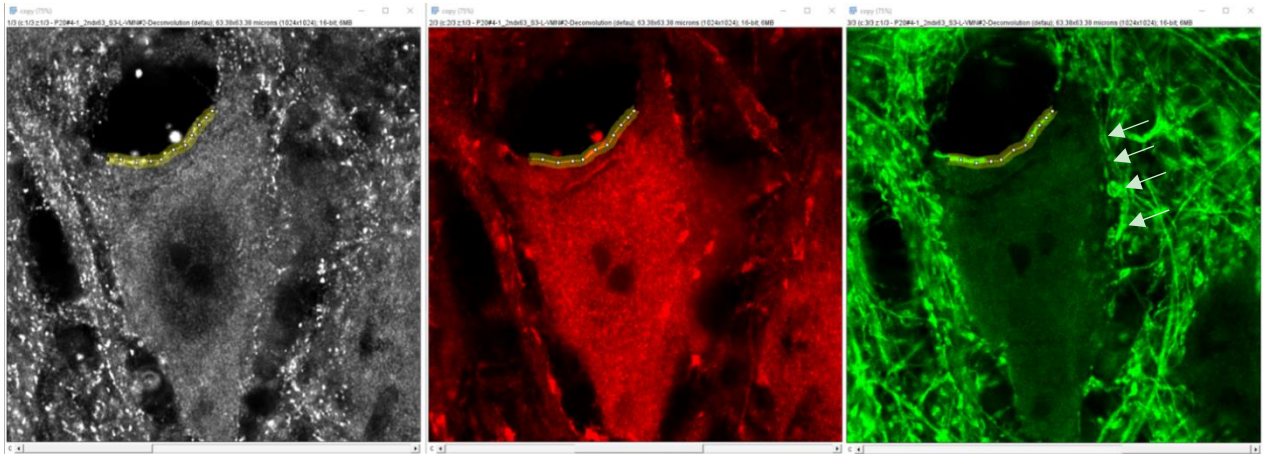
➔ It makes the analysis much more accurate, compared to selecting the whole MN soma periphery exhibiting part with **interference** and **missing signals**.

Interference signals come from numerous densely-packed GlyT2-positive fibers (white arrows in Fig.1A-C) and GlyR-ir spots with artefacts (white thick arrow in Fig.2). Missing signals of GlyT2-positive boutons are due to tissue damage (white thick arrow in Fig.3A-B).

#### ❖ Fig.1A P20#12-4th serie\_1st slide\_x63\_S3-R-DMN#3-Deconvolution (defaults)-05



❖ Fig.1B P20#4-1\_2ndx63\_S3-L-VMN#2-Deconvolution (defaults)-07



❖ Fig.1C P20#1-2\_2ndx63\_S1-L-DMN#4-Deconvolution (defaults)-01

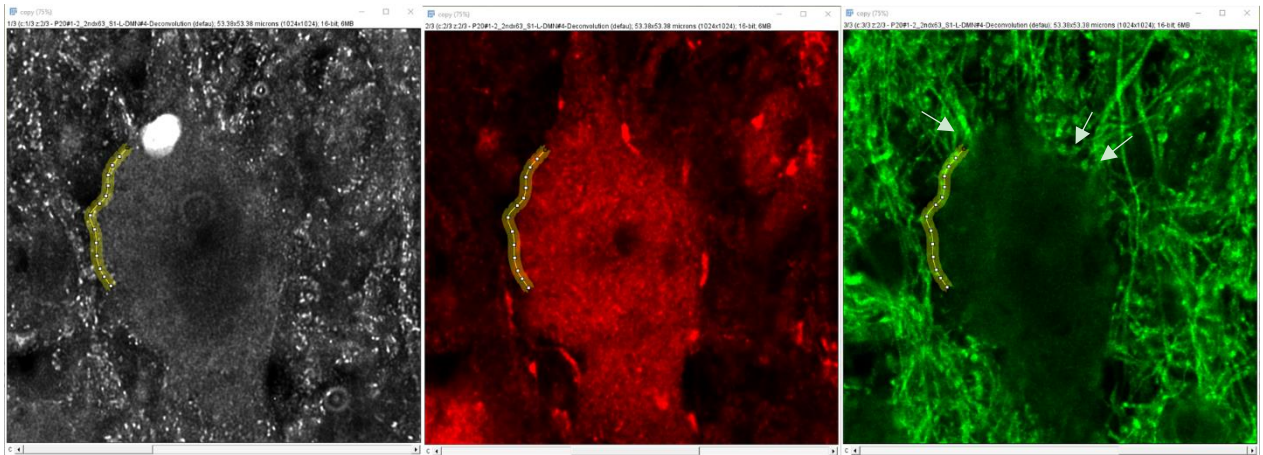


Fig.1. Examples of **Interference signals** (Confounding factor 1) generated from numerous densely-packed GlyT2-eGFP labelled fiber structures. (A-C) GlyT2-positive fibers and boutons revealed relatively frequent contacting to ChAT+ MN, making it not easy to identify positive GlyT2-boutons (see white thin arrow) because of the possibility to include some false-positive GlyT2-boutons. Only highlighted band-image, showing clear round-shape or flattened-shape cross-sectional boutons with particle size of above  $0.2 \mu\text{m}^2$ , were selected to present the GlyT2-positive boutons for quantitative analysis. Note all images were taken from band-image processing during running macro in Fiji.

❖ Fig.2. P20#4-1\_2ndx63\_S1-L-VMN#4-Deconvolution (defaults)-01

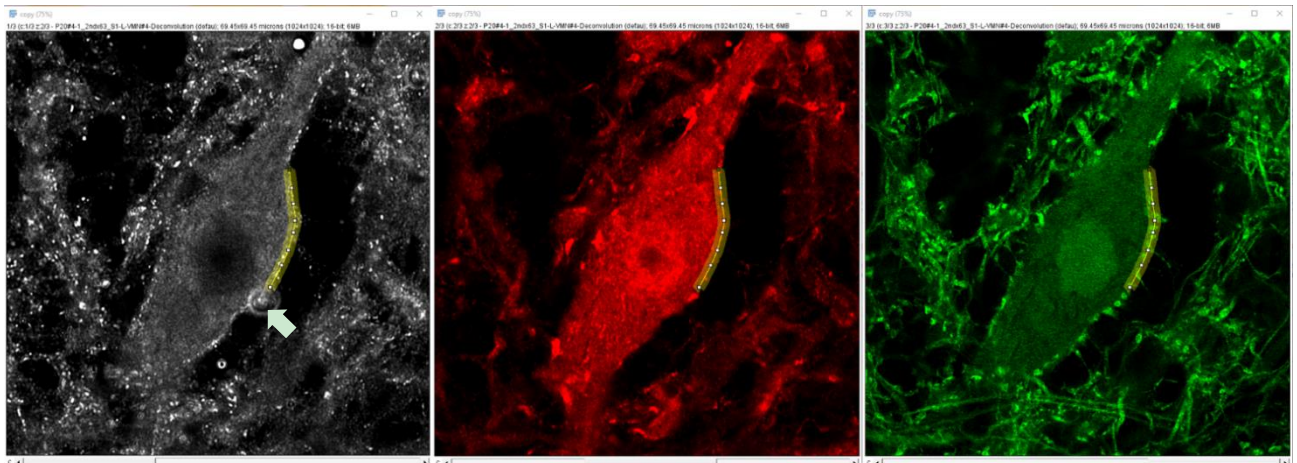
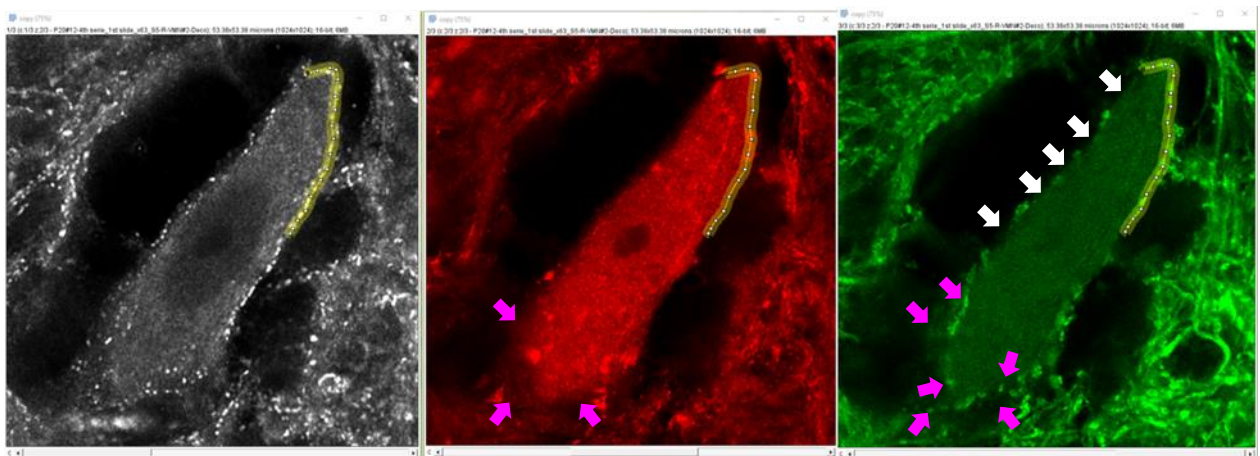


Fig.2. Examples of **Interference signals** (Confounding factor 2) generated from GlyR-immunoactive over-magnifying bright spots.

❖ Fig.3A P20#12-4th serie\_1st slide\_x63\_S5-R-VMN#2-Deconvolution (defaults)-05



❖ Fig.3B P20#12-4th serie\_1st slide\_x63\_S5-L-DMN#2-Deconvolution (defaults)-16

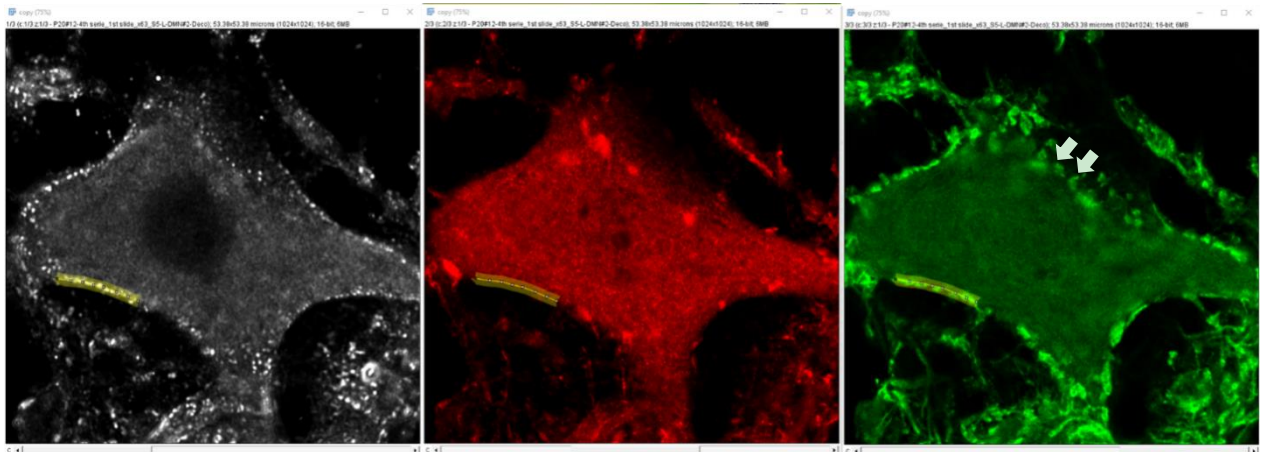


Fig.3. Examples of **missing signals** (Confounding factor 3) generated from the loss of **GlyT2-positive boutons caused by tissue damage**. (A) Only one band-image highlighted in yellow was selected as good band-image in FIJI. Other parts of soma displayed two problems, missing positive GlyT2 terminals caused by tissue damage during slicing in the cryostat (see white thick arrow) and unclear membrane boundary (see pink thick arrow), which were excluded for selection as band images. (B) Part of cell membrane is damaged, leading to the loss of GlyT2-positive boutons (see white thick arrow).

→ Darkness around ChAT-ir MNs suggests tissue deficiency or damage, which means that GlyT2 terminals may be missing.

## Second part

### Pre- and post-synaptic spots detection and colocalization analysis: theoretical aspect

Object-based and intensity-based colocalization analysis is used in the FIJI macro for detecting pre- and post-synaptic spots or particles:

- **object-based colocalization analysis:**

Only GlyT2 particles with area  $> 0.2\mu\text{m}^2$  (size= 0.2-Infinity) and GlyR particles with area  $> 0.02\mu\text{m}^2$  (size= 0.02-Infinity) are detected by the macro

For colocalization analysis, the criteria are set such as at least 30% area of a GlyR particle co-localizes with a GlyT2 bouton  $0.02\mu\text{m}^2 \times 0,3 = 0.006\mu\text{m}^2$ .

Overlap is measured using a binary quantification (8bit, 0-255)

- 100% coloc give 255 (max intensity in 8bit)
- 30% coloc give 76.5 (to normalize for collecting the overlap percentage)

### Pre- and post-synaptic spots detection and colocalization analysis: practical aspect

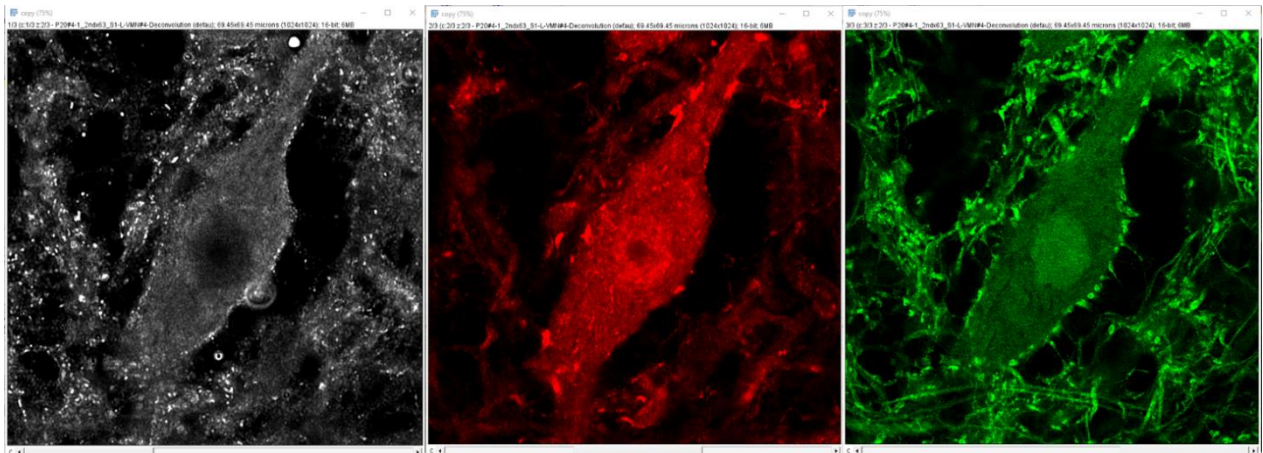
Results images are displayed as:

- 1) **RGB color mode** for each channel of interest:
  - ✓ **GlyR clusters** in **Red** on channel 1 (C1)
  - ✓ **GlyT2-boutons** in **Blue** on channel 3 (C3)
  
- 2) Color mode is changed to **Composite image** in order to see both C1 and C3 channels on the same image **after binary process**:
  - ✓ **GlyR clusters (Red)**
  - ✓ **GlyT2-boutons (Green)**
  - ✓ **Colocalization (Yellow)**  
>30% colocalization intensity between post/pre or pre/post will be defined as a **mature synapse**.
  
- 3) **Number and size of GlyR clusters, colocalizing or not with GlyT2-boutons, are collected by the macro in an csv sheet**

#### Example of the second part

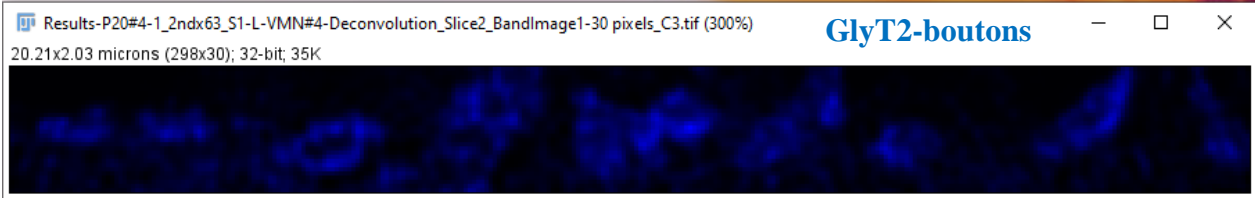
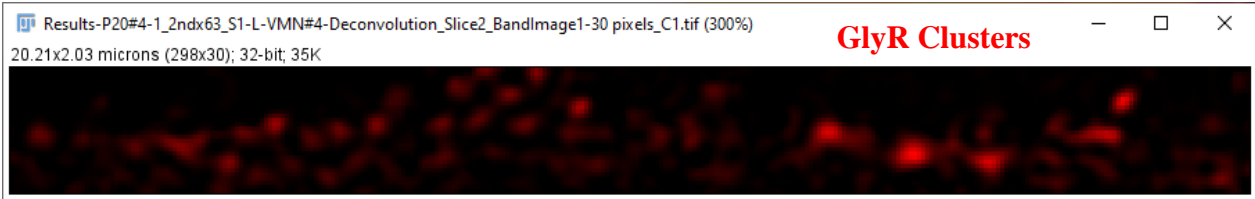
❖ P20#4-1\_2ndx63\_S1-L-VMN#4-Deconvolution (defaults)-01

Raw images displayed in FIJI

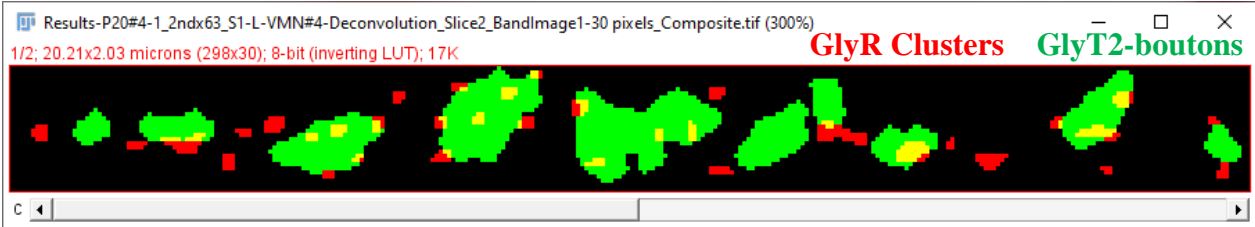


Result images were taken from the ROI of Fig.2:

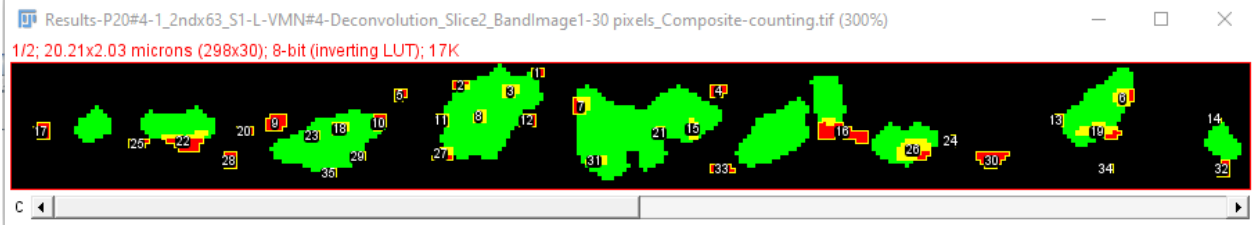
Original images in RGB color mode:



Composite image after binary process



Number and size of GlyR clusters, colocalizing or not with GlyT2-boutons, are collected



	bandimage_area	bandimage_perimeter	Count	GlyR_C1_area	GlyT2_C3_area	GlyR_C1_intColoc
1	41.118	656	1	0.028	1.674	66.667
2			2	0.037	0.860	25.000
3			3	0.051	0.359	100.000
4			4	0.051	2.217	0.000
5			5	0.037	0.796	0.000
6			6	0.078	0.239	82.353
7			7	0.069	0.492	53.333
8			8	0.037	1.145	100.000
9			9	0.083	0.524	0.000
10			10	0.051	0.248	54.545
11			11	0.041		44.444
12			12	0.051		18.182
13			13	0.037		25.000
14			14	0.023		0.000
15			15	0.041		100.000
16			16	0.193		11.905
17			17	0.064		0.000
18			18	0.051		100.000
19			19	0.120		80.769
20			20	0.032		0.000
21			21	0.028		100.000
22			22	0.147		37.500
23			23	0.028		100.000
24			24	0.023		0.000
25			25	0.041		0.000
26			26	0.161		88.571
27			27	0.055		25.000
28			28	0.055		0.000
29			29	0.023		80.000
30			30	0.106		0.000
31			31	0.037		100.000
32			32	0.046		0.000
33			33	0.051		0.000
34			34	0.023		0.000
35			35	0.028		0.000

## Reference

- Chang, Q., and Martin, L.J. (2009). Glycinergic Innervation of Motoneurons Is Deficient in Amyotrophic Lateral Sclerosis Mice A Quantitative Confocal Analysis. *Am J Pathol* 174, 574-585.
- Spike, R.C., Watt, C., Zafra, F., and Todd, A.J. (1997). An ultrastructural study of the glycine transporter GLYT2 and its association with glycine in the superficial laminae of the rat spinal dorsal horn. *Neuroscience* 77, 543-551.
- Verstraelen, P., Van Dyck, M., Verschuuren, M., Kashikar, N.D., Nuydens, R., Timmermans, J.P., and De Vos, W.H. (2018). Image-Based Profiling of Synaptic Connectivity in Primary Neuronal Cell Culture. *Front Neurosci* 12, 389.